EFFICIENT AND CONDITIONAL RELIABILITY ANALYSIS OF SLOPES IN SPATIALLY VARIABLE SOILS

LIU LEILEI

PhD

The Hong Kong Polytechnic University

2018

The Hong Kong Polytechnic University
Department of Civil and Environmental Engineering

Efficient and Conditional Reliability Analysis of Slopes in Spatially Variable Soils

Liu Leilei

A thesis submitted in partial fulfillment of the requirements for the degree of Doctor of Philosophy

January 2018

CERTIFICATE OF ORIGINALITY

I hereby declare that this thesis is my own work and that, to the best of my knowledge and belief, it reproduces no material previously published or written, nor material that has been accepted for the award of any other degree or diploma, except where due acknowledgement has been made in the text.

________________________________ (Signed)

Liu Lei-Lei (Name of student)

To my family

for their love and support

ABSTRACT

Spatial variability in soil properties has been widely recognized as an important issue. The influence of spatially variable soils on geotechnical structures such as a slope has attracted increasing notice in the past years. However, it is not a trivial task to accurately estimate the slope reliability with sufficient efficiency when the spatial variability of soil properties is incorporated into the slope stability model, because there are a great number of discretized random variables within the framework of random field theory. In addition, site investigation data, despite not much, are actually the exact values of the soil properties at some particular positions which are independent of the simulation methods. The traditional unconditional random field discards such known data, which is actually a serious drawback and a waste of site investigation effort. Neglecting the known data would also increase the simulation variance of the underlying random fields, which subsequently affects the responses of the whole slope system, such as the FS and the probability of failure (P_f). Furthermore, there is another kind of uncertainty—stratigraphic boundary uncertainty (SBU)—which widely exists in layered soils but is missing in most of the previous studies. However, how the SBU influences the slope stability is still an open question. This will subsequently affect the assessment of the estimated results based on the deterministic boundary assumptions. In view of these problems, this thesis mainly focuses on proposing an efficient approach for slope reliability analysis with consideration of the soil spatial variability and incorporating borehole/measurement data (i.e., conditional information) into slope reliability analysis.

Firstly, a simplified framework for efficient system reliability analysis of slopes in spatially variable soils is proposed based on multiple response surface method (MRSM) and Monte Carlo simulation (MCS). Within this framework, the equivalent spatially constant parameters, calculated from an explicit random variable model, are used to characterize the soil spatial variability such that the MRSM can be efficiently

performed. In addition, a variance reduction strategy is proposed to enable the framework applicable to slope reliability problems involving more than one type of shear strengths. The results show that the proposed simplified framework can well deal with slope reliability analysis in spatially variable soils, providing sound results that are comparable with those by MCS as reported in the literature. It is robust against changes of various cross-correlations, COVs and ACDs, which provides a practical tool for system reliability analysis of slopes in spatially variable soils.

Secondly, some attempts are made to estimate the failure probability of a slope characterized by soil spatial variability conditioned on a certain number of cored samples (or known data) from site investigation. Kriging method is used in combination with the Cholesky decomposition technique (CDT) to model the conditional random fields (CRFs) such that the simulated CRFs can be constrained by the measured data at particular locations. Then, the probability of slope failure is calculated by Subset simulation (SS). An example application is performed on a nominally "homogeneous" cohesion-frictional (c-φ) slope to illustrate the proposed approach. A series of parametric studies are conducted to investigate the influence of the layout of the cored samples on the P_f, FS, and the spatial variability of the critical slip surface (CSS). It is found that whether the CRFs can be precisely modelled relies highly on the relationship between the sample distance and the underlying auto-correlation distance (ACD). A smaller ratio of the sample distance to the ACD would provide a better simulation result. Moreover, compared with unconditional random field simulations, the simulation variance can be substantially reduced by CRF simulations. This finally produces a narrower variation range of the FS and the corresponding CSS location as well as a much lower P_f. The results also highlight the major significance of the CRF simulation at relatively large ACDs.

Thirdly, the influence of the system SBU on the system P_f and risk of a layered slope with spatially varied soil properties are studied. Within this contribution, the inherent soil spatial variability is modelled by non-stationary random fields that are obtained by using an extended CDT, while the random nature of the stratigraphic boundary location is simulated by a discrete random variable model. A series of comparative studies on the probabilistic analysis results obtained from considering and neglecting the system SBU have been conducted with respect to different statistics of soil properties. It is found that the system SBU has a significant influence on the slope failure mechanism. In addition, the slope failure risk would be overestimated for various statistics if the system SBU is not considered, except for small values of COV_{φ} (i.e., COV of φ), where the results are underestimated.

Finally, efforts are made to incorporate the inherent SBU into the reliability analysis of slopes in spatially variable soils using one-dimensional conditional Markov chain model, so as to investigate the influence of different borehole layout schemes on slope reliability analysis with and without considering the spatial soil variability. Detailed procedure for implementing the proposed approach on commonly used commercial software (e.g., ABAQUS and MATLAB) is described. It is found that both the location and number of boreholes have significant influence on the stratigraphic boundary simulation. Whether the soil spatial variability is neglected or not, the FS statistics and P_f do not increase or decrease with the borehole number, because there is an influence zone in the slope body and the boreholes located in this zone play a dominant role in the stability of the slope. However, the FS statistics and P_f can converge to the correct results if more and more boreholes are drilled. In addition, it is found that the conventional reliability analysis with an implicit assumption of DSB condition may overestimate the slope reliability. The difference between the DSB and RSB decreases with the increase of the vertical SOF. Compared with the effect of the system SBU, the inherent SBU is far more important to be considered in slope reliability analysis.

PUBLICATIONS ARISING FROM THE THESIS

1. **Leilei Liu**, Yungming Cheng, Xiaomi Wang, Shaohe Zhang, Zhonghu Wu. System reliability analysis and risk assessment of a layered slope in spatially variable soils considering stratigraphic boundary uncertainty. *Computers and Geotechnics*, 2017, 89: 213-225.

2. **Leilei Liu**, Yungming Cheng, Shuihua Jiang, Shaohe Zhang, Xiaomi Wang, Zhonghu Wu. Effects of spatial autocorrelation structure of permeability on seepage through an embankment on a soil foundation. *Computers and Geotechnics*, 2017, 87: 62-75.

3. **Leilei Liu**, Yungming Cheng, Shaohe Zhang. Conditional random field reliability analysis of a cohesion-frictional slope. *Computers and Geotechnics*, 2017, 82: 173-186.

4. **Leilei Liu**, Yungming Cheng, Shaohe Zhang. Response to the discussion on "Conditional random field reliability analysis of a cohesion-frictional Slope" by A. Johari and A. Gholampour. Computers and Geotechnics, 2018, DOI 10.1016/j.compgeo.2018.02.014.

5. **Leilei Liu**, Yungming Cheng, Xiaomi Wang. Genetic algorithm optimized Taylor Kriging surrogate model for system reliability analysis of soil slopes. *Landslides*, 2017, 14(2): 535–546.

6. **Leilei Liu**, Yungming Cheng. Efficient system reliability analysis of soil slopes using multivariate adaptive regression splines-based Monte Carlo simulation. *Computers and Geotechnics*, 2016, 79: 41-54.

7. Yungming Cheng, Liang Li, **Leilei Liu**. Simplified approach for locating the critical probabilistic slip surface in limit equilibrium analysis. *Natural Hazards*

and Earth System Science, 2015, 15(10): 2241–2256.

8. **Leilei Liu**, Yungming Cheng, Shaohe Zhang. System reliability analysis of soil slopes using advanced Kriging metamodel and quasi Monte Carlo simulation. *International Journal of Geomechanics (ASCE)*, 2018, 18(8): 06018019.

9. **Leilei Liu**, Shaohe Zhang, Yungming Cheng. Advanced reliability analysis of slopes in spatially variable soils using multivariate adaptive regression splines. *Geoscience Frontiers*, 2018, DOI: 10.1016/j.gsf.2018.03.013.

10. **Leilei Liu**, Zhiping Deng, Shaohe Zhang, Yungming Cheng. Simplified framework for system reliability analysis of slopes in spatially variable soils. *Engineering Geology*, 2018, 239: 330-343.

11. **Leilei Liu**, Qiujing Pan, Yungming Cheng, Daniel Dias. Incorporating stratigraphic boundary uncertainty into reliability analysis of slopes in spatially variable soils using one-dimensional conditional Markov chain model. *Landslides*, 2018. *Under review.*

ACKNOWLEDGEMENTS

First of all, I gratefully acknowledge my chief supervisor, Dr. Y.M. Cheng, for providing me the opportunity to pursue the Ph.D. degree in The Hong Kong Polytechnic University and for his patient guidance and constant encouragement in both my academic research and life. Without his help, the work presented in this thesis cannot be successfully achieved.

Then, I would like to express my profound gratitude to my former supervisor, Prof. Shaohe Zhang from the Central South University in mainland China, who firstly guided me to the academic world. Thanks for his continuous support and encouragement to help me overcome all the difficulties encountered during the past three years of the research work. His modesty and strict attitude towards academic research have been continuously impacting me.

Next, I own my sincere appreciation to other professors at the Department of Civil and Environmental Engineering in The Hong Kong Polytechnic University, who have taught me different kinds of professional knowledge; and my heartfelt gratitude also goes to my friends and members of the research group in The Hong Kong Polytechnic University, Dr. Yi Yang, Dr. Na Li, Mr. Kaihui Li, Mr. Lei Huang, Mr. Tao Zhou, Mr. Zhiyi Liao et al. for their helps and times to guide me through the highs and lows in both my life and research work.

Moreover, special thanks would go to Dr. Yu Wang at the City University of Hong Kong for offering me the chance to talk about my research, which is very inspiring.

Last but not least, I am forever indebted to my beloved parents and fiancée for their unconditional love and wordless support, although they cannot be thanked enough.

TABLE OF CONTENTS

LIST OF FIGURES

LIST OF TABLES

CHAPTER 1 INTRODUCTION

1.1 Research motivation

Hong Kong is well-known for slope failures with an average of approximately 300 such failures per year. In general, conventional slope stability analysis based on fixed constant parameters is used for the design of these slopes. Although the use of a deterministic approach for calculating the minimum factor of safety (FS) is useful for design purpose for most of the time, it is sometimes encountered that slopes with safety factors greater than unity are not necessarily safe. For example, it has been noted by the Hong Kong SAR Government that approximately 5% of the stabilized slopes in Hong Kong have eventually failed, and that many slopes with safety factors greater than 1.0 still ultimately fail.

Possible reason may lie in the fact that soil, by its very nature, generally presents a certain degree of uncertainties. In terms of sources of these uncertainties, they are mainly four-fold (e.g., **Phoon and Kulhawy 1999b**, **c; Cho 2012; Dasaka and Zhang 2012; Mašín 2015; Dithinde et al. 2016a**): inherent physical uncertainty (e.g., spatial variability of soil properties), system uncertainty arising from inevitable measurement errors induced by observers and measurement apparatuses (e.g., experiment uncertainty), epistemic uncertainty resulted from lack of sufficient site investigation data (e.g., sampling uncertainty), and model uncertainty (e.g., assumptions and simplifications in a slope stability model). Ideally, all these uncertainties should be appropriately considered in geotechnical stability analysis because they more or less simultaneously influence the performance of geotechnical structures such as slopes (e.g., **El-Ramly et al. 2002; Cho 2007; Griffiths et al. 2009; Mašín 2015; Dithinde et al. 2016a**). Obviously, conventional deterministic slope stability analysis using only the FS cannot well characterize all the uncertainties underlying the geotechnical problem. Hence, slope stability analysis within the framework of probability theory has been gaining more and more interests in the geotechnical engineering community in recent years, so as to quantify those uncertainties in a more reasonable acceptable manner.

Soil spatial variation is one of the most dominant uncertainties that affect the performance of geotechnical structures. Neglecting the spatial variability of soil properties would produce either an overestimated or underestimated slope failure probability (e.g., **Griffiths et al. 2009; Jha and Ching 2013; Li et al. 2017**). It is thus of great practical significance to consider such spatial variability of soils in the stability analysis of geotechnical structures such as slopes. In this regard, substantial efforts have been made by both scientists and engineers from geotechnical engineering field during the past two decades with fruitful achievements (e.g., **Griffiths and Fenton 2004; Griffiths et al. 2009; Huang et al. 2010; Griffiths et al. 2011; Wang et al. 2011; Low 2014; Griffiths and Yu 2015; Pantelidis et al. 2015; Zhu et al. 2015; Li et al. 2016c; Liu et al. 2017c**), such as the first/second-order reliability method (FORM/SORM) (e.g., **Cho 2013; Low 2014**), the random finite element method (RFEM) (e.g., **Griffiths and Fenton 2001; Griffiths and Fenton 2004**) and several analytical methods (e.g., **Cai et al. 2017**).

Although these methods have advanced the understanding and application of the probabilistic approaches in slope design (e.g., **Low and Tang 2007; Ching et al. 2009; Javankhoshdel and Bathurst 2014**), they are far from perfect and are not well accepted by engineering practitioners. For example, FORM/SORM cannot deal with highly nonlinear problems and slopes with significant system effect, which however are frequently encountered in engineering practice. Also, the analytical methods are suitable for simple slopes where the stability can be accurately represented by an explicit performance function. RFEM is probably the most common and robust approach to assess the effect of spatially auto-correlated soils on the slope stability. It is conceptually simple and easily understood by both geotechnical researchers and engineers. Due to this reason, RFEM has gained popularity in probabilistic slope stability analysis (e.g., **Griffiths and Fenton 2004; Griffiths et al. 2009; Huang et

al. 2010; Huang and Griffiths 2015; Zhu et al. 2015) since it was originally proposed by **Griffiths and Fenton (2001)** to investigate the effects of the spatial variation of the soil's undrained shear strength on the statistics of the bearing capacity. These works have demonstrated the RFEM to be a robust methodology for slope reliability evaluation involving spatially auto-correlated variables. However, it suffers from a major weakness of low efficiency because this method consumes extensive computing resources to obtain a reasonable accuracy of the probability of failure (P_f). This limitation of RFEM would be more serious when P_f is lower than 0.001 (e.g., **Ji and Low 2012; Li et al. 2016c**). As such, developing efficient slope reliability analysis approaches with the consideration of soil spatial variability continues to be an active topic in the geotechnical profession.

In addition, site investigation data, despite not much, generally exist in engineering practice. These data are actually the exact values of the soil properties at some particular positions, which are independent of the simulation methods. The traditional unconditional random field discards such known data, which is actually a waste of site investigation effort. Additionally, neglecting the known data would increase the simulation variance of the underlying random fields, which subsequently affects the responses of the whole slope system, such as the FS and P_f. Hence, it is of practical significance to take the known data into account in a slope reliability analysis, which can be considered as an effective tool for reducing the uncertainties in slope stability analysis. Hence, the conditional probabilistic analysis of a slope is needed for considering the effect of the known data.

Furthermore, there is another kind of uncertainty—stratigraphic boundary uncertainty (SBU)—which widely exists in layered soils, which has been commonly neglected in many previous studies. In terms of its source, SBU can be classified into two categories: system SBU induced by measurement error and inherent SBU caused by limited site investigation data. However, how this kind of uncertainty influences the slope stability is still an open question to date. This will subsequently affect the assessment of the results estimated based on deterministic boundary assumptions. In this thesis, this problem will be systematically solved with consideration of the influence of different soil statistics based on conditional simulations.

1.2 Research Objectives

With the abovementioned problems in mind, this study focuses mainly on the reliability analysis of slopes that are characterized by inherent spatial soil variability and SBU. The objectives of this study are as follows:

1. To propose an efficient approach for system reliability analysis of slopes in spatially variable soils, and to explore the robustness of accuracy and efficiency of the approach against the variations of various statistics, such as the anisotropic spatial variability through a series of parametric studies.

2. To propose an effective method for simulating conditional random fields that account for the known data from cored samples, and to efficiently evaluate the reliability of a slope based on the proposed method. To study the effects of different layouts of cored samples on the conditional random field simulation and the effects of the statistics of soil properties on the conditional simulation results.

3. To propose a useful model for characterizing the system SBU and to investigate the effect of the system SBU on the stability reliability and failure risk of a multi-layered soil slope. Meanwhile, it is also required to explore how SBU affects the assessment of the traditional reliability analysis results obtained based on the deterministic stratigraphic boundary (DSB) assumption when different degrees of spatial variability are considered.

4. To propose a useful model for characterizing the inherent SBU and to investigate the effect of the inherent SBU on the slope stability. To investigate the influence of different borehole layout schemes on slope reliability analysis with and without considering the spatial soil variability, and to find out the difference between

the results obtained based on DSB and those obtained based on the real stratigraphic boundary (RSB). In addition, to investigate how the soil spatial variability influences the difference between DSB and RSB.

1.3 Outline and Scope

To achieve the research objectives above, this thesis is divided into 7 chapters. Each chapter is briefly described as follows:

Chapter 1 introduces the research motivation, objectives and scope of this study.

Chapter 2 reviews extensively the literature relevant to this topic, which includes the available reliability approaches, commonly used probabilistic models for slope reliability analysis and frequently used random field discretization methods for characterizing the spatial variability of soil properties.

Chapter 3 proposes a simplified framework based on multiple response surface method (MRSM) and Monte Carlo simulation (MCS) for efficient system reliability analysis of slopes in spatially variable soils. Examples are studied to illustrate the accuracy and efficiency of the proposed framework, based on which the robustness of the proposed framework against various statistics such as the anisotropic spatial variability is fully demonstrated through a series of parametric studies. The strength and weakness of the proposed framework against MRSM is fully discussed.

Chapter 4 presents a Subset simulation (SS) based conditional random field reliability analysis approach for a cohesion-frictional soil slope to consider the effect of borehole data from site investigation. The effects of different layouts of cored samples on the conditional random field simulation and the effects of the statistics of soil properties on the conditional simulation results are studied.

Chapter 5 explores the influence of the system SBU on the system failure probability and risk of a layered slope characterized by spatially varied soil properties.

In this chapter, the stochastic nature of the stratigraphic boundary location is simulated by a discrete random variable; MCS is suggested for evaluating the system failure probability and risk. A series of comparative studies on the probabilistic analysis results obtained from considering and neglecting the system SBU have been conducted with respect to different statistics of soil properties.

Chapter 6 incorporates the inherent SBU into the reliability analysis of slopes in spatially variable soils using one-dimensional conditional Markov chain model. Based on the model, the influence of different borehole layout schemes on slope reliability analysis with and without considering the spatial soil variability is investigated. The difference between the results obtained based on DSB and those obtained based on the RSB is quantified. In addition, the question how the soil spatial variability influences the difference between DSB and RSB is answered.

Chapter 7 summaries the major work of this thesis and concludes the important findings from the work. The limitations of the current study are discussed and some suggestions for further studies are also proposed.

CHAPTER 2 LITERATURE REVIEW

2.1 Introduction

In this chapter, the most frequently used slope reliability approaches are first reviewed. In general, the available probabilistic analysis methods can be classified into four categories: analytical methods, approximate methods, sampling-based methods such as MCS, and the random finite element method (RFEM). The advantages and disadvantages of each class of method are summarized.

Based on the above reliability methods, the common probabilistic analysis models are then summarized, including random variable model (RVM), random field model (RFM) and conditional random field model (CRFM). The applicability of each model is introduced.

Finally, an extensive review of the studies on the reliability analysis of slopes in spatially variable soils in recent years is briefly summarized.

2.2 Review of the existed reliability approaches

2.2.1 Analytical methods

Several analytical methods for slope reliability analysis are available in the literature. For example, the first order second moment method (FOSM), in which the FS is approximately expressed by a Taylor series expansion and is truncated after the linear term (hence first order). Later, a modified expansion is used, along with the first two moments of the random variables, to determine the values of the first two moments of the dependent variables (hence second moment). The method is very easy to implement and can be used without knowing the specific probabilistic distribution functions of the underlying random variables. One only needs to know the first two moments of the underlying random variables, i.e., means and standard deviations.

However, it is difficult to apply this method to the situation where the FS cannot be explicitly expressed by random variables and the situation where the FS is highly nonlinear (e.g., **Fenton and Griffiths 2008**).

Another well-known analytical approach is the first order reliability method (FORM). It is defined based on a different reliability index, Hasofer and Lind reliability index (**Hasofer and Lind 1974**). The physical meaning of the Hasofer and Lind reliability index is that it indicates the minimum distance between the origin and the limit state surface in the standard normal space. Nevertheless, it suffers from the error induced by the linearization postulation of the complex non-linear performance function. More unfortunately, additional techniques must be adopted in order to assess exactly the induced error since FORM itself cannot validate it (e.g., **Echard et al. 2013**). Additionally, the pseudo partial differentiation adopted by finite difference scheme may severely affect the accuracy and efficiency in the presence of high-dimensional parameters space (e.g., **Cadini et al. 2014**).

Apart from FOSM and FORM, other methods such as point estimate method (PEM) (**Rosenblueth 1975**) and jointly distributed random variables method (JDRVM) (e.g., **Johari and Khodaparast 2015; Johari and Lari 2016**) are also used to assess the slope reliability in the literature. However, they are not frequently used in practice.

The abovementioned analytical approaches are very efficient in computation and can provide a relative accurate result to some extent, but it is not easy and possible to consider highly nonlinear problems. In addition, it is difficult to address the reliability analysis problems where the soil parameters are spatially auto-correlated.

2.2.2 Approximate methods

As for the probability of slope failure, it often involves evaluating a multiple integration with a multivariate joint probability density function of random variables of interest under a very complex integral domain (also termed as failure domain).

Obviously, it is very tough and even impossible to solve the n-fold integral equation for slope failure probability, especially when the number of random variables considered is extremely large. Therefore, approximate methods are resorted to. The surrogate model (or metamodel) is an efficient and recent popular alternative.

The last few decades have experienced an extensive application of several metamodels and their variants in different fields, among others, including response surface method (RSM) (e.g., **Li et al. 2015a; Li and Chu 2015; Jiang and Huang 2016; Li et al. 2016d; Li and Chu 2016; Zhang and Huang 2016**), stochastic response surface method (SRSM) based on polynomial chaos expansion (e.g., **Isukapalli et al. 1998; Li et al. 2011a; Ying 2012**), Kriging method (e.g., **Zhang et al. 2011a; Luo et al. 2012b; Zhang et al. 2013; Yi et al. 2015**), artificial neural network (ANN) (e.g., **Cho 2009**), Gaussian process regression (e.g., **Kang et al. 2015**) and support vector machine based RSM (e.g., **Kang and Li 2016; Kang et al. 2016**). A recent review on RSM is given elsewhere (e.g., **Li et al. 2016d**).

Generally, the fundamental concepts behind them rests on the approximation of the implicit performance function by an explicit model that are expressed in terms of the random variables within the framework of design of experiment (DOE). Thus, the computational efficiency is substantially improved, especially when computationally extensive finite element model is involved. The successful application of a metamodel generally depends highly on the number of DOEs, which are usually realized through sampling techniques such as MCS and Latin hypercube sampling (LHS). Intuitively, the larger the number of DOEs, the more accurate the metamodel fitting would be. However, more number of DOEs means more calls for the original implicit performance function, thus resulting in high computational cost and even overfitting problems. Hence, it is somewhat troublesome to achieve the balance between accuracy and efficiency (i.e., to find the optimal number of DOEs). Another factor affecting the accuracy of the metamodel is the location of the DOEs, which should be evenly distributed in the sample space and concentrate on the adjacent points of the limit state surface. Finally, the surrogate model is often impossible to control the approximation error, as discussed by **Cadini et al. (2014)**.

2.2.3 Sampling-based methods

The third group of the method is the sampling-based techniques. The probability of failure is usually expressed by a multi-fold integration, which is very difficult to solve. Fortunately, MCS can provide an unbiased estimation for this integration according to the law of large numbers. MCS estimates the failure probability of slope by calculating the ratio of the number of failure samples where the original performance function evaluation is less than a threshold to the total samples, which can be easily understood and implemented by engineers. Therefore, MCS is conceptually simple, robust and accurate as well as easily implementable (e.g., **Ang and Tang 2007**).

However, as is known to all, the variance of the failure probability is inversely proportional to the total number of samples. By definition, the total number of samples would be extremely high in order to obtain an acceptable variance when the failure probability is at a very small level. This would significantly increase the computational effort and render MCS inefficient. Furthermore, if the performance function is determined by a finite element method, the time and resources required for MCS would be prohibitively expensive.

To enhance the efficiency of MCS, lots of variance reduction methods have been proposed in the literature, such as importance sampling (IS) and Subset simulation (SS) (e.g., **Au and Beck 2003; Au et al. 2007; Rennen 2008; Ching et al. 2009; Wang et al. 2010; Angelikopoulos et al. 2015; Li et al. 2015c; Sundar 2015; Zhao et al. 2015; Li et al. 2016b; Li et al. 2016c**). The IS is performed by shifting the center of the PDF to the importance region where the most probably failure point or design point locates in, so that the failure samples can be generated with a relatively large probability (e.g., **Ching et al. 2009**). SS is originally proposed by **Au and Beck (2001)** for estimating the small failure probabilities in high dimensional problems. In this approach, a small failure probability is evaluated as the product of several larger conditional failure probabilities of some intermediate failure events. Thus, the simulation of a small failure probability event is converted to the simulations of a sequence of more frequently happened intermediate failure events. In addition, many other sampling techniques are produced based on the principles of increasing the occurance likelihood of failure samples, such as line sampling, Hasofer and Lind reliability based sampling (e.g., **Gong et al. 2015**) and other variants of SS or IS.

2.2.4 Random finite element method (RFEM)

RFEM is a combination of finite element method and random field theory, which can be applied to slope reliability analysis considering spatial variation of soil properties (e.g., **Griffiths and Fenton 1993; Griffiths and Lane 1999; Griffiths and Fenton 2001; Griffiths and Fenton 2004; Griffiths et al. 2009; Huang et al. 2010**). Unlike the deterministic slope stability analysis using limit equilibrium method, RFEM does not need any prior assumptions about the slip surfaces and internal slice forces, and gains more insight into the failure mechanism of a slope. However, RFEM is still not favored by engineers for routine design work because it requires significant modification of the existing deterministic numerical codes while the commercial software packages generally do not offer this option, and sometimes it also suffers from being time-consuming in certain special cases (e.g., **Cheng et al. 2007**). In addition, the strength reduction method is used to calculate the FS of a slope, of which the convergence criteria are still controversial (e.g., **Krahn 2006**).

To further enhance the application of RFEM in slope reliability analysis by engineers, non-intrusive stochastic finite element methods are gaining interest among researchers recently (e.g., **Jiang et al. 2014a; Li et al. 2016c**). In this kind of method, the deterministic and probabilistic analysis of slope stability are intentionally separated, which makes it a practical tool for engineers for slope reliability analysis without modifications of finite element codes.

2.3 Review of common probabilistic models for slope reliability analysis

In slope reliability analysis, two probabilistic models are frequently used by researchers: RVM and RFM. The RVM means soil properties are characterized by random variables that are subjected to particular distribution types. This indicates that in the same soil layer, the soil properties are the same in each random simulation. Several distribution types are often adopted to describe the stochastic properties of soil properties, such as normal, lognormal, beta, exponential, uniform, gamma and others. The non-normal variables can be easily transformed to normal variables by Nataf transformation (e.g., **Li et al. 2011a**). Among these distributions, the lognormal distribution is the most commonly used, mainly due to the non-negative property of the shear strength parameters. Many RVMs can be founded in the literature (e.g., **Wong 1985; Oka and Wu 1990; Christian et al. 1994; Chowdhury and Xu 1995; Low et al. 1998; Jimenez-Rodriguez et al. 2006; Low 2007; Zhao 2008; Ching et al. 2009; Li et al. 2011a; Li et al. 2011b; Zhang et al. 2011a; Zhang et al. 2011b; Luo et al. 2012a; Luo et al. 2012b; Tang et al. 2012; Cho 2013; Zhang et al. 2013; Peng et al. 2014; Johari and Khodaparast 2015; Li et al. 2015b; Yi et al. 2015; Johari and Lari 2016; Kang and Li 2016; Kang et al. 2016**).

On the other hand, the RFM is employed to characterize the spatial variability of soil properties. In RFM, the soil properties at a particular location are quite different from those far from it, but tend to be similar to the soil properties near the location (e.g., **Vanmarcke 1977a; Vanmarcke 1977b**). Similarly, lots of works can be tracked in the literature (e.g., **Hsu and Nelson 2006; Cho 2007; Hicks et al. 2008; Griffiths et al. 2009; Cho 2010; Suchomel and Mašín 2010; Wang et al. 2010; Cho 2012; Ji et al. 2012; Jha and Ching 2013; Ji 2013; Kim and Sitar 2013; Cho 2014; Jiang et al. 2014a; Li et al. 2014; Low 2014; Jiang et al. 2015; Li et al. 2015a; Li and Chu 2015; Low et al. 2015; Metya and Bhattacharya 2015; Pantelidis et al. 2015; Jiang and Huang 2016**). The failure probability calculated from RFM has been demonstrated to be quite different from that by RVM.

Another model is CRF, which is rarely utilized in slope reliability analysis in the literature, at least to the best of our knowledge. However, this model has been used to characterize the geological profiles or the soil properties (e.g., **Lloret-Cabot et al. 2012; Li et al. 2015d; Namikawa 2016**). In this model, the available data from site investigation are fully used, which seems to be more reasonable.

2.4 Review of random field discretization methods for characterizing the soil spatial variability

2.4.1 Spatial variability of soil properties

Generally, soil parameters at a particular location are more similar to the soil parameters at adjacent locations than those parameters at a remote location (e.g., **Li et al. 2015a**). This kind of property is referred to as the soil spatial variability that is governed by the auto-correlation structure underlying the soil properties. The auto-correlation coefficient between any two parameters at two different points is generally characterized by an auto-correlation function (ACF), which is very difficult to evaluate because of the limited site investigation data (e.g., **Liu et al. 2017c**). Instead, theoretical ACFs are often used as alternatives (e.g., **Li and Lumb 1987; Li et al. 2015a; Jiang and Huang 2016; Liu et al. 2017c; Liu et al. 2017d**). As far as the author knows, the single exponential and the squared exponential ACFs are likely to be the most frequently used ones in geotechnical stability analysis where the soil properties are considered spatially varied (e.g., **Griffiths and Fenton 2004; Cho 2010; Wang et al. 2011; Jiang et al. 2015; Liu et al. 2017d**). Furthermore, there are several other functions being occasionally used when appropriate, including the cosine exponential ACF, the binary noise ACF and the second-order Markov ACF (e.g., **Cheng et al. 2000; Cafaro and Cherubini 2002; Li et al. 2015a**). Obviously, differences must exist among these ACFs. For example, three of the above-mentioned five commonly used ACFs are not differentiable at the origin, except for the squared exponential ACF and the second-order Markov ACF (e.g., **Li et al. 2015a; Liu et al. 2017b**). Moreover, the autocorrelation matrix obtained from the squared exponential

ACF is generally not positive definite, and thus cannot be easily decomposed by the CDT that will be utilized in the following (e.g., **Liu et al. 2017c**). A more thorough and comprehensive comparison of these ACFs can also be found in the literature (e.g., **Li et al. 2015a; Liu et al. 2017b; Liu et al. 2017c**). However, the differences between the aforementioned ACFs have little influence on slope reliability analysis, as demonstrated by **Li et al. (2015a)**. Since the single exponential ACF is conceptually simple and easily implemented, it is utilized herein and described as (e.g., **Liu et al. 2017c**)

$$\rho\left(\tau_x, \tau_y\right) = \exp[-2(\frac{\tau_x}{\delta_h} + \frac{\tau_y}{\delta_v})] \tag{2.1}$$

where $\tau_x = \left|x_i - x_j\right|$ and $\tau_y = \left|y_i - y_j\right|$ are the absolute distances between two points in the horizontal and vertical directions, respectively; δ_h and δ_v are the horizontal and vertical scale of fluctuations (SOFs) of soil parameters, respectively.

2.4.2 Random field discretization methods

Random field theory has been extensively applied to characterize spatially variable soils in slope reliability analysis (e.g., **Griffiths and Fenton 2004; Cho 2007; Jha and Ching 2013; Kim and Sitar 2013; Jiang et al. 2015**). Within the framework of random process, the soil parameters at particular locations are often considered as random variables. The resultant random field is considered stationary or weakly stationary when the combination of the following three requirements is met **Vanmarcke 1977b; Phoon and Kulhawy 1999b; Li et al. 2015a; Jiang and Huang 2016**: (1) the statistics (i.e., means and standard deviations) of these random variables are constant over the domain of the random field; (2) the covariance between any two random variables at two points depends only on their absolute distances but not on their locations; (3) the probability density function (PDF) for the same number of random variables has nothing to do with their absolute locations; otherwise, the field is non-stationary (e.g., **Li et al. 2015d**). In slope reliability analysis, a weakly stationary random field is usually applied to model the spatial variability of a soil parameter in a homogeneous soil layer, whereas a non-stationary random field is suitable for multi-layered soils (e.g., **Li et al. 2015a**). Many methods such as the local average subdivision (LAS) (e.g., **Fenton and Vanmarcke 1990**), trend removal scheme (e.g., **Li et al. 2014**), Karhunen-Loève (K-L) expansion (e.g., **Phoon et al. 2002**), CDT (e.g., **Suchomel and Mašín 2010; Li et al. 2015a; Jiang and Huang 2016; Liu et al. 2017d**) and those given in **Fuglstad et al. (2014)** can be adopted. Since K-L expansion and CDT are the most commonly used by the author and in the literature (e.g., **Suchomel and Mašín 2010; Li et al. 2015a; Jiang and Huang 2016; Liu et al. 2017d**), they are detailed in the following sections based on the simulation of a set of non-Gaussian random fields of cohesion and friction angle.

2.4.3 K-L expansion for non-Gaussian random fields simulation

2.4.3.1 Introduction to K-L expansion

A random field $H(x, \theta)$ is a series of random variables associated with a continuous argument $x \in \Omega$, where Ω is an open set of R^n defining the system geometry, and $\theta \in \Theta$ is the coordinate in the outcome space. According to the K-L expansion, the random field $H(x, \theta)$ can be discretized based on the spectral decomposition of its ACF $\rho(x_1, x_2)$ that is generally bounded, symmetric and positive definite. The spectral decomposition is a process of solving for the eigenvalues and eigenfunctions of the homogeneous Fredholm integral equation as

$$\int_{\Omega} \rho(x_1, x_2) f_i(x_2) dx_2 = \lambda_i f_i(x_1) \tag{2.2}$$

where x_1 and x_2 denote the coordinates of two points; $f_i(x)$ and λ_i are the eigenfunctions and eigenvalues of the 1-D ACF $\rho(x_1, x_2)$, respectively. Generally, it is difficult to solve this equation analytically, depending on the type of the ACF. For example, in the case of the squared exponential ACF, numerical methods should be adopted because there are no analytical solutions for this ACF. Hence, the wavelet-Galerkin method is often employed to numerically solve the eigenvalue problem of Eq. (2.2). Details for this numerical technique are given elsewhere (e.g., **Phoon et al. 2002**).

Based on the set of deterministic eigenvalues and eigenfunctions obtained above, the random field $H(x, \theta)$ is expanded as

$$H(x, \theta) = \mu + \sum_{i=1}^{\infty} \sigma \sqrt{\lambda_i} f_i(x) \chi_i(\theta) \tag{2.3}$$

where $\chi_i(\theta)$ is a set of uncorrelated random variables with zero mean and unit variance; μ and σ are the mean and standard deviation of the random field $H(x, \theta)$, respectively. The series expansion in Eq. (2.3) is called the K-L expansion, which provides a second-moment representation of a random field in terms of the uncorrelated random variables and deterministic orthogonal functions (e.g., **Phoon et al. 2002; Jiang et al. 2014a**). It is known to converge in the mean square sense for any distribution of $H(x, \theta)$ (e.g., **Vořechovský 2008; Jiang et al. 2014a**). However, it is nearly impossible and computationally demanding to incorporate infinite terms in the series expansion in Eq. (2.3). Hence, the common way is to truncate the series at some high order term *M* to obtain the approximate estimation of the random field $H(x, \theta)$ as

$$\widehat{H}(x, \theta) = \mu + \sum_{i=1}^{M} \sigma \sqrt{\lambda_i} f_i(x) \chi_i(\theta) \tag{2.4}$$

where *M* is the number of K-L expansion terms to be retained, which is very critical to the accuracy and efficiency of the truncated series. As suggested by **Huang et al. (2001)** and **Laloy et al. (2013)**, the ratio of the expected energy ε can be used to measure the accuracy of the truncated series, which is defined as

$$\varepsilon = \frac{\int_{\Omega} E(\widehat{H}(x,\theta) - \mu)^2 dxdy}{\int_{\Omega} E(H(x,\theta) - \mu)^2 dxdy} = \sum_{i=1}^{M} \lambda_i \,/\, \sum_{i=1}^{\infty} \lambda_i \tag{2.5}$$

where $E(\cdot)$ is the expectation function and the eigenvalues λ_i are sorted in a descending order. Generally, the larger the value of ε, the higher the accuracy of the truncated series. Meanwhile, ε should be adjacent to 1 and as closely as possible to maintain a certain accuracy. However, a large value of ε also indicates a great cost of computation. To make a compromise between the accuracy and efficiency, **Huang et al. (2001)** and **Laloy et al. (2013)** suggested taking $\varepsilon \geq 95\%$ as a criterion for determining the value of M.

Extension to 2-D random field simulations is straightforward based on the aforementioned procedure for 1-D random field simulations. The method is to replace all eigenfunctions and eigenvalues of the 1-D ACF in Eq. (2.4) with the corresponding eigenfunctions and eigenvalues of the 2-D ACF. Hence, the discretization of a 2-D random field $H(x, y, \theta)$ can be defined as

$$\widehat{H}(x, y, \theta) = \mu' + \sum_{j=1}^{M'} \sigma' \sqrt{\lambda_j} f_j(x, y) \chi_j(\theta) \quad (2.6)$$

where μ' and σ' are the mean and standard deviation of the 2-D random field, respectively; $f_j(x, y)$ and λ_j are the eigenfunctions and eigenvalues of the 2-D ACF $\rho[(x_1, y_1), (x_2, y_2)]$, respectively; $\chi_j(\theta)$ is a set of uncorrelated random variables with zero mean and unit variance; and M' is the number of K-L expansion terms, which is determined based on Eq. (2.5) where, however, the eigenvalues λ_i are replaced by λ_j. It should be noted that the eigenmodes of a separable multidimensional ACF, such as the 2-D single exponential ACF in Eq. (2.1), can be easily calculated by multiplying with the eigenmodes of 1-D ACF (**Jiang et al. 2014a**). More details are given by **Huang et al. (2001)**.

2.4.3.2 Simulation of cross-correlated non-Gaussian random fields

In geotechnical engineering practice, a geotechnical structure is very often influenced by more than one soil parameters, and different parameters are commonly cross-correlated with each other (e.g., **Low 2007; Cho 2010; Li et al. 2011a; Jiang et**

al. 2014a). For example, the cohesion c and the friction angle φ are two key parameters that influence a slope stability, and they are generally negatively correlated (e.g., **Cho 2010**). Obviously, all these parameters should be simulated as cross-correlated random fields when the spatial variability of soil properties are considered. According to **Cho (2010)**, all random fields simulated over the same region Ω (e.g., a soil layer) share an identical ACF, and the cross-correlation structure between each pair of simulated fields can be simply defined by a cross-correlation coefficient. The underlying rationale of this statement lies in the fact that the spatial correlation structure is generally caused by changes in the constitutive nature of the soil over space (e.g., **Fenton and Griffiths 2003; Cho 2010**). Therefore, for a pair of cross-correlated random fields over a region Ω, only one evaluation of the eigenmodes of a given ACF is required. The resultant set of eigenfunctions and eigenvalues is then used in combination with two cross-correlated sets of random variables to expand the cross-correlated random fields. In the following, the simulations of cross-correlated random fields associated with c and φ are taken as examples to illustrate the procedure for cross-correlated random field simulations (e.g., **Cho 2010; Jiang et al. 2014a**).

As mentioned above, suppose the eigenmodes and the number of the K-L expansion terms under a given ACF (e.g., the squared exponential ACF in this study) are known, the cross-correlated random fields between c and φ can be simulated only if the cross-correlated sets of random variables are obtained. Denote the cross-correlation coefficient between c and φ as $\rho_{c\varphi}$, the cross-correlation matrix between them is written as

$$\boldsymbol{R} = \begin{bmatrix} 1 & \rho_{c\varphi} \\ \rho_{c\varphi} & 1 \end{bmatrix} \tag{2.7}$$

A vector of independent standard normal samples is then generated using LHS or a standard normal generator, which is finally partitioned into N_F vectors with a dimension of M' to form a sample matrix $(\boldsymbol{\chi})_{M' \times N_F}$, where N_F is the number of random fields to be simulated. For the number of two random fields simulated here, $N_F = 2$ and $\boldsymbol{\chi} = \{\boldsymbol{\chi}_c \quad \boldsymbol{\chi}_\varphi\}$, where $\boldsymbol{\chi}_c = \{\chi_{c1} \quad \chi_{c2} \quad \cdots \quad \chi_{cM'}\}^T$ and $\boldsymbol{\chi}_\varphi = \{\chi_{\varphi 1} \quad \chi_{\varphi 2} \quad \cdots \quad \chi_{\varphi M'}\}^T$. Next, a lower triangular matrix $\boldsymbol{L}$ is obtained by the CDT of $\boldsymbol{R}$. Based on $\boldsymbol{\chi}$ and $\boldsymbol{L}$, the cross-correlated standard normal sample matrix $\boldsymbol{\xi}$ is obtained as

$$\boldsymbol{\xi} = \boldsymbol{\chi}\boldsymbol{L}^T = \{\boldsymbol{\xi}_c \quad \boldsymbol{\xi}_\varphi\} \tag{2.8}$$

where $\boldsymbol{\xi}_c = \{\xi_{c1} \quad \xi_{c2} \quad \cdots \quad \xi_{cM'}\}^T$ and $\boldsymbol{\xi}_\varphi = \{\xi_{\varphi 1} \quad \xi_{\varphi 2} \quad \cdots \quad \xi_{\varphi M'}\}^T$.

Now, knowing the eigenmodes and the cross-correlated standard normal sample matrix $\boldsymbol{\xi}$, the cross-correlated Gaussian random fields underlying c and φ are discretized as

$$\hat{H}_i^G(x,y) = \mu_i + \sum_{j=1}^{M'} \sigma_i \sqrt{\lambda_j} f_j(x,y) \xi_{ij}, \text{(for } i = c, \varphi) \tag{2.9}$$

The isoprobability transformation (e.g., **Li et al. 2011a**) is then utilized to obtain the cross-correlated non-Gaussian random fields component-to-component as

$$\hat{H}_i^{NG}(x,y) = G_i^{-1}\{\Phi_i[\hat{H}_i^G(x,y)]\}, \text{(for } i = c, \varphi) \tag{2.10}$$

where $G_i^{-1}(\cdot)$ is the inverse cumulative distribution function (CDF) of each non-Gaussian random field $H_i^{NG}(x,y)$, and $\Phi_i(\cdot)$ is the CDF of each Gaussian random field $H_i^G(x,y)$. For example, if the c and φ are assumed to be cross-correlated lognormal random fields, then the approximations of the lognormal fields can be easily obtained by exponentiating their approximate Gaussian random fields as

$$\hat{H}_i^{LNG}(x,y) = \exp\left[\mu_{\ln_i} + \sum_{j=1}^{M'} \sigma_{\ln_i} \sqrt{\lambda_j} f_j(x,y) \xi_{ij}\right], \text{(for } i = c, \varphi) \tag{2.11}$$

where $\mu_{\ln_i}$ and $\sigma_{\ln_i}$ are the mean and standard deviation of the Gaussian random field $\ln i$, respectively. The relationship between (μ_i, σ_i) and $(\mu_{\ln_i}, \sigma_{\ln_i})$ is given as

$$\begin{cases} \mu_{\ln_i} = \ln \mu_i - 0.5\sigma_{\ln\ i}^2 \\ \sigma_{\ln_i} = \sqrt{\ln\ [1 + (\sigma_i/\mu_i)^2]} \end{cases} \tag{2.12}$$

If the above procedure is repeated N_s times, N_s simulations of the random fields will be obtained, based on which the statistical analysis can be performed.

2.4.4 CDT for non-Gaussian random fields simulation

Consider in a soil layer, if the considered random fields are to be discretized at the centroids of the random field elements, an autocorrelation matrix can be formed as

$$\boldsymbol{C} = \begin{bmatrix} 1 & \rho(\tau_{x_{12}}, \tau_{y_{12}}) & \cdots & \rho\left(\tau_{x_{1n_e}}, \tau_{y_{1n_e}}\right) \\ \rho(\tau_{x_{21}}, \tau_{y_{21}}) & 1 & \cdots & \rho\left(\tau_{x_{2n_e}}, \tau_{y_{2n_e}}\right) \\ \vdots & \vdots & \ddots & \vdots \\ \rho\left(\tau_{x_{n_e1}}, \tau_{y_{n_e1}}\right) & \rho\left(\tau_{x_{n_e2}}, \tau_{y_{n_e2}}\right) & \cdots & 1 \end{bmatrix} \tag{2.13}$$

where $\rho\left(\tau_{x_{ij}}, \tau_{y_{ij}}\right)$ denotes the autocorrelation coefficient between spatial quantities at any two points, in which the lags $\tau_{x_{ij}} = |x_i - x_j|$ and $\tau_{y_{ij}} = |y_i - y_j|$ denote the absolute distances between the centroid coordinates of the i^{th} element and the j^{th} element in the horizontal and vertical directions, respectively; n_e is the number of the discretized random field elements. Based on Eq. (2.13) and isoprobability transformation, one realization of the cross-correlated non-normal random fields $\boldsymbol{Z}^{CNN}$ of c and φ can be obtained as (e.g., **Li et al. 2015a**)

$$\boldsymbol{Z}_i^{CNN}(x,y) = F_i^{-1}\{\Phi[\boldsymbol{Z}_i^{CN}(x,y)]\}, (i = c, \varphi) \tag{2.14}$$

where $F_i^{-1}(\cdot)$ is the inverse function of the marginal cumulative distribution of the i^{th} random field; $\Phi(\cdot)$ is the standard normal cumulative distribution function; $\boldsymbol{Z}^{CN}$ is a typical realization of the cross-correlated normal random fields, which is obtained by

$$\boldsymbol{Z}^{CN} = \boldsymbol{L_1}\boldsymbol{\xi}(\boldsymbol{L_2})^{\boldsymbol{T}} \tag{2.15}$$

where $\boldsymbol{\xi}$ is a randomly sampled standard normal matrix with a dimension of $n_e \times 2$; $\boldsymbol{L_1}$ and $\boldsymbol{L_2}$ are the lower triangular matrices decomposed from the autocorrelation matrix $\boldsymbol{C}$ and the cross-correlated matrix $\boldsymbol{R}$ in Eq. (2.7), respectively, using the CDT as

$$\boldsymbol{L_1}(\boldsymbol{L_1})^{\boldsymbol{T}} = \boldsymbol{C} \tag{2.16}$$

$$\boldsymbol{L_2}(\boldsymbol{L_2})^{\boldsymbol{T}} = \boldsymbol{R} \tag{2.17}$$

Similarly, if the above procedure is repeated N_s times, N_s simulations of the random fields will be obtained, based on which the statistical analysis can be performed.

To conclude, it should be pointed out that extension of the above procedure for the simulation of non-stationary random fields is straightforward. Details are given elsewhere (e.g., **Lu and Zhang 2007; Jiang and Huang 2016**) and are not described here. Finally, it should be noted that the nonlinear isoprobabilistic transformation would induce a certain amount of error which, however, is very small and can be neglected, as demonstrated by **Li et al. (2011a)**, **Cho and Park (2010)**, **Al-Bittar and Soubra (2013)** and **Jiang et al. (2014b)**.

CHAPTER 3 SIMPLIFIED FRAMEWORK FOR SYSTEM RELIABILITY ANALYSIS OF SLOPES IN SPATIALLY VARIABLE SOILS

3.1 Introduction

In general, a robust estimation of the reliability result such as the probability of failure (P_f) arises from a large number of repeatedly call of the performance function of slope stability in the framework of Monte Carlo simulation (MCS). This suggests that the major sources of the computational cost of the slope reliability analysis are the evaluation of performance function and the number of MCS samples. Hence, to enhance the computation efficiency of slope reliability analysis, most of the previous studies in the literature focused mainly on the following two aspects: (1) simplifying the performance function of slope stability, such as using explicit performance functions as replacements of the original implicit ones (e.g., **Jiang et al. 2015; Li et al. 2015a; Pan and Dias 2017; Pan et al. 2017**); (2) reducing the MCS sample size as much as possible, such as importance sampling (IS) and Subset simulation (SS) (e.g., **Wang et al. 2011; Huang et al. 2016; Li et al. 2016c**). Response surface methods (RSMs) fall into the first category. These methods generally start with the construction of the explicit response surface for the original implicit performance function, followed by the MCS performed directly on the response surface to obtain the P_f (e.g., **Li et al. 2015a**). Since it is more efficient to evaluate the factor of safety (FS) from the explicit performance function (i.e., response surface) than from the original stability model that is often implicit and highly nonlinear (e.g., a finite element model), the total time for the reliability analysis is substantially reduced. The only time-consuming portion of the whole analysis lies in the construction of the response surface. A computationally efficient process of establishing the response surface would have no doubt to improve the efficiency of the reliability analysis, and vice versa. Likewise, RSMs can be inefficient when the random fields associated with the soil properties are discretized into thousands of random variables, because in this situation the number of training samples shall be very high in order to fully calibrate the response surface. Therefore, the RSM should be used with caution for slope reliability problems involving spatially correlated variables.

On the other hand, sample reduction methods, represented by SS, have now gained an increasing popularity in slope reliability community as well as other geotechnical divisions, because they can evaluate the P_f with a smaller sampling size while providing sound accuracy. For example, **Wang et al. (2011)** combined the SS with a limit equilibrium method (LEM) in a spreadsheet to calculate the P_f of slopes in spatially variable soils, and found that the computation efficiency was increased by nearly 50% compared with the direct MCS. **Li et al. (2016c)** then incorporated the SS into the FEM for slope reliability analysis and risk assessment, which substantially enhanced the computation efficiency of the random finite element method (RFEM) proposed by **Griffiths and Fenton (2004)**. However, as pointed out by **Huang et al. (2016)**, if the strength reduction method is used for calculating the FS in FEM, the SS-based RFEM is not necessarily more efficient than RFEM because more computation time is required to search for the FS, although the sampling times is significantly reduced. To this end, **Huang et al. (2016)** proposed using the value of yield function as a measure of the safety margin to avoid the search of FS, thus improving the computation efficiency. Unfortunately, the method by **Huang et al. (2016)** is only suitable for problems with failure probability level as low as 0.0001, and may be less efficient than the traditional RFEM when P_f is around 0.005. Moreover, it is noted that SS is sensitive to the sample size in each simulation level, and generally a relatively large value of the sample size in each level is warranted to obtain a robust estimation of the P_f. Likewise, SS shall be inefficient, especially when coupled with FEM, leaving efficient reliability analysis in spatially variable soils still to be a difficult problem.

Apart from the aforementioned efforts for efficient reliability analysis, many other beneficial attempts have also been made in the literature, such as the first-order reliability method (FORM) combined with LEM and random field theory (e.g., **Low et al. 2015**) and some simplified reliability models (e.g., **Luo et al. 2012c; Jha and Ching 2013; Li et al. 2017**). A common characteristic of these methods is that they make full use of the advantages of the high efficiency of the reliability approaches, assuming soil properties fully correlated (e.g., FORM) to account for the soil spatial variability in slope reliability analysis. Within this framework, the aforementioned RSMs and SS are expected to be more efficient because the number of random variables is generally small (e.g., less than ten for general slopes). For example, **Li et al. (2017)** used equivalent soil parameters to characterize the spatially varied soil parameters so that the efficient FORM approach for perfectly correlated random soils can be extended for reliability analysis of slopes in spatially variable soils. The efficiency and accuracy of the equivalent approach have been fully illustrated by applications to a “homogeneous” cohesive slope and a two-layered cohesive slope. However, the following issues are remained to be answered: (1) the system effect of slope failure is ignored, whereas there are generally multiple failure modes in a slope and different groups of two failure modes are often characterized by different correlations (e.g., **Oka and Wu 1990; Chowdhury and Xu 1994**, **1995**); (2) only one kind of strength parameter (i.e., the s_u) is considered, which does not stand for slopes with multiple strength parameters (e.g., cohesion and friction angle); (3) the influence of different statistics of soil properties, such as coefficients of variation (COVs) of different strengths, cross-correlation coefficient between two kinds of strengths and ACDs (ACDs) in both horizontal and vertical directions, are not fully investigated, although the effect of the isotropic spatial variation of soil properties has been studied; (4) the time consumption for calculating the equivalent parameters might be too large to affect the computation efficiency.

With the above-mentioned problems in mind, this chapter proposes a simplified framework based on multiple response surface method (MRSM) and MCS for efficient system reliability analysis of slopes in spatially variable soils. Within this framework, the equivalent parameters, which are efficiently calculated from an explicit response surface, are utilized to characterize the soil spatial variability. Then, the means, standard deviations, and the associated probability distribution functions (PDFs) of the equivalent parameters are determined. Multiple response surfaces are subsequently built based on the equivalent parameters, based on which MCS is performed to evaluate the system P_f. The framework is finally illustrated through an undrained cohesive slope and a cohesive-frictional (c-φ) slope, based on which the influence of different statistics is fully checked.

3.2 Proposed simplified reliability analysis framework

3.2.1 General

The major idea of this framework is to make a random field model (RFM) of slope stability considering soil spatial variability equivalent to a random variable model (RVM) based on the requirement that the two models offer comparable system P_f values. As such, the commonly used RVM based reliability approaches (e.g., FORM and RSM) can be effectively used to consider spatially variable soils, and thus improving the computation efficiency of the slope reliability analysis that involves spatially variable soils. The spatial variability of soil properties is considered in the RVM by the equivalent random parameters that are spatially constant of the original spatially variable soil properties. Herein, it is deemed in this study that the two kinds of parameters (i.e., the random variable versus the random field) are equivalent in the sense that they produce the same FS value when they are substituted into the RVM and RFM, respectively. For example, Figure 3.1(a) shows the FS for a random realization of the random field of the undrained strength s_u at the case of COV=0.3, l_h=20 m and l_v=2 m, which is nearly the same as that shown in Figure 3.1(b) where the value of the random variable s_u is equal to 24.7 kPa. Under this circumstance, we call the random variable value of 24.7 kPa is the equivalent value of the random field s_u at the case of COV=0.3, l_h=20 m and l_v=2 m for this realization. However, it might be argued that Figures 3.1(a) and (b) are not fully equivalent because the shape and location of the critical slip surfaces in the two figures are not completely the same. Nevertheless, the FS value based equivalence still appears to hold, because the focus of this study is not on the risk assessment that may be affected by the location and shape of the slip surface but on the failure probability analysis that depends only on the distribution of FS value. In the following sections, the techniques comprised of the framework will be introduced in detail.

3.2.2 Random field modeling of spatially variable soil properties

As mentioned above, one of the prerequisites for establishing the RFM is to characterize the spatial variability of soil properties, which is often simulated based on random field theory in the literature (e.g., **Vanmarcke 1977b; Griffiths and Fenton 2004; Vanmarcke 2010**). For this purpose, several techniques can be employed, such as the local average subdivision method (e.g., **Fenton and Vanmarcke 1990**), the Karhunen–Loève expansion method (e.g., **Phoon et al. 2002**), and the Choleskey decomposition method (e.g., **Li et al. 2015a; Liu et al. 2017c**). The Choleskey decomposition method is adopted in this study due to its simple concept and ease in implementation in the program, but also on the fact that the aforementioned techniques show little difference on the reliability results (e.g., **Li et al. 2015a; Jiang et al. 2017**). Detailed procedures have been given in Chapter 2.

3.2.3 Evaluation and statistical analysis of equivalent parameters

3.2.3.1 Evaluation of equivalent parameters

Accurate and efficient evaluation of equivalent parameters is a key component of the proposed framework, which requires back calculation of the strength parameters from a slope stability model (i.e., RVM) for a given FS value. This is generally achieved by trial and error in previous studies (e.g., **Li et al. 2017**). However, this method has at least the following two limits: (1) it requires repeated iterations to obtain accurate results, which may be very time-consuming, especially for those FEM-based models;

(2) it is only applicable to simple slopes, of which the stability is only governed by one strength parameter (e.g., the homogenous undrained cohesive slope), because different groups of strength parameters may have the same FS in those more complicated slopes (e.g., the c-φ slope). Therefore, to accommodate for more general cases, this study proposes back calculating the equivalent parameters on the basis of the explicit response surface function of the RVM (referred to as the explicit RVM, and abbreviated with ERVM hereafter).

The ERVM is established based on the regression analysis of a specific number (e.g., N_t) of data ($\boldsymbol{X}$, $\boldsymbol{FS}$), where $\boldsymbol{X}$ is a matrix with a dimension of $N_t \times n$ and n is the number of the strength parameters, $\boldsymbol{FS}$ is a column vector of N_t FS values that are evaluated from the RVM for these given N_t combinations of strength parameters (i.e., $\boldsymbol{X}$). Once the ERVM is established successfully, the back calculation of equivalent strength parameters for a given equivalent FS value that is obtained in advance from the RFM for a typical realization of random fields is as easy as solving algebraic equations. Obviously, for those simple slopes involving only one strength parameter, giving an FS will, admittedly, output one parameter. However, for those slopes containing more than one strength parameter, the solution for the equation of the ERVM is not unique, since only one known value (i.e., the equivalent FS) is given. For this problem, the following strategy is employed in this study:

1. Determine one of the strength parameters to be back calculated for a given equivalent FS.

2. Perform variance reduction technique (e.g., **Vanmarcke 2010**) on the remaining n-1 strength parameters that are simulated by random fields to consider them as random variables in a specific domain. Note that the variance reduction factor for 2-D single exponential ACF is used in this study (e.g., **Luo et al. 2012c**).

3. Randomly generate n-1 random variable samples based on the statistics of the n-1 random variables that are deduced in step 2, and substitute them into the

ERVM together with the given FS to calculate the equivalent value of the strength parameter that is pre-specified in step 1.

The strategy indicates that only one kind of equivalent parameter is required to be back calculated for a given equivalent FS. Likewise, the proposed approach can deal with complicated slope examples that have more than one type of strength parameter, of which the effectiveness will be shown later in Section 3.5.

3.2.3.2 Statistical analysis of equivalent parameters

Due to the random nature of the spatially variable soil properties, the equivalent parameters are also randomly varied. To accurately estimate the statistics of the equivalent parameters, a certain amount (e.g., N_s) of equivalent samples should be obtained first. This requires generating N_s random fields to obtain the corresponding N_s equivalent FS values from the RFM, which is then followed by the N_s evaluations of the equivalent samples using the suggested method in Section 3.2.3.1. Suppose N_s equivalent samples have been obtained, the problem is evolved to find the mean, standard deviation, and PDF of the equivalent parameter. In the current study, the mean and standard deviation are easily estimated using the basic statistical theory, while the marginal PDF is determined based on the information criteria that are commonly used for the PDF estimation of geotechnical parameters (e.g., **Phoon and Ching 2014**), such as the Akaike information criterion (AIC) and the Bayesian information criterion (BIC), although many goodness-of-fit test methods are available for this purpose. According to the information criteria, the best-fit PDF for a number of given samples is identified as the one that results in the smallest AIC and BIC values. The AIC and BIC are defined, respectively, as (e.g., **Phoon and Ching 2014**)

$$\mathrm{AIC} = -2\sum_{i=1}^{N_s} \ln f(x_i; p, q) + 2k \tag{3.1}$$

$$\mathrm{BIC} = -2\sum_{i=1}^{N_s} \ln f(x_i; p, q) + k \ln N_s \tag{3.2}$$

where $f(x_i; p, q)$ is the candidate PDF for the equivalent samples; x_i is the sample value; k is the number of distribution parameters in the candidate PDF; p and q are distribution parameters related to the mean and standard deviation of the candidate PDF. Since the non-negative property of the geotechnical parameters, four candidate PDFs—TruncNormal (i.e., Normal truncated below zero), Lognormal, TruncGumbel (i.e., Gumbel truncated below zero), and Weibull distributions—are selected and checked by the AIC and BIC criteria in this study. Details on the best-fit PDF identification process based on AIC and BIC criteria and the expressions of the four PDFs as well as their associated parameter relationships can be found in the book by **Phoon and Ching (2014)**, to which the reader is referred.

Additionally, it should be noted that there might be cross-correlations between the equivalent parameter and the reduced random variables in the presence of multiple strength parameters, which can be evaluated by the Pearson's correlation coefficient (e.g., **Mari and Kozt 2001**) as

$$\rho = \frac{\sum_{i=1}^{N_S}(x_{1i}-\overline{x_1})(x_{2i}-\overline{x_2})}{\sqrt{\sum_{i=1}^{N_S}(x_{1i}-\overline{x_1})^2}\sqrt{\sum_{i=1}^{N_S}(x_{2i}-\overline{x_2})^2}} \tag{3.3}$$

where x_{1i} denotes the i^{th} equivalent sample value; x_{2i} denotes the i^{th} reduced variable sample value; $\overline{x_1}$ and $\overline{x_2}$ denote the sample means of the equivalent parameter and the reduced variable considered, respectively.

With the above-mentioned equivalent statistics, the slope failure probability can be easily estimated based on those random variable reliability approaches, which will be introduced in the following section.

3.2.4 MRSM for evaluating the system P_f

Having obtained the equivalent parameters that are spatially constant, the original reliability analysis based on the RFM can now be represented by the reliability analysis based on the RVM. Thus, the conventional reliability analysis methods considering random variables can be easily used. In addition, it has been widely recognized that there are generally multiple potential failure modes in a slope, and different failure modes are often characterized by different correlations (e.g., **Oka and Wu 1990**). This indicates the slope reliability should be analyzed from a systematic view of point. To this end, MCS is often resorted to. However, direct MCS on the RVM is still time-consuming, because thousands of evaluations of the RVM are at least needed to obtain a robust estimation of the P_f. To enhance the efficiency, the MRSM, which has been demonstrated to be effective and efficient for a wide range of slope reliability problems (e.g., **Li et al. 2015a; Li et al. 2016d**), is adopted here. It should be pointed that compared with the MRSM for spatially variable soils MRSM for spatially constant soils is much more efficient, because the unknown coefficients are substantially deduced, suggesting much less evaluations of the RVM required. The MRSM proceeds with the following two steps (e.g., **Li et al. 2015a**):

1. *Select a suitable response surface form for each potential slip surface*. The quadratic polynomial chaos expansion without cross terms is used here and written as

$$FS_i(\boldsymbol{X}) = a_{1i} + \sum_{j=1}^{n} b_{ij} x_j + \sum_{j=1}^{n} c_{ij} x_j^2 \tag{3.4}$$

where $FS_i(\boldsymbol{X})$ is the FS for the i^{th} potential slip surface; $\boldsymbol{X} = (x_1, x_2, \cdots, x_n)^T$ is the random variable vector, particular the equivalent parameters herein; a_{1i}, b_{ij} and c_{ij} are unknown coefficients with a totally number of $2n$+1.

2. *Calibrate the unknown coefficients*. Firstly, generate the following $2n$+1 samples using the central composite design (CCD) method (e.g., **Bucher and Bourgund 1990**): $(\mu_{x_1}, \mu_{x_2}, \cdots, \mu_{x_n})$, $(\mu_{x_1} \pm m\sigma_{x_1}, \mu_{x_2}, \cdots, \mu_{x_n})$, $(\mu_{x_1}, \mu_{x_2} \pm m\sigma_{x_2}, \cdots, \mu_{x_n})$, $\cdots$, and $(\mu_{x_1}, \mu_{x_2}, \cdots, \mu_{x_n} \pm m\sigma_{x_n})$, where μ_{x_i} and σ_{x_i} are the mean and standard deviation of the i^{th} random variable, respectively; m is a coefficient for generating sample points, and is generally taken as 2 (e.g., **Zhang et al. 2011b**). Then, evaluate the FS for each CCD sample from the RVM. Finally, the unknown

coefficients are obtained by solving a system of $2n+1$ linear algebraic equations.

3. *Establish the remaining response surfaces.* Repeat steps 1 and 2 for N_p times to establish N_p response surfaces, which, as a whole, are finally taken as the surrogate of the RVM.

4. *MCS to evaluate P_f.* Generate N_{sim} samples and substitute them to the surrogate established in step 3 to estimate the system P_f as

$$P_f = \frac{1}{N_{sim}} \sum_{i=1}^{N_{sim}} I\left\{\left[\min_{j=1,2,\cdots N_p} FS_j(X_i)\right] < 1\right\} \tag{3.5}$$

where $I\{\cdot\}$ is an indicator function which is equal to unity if $\left[\min_{j=1,2,\cdots N_p} FS_j(X_i)\right] < 1$ and zero, otherwise.

3.3 Implementation procedure of the proposed framework

To further facilitate the understanding and application of the framework, Figure 3.2 schematically shows the flowchart of the proposed system reliability analysis framework. In general, the whole flowchart consists mainly of five steps, which are detailed as follows:

1. Collect the required data of both geotechnical and geometrical parameters for slope stability analysis, including but not limited to shear strengths, unit weights, slope angle and slope height. Then, single out the stochastic parameters and characterize their statistics, which include the means, COVs, PDFs, ACFs, ACDs and cross-correlation coefficients.

2. Use the mean values obtained in step 1 to establish two slope stability models: RVM and RFM. Traditional slope stability analysis methods such as LEM can be adopted for this purpose. Additionally, it should be pointed out that the soil properties are spatially constant in RVM but spatially variable in RFM. Hence, the slope domain in RFM is required to be discretized into finite elements in advance in order to

characterize the spatial variability of soil properties, as schematically shown in Figure 3.1(a).

3. Evaluate the RVM for a specific number (e.g., N_t) of groups of strength parameters (e.g., $\boldsymbol{X}$ in Figure 3.2) to obtain the corresponding FS values, and regression analysis is performed to establish an explicit response surface function (i.e., ERVM) between FS and $\boldsymbol{X}$, i.e., $FS=f(\boldsymbol{X})$, which will contribute greatly to the efficient back calculation of the equivalent parameters in the following steps. Additionally, within the ERVM, it is easy to deal with soils involving more than two types of strength parameters with effectiveness, which, however, cannot be achieved in the work by **Li et al. (2017)**.

4. Generate N_s random fields associated with the spatially variable soil properties and incorporate them into the RFM to obtain N_s FS values, which are referred to as the equivalent FS values (i.e., $\boldsymbol{FS}_{eq}$) to differentiate them from the N_t FS values obtained from the RVM in step 3. The equivalent FS values are then substituted to the established response surface in step 3 for back calculating the equivalent soil parameter values, i.e., $\boldsymbol{X} = f^{-1}(\boldsymbol{FS}_{eq})$. Based on the equivalent parameter values, statistical analysis is then performed to obtain the means, COVs, PDFs and cross-correlations of equivalent parameters. Note that, for soils involving more than one type of strength parameter, the technique introduced in Section 3.2.3.1 should be employed before the regression analysis in order to determine the strength parameter to be back calculated and to obtain the reduced strength parameters.

5. Use the equivalent statistics obtained in step 4 in a random variable reliability approach such as the MRSM (e.g., **Zhang et al. 2011b**) to evaluate the system P_f.

3.4 Example I: Application to an undrained cohesive slope

3.4.1 Model preparation

To illustrate the proposed framework, it is first applied to an undrained cohesive slope, of which the stability is governed only by the undrained shear strength s_u. Figure 3.3 schematically plots the geometry of the slope, which has a slope height of 5 m and a slope angle of 26.6°. The slope consists only of a homogeneous clay layer with a thickness of 10 m and a total unit weight of 20 kN/m^3. The s_u of the clay is assumed to be subjected to lognormal stationary random field with the mean μ_{s_u} of 23 kPa, the COV COV_{s_u} of 0.3, the horizontal ACD l_h of 20 m, and the vertical ACD l_v of 2 m. For convenience purpose, these values are directly taken from **Jiang et al. (2015)** and **Cho (2010)** so that the results in these references can be referred to. Based on these values, the RVM is firstly built based on Bishop's simplified method, which provides an FS of 1.355 when the s_u is taken as a spatial constant with a value of μ_{s_u}. The FS value is very close to those (i.e., both 1.356) reported by **Jiang et al. (2015)** and **Cho (2010)**, and its associated slip surface (known as critical deterministic slip surface, CSS), which is identified among 4,851 predefined potential slip surfaces, is nearly the same with that found by **Jiang et al. (2015)**, as shown in Figure 3.3. The comparable results with the literature thus indicate the effectiveness of the established RVM, which ensures the accuracy of the following analysis.

To consider the spatial variability of s_u in slope stability analysis, the random field of s_u is firstly modeled by 910 spatially correlated random variables, which are respectively located at the centroids of 910 random field elements that are discretized with a side length of 0.5 m, as schematically shown in Figure 3.4. Note that the size of the discretized random field element here is consistent with that used by **Jiang et al. (2015)**. The random variable values associated with all elements are generated from the realization of the random field of s_u using Eq. (2.14). As an illustration, Figure 3.4 shows a typical realization of the random field of s_u, where darker color indicates larger s_u values and lighter color represents smaller s_u values. Based on the discretized random field, traditional stability analysis methods (e.g., Bishop's simplified method) can be employed to evaluate the FS for this realization. The slope stability model that takes the soil spatial variability into account here and hereafter signifies the so-called

RFM in this study. Note that, if the random variable values are all assigned a value of the μ_{s_u}, the RFM is expected to obtain the same FS (i.e., 1.355) and CSS as those produced by the RVM, as shown in Figure 3.4. Conventional reliability approaches are directly performed based on the RFM, which is very time-consuming. However, the RFM here in this study is mainly used for the generation of equivalent parameters, as will be introduced later.

3.4.2 Determination of equivalent undrained shear strength $s_{u_{eq}}$

In this section, the equivalent undrained shear strength $s_{u_{eq}}$ is determined. According to the procedure described in Section 3.3, the first step for identifying the $s_{u_{eq}}$ is to establish the ERVM of the slope stability. To this end, a certain number (e.g., N_t=21 for this example) of samples that were evenly selected from the range of $(\mu_{s_u} - 3\sigma_{s_u}, \mu_{s_u} + 3\sigma_{s_u})$ were substituted to the RVM to obtain the corresponding FS values, which comprises a set of training data. Based on the data set, a linear regression analysis was then performed to obtain the linear ERVM between the FS and s_u, because previous studies generally indicate that the FS is linearly correlated with the s_u for homogeneous undrained cohesive slopes (e.g., **Griffiths et al. 2009; Huang et al. 2017**). The explicit expression of the ERVM was finally obtained as

$$FS(s_u) = 0.0589 s_u \tag{3.6}$$

To valid the accuracy of the ERVM, Figure 3.5 compares the FS values predicted by Eq. (3.6) for 100 randomly generated values of s_u with those obtained from the RVM using Bishop's simplified method. As can be seen from the figure, the FS values from the two models are in good agreement with each other. This suggests that the ERVM can be effectively used to back calculate the equivalent undrained strength value when an equivalent FS is given.

The second step is to determine the statistics of the $s_{u_{eq}}$. As shown in Figure 3.2, N_s random field realizations of s_u are generated to obtain N_s equivalent FS values, which are subsequently substituted to Eq. (3.6) to get the N_s equivalent values of s_u. Statistical analysis is then performed on the N_s equivalent values based on the method introduced in Section 3.2.3.2 to determine the mean $\mu_{s_{u_{eq}}}$, standard deviation $\sigma_{s_{u_{eq}}}$, and PDF of the $s_{u_{eq}}$. Therefore, the value of the N_s is very critical to the accuracy of the estimations of the statistics of the $s_{u_{eq}}$. A large value would definitely increase the accuracy, but it also decreases the computational efficiency. To obtain the optimal value of N_s, a sensitivity study was conducted with N_s varying from 100 to 10,000. Figure 3.6(a) shows the variations of the $\mu_{s_{u_{eq}}}$ and $\sigma_{s_{u_{eq}}}$ with respect to N_s. It is found that both $\mu_{s_{u_{eq}}}$ and $\sigma_{s_{u_{eq}}}$ keep nearly invariant with N_s when N_s is larger than about 3,000. To make a compromise between the efficiency and accuracy, N_s=3,000 is selected, with which the standard errors of the estimated $\mu_{s_{u_{eq}}}$ and $\sigma^2_{s_{u_{eq}}}$ are estimated as $\sqrt{COV_{s_u}/N_s} = 0.018\sigma_{s_u}$ and $COV_{s_u}\sqrt{2/(N_s-1)} = 0.026COV_{s_u}$, which are less than 3% of their true quantities (e.g., **Griffiths and Fenton 2001; Li et al. 2017**). Additionally, AIC and BIC criteria show that the 3,000 equivalent samples are best fitted by the lognormal distribution, which can also be deduced from Figure 3.7(a) where Lognormal matches well with the histogram of the 3,000 samples. Next, reliability analysis using these statistics can be easily performed using the suggested method in Section 3.2.4.

3.4.3 System reliability analysis results

Table 3.1 lists the system failure probability results of this slope calculated by this study and taken out from **Cho (2010)** and **Jiang et al. (2015)**. The system P_f evaluated using the proposed framework [denoted as "EQP (equivalent parameter)+MRSM+MCS" in the Table 3.1 and hereafter] is 7.40×10^{-2}, which matches well with the value of 7.73×10^{-2} that is estimated by direct MCS on the RFM with 10,000 random field samples. However, it might be argued that the high accuracy of the framework can be a compromise between the use of equivalent parameters and MRSM, because both of the two techniques are approximate. To eliminate such concern, direct MCS on the RVM (denoted as “EQP+ MCS” in the Table 3.1 and hereafter) with 10,000 random variable samples generated using the equivalent parameter (i.e., $s_{u_{eq}}$) was also performed to evaluate the P_f, which shows to be identical with the result (i.e., 7.40×10^{-2}) from the proposed framework. Indeed this can be expected from previous studies (e.g., **Li et al. 2016d**) that has demonstrated the accuracy of the MRSM for reliability analysis of slopes involving random variables. Overall, the good agreement between the three methods (i.e., MCS, “EQP+MCS” and “EQP+MRSM+MCS”) validates the accuracy of the proposed framework. Additionally, it is found that the reliability results in this study are comparable with those (i.e., 7.60×10^{-2}, 8.30×10^{-2} and 7.90×10^{-2}) reported by **Cho (2010)** and **Jiang et al. (2015)**, respectively. This finding further validates the reliability of the results by this study. It should be pointed out that the larger values provided by these references than those in this study are mainly because the squared exponential was used by **Cho (2010)** and **Jiang et al. (2015)**, which, by its function nature, may result in larger estimations of the P_f, as proved by **Li et al. (2015a)**. Nevertheless, the difference is minimal.

As for the efficiency of the proposed framework, it is obviously much more efficient than direct MCS and “EQP+MCS”, because only 3,000 evaluations of the RFM and 21 evaluations of the RVM are required. However, as stated by **Jiang et al. (2015)**, Latin hypercube sampling (LHS) with only 1,000 samples can yield a satisfactory estimation of the P_f (i.e., 8.30×10^{-2}), which shows to be more efficient and seems that it is not necessary to use the proposed framework. This lies in the fact that the failure probability level is in the order of magnitude of 10^{-2}, which is relatively large and can be accurately estimated based on a small number of samples. However, this is not always the truth for slopes with a relatively small P_f, e.g., less than 0.001, as will be illustrated for the case of $COV_{s_u} = 0.15$.

Table 3.2 shows the reliability results for $COV_{s_u} = 0.15$ by various approaches. Following the aforementioned procedure employed for $COV_{s_u} = 0.3$, N_s=4,000 is selected based on the sensitivity study shown in Figure 3.6(b), and the $s_{u_{eq}}$ is best fitted by the lognormal distribution, as seen from Figure 3.7(b). It should be noted that when COV_{s_u} is decreased to 0.15, there is no need to establish again the ERVM. Based on the $s_{u_{eq}}$, the P_f for the case of $COV_{s_u} = 0.15$ is estimated as 1.40×10^{-4} using the proposed framework, which is comparable with those (i.e, 2.50×10^{-4} and 1.25×10^{-4}) obtained by direct LHS and "EQP+LHS", respectively. However, the computational effort (i.e., 4,000 RFM+24 RVM) required by the proposed method is much less than those (i.e., 40,000 RFM and 4,000 RFM+40,024 RVM) by direct LHS and "EQP+LHS", respectively. This thus highlights the advantage of efficiency of the proposed method when facing with such a small level of failure probability. Additionally, Table 3.2 also gives the reliability results reported by **Jiang et al. (2015)**, which are comparable with those in this study. Again, similar to the case of $COV_{s_u} = 0.3$, the results by **Jiang et al. (2015)** are slightly overestimated, because the squared exponential ACF is used. Nevertheless, such finding further validates the reliability of the results by this study.

3.4.4 Influence of spatial variability of s_u on the accuracy of the proposed framework

This section investigates the influence of horizontal and vertical ACDs on the system P_f of this slope example using the proposed framework, which aims at examining the applicability of the framework for reliability analysis with different degrees of spatial variability. A series of parametric studies were performed to consider the different spatial autocorrelations with the l_h varying between 10 m and 40 m, and the l_v

varying between 0.5 m and 3.0 m. The variation ranges are following those used by **Jiang et al. (2015)**, which are the typical statistics for a wide range of spatially variable soils (e.g., **Phoon and Kulhawy 1999b**). For each combination of the l_h and l_v, the system P_f was evaluated by the proposed framework, direct MCS, and "EQP+MCS". In addition, results from **Jiang et al. (2015)** were also referred as a reference to this study for a consistent comparison purpose.

Figure 3.8(a) shows the variations of the system P_f associated with the four methods with respect to l_h with l_v fixed at 2.0 m. As expected, the reliability results obtained by the four methods increase slightly with the increase of l_h. The results associated with the four methods are generally consistent with each other. For example, for a given $l_v = 2.0$ m, the values of P_f for the four methods are respectively 5.48×10^{-2}, 5.65×10^{-2}, 5.65×10^{-2} and 5.43×10^{-2} when $l_h = 10$ m, which are increased to 8.79×10^{-2}, 8.92×10^{-2}, 8.92×10^{-2} and 8.40×10^{-2} when $l_h = 40$ m, respectively. This thus validates the accuracy of the proposed framework for a wide range of l_h. Figure 3.8(b) compares the reliability results obtained by the aforementioned four methods for various values of l_v with l_h fixed at 20 m. Compared with Figure 3.8(a), the results shown in Figure 3.8(b) increase more significantly with the increase of the l_v. For example, for a given $l_h = 20$ m, the P_f estimated by the proposed framework increases from 7.80×10^{-3} to 9.88×10^{-2} as l_v changes from 0.5 m to 2.0 m. This mainly lies on the fact that it is more likely to form a continuous weak zone when the vertical spatial variability is underestimated (e.g., **Jiang et al. 2015**). Such finding is also consistent with many available studies in the literature (e.g., **Cho 2007; Jiang et al. 2015; Li et al. 2015a**). In addition, the difference among the four methods is minimal even at small l_v values where, for example, the estimated failure probability results at $l_v = 0.5$ m are 8.40×10^{-3}, 7.80×10^{-3}, 7.80×10^{-3} and 4.67×10^{-3}, respectively. Therefore, the results in Figure 3.8 indicate that the proposed framework is accurate enough for reliability analysis of the undrained cohesive slope considering different spatial variability of s_u.

3.5 Example II: Application to a c-φ slope

This section extends the proposed framework for a more complex slope with two types of shear strength parameters (i.e., c and φ), which remains unanswered and appears to be difficult by the method proposed by **Li et al. (2017)**.

3.5.1 Model preparation

Figure 3.3 shows the geometry of the second slope example, which has a slope height of 10 m and a slope angle of 45°. This is a hypothetical c-φ slope, which has been previously investigated by many researchers (e.g., **Cho 2010; Li et al. 2015a**). Following the literature, the shear strength parameters c and φ are modeled by cross-correlated lognormal random fields, while the unit weight of the soil is considered as a constant. The statistics of theses parameters are summarized in Table 3.3, which are directly taken from **Li et al. (2015a)** and **Cho (2010)** so that the results in these references can be easily utilized to demonstrate the proposed framework. Based on the mean values in Table 3.3, the RVM was firstly built based on Bishop's simplified method, which estimated the FS as 1.205. The FS value is very close to the values of 1.208 and 1.204 reported by **Li et al. (2015a)** and **Cho (2010)**, respectively, and its associated CSS, which was identified among 9,261 potential slip surfaces, is nearly the same with that found by **Li et al. (2015a)**, as shown in Figure 3.9.

The slope domain was then discretized into 1,210 random field elements to consider the spatial variability of the c and φ. The random field mesh is schematically shown in Figure 3.10, which consists mainly of 4-noded quadrilateral elements with a side length of 0.5 m. Random field simulation procedure described in Section 3.2.2 was subsequently invoked to generate the cross-correlated random fields of the c and φ, as schematically show in Figures 3.10(a) and (b). Based upon the random fields, RFM was established for this slope with the consideration of spatial soil variability. Again, similar to Example I, the RFM is mainly used for the generation of equivalent c and φ.

3.5.2 Determination of equivalent shear strengths

To determine the equivalent parameters, 361 data points (c, φ) are first generated from all possible combinations of $c = \{1, 2, \cdots, 19\}$ and $\varphi = \{12, 14, \cdots, 48\}$, which are then submitted to the RVM to obtain the corresponding FS values to form a training data set in the form of (c, φ, FS). Based on the data set, a quadratic regression analysis is performed to obtain the quadratic ERVM between the FS and c and φ, which is described as

$$FS(c, \varphi) = 8.28 \times 10^{-2} + 4.61 \times 10^{-2}c + 1.23 \times 10^{-2}\varphi - 7.9404 \times 10^{-4}c^2 + 2.4971 \times 10^{-4}\varphi^2 + 5.0388 \times 10^{-4}c\varphi \tag{3.7}$$

To valid the accuracy of the ERVM, Figure 3.11 compares the FS values predicted by Eq. (3.7) with those obtained from the RVM using Bishop's simplified method for 100 randomly generated sample points. As can be seen from the figure, the FS values from the two models are in good agreement with each other. This suggests that the ERVM can be effectively used to back calculate the equivalent strength values when an equivalent FS is given.

It is noted that there are two types of shear strengths in this slope example, so for a given FS value it is not a trivial task to back calculate both the two equivalent parameters simultaneously, which is also a challenge for the method proposed by **Li et al. (2017)**. Hence, the suggested technique in Section 3.2.3.1 is proposed mainly for this purpose. With the aid of this technique, two types of equivalent manners are derived: equivalent cohesion c_{eq} by reducing the friction angle (RFA) and equivalent friction angle φ_{eq} by reducing the cohesion (RC). Both of the two manners are examined in the following to check the effectiveness of the proposed framework. For the case listed in Table 3.3, internal sensitivity studies show that N_s=3,000 can yield relatively robust statistics for both the c_{eq} and φ_{eq}, with the standard errors of the estimated means and COVs of both the two equivalent parameters less than 3% of their true quantities (e.g., **Griffiths and Fenton 2001; Li et al. 2017**). Additionally, AIC and BIC criteria show that the c_{eq} and φ_{eq} can be best described by the truncated normal distribution and Weibull distribution, respectively. In the following, reliability analysis of this slope can be easily performed based on these statistics.

3.5.3 System reliability analysis results

Table 3.4 summarizes the reliability analysis results of the second slope example obtained from this study and reported by **Cho (2010)** and **Li et al. (2015a)**. As seen from the table, the system P_f (i.e., 1.36×10^{-2}) evaluated using the proposed framework with equivalent friction angle (i.e., "EQP+RC+MRSM+MCS" in the table) is comparable with the value of 1.60×10^{-2} that is directly estimated by MCS, and matches well with those (i.e., 1.71×10^{-2} and 1.87×10^{-2}) reported by **Cho (2010)** and **Li et al. (2015a)**, respectively. It should be noted that the value of 1.36×10^{-2} by the proposed "EQP+RC+MRSM+MCS" is very consistent with the value of 1.35×10^{-2} that is obtained by "EQP+RC+MCS". This can be expected from the evidence that MRSM is accurate enough for reliability analysis of slopes involving cross-correlated random variables, as demonstrated by **Li et al. (2016d)**. These results suggest that the proposed framework can provide sufficiently accurate estimations of the reliability results for slopes characterized by cross-correlated random fields. In addition, the P_f for this slope example was also evaluated using the proposed framework with equivalent cohesion (i.e., "EQP+RFA+MRSM+MCS" in the table), and the value was estimated as 1.18×10^{-2}, which is very consistent with that (i.e., 1.18×10^{-2}) obtained by "EQP+RFA+MCS", as expected. The result by "EQP+RFA+MRSM+MCS" appears to be underestimated compared with that (i.e., 1.60×10^{-2}) obtained by direct MCS, but the difference between them is minimal.

To gain more insights into the proposed variance reduction technique, the reliability of this slope example was also evaluated by the proposed framework that does not consider reduction on the parameter variance, that is, the reduction factor is taken as unity. To differentiate this framework from the original one, the parameter to be reduced is referred to as fixed variables at this situation. Likewise, there are four methods to be evolved: (1) "EQP+FC+MRSM+MCS"—MRSM based MCS with equivalent friction angle but fixed cohesion (FC); (2) "EQP+FFA+MRSM+MCS" —MRSM based MCS with equivalent cohesion but fixed friction angle (FFA); (3) Similarly, "EQP+FC+MCS"—MCS with equivalent friction angle but fixed cohesion; (4) "EQP+FFA+MCS" —MCS with equivalent cohesion but fixed friction angle. Table 3.4 also lists the P_f results associated with the abovementioned four approaches. It is found that, as expected, the MCS- and MRSM-based methods are in good agreements, which again validates the effectiveness of the use of MRSM in this study. It is also observed that the results by FC-based methods are much closer to the "accurate" result (i.e., 1.60×10^{-2}) than those by FFA-based methods. Compared with the original framework, the framework without reduction appears to overestimate the system failure probability, particularly the "EQP+FFA+MRSM+MCS" method. This may be mainly attributed to the fact that taking random field parameters as random variables yet neglecting the effect of variance reduction might substantially underestimate the spatial variability. In particular, the spatial variability of the friction angle plays a much more significant role in the slope stability than the spatial variability of the cohesion (e.g., **Li et al. 2015a**). Therefore, in the following analysis, only the "EQP+RC+MRSM+MCS" and "EQP+FC+MRSM+MCS" are considered to examine the effectiveness and accuracy of the proposed framework.

3.5.4 Influence of variation of cross-correlated random fields of c and φ on the accuracy of the proposed framework

This section further investigates the sensitivity of the accuracy of the proposed framework to the variation of the cross-correlated random fields of c and φ. For this purpose, a series of parametric studies of P_f with respect to such statistics as cross-correlation coefficient, COVs and ACDs are conducted with the $\rho_{c\varphi}$, COV_c, COV_φ, l_h and l_v varying between [-0.7, 0.5], [0.1, 0.7], [0.05, 0.2], [5, 30] and [0.5, 3], respectively. It should be noted that, for simplicity and consistent comparison with literature (e.g., **Li et al. 2015a**), in each parametric sensitivity study, only one parameter is changed whereas the others are kept the same as the values in the nominal case where $\rho_{c\varphi} = 0$, $COV_c = 0.3$, $COV_\varphi = 0.2$, $l_h = 20$ m and $l_v = 2$ m.

Figure 3.12 compares the values of P_f obtained by this study and reported in the literature for various cross-correlation coefficients. In general, the results obtained by MCS, "EQP+RC+MRSM+MCS" and "EQP+FC+MRSM+MCS" in this study present a very similar variation trend—increasing with the increase of $\rho_{c\varphi}$, which is the same as those reported by **Li et al. (2015a)** and **Cho (2010)**. The results obtained from the proposed "EQP+RC+MRSM+MCS" are also in good agreement with those evaluated by MCS and reported in the literature, suggesting the accuracy of the proposed framework. In contrast, the results evaluated by the proposed framework that has no consideration of variance reduction (i.e., "EQP+FC+MRSM+MCS") are slightly overestimated compared with the other four methods, although the difference between them decreases with the increase of $\rho_{c\varphi}$, is not significant and still in the same order of magnitude even at the smallest $\rho_{c\varphi}$. The overestimation of the "EQP+FC+MRSM+MCS" is expected from the fact that taking random field parameters as random variables yet neglecting the effect of variance reduction might substantially underestimate the spatial variability, thus leading to higher estimations of the P_f. These results indicate that the proposed framework can well account for the influence of the $\rho_{c\varphi}$ on the P_f.

Figures 3.13(a) and (b) show the variations of reliability results associated with different methods with respect to COV_c and COV_φ, respectively. In both the two subfigures, the results evaluated by the proposed framework agree well with those obtained from MCS and reported in the literature. In particular, it is observed that the proposed framework is still accurate enough at small probability levels (e.g., in the order of magnitude of 10^{-4}). For example, when $COV_\varphi = 0.05$, the P_f is estimated as 1×10^{-3} using the proposed framework (i.e., "EQP+RC+MRSM+MCS"), which is comparable with the "exact" value of 9.3×10^{-4} obtained by MCS in this study. However, as expected, the value of 3.3×10^{-3} obtained by "EQP+FC+MRSM+MCS" for $COV_\varphi = 0.05$ is admittedly overestimated. Additionally, it is noticed that the P_f is much more sensitive to COV_φ than to COV_c, which is captured by all the methods in the figure. These observations thus demonstrate the accuracy and robustness of the proposed framework versus the variations of c and φ.

Figures 3.14(a) and (b) show the variations of reliability results associated with different methods with respect to various horizontal and vertical ACDs, respectively. Similar to Figs. 12 and 13, the results evaluated by the proposed framework agree well with those obtained from MCS and reported in the literature for the considered ranges of l_h and l_v. This indicates that the proposed framework can provide accurate estimations of the P_f for slopes characterized by different spatially variable soil properties. Furthermore, it is also captured by the proposed framework that the vertical ACD influences the P_f more significantly than the horizontal ACD, which is in good accordance with those in the literature (e.g., **Li et al. 2015a**). This thus verifies the robustness of the proposed framework versus the spatial soil variability.

3.6 Discussion

Through the applications of the proposed framework to the aforementioned slope examples, it is found that, in general, a few thousand (e.g., 3,000 to 4,000) times of evaluations of the RFM are sufficient to obtain reasonable reliability results for the considered ranges of different statistics such as COVs and ACDs in this study. Therefore, it can be admittedly concluded that the proposed framework is more efficient than direct MCS, especially for reliability problems with low probability levels (e.g., $P_f \leq 10^{-3}$). However, it might be argued that the equivalent process in this study is redundant and the proposed framework might be less efficient than the traditional MRSM, because the traditional MRSM has already been demonstrated to be a very efficient approach in the literature (e.g., **Li et al. 2015a; Li et al. 2016d**). To this end, this section further discusses the efficiency of the proposed method against the traditional MRSM.

Figure 3.15 compares the computational costs (measured by evaluation times of the RFM) required by the proposed framework and the MRSM for the aforementioned two slope examples. For simplicity purpose, only the variation of computational cost with respect to the vertical ACD is considered in the figure, because failure probability is more sensitive to the vertical ACD and can vary within a larger probability interval. According to Figure 3.15(a), for the considered vertical ACDs in Example I, the proposed framework requires to evaluate around 4,000 times of the RFM to estimate the P_f, which is larger than 1,821 required by MRSM (**Li et al. 2015a**). It seems that the MRSM is more efficient than the proposed framework. However, this would not always be the truth, as illustrated in Figure 3.15(b) where the proposed framework is shown to be more efficient. The reason lies in the fact that there are more random field elements (i.e., 1,210) as well as shear strengths in Example II, which consequently results in more unknown coefficients (i.e., 4,841) to be calibrated in the MRSM.

To gain more insight into the proposed framework, Figure 3.16 qualitatively investigates the influence of the number of random field elements on the computational efficiency of the proposed framework and MRSM. As expected, the computational cost of MRSM increases sharply with the increase of the number of the random field elements, while the computational cost of the proposed method keeps nearly unchanged. In particular, for the illustrative Example I, the proposed framework, in turn, may outperform the MRSM in terms of the computational efficiency when the number of random field elements reaches a critical value. Overall, both the proposed framework and the MRSM are relatively efficient compared with direct MCS, and each of the two methods may have its own suitability. Nevertheless, the proposed framework provides a good alternative to efficient slope reliability analysis.

3.7 Summary and conclusions

This chapter presents a simplified framework for system reliability analysis of slopes in spatially variable soils. The basis and implementation procedure of the framework are thoroughly described. In particular, the ERVM is proposed to back calculate the equivalent spatially constant soil parameters such that the computational efficiency can be improved. Additionally, a variance reduction strategy is introduced to enable the proposed framework applicable to slope reliability problems involving more than one type of shear strength. Two slope examples are studied to illustrate the accuracy and efficiency of the proposed framework, based on which the robustness of the proposed framework against various statistics such as the anisotropic spatial variability is fully demonstrated through a series of parametric studies. Moreover, the strength and weakness of the proposed framework against MRSM is discussed. From this study, the following conclusions are made:

1. The proposed simplified framework can well deal with slope reliability analysis in spatially variable soils, providing sound results that are comparable with those by MCS and reported in the literature. It is robust against changes of various cross-correlations, COVs and ACDs, which provides a practical tool for system reliability analysis of slopes in spatially variable soils.

2. The high accuracy and robustness of the proposed framework demonstrates the effectiveness of the ERVM. This indicates the back-calculated equivalent spatially constant soil parameters can well represent the spatial variability of the original spatially variable soils. However, it is found that the distributions of the equivalent parameters may be different from the original ones. By using the ERVM, the computational efficiency of the proposed framework is substantially improved.

3. The variance reduction technique designed for slope reliability problems involving more than one type of shear strength is shown to be effective through the application of the proposed framework to a c-φ slope. Particularly, by using this

technique, the reliability results are further refined.

4. The proposed framework is much more efficient than direct MCS, especially for reliability problems with low probability levels (e.g., $P_f \leq 10^{-3}$). However, compared with MRSM, its relative efficiency is case dependent. For the slope where the number of random field elements is relatively large and more than one type of shear strength is dealt with, the proposed framework is much more efficient; otherwise, it is less efficient. Nevertheless, the proposed framework provides a good alternative for efficient slope reliability analysis.

Table 3.1 Reliability analysis results for $COV_{s_u} = 0.3$ in Example I

Method	P_f	Source
MCS (10,000)	7.73×10^{-2}	This study
EQP+MCS (10,000)	7.40×10^{-2}	This study
EQP+MRSM+MCS (10,000)	7.40×10^{-2}	This study
MCS (100,000)	7.60×10^{-2}	**Cho (2010)**
LHS (1,000)	8.30×10^{-2}	**Jiang et al. (2015)**
SRSM+RSSs+MCS (500,000)	7.90×10^{-2}	**Jiang et al. (2015)**

Table 3.2 Reliability analysis results for $COV_{s_u} = 0.15$ in Example I

Method	P_f	Source
LHS (40,000)	2.50×10^{-4}	This study
EQP+LHS (40,000)	1.25×10^{-4}	This study
EQP+MRSM+MCS (500,000)	1.40×10^{-4}	This study
LHS (40,000)	3.80×10^{-4}	**Jiang et al. (2015)**
SRSM+RSSs+MCS (500,000)	2.80×10^{-4}	**Jiang et al. (2015)**

Table 3.3 Statistics of soil parameters for Example II

Parameter	Mean	COV	Distribution	ACD	$\rho_{c\varphi}$
c	10 kPa	0.3	Lognormal	$l_h = 20$ m, $l_v = 2$ m	-0.5
φ	30°	0.2	Lognormal	$l_h = 20$ m, $l_v = 2$ m	
γ	20 kN/m³	–	–	–	–

Table 3.4 Reliability analysis results for Example II

Method	P_f	Source
MCS (10,000)	1.60×10^{-2}	This study
MCS (50,000)	1.71×10^{-2}	**Cho (2010)**
MRSM	1.87×10^{-2}	**Li et al. (2015a)**
EQP+RC+MCS (10,000)	1.35×10^{-2}	This study
EQP+RC+MRSM+MCS (10,000)	1.36×10^{-2}	This study
EQP+RFA+MCS (10,000)	1.18×10^{-2}	This study
EQP+RFA+MRSM+MCS (10,000)	1.18×10^{-2}	This study
EQP+FC+MCS (10,000)	2.52×10^{-2}	This study
EQP+FC+MRSM+MCS (10,000)	2.61×10^{-2}	This study
EQP+FFA+MCS (10,000)	5.10×10^{-2}	This study
EQP+FFA+MRSM+MCS (10,000)	5.16×10^{-2}	This study

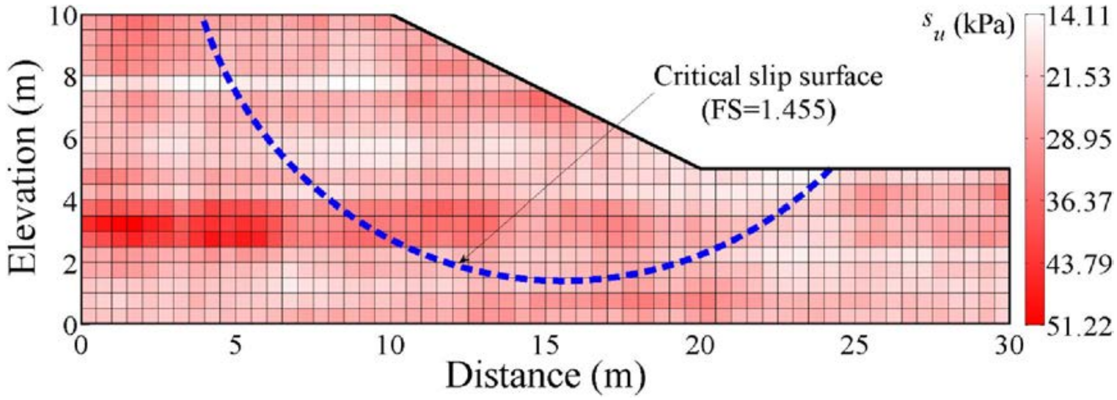

(a) RFM (COV=0.3, l_h=20 m and l_v=2 m)

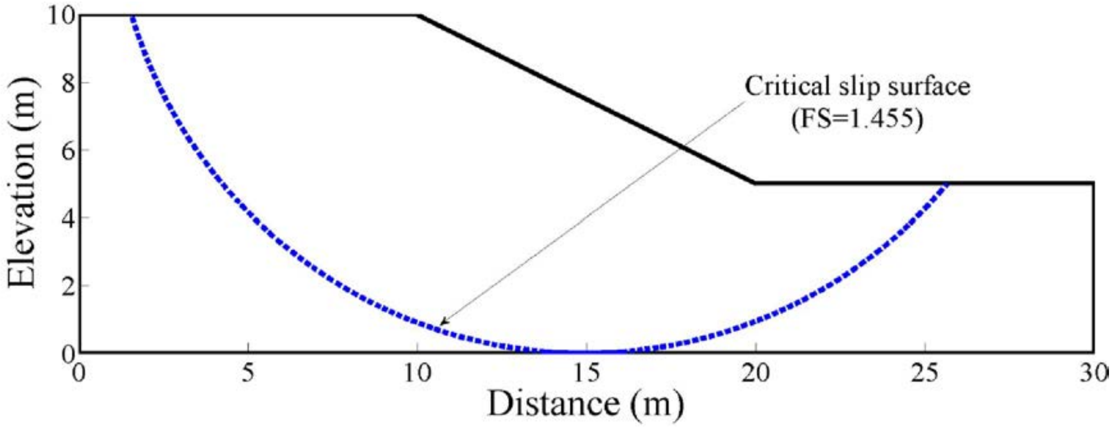

(b) RVM (s_u=24.7 kPa)

Figure 3.1 Schematics of the equivalence between the RVM and RFM

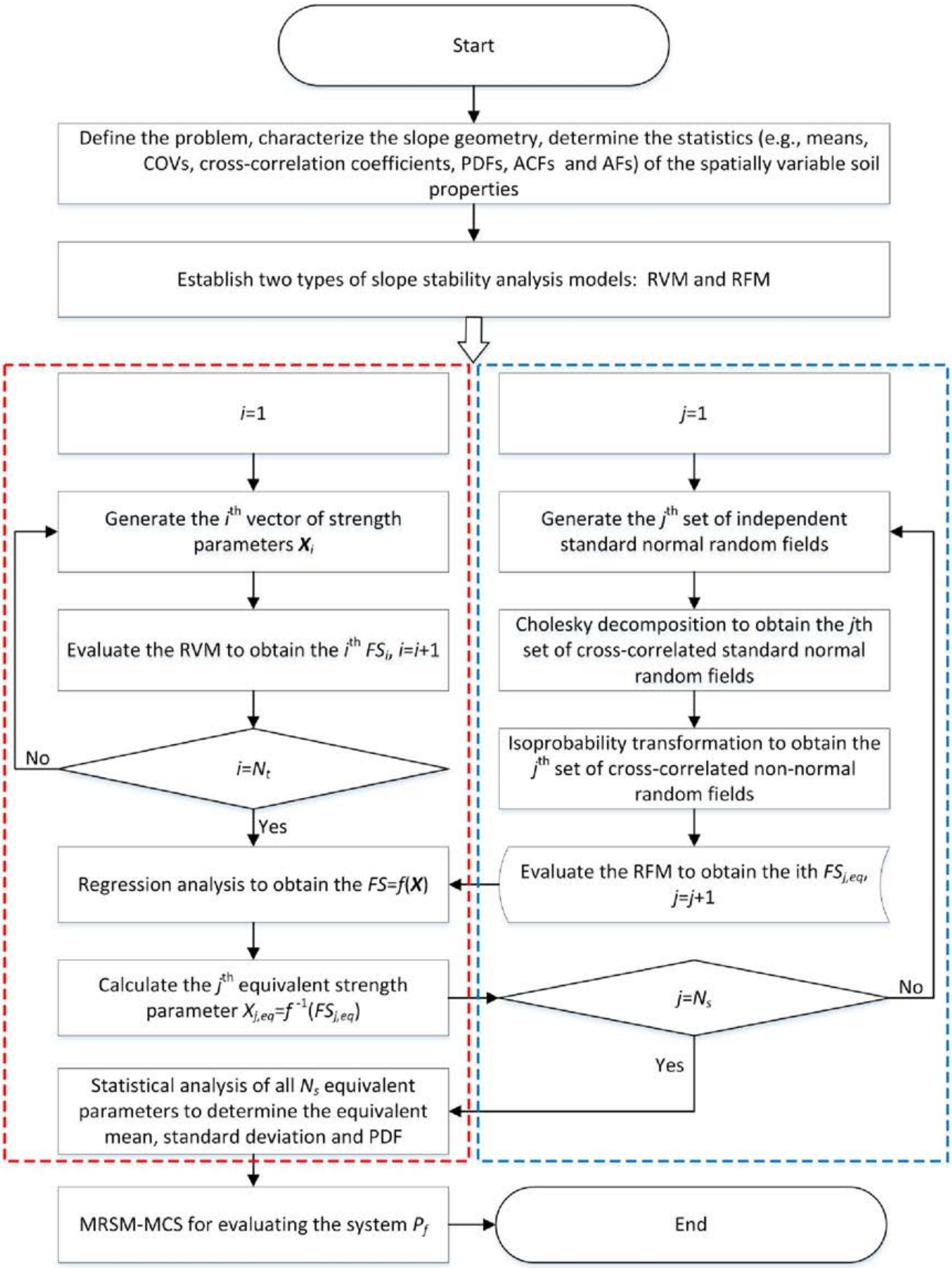

Figure 3.2 Flowchart of the proposed simplified reliability analysis framework

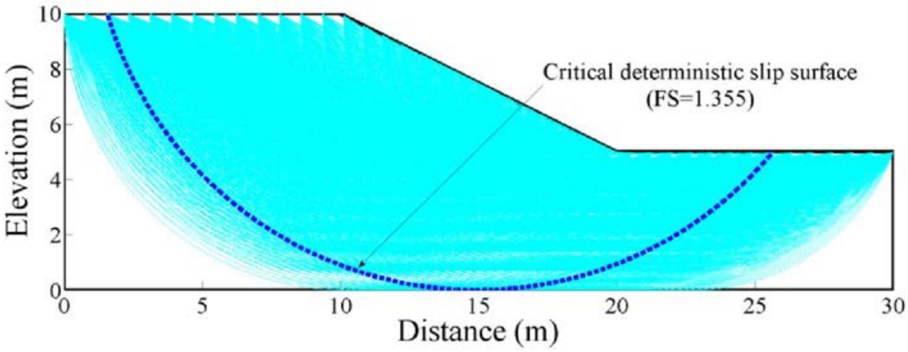

Figure 3.3 Geometry of the undrained cohesive slope with 4,851 potential slip surfaces

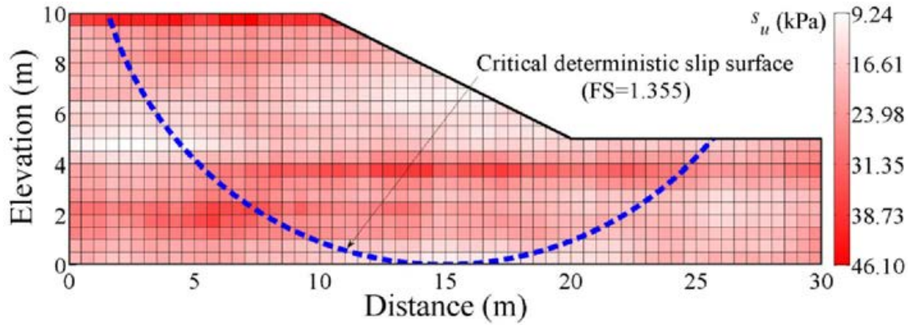

Figure 3.4 Random field elements mesh of the undrained cohesive slope with a typical realization of the random field of s_u ($COV_{s_u} = 0.3$, l_h=20 m, l_v=2 m)

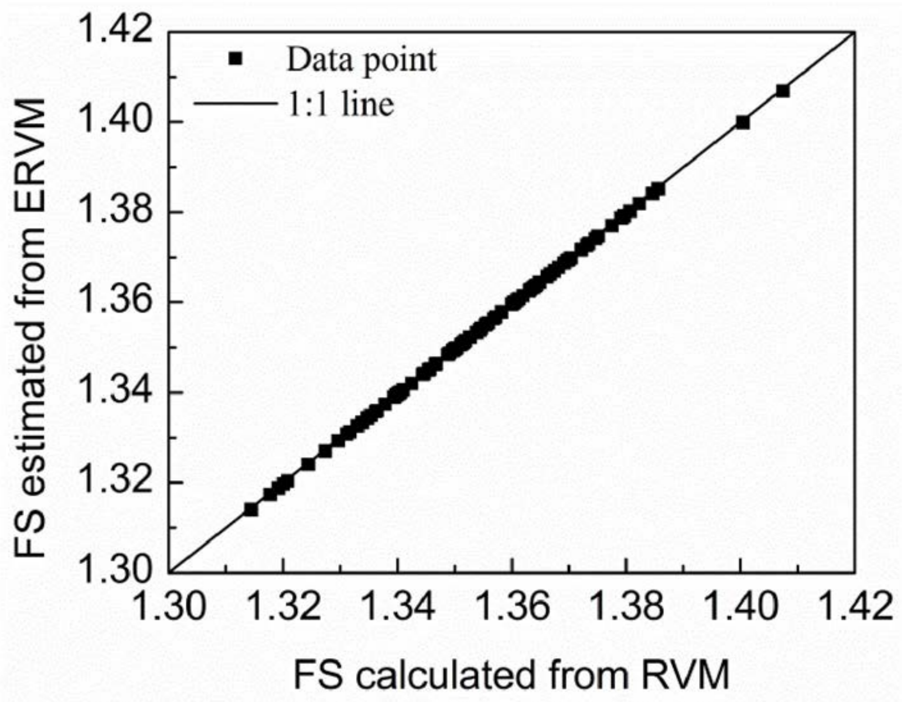

Figure 3.5 Validation of the ERVM for Example I (R^2=1)

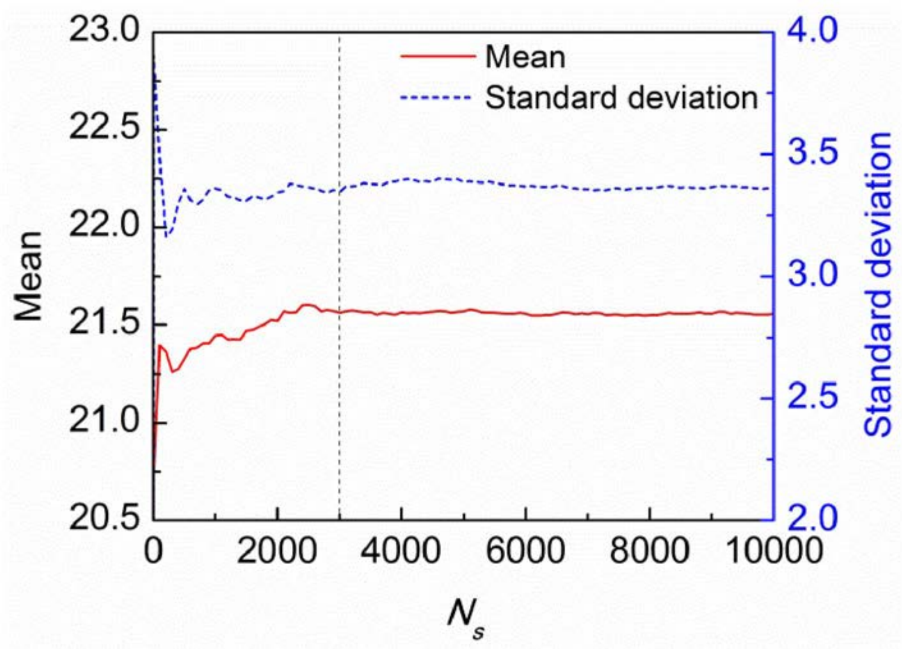

(a) $COV_{s_u} = 0.3$

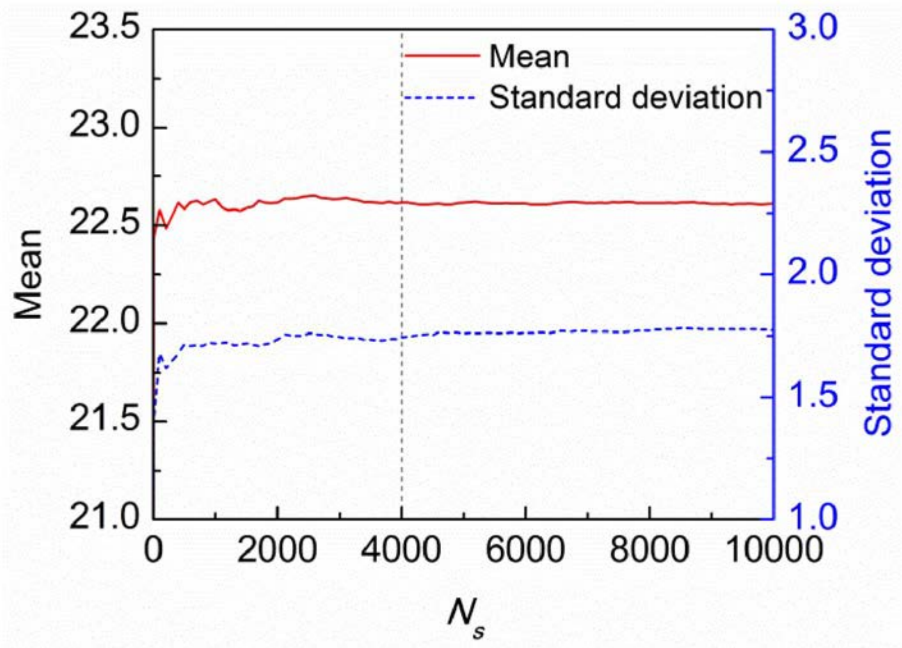

(b) $COV_{s_u} = 0.15$

Figure 3.6 Variations of the mean and standard deviation of the $s_{u_{eq}}$ with N_s

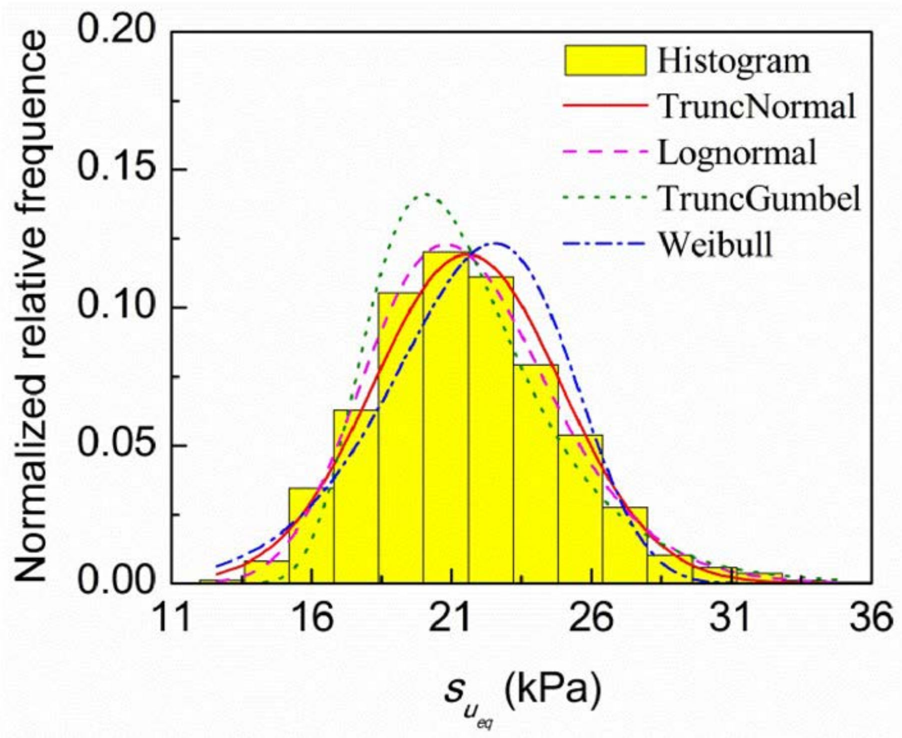

(a) COV=0.3

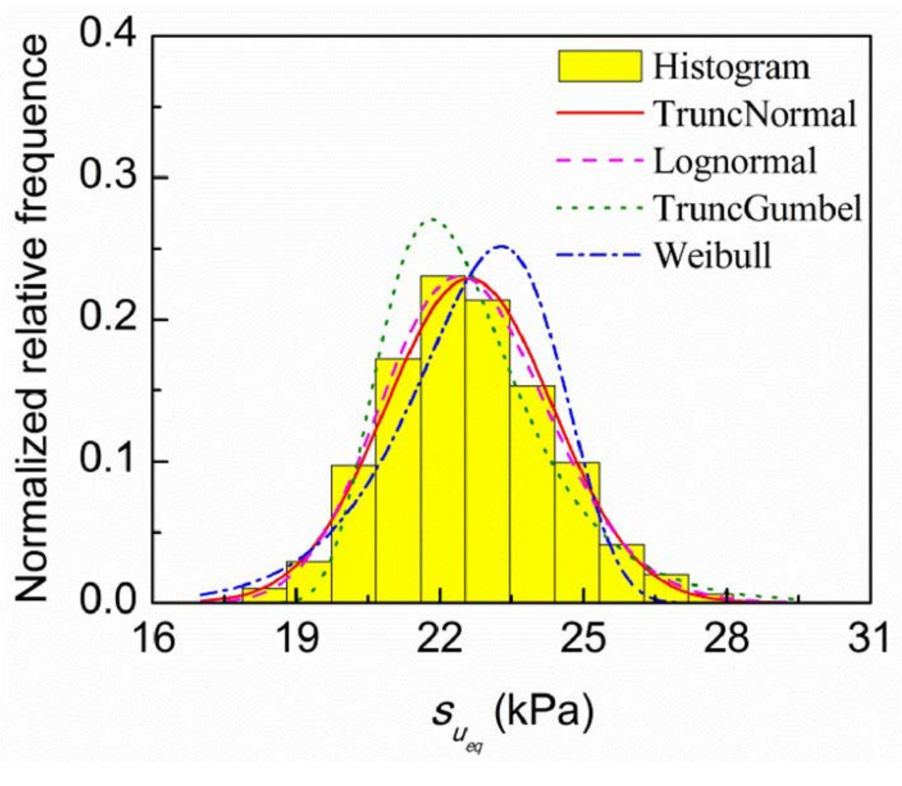

(b) COV=0.15

Figure 3.7 Histograms and fitted PDFs of the $s_{u_{eq}}$

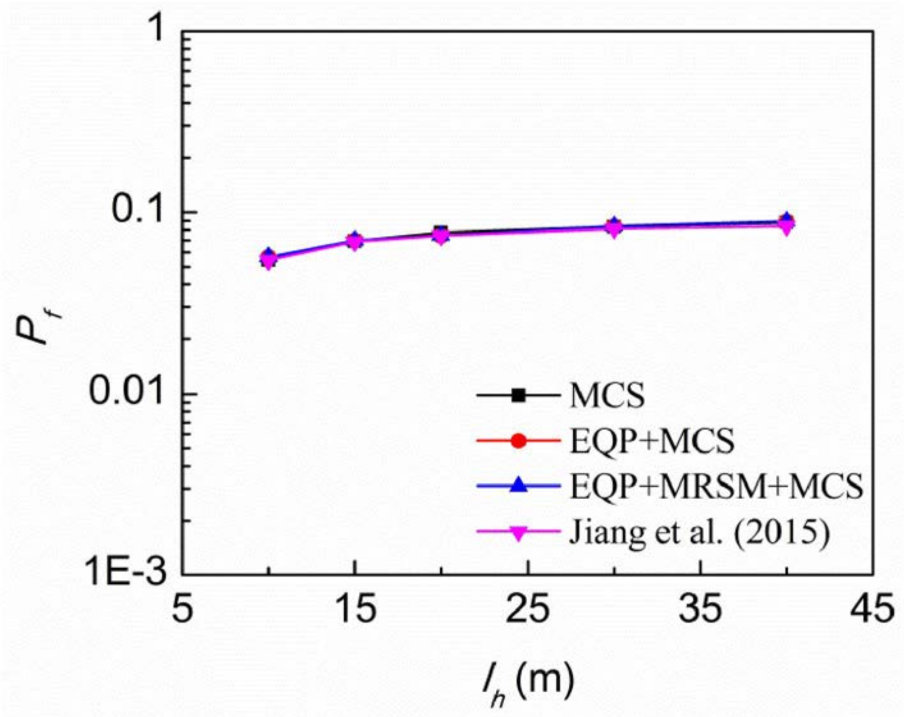

(a) Horizontal ACD

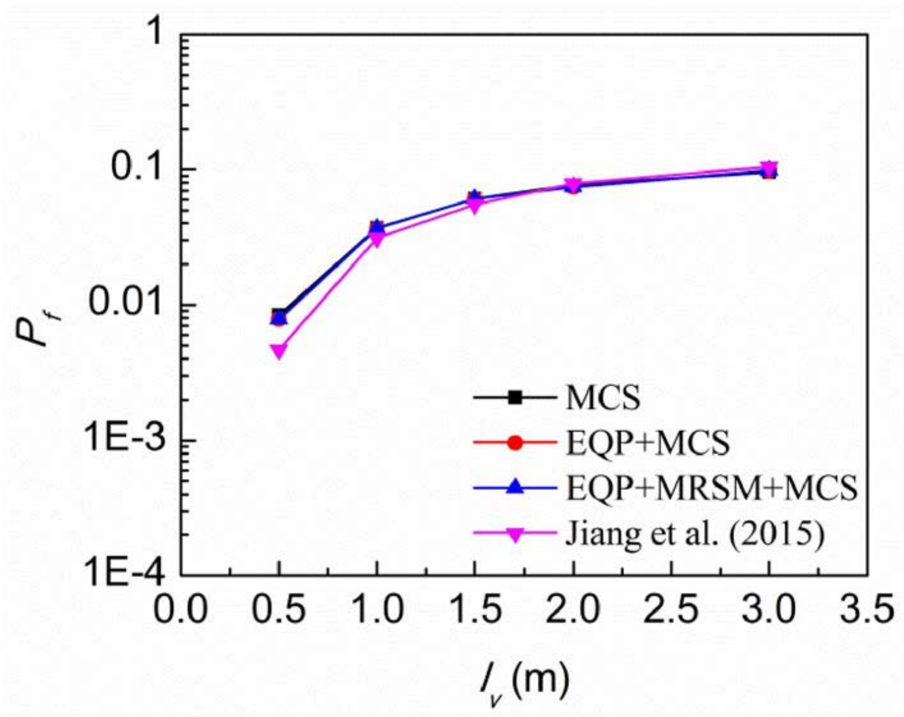

(b) Vertical ACD

Figure 3.8 Variation of the P_f with respect to spatial variability

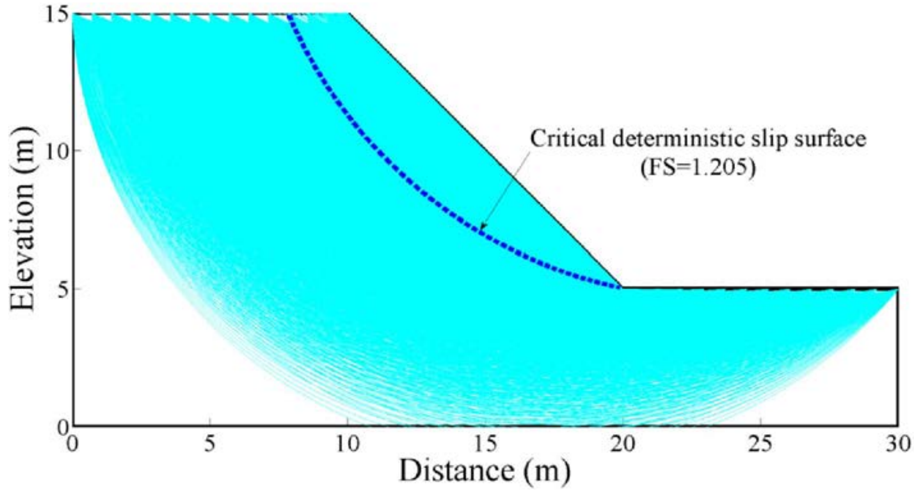

Figure 3.9 Geometry of the *c*-*φ* slope with 9,261 potential slip surfaces

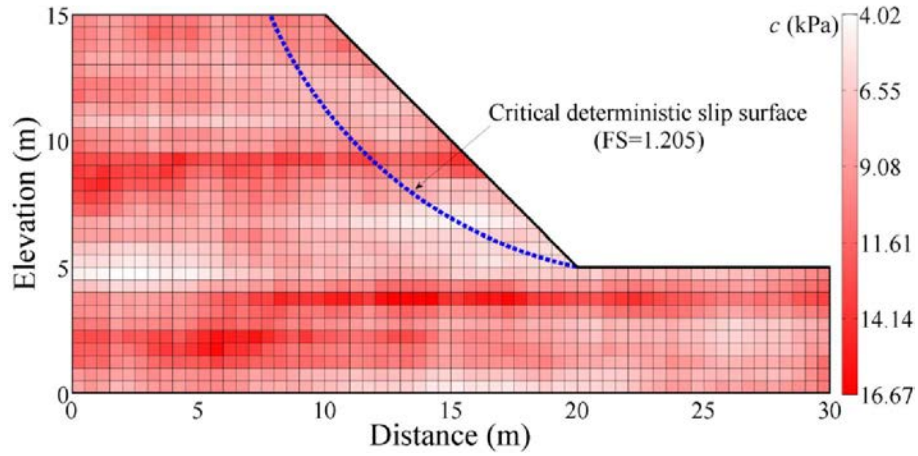

(a) Cohesion

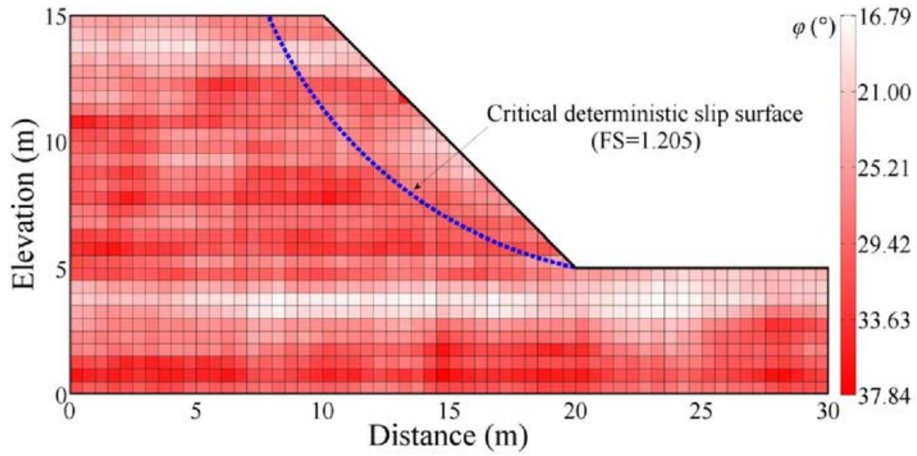

(b) Friction angle

Figure 3.10 Random field elements mesh of the *c*-*φ* slope with typical realizations of the random fields underlying the *c* and *φ*

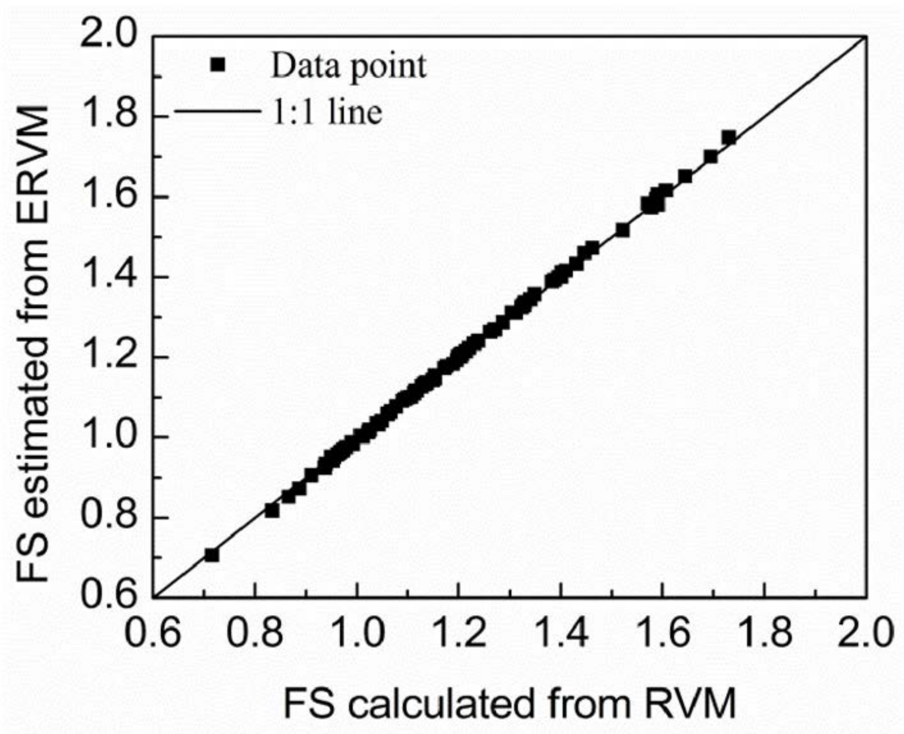

Figure 3.11 Validation of the ERVM for Example II (R^2=0.9996)

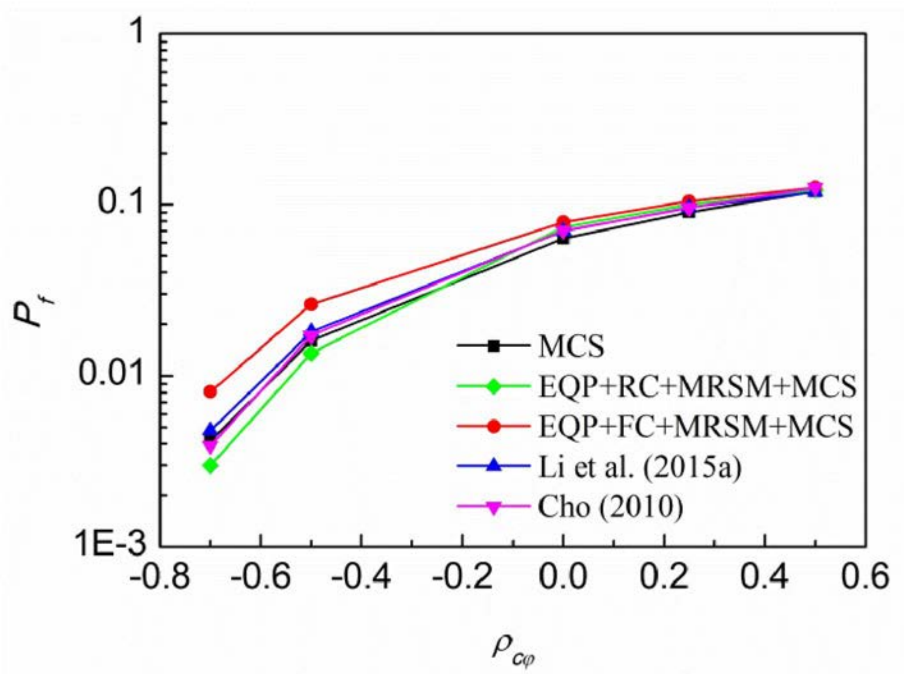

Figure 3.12 Variation of the P_f with respect to $\rho_{c\varphi}$

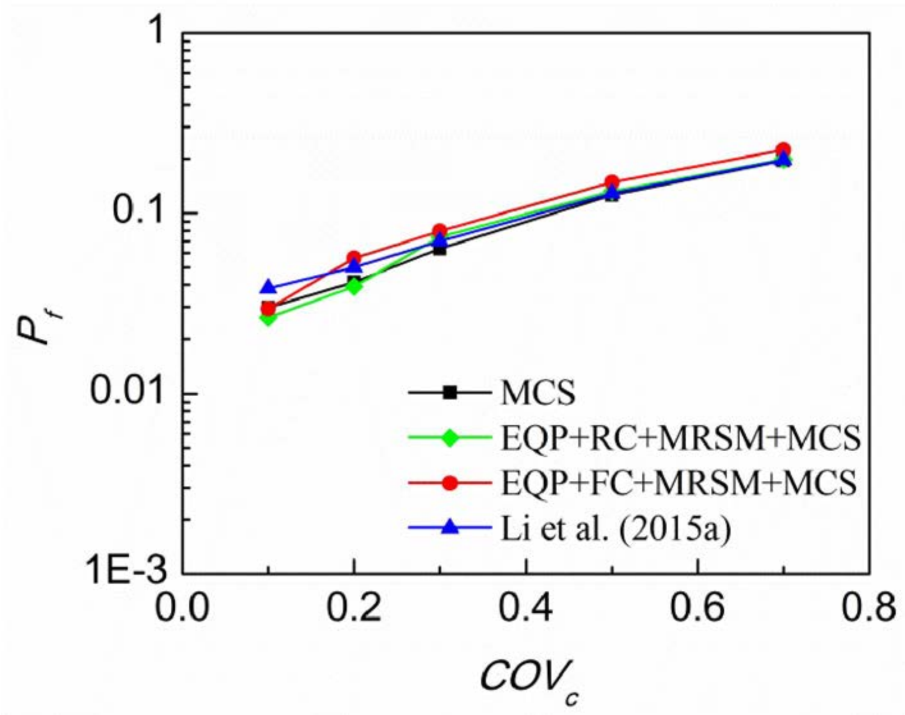

(a) Cohesion

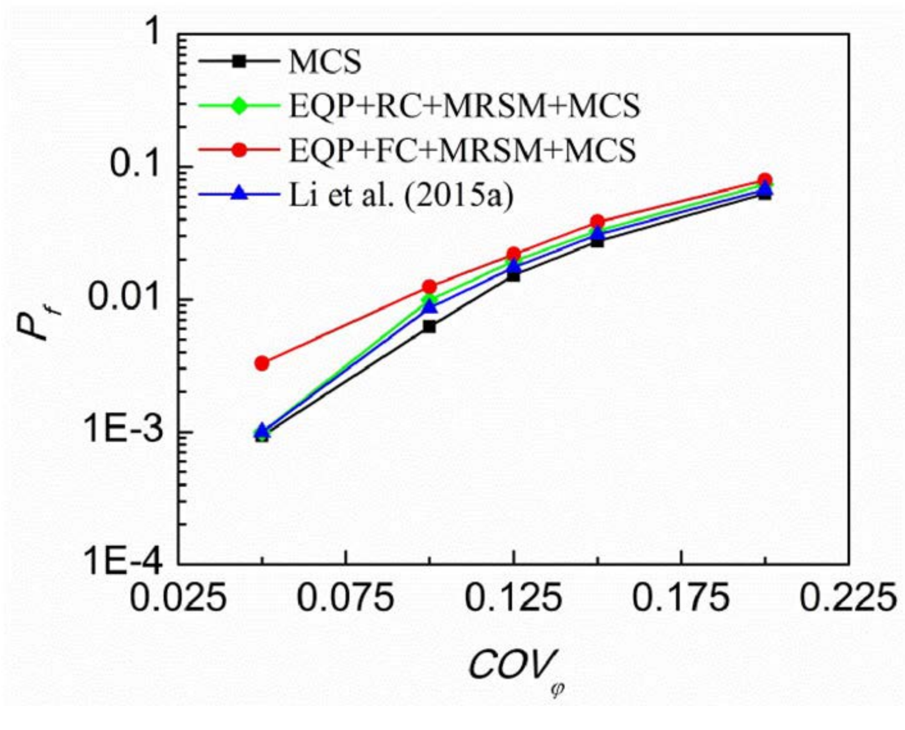

(b) Friction angle

Figure 3.13 Variation of the P_f with respect to COV_c and COV_φ

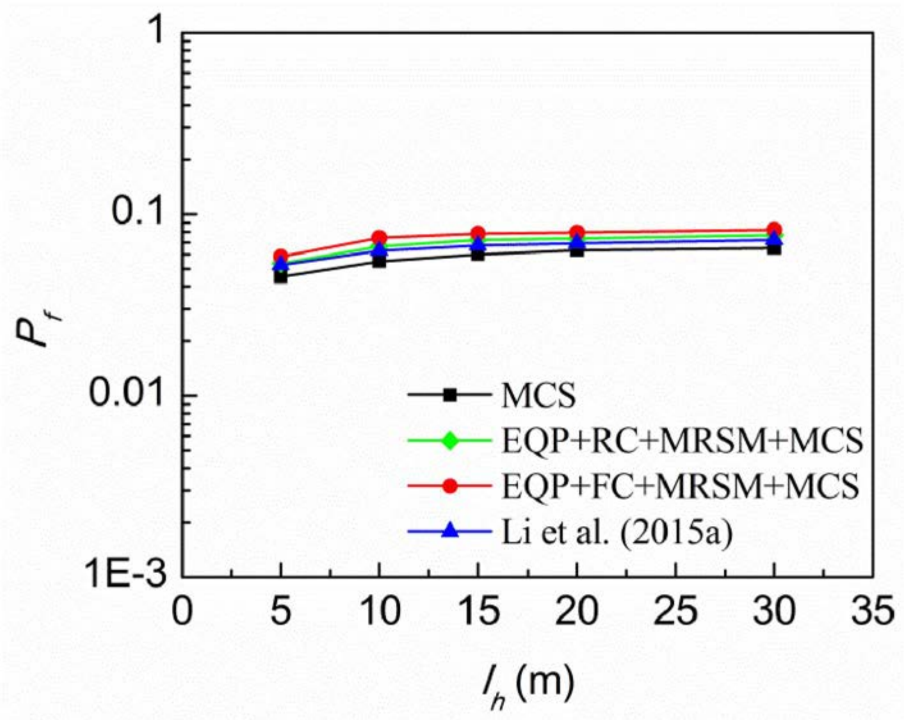

(a) Horizontal ACD

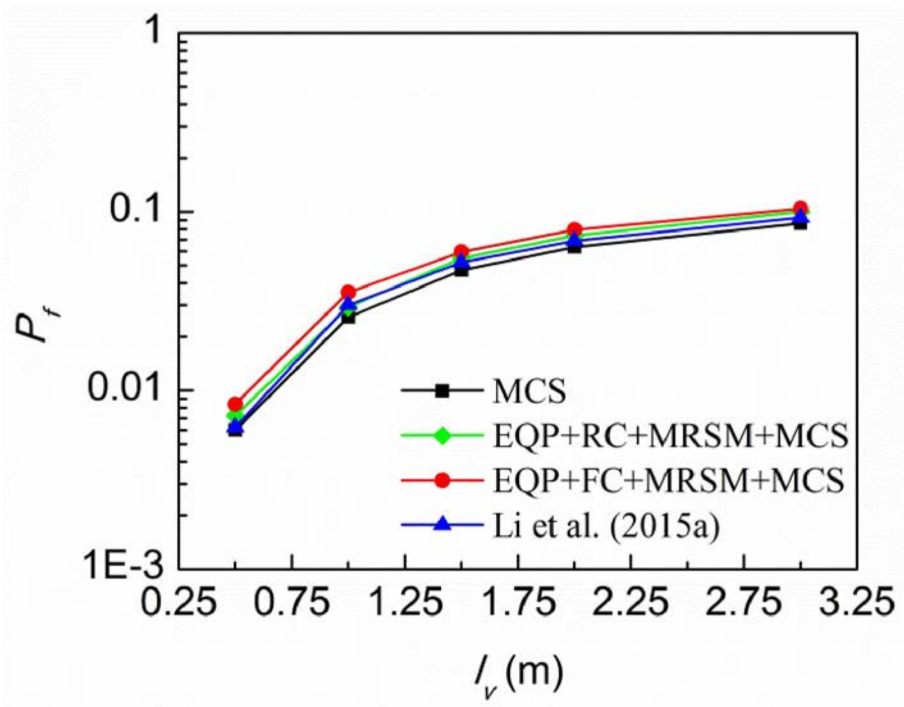

(b) Vertical ACD

Figure 3.14 Variation of the P_f with respect to ACDs

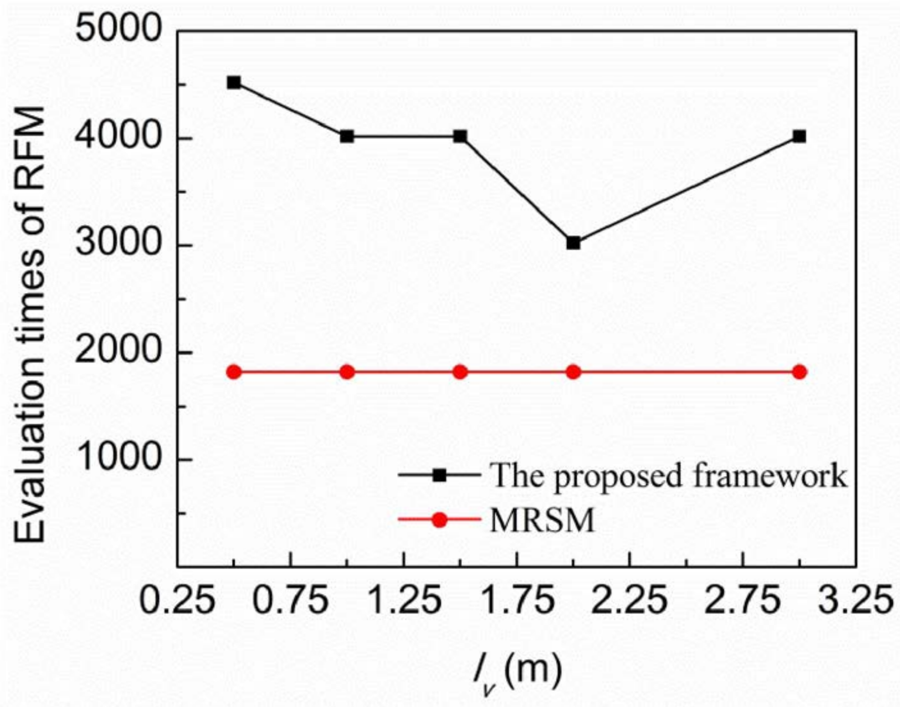

(a) Example I

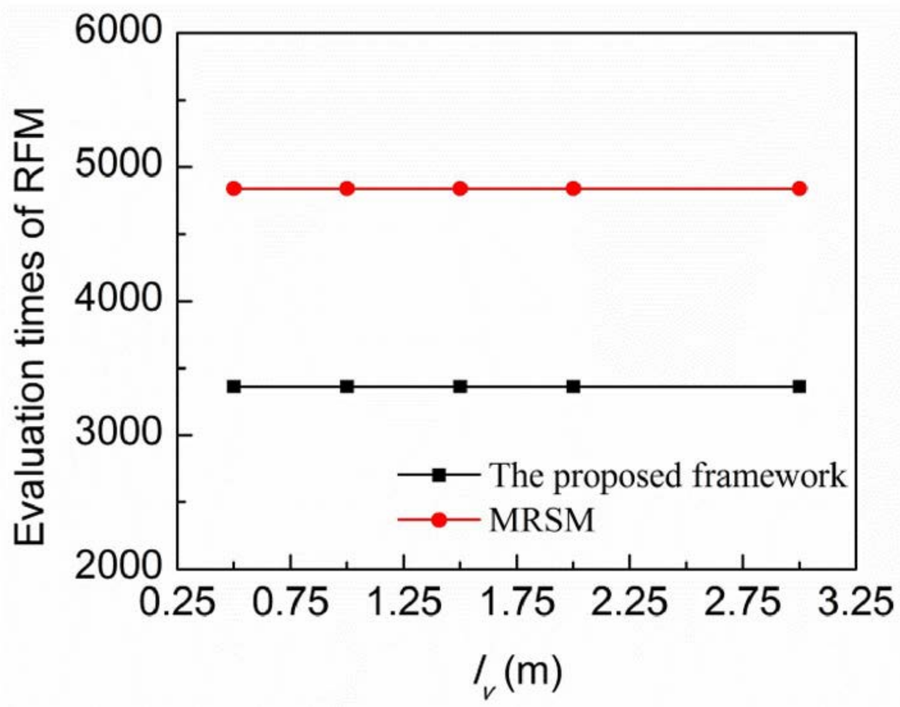

(b) Example II

Figure 3.15 Comparison of the computational efficiency between the proposed framework and MRSM

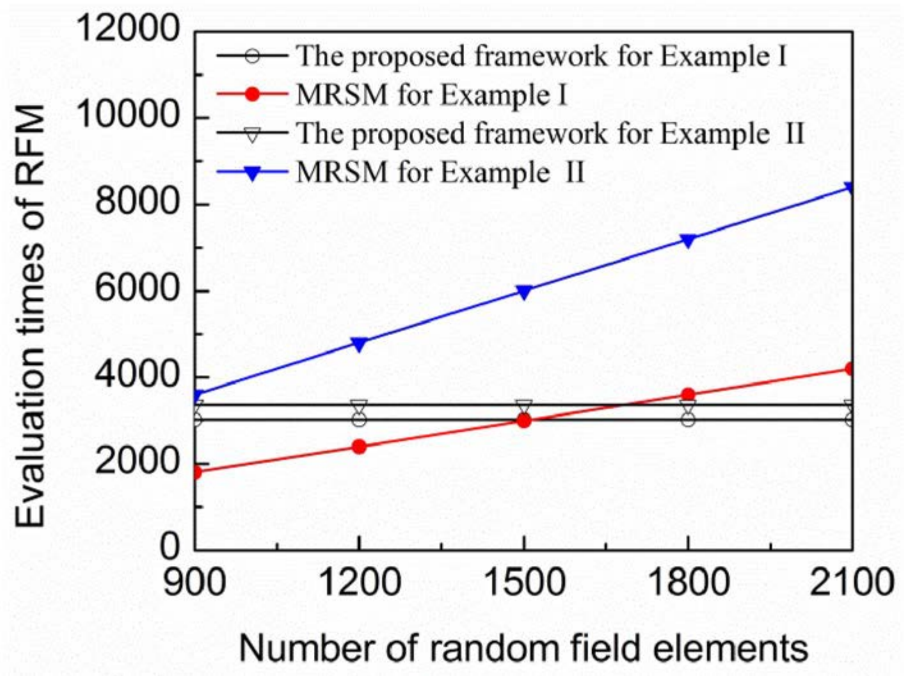

Figure 3.16 Influence of the number of random field elements on the computational efficiency of the proposed framework and MRSM

CHAPTER 4 CONDITIONAL RELIABILITY ANALYSIS OF A COHESION-FRICTIONAL SLOPE CONSIDERING SPATIAL SOIL VARIABILITY

4.1 Introduction

Slope stability is a serious geotechnical problem that is characterized by various uncertainties (e.g., **El-Ramly et al. 2002**). These uncertainties generally originate from the inherent soil spatial variation (e.g., **Vanmarcke 1977a; Vanmarcke 1977b**), the limited site investigation data, the assumptions and simplifications in the adopted stability model etc. (e.g., **Ang and Tang 2007**). Among these sources, the inherent spatial variability has been identified as the most dominating one in geotechnical engineering (e.g., **Christian et al. 1994; Phoon and Kulhawy 1999a; Lloret-Cabot et al. 2014**). Therefore, random field theory (e.g., **Vanmarcke 2010**) is often utilized to effectively characterize the soil spatial variability in a slope stability model. Based on this framework, slope reliability analysis is then performed using a probabilistic analysis approach.

Various reliability approaches that are able to consider the spatial variability of soil properties have been proposed in recent decades. Some of these approaches are briefly described as follows: **El-Ramly et al. (2002)** employed 1-D weak stationary random fields to consider the spatial variability of soil properties along a slip surface by the limit equilibrium method (LEM). **Griffiths and Fenton (2004)** investigated the effects of spatial variation of the undrained cohesion on the slope system reliability using a random finite element method (RFEM). **Cho (2007)** proposed a numerical procedure-based MCS for probabilistic slope stability analysis in spatially variable soils. **Wang et al. (2011)** implemented an enhanced MCS termed Subset simulation (SS) in a spreadsheet to perform slope reliability analysis with the ability to consider spatial variation of soil properties. **Ji et al. (2012)** proposed two 2-D random field discretization methods known as interpolated autocorrelations and auto-correlated slices for slope reliability analysis in the presence of spatially varying soil parameters. **Jiang et al. (2015)** adopted a multiple stochastic response surface method (SRSM) and MCS to efficiently evaluate the failure probability of a slope in spatially variable soils. Other methods are summarized in Table 4.1 in chronological order.

Based on Table 4.1, it is found that great achievements have been obtained in the area of slope reliability analysis for spatially variable soils. On the other hand, it is observed that most of the studies focus mainly on the unconditional random field simulation, which is realized using only the statistics (e.g., means, standard deviations and ACDs) of the limited site investigation data and discards the actual deterministic data. In general, site investigation data are available in an engineering project, although the volume of the data might not be too much. These data are the exact values of the soil properties at some particular positions, which are supposed to be independent of the simulation methods. The traditional unconditional random field discards such known data, which is actually site investigation labor lost. Additionally, neglecting the known data increases the simulation variance of the underlying random fields, which subsequently affects the responses, such as the factor of safety (FS) and the probability of failure, of the whole slope system. Hence, it is of practical significance to take the known data into account in slope reliability analysis, which can be considered as an effective tool for reducing the uncertainties in slope analysis.

In the literature, there are very few previous works on slope reliability analysis based on conditional random fields (e.g.,**Wu et al. 2009; Kim and Sitar 2013**), and these previous works suffer from many deficiencies, which should be addressed. For example, **Kim and Sitar (2013)** only investigated the effect of a specific number of cored samples on the probability of slope failure. However, the effect of the number of samples was not evaluated or quantified. Additionally, only one slip surface was considered in their work, which would obviously underestimate the failure probability of the slope because various works have demonstrated that the system effect of the slope reliability (e.g., **Oka and Wu 1990; Huang et al. 2010; Zhang et al. 2011b**) can be more controlling in many cases. As another example, **Wu et al. (2009)** studied the effect of conditional samples on the reliability of a homogeneous cohesive slope using RFEM. The isotropic 2-D random field was considered in their paper; however, the spatial variations in the soil properties in the horizontal and vertical directions are quite different in reality (e.g., **Phoon and Kulhawy 1999a; Li et al. 2015a**). Furthermore, the failure probability of the slope analysed in their paper is also very large. However, events with small failure probabilities in slope reliability analysis are of greater interest to researchers and engineers. Similar problems to those in the works by **Kim and Sitar (2013)** are also identified.

The present work is thus inspired by the limitations of the previous works. The objectives of this chapter are to (1) propose an effective method for simulating conditional random fields that account for the known data from cored samples, (2) efficiently evaluate the reliability of a slope based on the proposed method, (3) study the effects of different layouts of cored samples on the conditional random field simulation, and (4) investigate the effects of the statistics of soil properties on the conditional simulation results. To achieve these objectives, the remainder of this chapter is organized as follows. Sections 4.2 and 4.3 introduce the simulation of the unconditional and conditional random fields, respectively. Section 4.4 describes the probabilistic analysis approach adopted in this study. The implementation procedure for the proposed conditional probabilistic analysis of slope stability is then detailed in Section 4.5. The stability of a hypothetical cohesive-frictional slope is evaluated as an example to illustrate the proposed method in Section 4.6. The summary and conclusions of this study are given in Section 4.7.

4.2 Simulation of unconditional random field

The method suggested in Section 2.4.4 in Chapter 2 is used.

4.3 Simulation of conditional random field

A conditional random field is required when the soil properties at some locations are known. It is employed to ensure that the simulated random fields exactly match the soil properties at these particular locations. This indicates that, in each realization of a conditional random field, the soil properties at these particular locations are constants, and the soil properties at the other locations are random variables. To achieve this, the ordinary Kriging method is employed because it provides the best estimates of soil properties at the unknown points while considering the spatial correlations and weights of the known data. This method is used in combination with the RFM (i.e., unconditional random fields) to conduct the conditional random field simulation (e.g., **Fenton 2007**). The simulation of a realization of the CRF is detailed below.

As stated in Section 4.2, the underlying random field is characterized by a total of n_e random variables at the corresponding centroids of the n_e random field elements. Hence, there are actually a total of n_e values at n_e points to be determined. Suppose that the soil properties at points $(x_1, y_1), (x_2, y_2), \cdots, (x_p, y_p)$ have been measured from practice. A 2-D conditional random field $\boldsymbol{X}^C(x, y)$ is generated to match the known data at the measured locations and to simulate the soil properties at the remaining unknown points $(x_{p+1}, y_{p+1}), (x_{p+2}, y_{p+2}), \cdots, (x_{n_e}, y_{n_e})$ with the following steps:

Step 1: Generate a Kriging random field $\boldsymbol{X}^K(x, y)$, in which the soil properties at the known points exactly match the measured data. The soil properties at the unknown points are calculated from the system equations of the Best Linear Unbiased Estimation, also known as the Kriging (e.g., **Henderson 1975; Fenton 2007**). In general, the ordinary Kriging method is sufficient to obtain reliable and accurate results and is utilized herein as

$$\begin{bmatrix} \boldsymbol{K} & \boldsymbol{I} \\ \boldsymbol{I}^T & 0 \end{bmatrix} \begin{bmatrix} \boldsymbol{\beta} \\ \lambda \end{bmatrix} = \begin{bmatrix} \boldsymbol{k} \\ 1 \end{bmatrix} \tag{4.1}$$

$$\boldsymbol{K} = \begin{bmatrix} K_{11} & K_{12} & \cdots & K_{1p} \\ K_{21} & K_{22} & \cdots & K_{2p} \\ \vdots & \vdots & \cdots & \vdots \\ K_{p1} & K_{p2} & \cdots & K_{pp} \end{bmatrix} \tag{4.2}$$

$$\boldsymbol{\beta} = \begin{bmatrix} \beta_1 & \beta_2 & \cdots & \beta_p \end{bmatrix}^T \tag{4.3}$$

$$\boldsymbol{k} = \begin{bmatrix} K_{i1} & K_{i2} & \cdots & K_{ip} \end{bmatrix}^T, (i \in [1, n_e] \text{ and } i \neq 1, 2, \cdots, p) \tag{4.4}$$

where $\boldsymbol{K}$ is the Kriging covariance matrix; $\boldsymbol{I}$ is a column vector of all ones with a length of p; $\boldsymbol{\beta}$ is the vector of weights of the known data with $\sum_{i=1}^{p} \beta_i = 1$; $\boldsymbol{k}$ is the vector of covariance between the estimated point and the known points; and λ is a Lagrange multiplier. Note that K_{ij} is the covariance between any two points, which is characterized by the same autocorrelation function that is used to simulate an unconditional random field and is expressed as

$$K_{ij} = \sigma^2(x, y)\rho_{ij} \tag{4.5}$$

where $\sigma^2(x,y)$ is the variance of the simulated random field and ρ_{ij} is calculated by Eq. (2.13). The weight vector $\boldsymbol{\beta}$ is easily obtained by solving Eq. (4.1). The Kriging random field $\boldsymbol{X}^K(x,y)$ is then estimated as

$$\boldsymbol{X}^K(x, y) = \sum_{i=1}^{p} \beta_i X(x_i, y_i) \tag{4.6}$$

where we can deduce that the simulated random fields match well with the known data at the given p points. Note that Eq. (4.6) is suitable for both stationary and non-stationary random fields.

Step 2: Simulate an unconditional random field $\boldsymbol{X}^{UC}(x,y)$. Based on the statistics of the soil properties, such as means, standard deviations and ACDs, an unconditional random field is generated using the method that is described in the proceeding section.

Step 3: Extract the values at the known data locations from the generated unconditional random field $\boldsymbol{X}^{UC}(x,y)$ and take them as the simulated true data. Then, the Kriging method described in Step 1 is reused to generate another Kriging random field, which is referred to as the simulated Kriging random field $\boldsymbol{X}^{SK}(x,y)$.

Step 4: Superimpose the three constructed random fields to obtain the objective conditional random field $\boldsymbol{X}^{C}(x,y)$ as

$$\boldsymbol{X}^{C}(x,y) = \boldsymbol{X}^{K}(x,y) + [\boldsymbol{X}^{UC}(x,y) - \boldsymbol{X}^{SK}(x,y)] \tag{4.7}$$

Note that the conditional random field exactly matches the data at the known locations where $\boldsymbol{X}^{UC}(x,y) = \boldsymbol{X}^{SK}(x,y)$. At the unknown locations, the soil properties are represented by the Kriging random field with a stochastic deviation of $|\boldsymbol{X}^{UC}(x,y) - \boldsymbol{X}^{SK}(x,y)|$, which increases with the separation distance between the unknown and known points.

4.4 Probabilistic analysis of a slope based on SS

The probability of failure of a slope can be generally computed by MCS. However, MCS is very time-consuming for events with relatively small values of P_f. This shortcoming becomes more serious when the spatial variability of soil properties is concerned. As in such situations, more random variables are required, which subsequently significantly increases the time required to generate the random samples and evaluate the performance function. Hence, SS, which can be seen as an enhancement of MCS, is utilized to efficiently estimate the slope failure probability.

SS was originally proposed by **Au and Beck (2001)** for estimating the small failure probabilities in high-dimensional problems. In this approach, the small failure probability is expressed as a product of several larger conditional failure probabilities of some intermediate failure events. Thus, the simulation of a small failure probability event is converted into the simulations of a sequence of more frequently occurring intermediate failure events. For example, the failure probability of a slope is expressed as

$$P_f = P(FS < 1) = P(F_m) = P(F_1)\prod_{i=2}^{m} P(F_i \mid F_{i-1}) \tag{4.8}$$

where $P(\bullet)$ denotes the probability of an event; $F_i = \{FS < fs_i, i = 1, 2, \cdots, m\}$ denote a set of intermediate failure events that are defined by a decreasing sequence of threshold FS values $fs_1 > fs_2 > \cdots > fs_m$, respectively; $P(F_1) = P(FS < fs_1)$ and $P(F_i \mid F_{i-1}) = P(FS < fs_i \mid FS < fs_{i-1})$; and m denotes the number of levels of SS, which is identified as $fs_m \le 1$. As suggested by **Au and Beck (2001)**, the threshold values $fs_1, fs_2, \cdots, fs_m$ are automatically determined so that the probabilities of the intermediate events correspond to a specified value p_0. The process of SS is schematically shown in Figure 4.1 and detailed below (e.g., **Au and Beck 2001; Jiang and Huang 2016; Li et al. 2016c**).

As shown in Figure 4.1, SS begins by directly performing MCS with a small number (e.g., N_0) of samples. Each sample consists of the realization of a conditional random field that is generated according to the procedure in the proceeding section. The FS values of the N_0 samples are calculated by a deterministic slope stability method, such as FEM or LEM, and are then ranked in ascending order. The $(N_0 p_0 + 1)^{\text{th}}$ FS value is chosen as fs_1 so that the probability of the event F_1, i.e., $P(F_1) = P(FS < fs_1)$, is equal to p_0. Then, a modified Metropolis algorithm (e.g., **Au and Beck 2001**) is employed to perform a Markov Chain Monte Carlo simulation (MCMCS), during which $(1-p_0)N_0$ extra conditional samples are produced based on the $N_0 p_0$ sample seeds with $F_1 = \{FS < fs_1\}$. The FS values of the $(1-p_0)N_0$ MCMCS samples are also evaluated by the foregoing deterministic slope stability method. Therefore, a total of N_0 samples with $F_1 = \{FS < fs_1\}$ are obtained, of which the N_0 FS values are ranked again in ascending order. The $(N_0 p_0 + 1)^{\text{th}}$ FS value is chosen as fs_2, which defines the event $F_2 = \{FS < fs_2\}$. Note that the probability of event F_2, which is conditioned on event F_1, is also equal to p_0, i.e., $P(F_2 \mid F_1) = P(FS < fs_2 \mid FS < fs_1) = p_0$. Similarly, the above procedure is repeated *m*-2 times until the final event $F_m = \{FS < fs_m\}$ reaches the boundary of the failure space or the event is included in the failure space. Therefore, for a slope reliability analysis, the termination criterion of the SS is that the fs_m is less than or equal to the unity. Lastly, a total number of *m* levels of simulations, which consist of one level of crude MCS and *m*-1 levels of MCMCS, are conducted. This results in a total of N samples in an SS as

$$N = N_0 + (m-1)(1-p_0)N_0 \tag{4.9}$$

Based on the N samples and the procedure above, the P_f in Eq. (4.5) is further calculated as

$$P_f = p_0^{m-1} \frac{N_f}{N_0} \tag{4.10}$$

where N_f denotes the number of failure samples with $F = \{FS < 1\}$ in the final level of the SS. According to Eq. (4.8), the estimation error COV_{P_f} of P_f depends on the correlation among the estimators of $P(F_1)$ and $P(F_i \mid F_{i-1}), i = 2, 3, \cdots, m.$ Following **Au and Beck (2001)**, assuming that these estimators are uncorrelated, COV_{P_f} can be expressed as

$$COV_{P_f} = \sqrt{COV_{P(F_1)}^2 + \sum_{i=2}^{m} COV_{P(F_i|F_{i-1})}^2} \tag{4.11}$$

where $COV_{P(F_1)} = \sqrt{\frac{1-P(F_1)}{N_0 P(F_1)}}$ and $COV_{P(F_i|F_{i-1})} = \sqrt{\frac{1-P(F_i|F_{i-1})}{N_0 P(F_i|F_{i-1})}(1+\gamma_i)}$ are the coefficients of variation (COVs) of $P(F_1)$ and $P(F_i \mid F_{i-1})$, respectively; γ_i is the correlation factor which can be estimated based on the conditional samples generated by MCMCS in the i^{th} Subset simulation level. Previous studies have shown that Eq. (4.11) can well approximate the COV_{P_f} in SS, although the estimators of $P(F_1)$ and $P(F_i \mid F_{i-1}), i = 2, 3, \cdots, m,$ are generally correlated (e.g., **Au and Beck 2001; Li et al. 2016c**). More details can be found in the works by **Au and Beck (2001)** and **Au and Wang (2014)** on the COV_{P_f} in SS.

4.5 Implementation procedure of conditional probabilistic analysis

Having introduced the methodologies for generating conditional random fields and performing probabilistic analysis of a slope, this section mainly focuses on the practical implementation of the conditional probabilistic analysis for a slope in spatially variable soils. Figure 4.2 schematically presents the major steps for using the proposed approach. In general, the whole procedure consists of three parts: SS for uncertainty propagation, the deterministic slope stability analysis for calculating the FS value of a slope, and the conditional random field simulation for considering the effects of the measured data. In this way, the probabilistic analysis of a slope can be considered as an extension of the conventional slope stability analysis. This allows the probabilistic analysis and the conventional stability analysis of a slope to be performed separately. Thus, the process facilitates the application of the conditional reliability analysis of slope stability in geotechnical practice.

To achieve this objective, SS and the conditional random field simulation are programmed as user functions in MATLAB in this study. The user functions can be conveniently used by geotechnical practitioners with little knowledge about reliability analysis. As such, engineers are required to concentrate merely on the construction of the conventional stability model using either their in-house codes or the available software. Then, once the user functions are called by a geotechnical engineer, the deterministic slope stability model would be invoked repeatedly to complete the whole conditional reliability analysis.

For illustration, a detailed description of the conditional probabilistic analysis of a slope is given as follows:

Step 1: Determine the probabilistic distributions and statistics (e.g., means, standard deviations, cross-correlations and ACDs) of soil properties, and characterize the geometry of the slope under study.

Step 2: Establish a deterministic slope stability model, such as an FEM or an LEM, with the mean values of the soil properties. Then, based on this model, discretize the domain of the random field and extract the centroid coordinates of each random field element.

Step 3: Collect the information of the measured data, including the specific values of soil properties and the corresponding data locations. Then, transform the collected data into standard Gaussian random samples.

Step 4: Generate N_0 mutually independent standard normal samples using direct MCS in the first level of SS. Note that each sample is an $n_e \times m$ matrix. Then, the N_0 samples are taken as inputs in Step 5 (i.e., the conditional random field simulation) to generate the cross-correlated conditional random fields.

Step 5: Use Eq. (2.15) to generate cross-correlated standard Gaussian random fields $\boldsymbol{X}^{UC}$; the preprocessed data are used to construct the Kriging random fields $\boldsymbol{X}^{K}$, and the simulated Kriging random fields $\boldsymbol{X}^{SK}$ are generated according to Step 3 in the section of "Simulation of conditional random fields". Eq. (4.7) is then utilized to generate cross-correlated standard Gaussian conditional random fields which are then transformed into cross-correlated non-Gaussian conditional random fields in the sample space using Eq. (2.14).

Step 6: Substitute the generated conditional random fields into the deterministic slope stability model to obtain the corresponding FS values. Then, rank the N_0 values in ascending order, and take the samples corresponding to the first $N_0 p_0$ FS values as the "seeds" for MCMCS in the next simulation level.

Step 7: Check if the $(N_0 p_0 + 1)^{\text{th}}$ FS value is greater than the unity. If yes, go to the next level of SS to generate another set of $N_0(1-p_0)$ conditional samples using MCMCS based on the selected "seeds" in Step 6, and then back to Step 5 and continue; otherwise, go to Step 8.

Step 8: Calculate the P_f of the slope under study using Eq. (4.10).

4.6 Illustrative example

4.6.1 Basic model

For illustration, this section applies the proposed SS-based conditional probabilistic analysis approach to evaluate the probabilistic response of a hypothetical cohesion-frictional slope. The slope has also been successively studied by **Cho (2010)** and **Li et al. (2015a)** in the literature. As seen from Figure 4.3, the slope has a height of 10 m and a slope angle of 45°, and the slope consists of a single soil layer with a unit weight of 20 kN/m³. Following **Cho (2010)** and **Li et al. (2015a)**, the cohesion c and friction angle φ of this soil layer are modeled as cross-correlated lognormal random fields with a cross-correlation coefficient of $\rho_{c,\varphi}=-0.5$. The mean values of c and φ are 10 kPa and 30°, respectively, and their COVs are 0.3 and 0.2, respectively. Based on the mean values of c and φ, the deterministic slope stability model is preliminarily established using Bishop's simplified method (BSM), which provides a similar FS value (1.205) to the values (i.e., 1.204 and 1.208) calculated by **Cho (2010)** and **Li et al. (2015a)** with the same method, respectively. The corresponding CSS based on deterministic stability analysis is also shown in Figure 4.3.

To take the spatial variability of the soil properties into consideration, the random field domain in question is first discretized into 1,210 elements (i.e., n_e=1,210) with 1,281 nodes, as done in **Li et al. (2015a)** and schematically shown in Figure 4.3. The discretized random field elements mainly consist of 4-noded quadrilateral elements, which are degenerated into 3-noded triangular elements near the slope surface. Note that the influence of the size of the random field discretization is not considered in this study. More details on the selection of the random field element size are given elsewhere (e.g., **Ching and Phoon 2013**). Then, the single exponential autocorrelation function, i.e., Eq. (4.1), is selected to characterize the spatial correlation structure among a random field, in which the horizontal and vertical ACDs are chosen as l_h=20 m and l_v=2 m, respectively (e.g., **Cho 2010; Li et al. 2015a**). Note that, for simplicity, the values of l_h and l_v are assumed to be applicable to both random fields of c and φ. As a reference, these parameters are taken as the baseline case as well as the other statistics of soil properties mentioned in the last paragraph. For clarity, they are summarized in Table 4.2.

4.6.2 Reliability results based on unconditional random fields

Based on the basic model, simulations of unconditional random fields, which are realized by the CDT, are performed using the baseline parameters. Then, the P_f of the slope is evaluated as 2.04×10^{-2} using SS with N_0=500 and p_0=0.1. For the same slope,

Li et al. (2015a) and **Cho (2010)** estimated the failure probabilities as 1.87×10^{-2} and 1.71×10^{-2} by the multiple response surface method (MRSM) and MCS, respectively, which are very close to the result (i.e., 2.04×10^{-2}) in this study. Additionally, the probabilities of failure were also evaluated for two other different sets of ACDs. Table 4.3 lists the corresponding results and the statistics of the FS, including the results obtained by MRSM and MCS for comparison. As seen from this table, the reliability results obtained by different methods are similar to each other for these two cases, and the resulting statistics of the FS also seem to be consistent. Hence, this demonstrates the capacity of the proposed reliability approach for considering different spatial variations in soil properties.

Figure 4.4 compares the probability of slope failure obtained from this study with the results from **Li et al. (2015a)** and **Cho (2010)** when the cross-correlation coefficient varies from −0.7 to 0.5. In general, the cross-correlation coefficient significantly affects the probability of slope failure. The estimation of the failure probability in this study increases from 4.30×10^{-3} to 0.13 as the cross-correlation coefficient varies between −0.7 to 0.5. It is also noted that the reliability results from the three methods are consistent, which indicates that the method in this study can accurately estimate the failure probability at both high and relatively low levels. Overall, the results in Table 4.3 and Figure 4.4 have validated the feasibility and the correctness of the proposed reliability method, which enhances the confidence of extending the method to the conditional reliability analysis in the next section. Additionally, the method only requires 1,500 evaluations of the deterministic stability analysis to obtain a reasonable estimation of the failure probability of $\rho_{c,\varphi}=-0.7$ compared with more than 10,000 runs by MCS. This indicates the high efficiency of the SS for reliability analysis.

4.6.3 Reliability results based on conditional random fields

4.6.3.1 Construction of conditional random fields using virtual samples

As mentioned before, a conditional random field simulation requires known data of soil properties at some particular locations. However, there are no real cored samples available because the slope in question is hypothetical. Therefore, virtual samples are used as replacements to simulate the real cases. To reflect the general situation of site investigations, five virtual samples located under the slope crest, the slope surface and the slope toe are designed in this study. Figure 4.5 shows the layout of the five virtual samples, which are marked consecutively as A, B, C, D and E. The horizontal and vertical intervals between the samples are 5 m and 3 m, respectively. Such a design is reasonable because this is a homogeneous soil layer with large ACDs and the horizontal and vertical sample intervals also meet the site investigation requirements of the Chinese Design code.

Shear strength values are assigned to each of the samples, and without loss of generality, these values are randomly determined based on the statistical properties of the underlying soil properties. For instance, for the baseline case (i.e., Table 4.2), the shear strength values of the virtual samples are identified from one random realization of the corresponding random fields that are generated using the given statistics of this case. This realization of the random fields, for a specific case (e.g., the baseline case), is referred to as the reference "real" distributions of sample values for this case. This indicates that different statistics of soil properties would yield different reference "real" random fields, thus resulting in different sets of known data. Based on this principle, various parametric sensitivity studies are conducted in the next section to investigate the effects of $\rho_{c,\varphi}$, COV_c, COV_φ, l_h and l_v on the probabilistic responses of the slope under the framework of conditional random fields. The ranges of variation of these parameters follow **Li et al. (2015a)** and **Cho (2010)**. The resulting known data of the five virtual samples are summarized in Table 4.4 for various cases. Note that, in this table, only one parameter is changed in each case, and the other parameters remain the same as in the baseline case. With these available data, CRFs can be readily modelled using the method suggested in this study.

4.6.3.2 Effects of conditional random fields on the FS

This section investigates the effect of conditional random fields on the FS of the slope for various cases listed in Table 4.4. For each case, N_{sim} conditional random fields are simulated and evaluated by BSM to obtain the corresponding FS values. Then, the statistics of the N_{sim} FS values can be estimated. To effectively estimate these statistics, a suitable value of N_{sim} is essential and is determined by a sensitivity analysis, which demonstrates that the statistics of the FS present minor differences when N_{sim} is chosen as 500 and 10,000. Hence, N_{sim} is selected as 500 for this purpose. Moreover, it has been noted that the construction of conditional random fields depends on the layout and amount of known data. Hence, in this study, the number (N_d) of known data points in each case is intentionally set to 2, 3 and 5 to investigate its effect on the FS. Specifically, the soil properties of samples A and E are used as known data when N_d=2; the soil properties of samples A, C and E are used as known data when N_d=3, and all five virtual samples are termed as known data when N_d=5. For comparison, the results obtained by the unconditional random field simulation are also provided herein and are denoted by N_d=0.

Figure 4.6 shows the standard deviation of the FS as a function of the cross-correlation coefficient under unconditional and conditional random fields. For all cases, the standard deviation increases with the $\rho_{c,\varphi}$. It is also observed that the variability of the FS decreases when conditional random fields based on 3 and 5 known data points are considered. This observation indicates that the simulation variance of the conditional random fields can be efficiently reduced by the known data. In addition, the results from N_d=3 and N_d=5 suggest that more known data results in the spatial variation of soil properties being better represented. However, the FS results with N_d=2 present a larger variation than do the results from the unconditional random field simulation (i.e., N_d=0). This is because in this case the sample distance is significantly larger than the ACD in the vertical direction (12 m vs. 2 m), which means only one effective known data point is used to interpolate other points in the range of the ACD in the Kriging method. In other words, it indicates that the additional known data provide little or even no extra information for the middle 8 m range, which brings lots of uncertainty and increases the Kriging predictive variance, thus increasing the simulation variance of conditional random fields.

To further illustrate the abovementioned point, two additional cases with different ACDs are considered, as shown in Table 4.5. Both unconditional and conditional random field simulations are conducted for all the cases. Note that the conditional random field remains established based on N_d=2. Comparing cases 2 and 3 with case 1, it is found that the conditional random field effectively reduces the variance of the FS when the supposed vertical ACD is equal to or greater than the sample interval in the vertical direction. Hence, this indicates that the sample interval is critical to the establishment of the conditional random field when the ACDs are determined. This is also expected to contribute to the layout of the sample points in practice. To accurately reflect the spatial variation of soil properties, it is suggested from this study that the sample interval should be equal to or less than the ACD during the period of the site investigation. In addition, more effective and accurate conditional random fields can also be simulated using advanced approaches, such as Bayesian method (e.g., **Li et al. 2015d; Namikawa 2016**).

Figure 4.7 shows the variation of the standard deviation of the FS with respect to the COVs of the cohesion. As expected, the results obtained using both the unconditional random field simulation and the conditional random field simulation increase slightly with COV_c. Similar to Figure 4.6, the variance of the FS is reduced significantly when the conditional random fields based on three and five samples are considered. However, it overestimates the variation of the FS when N_d=2 because the two samples, which have a large vertical sample distance, are not sufficient to reflect the spatial variation of soil properties, as illustrated above and in Table 4.5.

Figure 4.8 shows the standard deviations of the FS obtained using unconditional and conditional random fields for various COVs of the friction angle. As seen from this figure, similar observations and conclusions to Figure 4.7 can be found. Comparing Figure 4.8 with Figure 4.7, it is also observed that the standard deviation of the FS is more sensitive to the friction angle than to the cohesion.

To investigate the effect of ACDs on the FS, Figure 4.9 shows the standard deviations of the FS obtained from unconditional and conditional random fields for various horizontal ACDs. Generally, the standard deviation of the FS in the unconditional random field simulation increases slightly with l_h, whereas the results from the conditional random field simulation present an inverse trend. This indicates that the conditional random field simulation is more efficient and necessary for a high value of l_h. It is also observed that the variances of the FS based on N_d=5 are smaller than those of the results obtained using the unconditional random field simulation for various values of l_h. For the case of N_d=3, the advantage of the conditional random field simulation is not evident for small values of l_h due to the poor estimation of the Kriging random field in this case. For example, when l_h=5 and N_d=3, the ratio of the sample distance in the horizontal direction (i.e., 10 m) and l_h is 2, as illustrated above and in Table 4.5, which means that only one known data point is used to interpolate the unknown points within the variance distance in the Kriging. Similarly, the conditional simulation based on N_d=2 also yields unsatisfactory results. It is also found that a smaller ratio produces a more efficient CRF simulation. This is because the effective number of samples increases with increasing l_h.

Figure 4.10 shows the standard deviation of the FS as a function of the various vertical ACDs. Similar to Figure 4.9, the results obtained by the conditional random field simulation based on N_d=3 and N_d=5 decrease with l_v, whereas the results obtained by the unconditional random field simulation increase with l_v. This would lead to a large difference between the unconditional and conditional random field simulations for large l_v, which demonstrates the superiority of the CRF simulation. As expected, the conditional random field simulation based on N_d=2 erroneously estimates the spatial variation of soil properties; in addition, note that the sample distance in the vertical direction is approximately 4-24 times l_v. Interestingly, at l_v=0.5, it seems that the unconditional random field simulation is more effective than the conditional random field simulation. This is due to the large ratios between the vertical sample distance and l_v with the values of 24, 12 and 6 for N_d=2, N_d=3 and N_d=5, respectively, which means that only a few known data points are involved in the Kriging estimation, as illustrated above and in Table 4.5. However, for large values of l_v, as can be expected, the conditional random field simulations based on N_d=3 and N_d=5 perform better than the unconditional random field simulation, which suggests the necessity of conditional random field simulations in such a case. In addition, it is observed that when the ratio between the sample distance in the vertical direction and l_v greater than 3, the results tend to be unreasonable, as seen from the cross-points in Figure 4.10. Finally, comparing Figure 4.10 with Figure 4.9, it is found that the results are more sensitive to l_v than to l_h.

4.6.3.3 Effects of conditional random fields on the spatial variation of the critical slip surface

In this section, both unconditional and conditional random fields are simulated 1,000 times for the case of $\rho_{c,\varphi}$=−0.5 to investigate the effects of the conditional samples (N_d=5) on the spatial variation of the critical slip surface. Within the framework of the LEM, a CSS can be located for each random field simulation. Therefore, there are theoretically 1,000 CSSs for each type of the field modelling. However, many of those CSSs would be the same surface, resulting in the number of CSSs being much less than 1,000. Figs. 11(a) and (b) schematically show the locations of the critical slip surfaces obtained from 1,000 unconditional and conditional random field simulations, respectively. Based on the unconditional random field simulation, 126 critical slip surfaces are identified; most surfaces nearly pass through the slope toe, as shown in Figure 4.11(a). By contrast, only 84 critical slip surfaces are determined when conditional samples are considered in the random field simulation. Similar to Figure 4.11(a), most of the 84 slip surfaces also nearly pass through the slope toe. However, it is observed that the potential slip band under the conditional simulation is narrower than the slip band obtained by the unconditional simulation. This indicates the superiority of the conditional simulation in reducing the uncertainty of the spatial variation of the critical slip surface. Additionally, similar results are observed for other cases in the internal studies which are not presented herein.

4.6.3.4 Effects of conditional random fields on the probability of failure

The probability of failure of a slope is the likelihood of a failure event that has an FS value not greater than the unity, which depends highly on the distribution of the FS. Hence, this section performs a series of parametric studies to investigate the effects of conditional random fields on the probability of failure of the slope. For computational efficiency and because the conditional random fields cannot be accurately simulated when N_d is small, only the results based on N_d=5 are calculated and presented herein. The failure probabilities that are obtained by the unconditional random field simulation are also provided for comparisons.

Figure 4.12 compares the results obtained by the unconditional and conditional random field simulations for various cross-correlation coefficients. It is observed that both results increase with the cross-correlation coefficients. This observation is expected because the variance of the FS is proportional to the cross-correlation coefficient, as shown in Figure 4.6. Moreover, the results based on conditional random field simulations decrease by several orders of magnitude when compared with the results from unconditional random field simulations. For example, the probabilities of failure obtained by the unconditional and conditional random field simulations are 3.40×10^{-3} and 2.84×10^{-10}, respectively; a difference of approximately 7 orders of magnitude is identified. This indicates that the traditional unconditional random field simulation overestimates the probability of slope failure, whereas the conditional random field simulation can effectively reduce the uncertainties and provide more reasonable results. It is also worth noting that the difference between the results obtained by the unconditional and conditional simulations decreases with the cross-correlation coefficient but remains of a relative large order of magnitude (e.g., 2 at $\rho_{c,\varphi}$=0.5).

Figures 4.13(a) and (b) show the effects of the conditional samples on the probability of failure for various COVs of cohesion and frictional angle, respectively. Similar to Figure 4.12, the results obtained by the conditional random field simulation are significantly lower than the results of the unconditional random field simulation, with a difference changing from 2 to 7 orders of magnitude. Additionally, the differences in both of the figures decrease with the COVs; however, they remain very large, especially for the largest value of COV_{φ}, where a difference of approximately 4 orders of magnitude is observed.

Figure 4.14(a) and (b) show the results from two types of random field simulation for various ACDs in the horizontal and vertical direction, respectively. In general, the results obtained by the unconditional random field simulation increase with both horizontal and vertical ACDs and are more sensitive to the vertical ACD. This finding is also consistent with the results of **Li et al. (2015a)**. By contrast, as is expected from Figs. 9 and 10, the results from the CRF simulation decrease with both horizontal and vertical ACDs. This is because a larger value of the ACD means more known data being used in the construction of the conditional random field, thus reducing the simulation variance. As such, the resulting inverse variation trends lead to an increase in the difference between the unconditional and conditional random field simulations. This suggests the high necessity of the consideration of sample information for large ACDs.

4.7 Summary and Conclusions

In this chapter, the achievements of slope reliability analysis considering spatial variation of soil properties in the last 15 years are briefly summarized. The fundamental basis of both unconditional and conditional random field simulations are fully introduced. The underlying principles and implementation procedure of SS for evaluating the probability of slope failure are also described in detail. This chapter has proposed to combine SS with the Kriging method for assessing the reliability of a slope in spatially variable soils where some known data at particular locations are available. This proposal is novel to the best of our knowledge, and has been demonstrated to be effective and efficient. An example application is performed on a nominally "homogeneous" cohesion-frictional (c-φ) slope to illustrate the proposed approach. Based on this example application, a series of parametric studies are conducted to investigate the influence of the layout of the cored samples on the P_f, FS, and the spatial variability of the CSS. Such a type of systematic parametric study for conditional field simulation is rarely seen in the literature. Based on the present study, several conclusions can be made and are presented as follows:

1. The results of unconditional random field simulations indicate that the proposed method can accurately determine the probability of failure of a slope in spatially variable soils. Compared with direct MCS, this method is very efficient and is especially suitable for a slope with a relatively low failure probability. The unconditional random fields underlying the soil properties can be effectively simulated by the CDT which can be realized fairly easily.

2. The conditional random field can effectively reduce the simulation variance of the underlying random fields if the Kriging method can accurately reflect the spatial variation of the soil properties based on a specific amount of known data; otherwise, the established conditional random fields are of no practical significance. The realization of a CRF heavily relied on the ratio of the sample distance to the ACD. It is found in this study that the random fields can be accurately simulated when the ratios in the horizontal and vertical direction are less than or equal to 1 and 3, respectively. A smaller ratio of the sample distance to the ACD would provide a better simulation result.

3. The variation of the FS obtained by the conditional random field simulation increase with the cross-correlation coefficients, the COVs of the soil properties, and decrease with the ACDs. Of great importance is the fact that the variation of the FS obtained by the conditional random field simulation is smaller than that obtained by the unconditional random field simulation. Furthermore, the spatial variation of the critical slip surface region is also narrower when conditional random fields are considered.

4. The failure probabilities can be reduced significantly by the CRF simulation. In general, the probabilities of failure follow similar trends as the results obtained by the unconditional random field simulation with respect to the cross-correlation coefficients and the COVs of the soil properties. However, the probabilities of failure present inverse trends with respect to the ACDs, which indicate that the conditional random field simulation is of significant benefit at relatively large ACDs.

5. The effect of conditional random fields is investigated only for a hypothetical homogeneous cohesion-frictional slope in this study because the computational demand increases sharply when heterogeneous slopes are considered. Although SS can enhance the simulation efficiency to some extent, it still requires several thousands of evaluations of the deterministic stability model. In addition, the current conditional information focuses only on a specific number of samples and does not consider practical borehole layouts. Hence, further research is required to study the influence of borehole locations on the practical slope reliability, therein employing more advanced probabilistic approaches.

Table 4.1 Summary of slope reliability analysis considering spatially varied soils

No.	Sources	Reliability methods	Random field simulation methods	Simulation types
1	**El-Ramly et al. (2002)**	MCS	Local average	U
2	**Low (2003)**	FORM	Midpoint method	U
3	**Griffiths and Fenton (2004)**	RFEM	Local average	U
4	**Fenton and Griffiths (2005)**	RFEM	Local average	U
5	**Hsu and Nelson (2006)**	MCS	Local average	U
6	**Cho (2007)**	MCS	Midpoint method	U
7	**Hicks et al. (2008)**	MCS	Local average	U
8	**Griffiths et al. (2009)**	RFEM	Local average	U
9	**Wu et al. (2009)**	RFEM	Local average	C
10	**Cho (2010)**	MCS	Karhunen-Loève (K-L) expansion	U
11	**Huang et al. (2010)**	RFEM	Local average	U
12	**Wang et al. (2011)**	SS	Midpoint method	U
13	**Ji et al. (2012)**	FORM	Interpolated autocorrelations	U
14	**Kim and Sitar (2013)**	FOSM	Local average	C
15	**Jha and Ching (2013)**	RFEA	Local average	U
16	**Low (2014)**	FORM/SORM	Interpolated autocorrelations	U
17	**Jiang et al. (2014a)**	NISFEM	K-L expansion	U
18	**Jiang et al. (2015)**	SRSM-based MCS	K-L expansion	U
19	**Li et al. (2015a)**	MRSM-based MCS	Midpoint method	U
20	**Li et al. (2016c)**	RFEM-based SS	Midpoint method	U

Note: “U” and “C” in the Table 4.denote the unconditional and conditional simulation, respectively.

Table 4.2 Statistics of soil properties

Soil parameters	Mean	COV	Distribution	ACD	Cross-correlation
c (kPa)	10	0.3	Lognormal	l_h=20 m, l_v=2 m	$\rho_{c,\varphi}$=−0.5
φ (°)	30	0.2	Lognormal	l_h=20 m, l_v=2 m	
γ (kN/m³)	20	–	–	–	–

Note: The symbol "–" means not applicable.

Table 4.3 Reliability results obtained by different methods

Methods	l_h (m)	l_v (m)	Mean	Standard deviation	P_f
This study	20	2	1.197	0.103	2.04×10^{-2}
MRSM by **Li et al. (2015a)**			1.195	0.102	1.87×10^{-2}
MCS by **Cho (2010)**			1.199	0.106	1.71×10^{-2}
This study	20	4	1.199	0.126	4.10×10^{-2}
MRSM by **Li et al. (2015a)**			1.195	0.119	3.97×10^{-2}
MCS by **Cho (2010)**			1.202	0.126	3.70×10^{-2}
This study	40	2	1.200	0.107	2.20×10^{-2}
MRSM by **Li et al. (2015a)**			1.196	0.104	2.06×10^{-2}
MCS by **Cho (2010)**			1.200	0.109	1.91×10^{-2}

Table 4.4 The known data of the five virtual samples for various cases

Parameter		c (kPa)					φ (°)					FS
		A	B	C	D	E	A	B	C	D	E	
$\rho_{c,\varphi}$	−0.7	9.07	9.80	9.38	7.82	9.16	32.11	32.68	29.98	41.20	28.61	1.211
	−0.5	9.07	9.80	9.38	7.82	9.16	32.30	33.60	29.96	42.20	28.15	1.216
	0	9.07	9.80	9.38	7.82	9.16	32.09	34.60	29.80	41.23	27.48	1.223
	0.5	9.07	9.80	9.38	7.82	9.16	31.14	34.11	29.54	36.80	27.32	1.223
COV_c	0.1	9.77	10.03	9.88	9.29	9.80	32.30	33.60	29.96	42.20	28.15	1.231
	0.3	9.07	9.80	9.38	7.82	9.16	32.30	33.60	29.96	42.20	28.15	1.216
	0.5	8.20	9.27	8.65	6.46	8.33	32.30	33.60	29.96	42.20	28.15	1.195
	0.7	7.29	8.60	7.84	5.30	7.45	32.30	33.60	29.96	42.20	28.15	1.172
COV_φ	0.05	9.07	9.80	9.38	7.82	9.16	30.68	30.98	30.10	32.82	29.63	1.198
	0.1	9.07	9.80	9.38	7.82	9.16	31.29	31.92	30.13	35.80	29.19	1.209
	0.15	9.07	9.80	9.38	7.82	9.16	31.83	32.79	30.08	38.93	28.70	1.216
	0.2	9.07	9.80	9.38	7.82	9.16	32.30	33.60	29.96	42.20	28.15	1.216
l_h (m)	5	9.29	10.34	8.39	6.33	8.37	32.42	37.21	30.83	45.50	30.11	1.334
	10	9.20	9.96	8.68	7.22	9.02	32.21	35.14	30.30	43.58	29.12	1.266
	20	9.07	9.80	9.38	7.82	9.16	32.30	33.60	29.96	42.20	28.15	1.216
	30	9.01	9.73	9.76	7.88	9.09	32.37	33.09	30.14	41.60	27.65	1.202
l_v (m)	0.5	9.78	9.04	8.82	8.54	9.16	30.62	39.24	33.06	43.24	28.15	1.241
	1	9.59	9.50	9.56	7.70	9.16	31.69	35.92	30.41	44.76	28.15	1.218
	2	9.07	9.80	9.38	7.82	9.16	32.30	33.60	29.96	42.20	28.15	1.216
	3	8.92	9.64	9.23	8.22	9.16	31.87	32.82	30.16	39.93	28.15	1.220

Table 4.5 Standard deviation of the FS for different cases using conditional random fields when N_d=2

No. of case	l_h (m)	l_v (m)	N_d=0	N_d=2
1	20	2	0.1033	0.1549
2	20	12	0.1527	0.1128
3	20	20	0.1584	0.1015

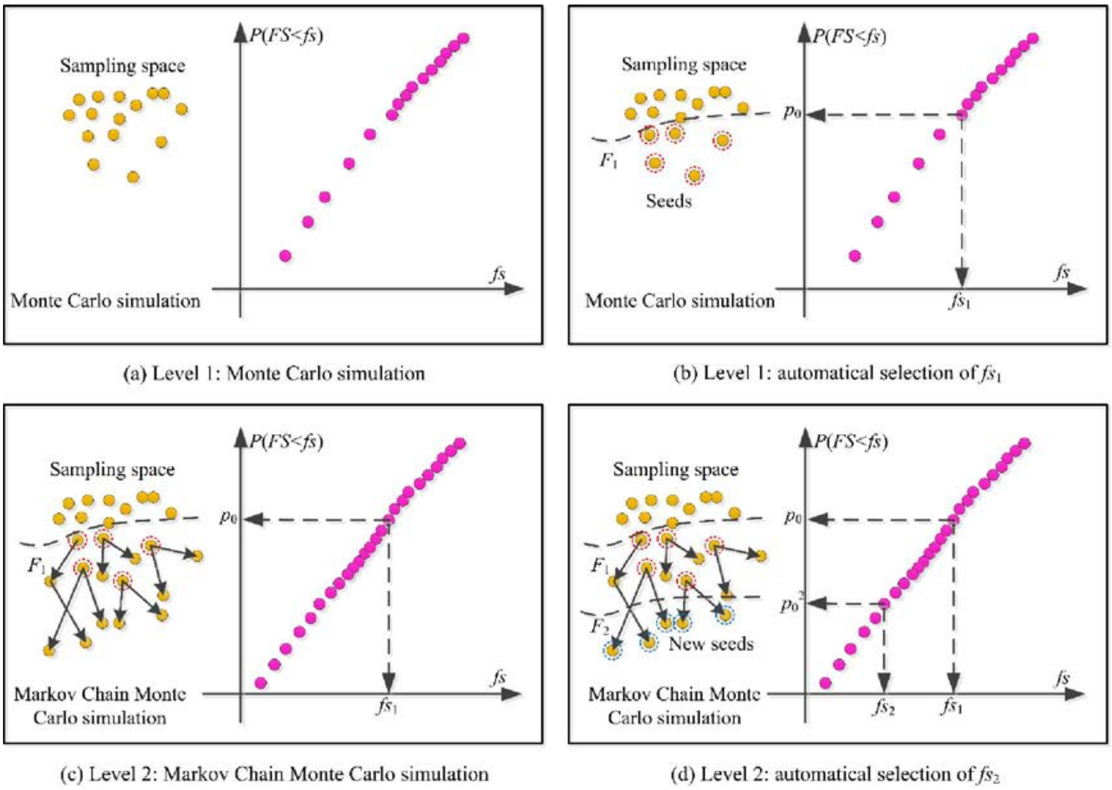

Figure 4.1 The schematic of the Subset simulation (modified from **Au et al. (2010)** and **Li et al. (2016c)**)

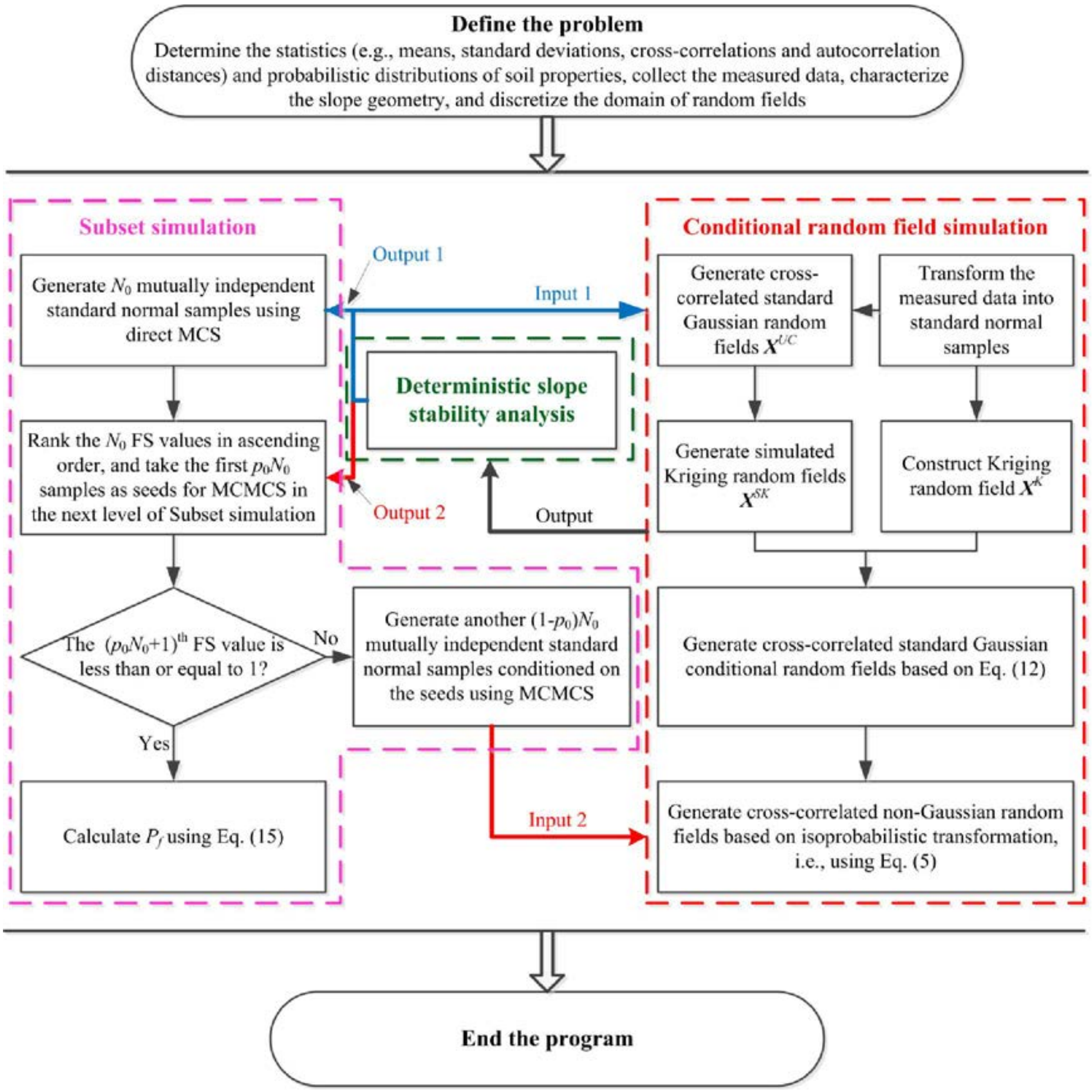

Figure 4.2 Flowchart of reliability analysis based on CRF

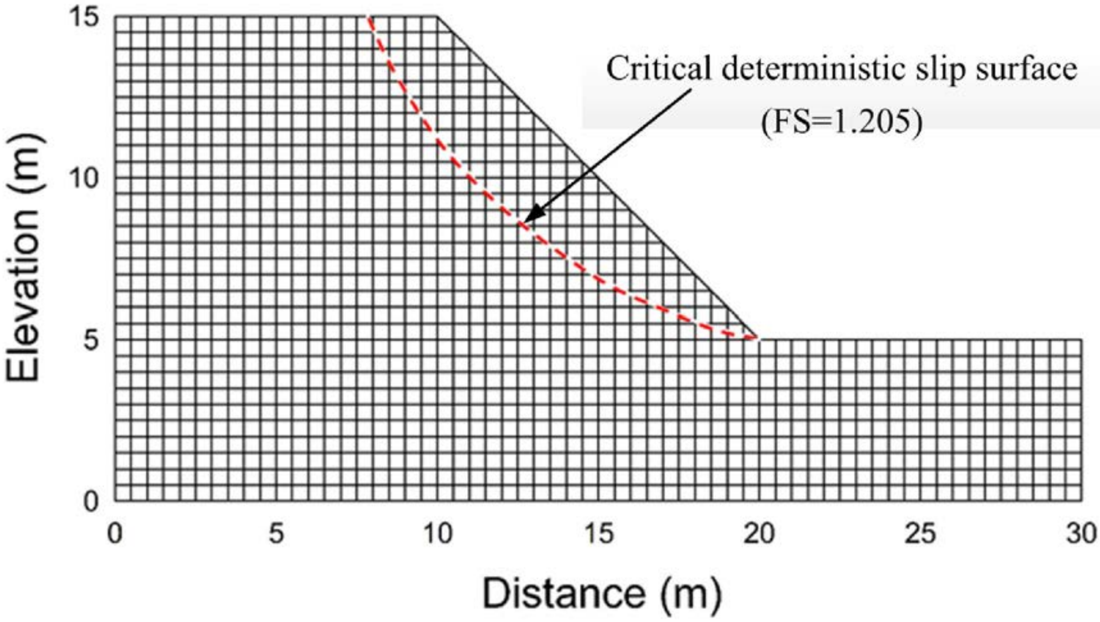

Figure 4.3 The cross-section and random field discretization of the slope

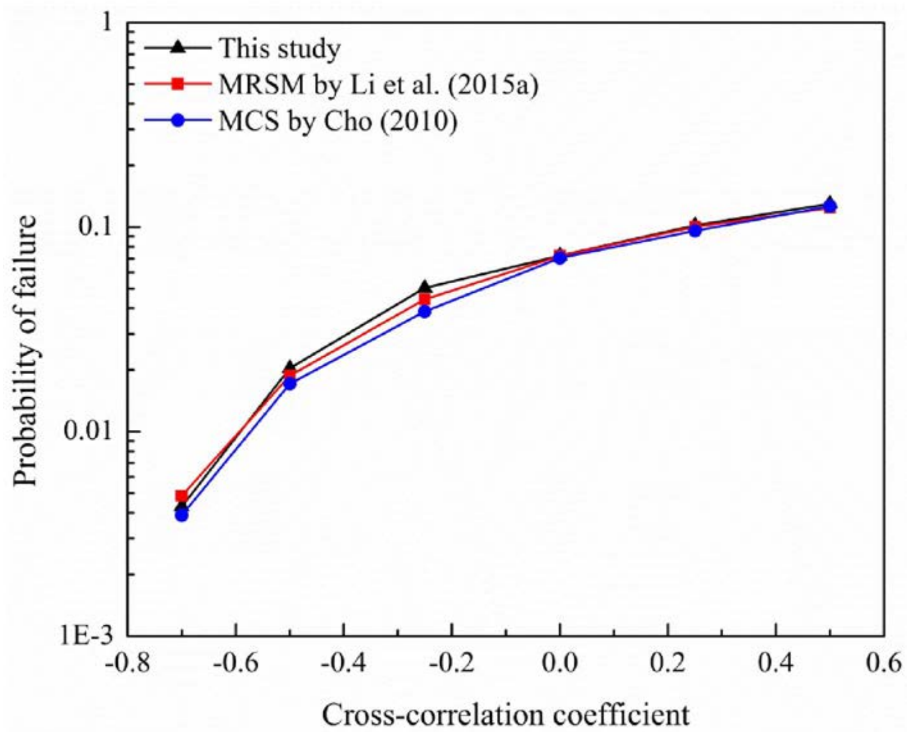

Figure 4.4 Comparison of the P_f results evaluated by different approaches

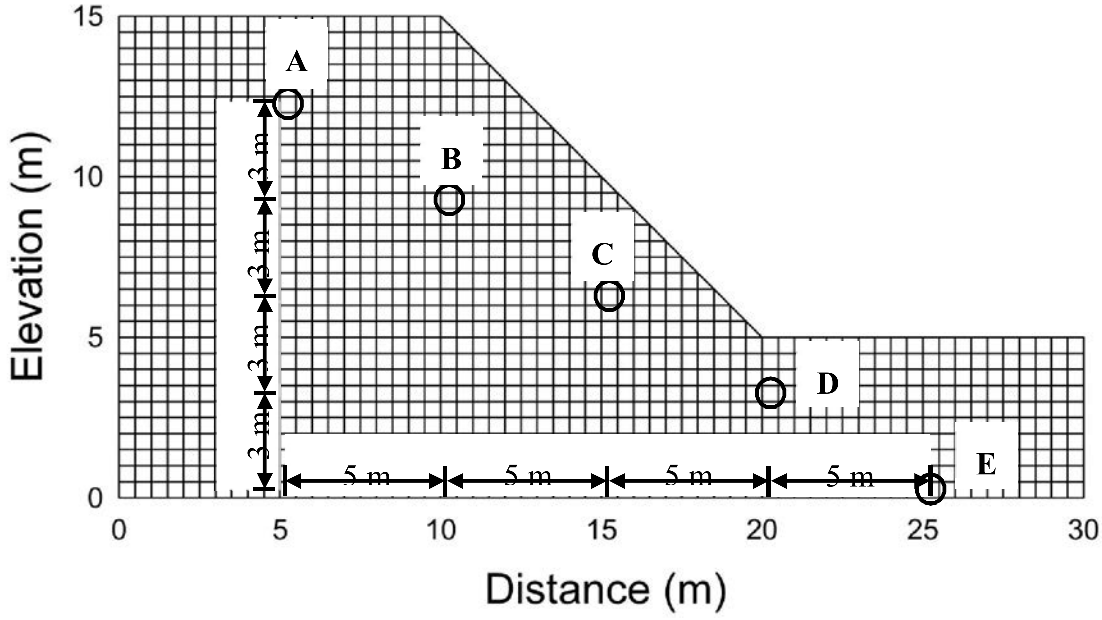

Figure 4.5 Layout of the virtual samples

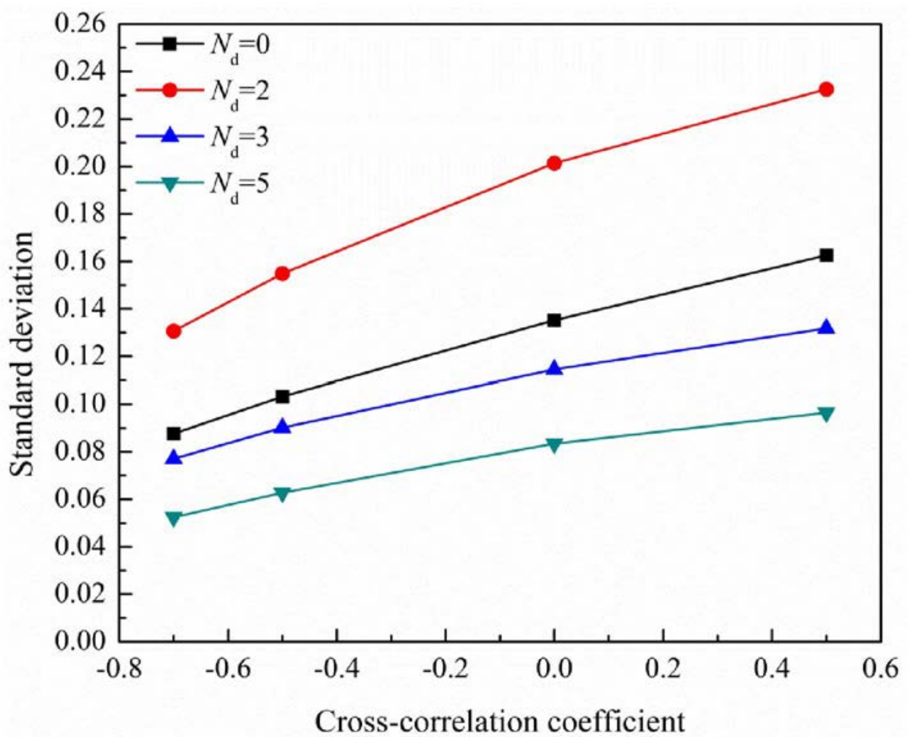

Figure 4.6 Standard deviation of the FS calculated using unconditional and conditional random fields for various cross-correlation coefficients

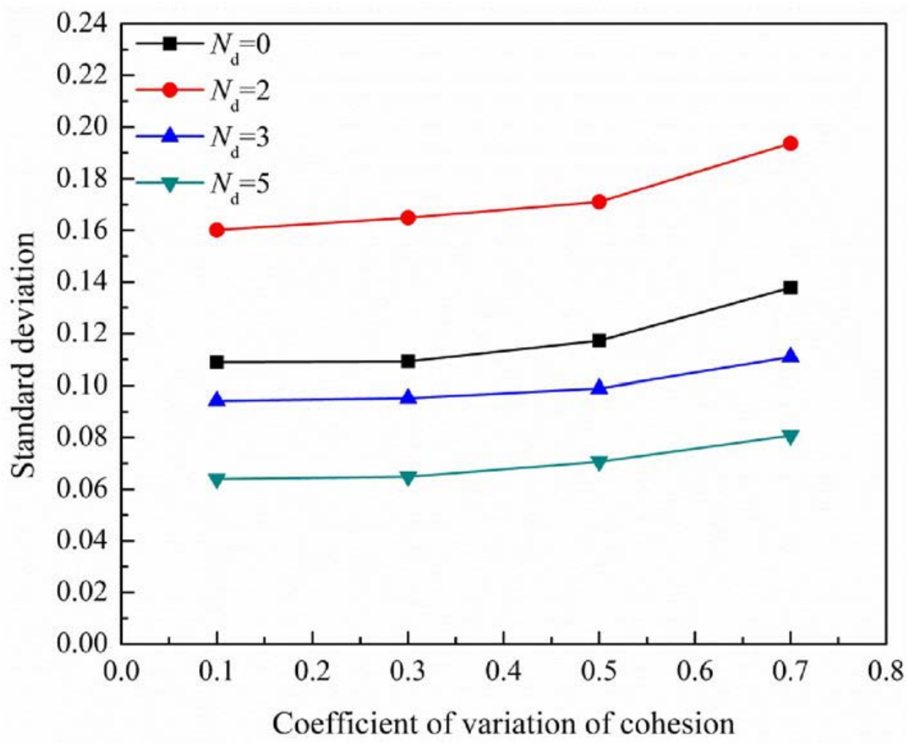

Figure 4.7 Standard deviation of the FS calculated using unconditional and conditional random fields for the coefficients of variation of cohesion

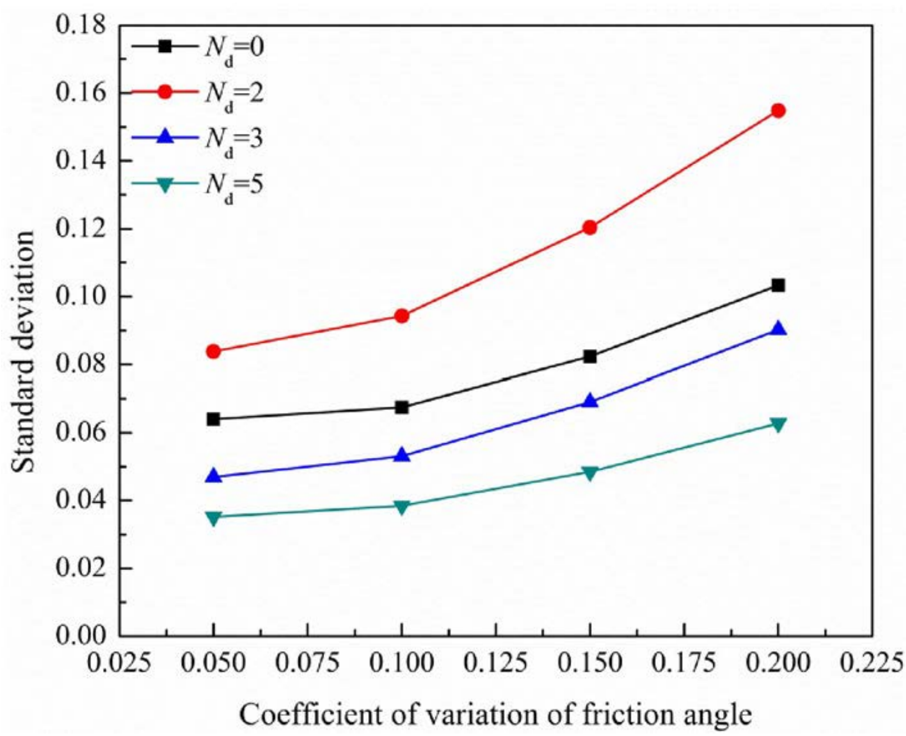

Figure 4.8 Standard deviation of the FS calculated using unconditional and conditional random fields for various coefficients of variation of friction angle

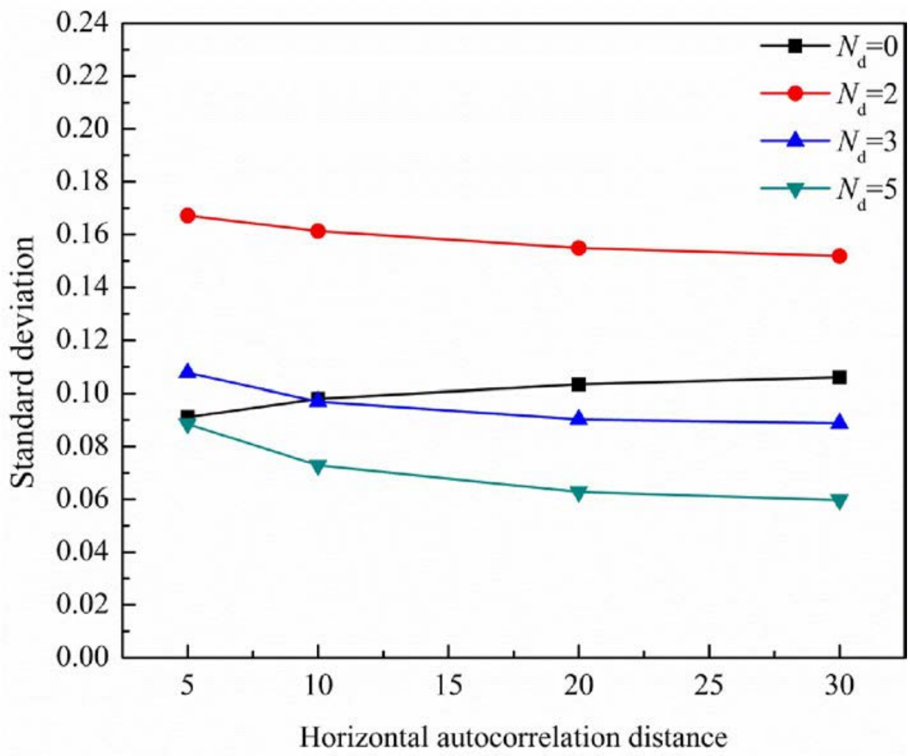

Figure 4.9 Standard deviation of the FS calculated using unconditional and conditional random fields for various horizontal ACDs

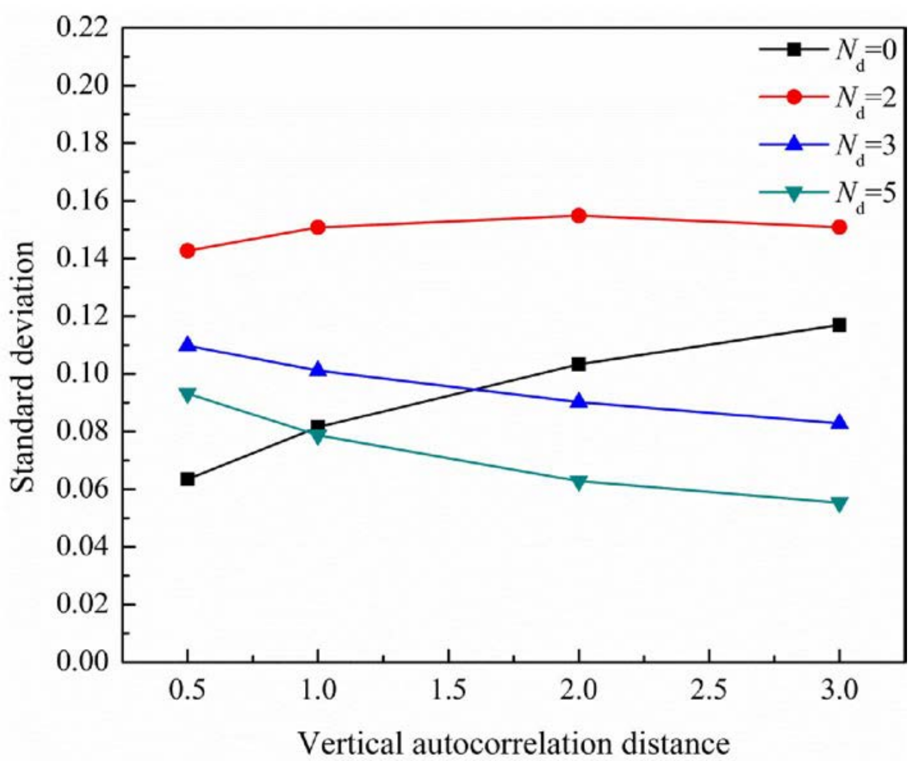

Figure 4.10 Standard deviation of the FS calculated using unconditional and conditional random fields for various vertical ACDs

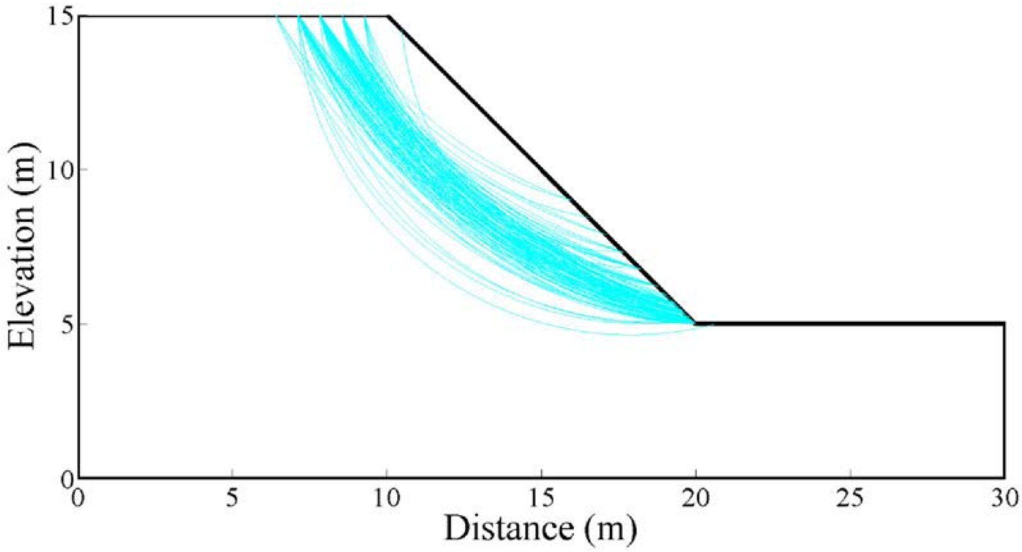

(a) Unconditional random field simulation

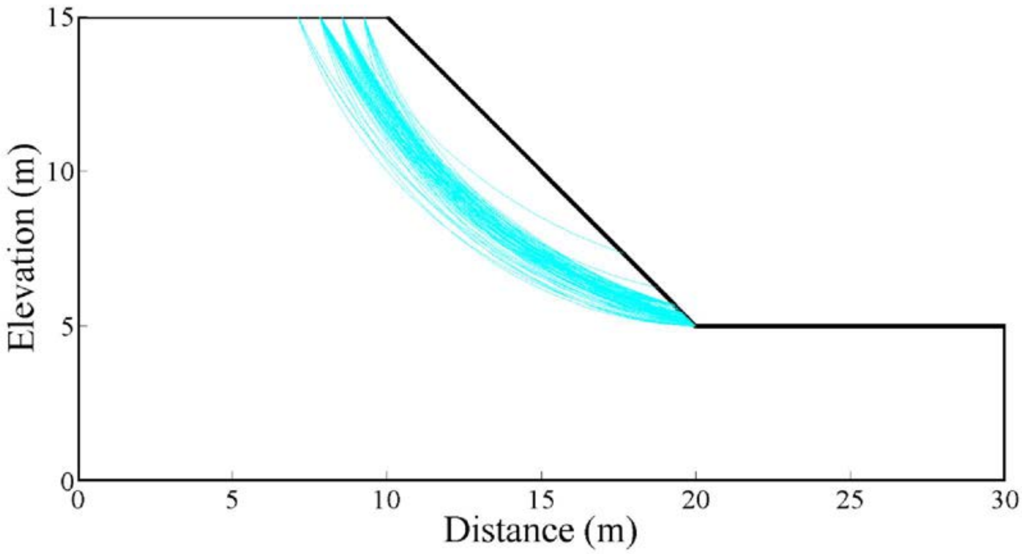

(b) Conditional random field simulation

Figure 4.11 Spatial variation of the critical slip surfaces obtained from unconditional and conditional random field simulations for the case of $\rho_{c,\varphi}$=−0.5

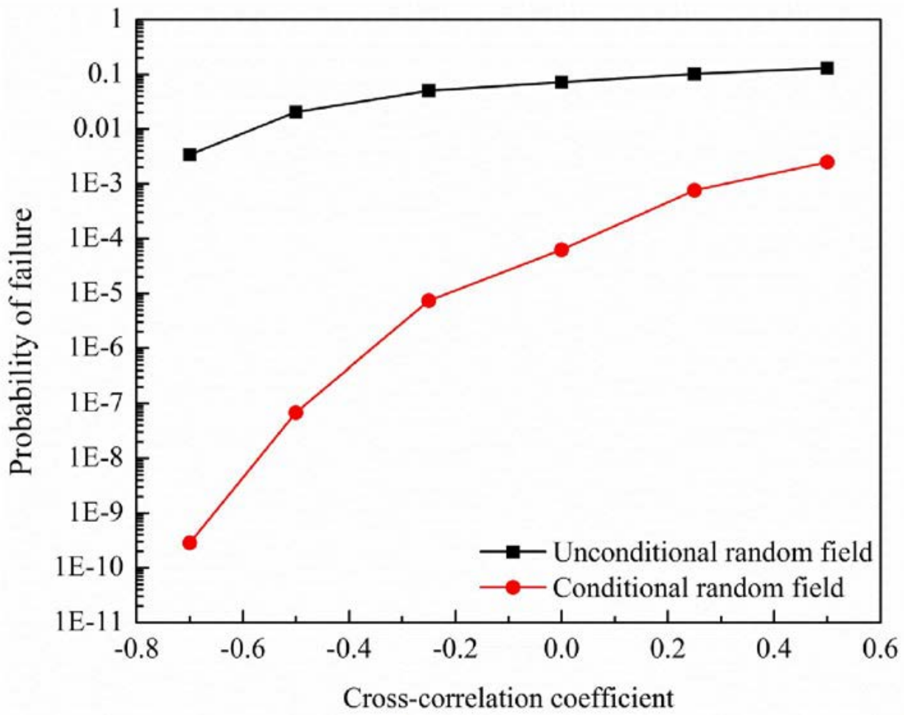

Figure 4.12 Comparison of probabilities of failure calculated by unconditional and conditional random field simulations for various cross-correlation coefficients

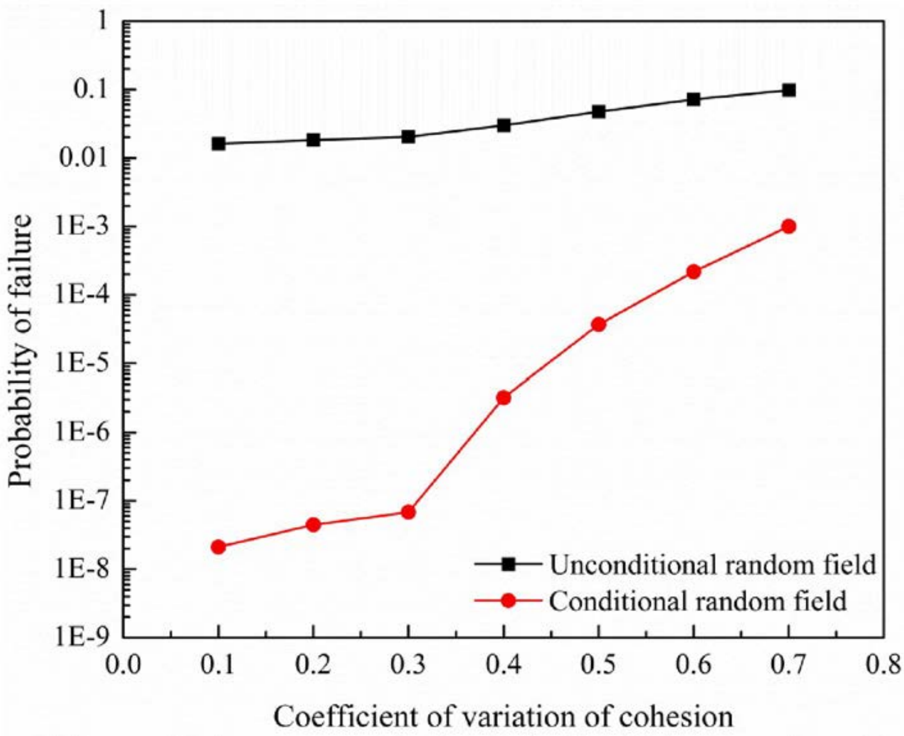

(a) Cohesion

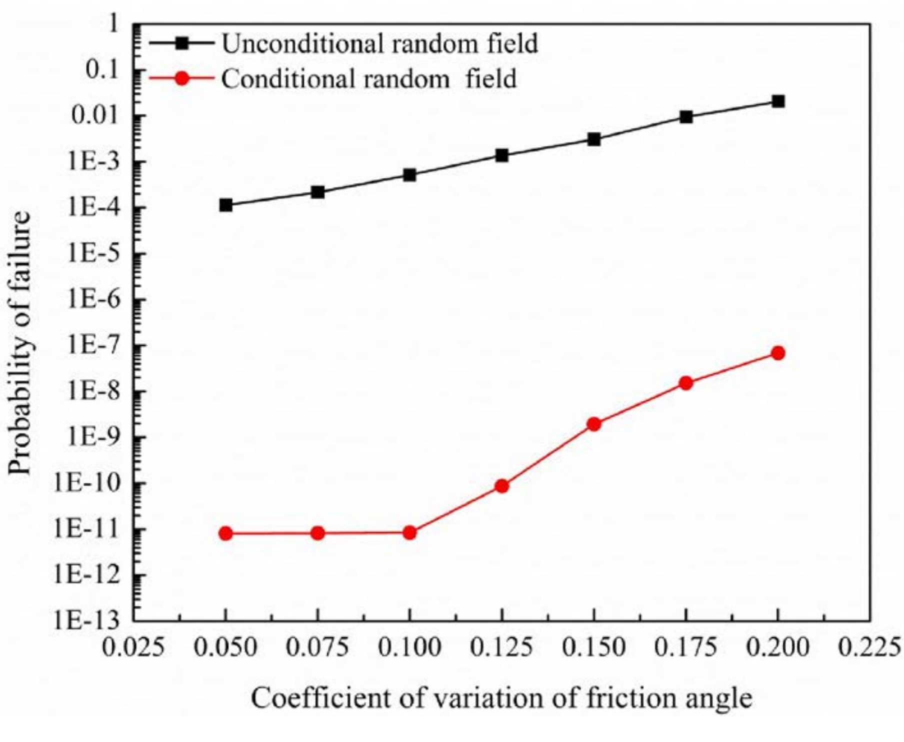

(b) Friction angle

Figure 4.13 Comparison of probabilities of failure calculated using the unconditional and conditional random field simulation for various coefficients of variation of shear strength parameters

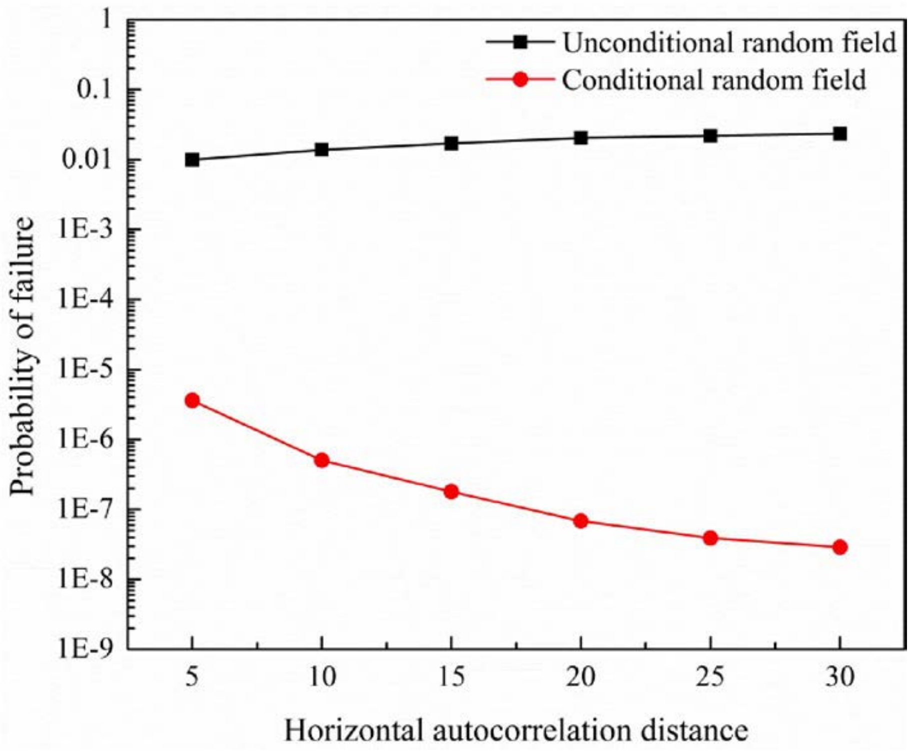

(a) Horizontal ACD

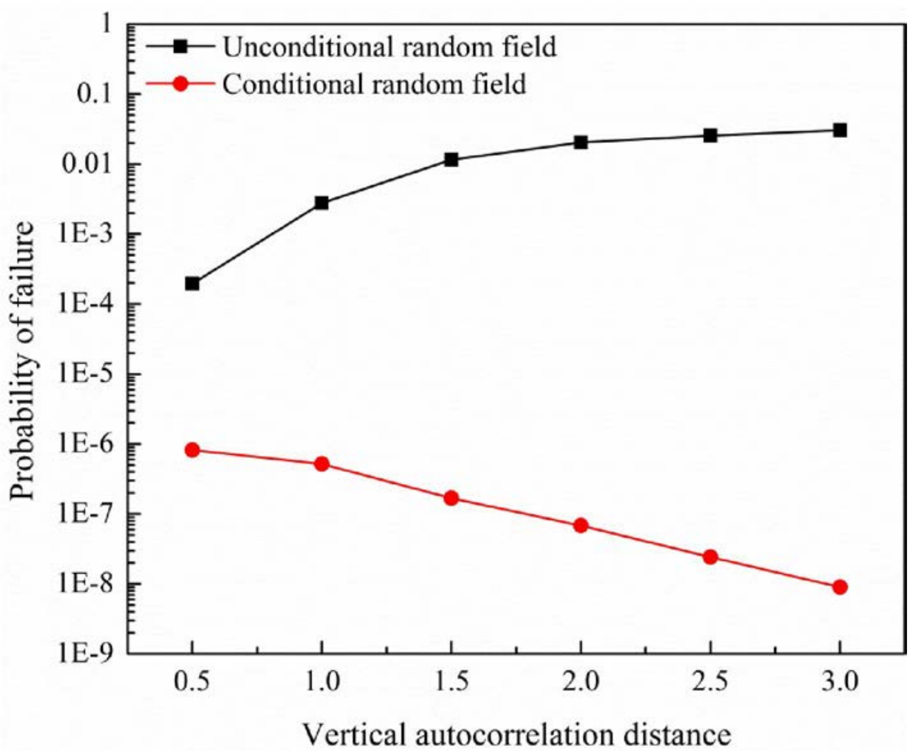

(b) Vertical ACD

Figure 4.14 Comparison of probabilities of failure calculated using the unconditional and conditional random field simulation for various ACDs

CHAPTER 5 EFFECT OF SYSTEM STRATIGRAPHIC BOUNDARY UNCERTAINTY ON SYSTEM RELIABILITY AND RISK OF A LAYERED SLOPE IN SPATIALLY VARIABLE SOILS

5.1 Introduction

During the past few decades, the inherent spatial variability of soil properties has been widely considered in slope reliability analysis and risk assessment. For instance, **Griffiths and Fenton (2004)** studied the reliability of a cohesive slope using the RFEM and found that neglecting the spatial variability of soil properties would underestimate the P_f. Such an observation would be more outstanding as the COV of the soil strength increases. Similar observations were also reported by other researchers (e.g., **Jiang et al. 2014a**). Recently, **Li et al. (2015a)** compared the influence of using different theoretical ACFs to simulate the spatial variability of soils on the slope reliability by using a multiple response surface method (RSM), and reported that no significant differences exist among different ACFs. Additionally, many other remarkable achievements (e.g., **El-Ramly et al. 2002; Cho 2007**, **2010; Hicks and Spencer 2010; Wang et al. 2011; Ji and Low 2012; Huang et al. 2013; Jha and Ching 2013; Hicks et al. 2014; Jiang et al. 2015; Low et al. 2015; Dithinde et al. 2016b; Li et al. 2016c; Xiao et al. 2016; Liu et al. 2017d**) have also been made using different probabilistic approaches. These contributions have benefited significantly to the geotechnical stability community for comprehending the failure mechanism of slopes in spatially variable soils. Nevertheless, they are far from perfect and are subjected to a common criticism of ignoring the stratigraphic boundary uncertainty (SBU) between different soil layers.

In general, the SBU widely appears in layered soils where the soil properties (e.g., c and φ) are characterized by significant variability and heterogeneity on various scales (e.g., **Nataf 1962; Luo et al. 2011; Cho 2012**). This variability and heterogeneity originates not only from the complex geological, chemical and environmental processes but also from the limited amount of site investigation data that we can obtain in engineering practice (e.g., **Vanmarcke 1977b**). Identification of the SBU is of great importance to geotechnical stability design. Many efforts have been made to characterize this uncertainty in the literature (e.g., **Wang et al. 2013, 2014; Li et al. 2015d; Li et al. 2016e; Wang et al. 2016**). The most commonly used methods in these studies are the Bayesian methods, which estimate the soil profile based on the posterior probability distribution of the available site investigation data such as cone penetration test (CPT) data. In addition, it is found that few of the available investigations have considered the SBU in probabilistic slope stability analysis, because they mainly concentrate on the nominally homogeneous slopes rather than the heterogeneous or layered slopes. However, in geotechnical engineering practice, it is more common to encompass layered soils than nominally homogeneous soil layers. Unfortunately, hardly can the works related to the influence of the system SBU on the slope stability be seen in the literature.

If the above-mentioned uncertainties are accounted for in a slope stability model, the CSS is also uncertain, which consequently leads to numerous possible failure modes of a slope. Slope failure occurs when a slope slides along any individual slip surface, and the failure probability and failure consequence associated with different potential slip surfaces might be different. Therefore, the slope reliability and failure risk evaluated based on a single slip surface such as the CSS would be non-conservative (e.g., **Fenton and Vanmarcke 1990**). On the other hand, evaluation of the slope stability based on the summation of the reliability and risk results associated with all the potential slip surfaces would also be inaccurate since the FSs of different potential slip surfaces are generally highly correlated (e.g., **Zhang and Huang 2016**). Therefore, the overall probability of failure and consequences of a slope should be calculated considering all the possible failure modes in a systematic manner, especially in layered soils where the systematic effects are more significant (e.g., **Ditlevsen 1979; Chowdhury and Xu 1995; Zhang et al. 2011b; Liu and Cheng 2016**). Many of investigations on slope reliability considering multiple slip surfaces have been reported in the literature (e.g., **Zhang et al. 2011b; Jiang et al. 2015; Li et al. 2015a; Li et al. 2016c; Liu and Cheng 2016; Xiao et al. 2016**), but few of these studies involved a quantitative risk assessment, with the exception of **Huang et al. (2013)**, **Li and Chu (2016)** and **Zhang and Huang (2016)**. To the best of our knowledge, perhaps **Huang et al. (2013)** are the first to investigate the systematic effect on slope failure risk assessment using limit analysis and MCS. However, only undrained cohesive slopes are considered in their work, and the influence of cross-correlations and COVs of different shear strengths on failure risk have not yet been fully explored. Recently, inspired by **Huang et al. (2013)**, **Li and Chu (2016)** developed a quantitative approach for risk assessment of slope failure based on several representative slip surfaces within the framework of an LEM, which provides an efficient and quantitative tool for identifying the key group of representative slip surfaces in the planning of slope risk mitigation. **Zhang and Huang (2016)** proposed an efficient RSM-based MCS for risk assessment considering multiple failure surfaces, but they did not consider the heterogeneity of soils. Obviously, none of these studies address the consideration of the SBU. In summary, the question of how to quantify the systematic effects of the SBU on slope reliability and risk remains unanswered.

In view of the above problems, this chapter concentrates on the analysis of the reliability and failure risk of multi-layered soil slopes, with a particular emphasis on the influence of the SBU. The chapter begins with the representation of the uncertainties in multilayered soils, followed by the evaluation of system reliability analysis and risk assessment using MCS. Next, a detailed implementation procedure for accomplishing the whole study is introduced. Later on, an example application is performed on a hypothetical layered slope to illuminate the influence of the SBU on the slope stability. Lastly, the major conclusions from this chapter are provided.

5.2 Characterization of uncertainties in layered soils

5.2.1 Simulation of inherent spatial variability of soil properties

Consider, for instance, a slope with N soil layers, and each layer is discretized into a certain number of random field elements. For the k^{th} layer, suppose the centroid coordinates of each element are denoted as (x_i, y_i), where $i = 1, 2, \cdots, n_e^k$, and n_e^k is the number of the discretized random field elements in the k^{th} layer. Based on Eq. (2.13) and these coordinates, the autocorrelation matrix $\boldsymbol{C}^k$ for the k^{th} layer is expressed as

$$\boldsymbol{C}^k = \begin{bmatrix} 1 & \rho(\tau_{x_{12}}, \tau_{y_{12}}) & \cdots & \rho(\tau_{x_{1n_e^k}}, \tau_{y_{1n_e^k}}) \\ \rho(\tau_{x_{21}}, \tau_{y_{21}}) & 1 & \cdots & \rho(\tau_{x_{2n_e^k}}, \tau_{y_{2n_e^k}}) \\ \vdots & \vdots & \ddots & \vdots \\ \rho(\tau_{x_{n_e^k 1}}, \tau_{y_{n_e^k 1}}) & \rho(\tau_{x_{n_e^k 2}}, \tau_{y_{n_e^k 2}}) & \cdots & 1 \end{bmatrix} \tag{5.1}$$

where the dimension of $\boldsymbol{C}^k$ is $n_e^k \times n_e^k$; $k = 1, 2, \cdots, N$; $\rho(\tau_{x_{ij}}, \tau_{y_{ij}})$ denotes the autocorrelation coefficient between spatial quantities at any two points, in which the lags $\tau_{x_{ij}} = | x_i - x_j |$ and $\tau_{y_{ij}} = | y_i - y_j |$ denote the absolute distances between the centroid coordinates of the i^{th} element and the j^{th} element in the horizontal and vertical directions, respectively.

Regarding the simulation of non-stationary random fields, the simulation domain is required to be divided into several non-overlapping subdomains, and soil properties at any two points in different subdomains are assumed to be uncorrelated (e.g., **Lu and Zhang 2007; Jiang and Huang 2016; Liu et al. 2017c; Liu et al. 2017d**). Herein, each layer can be considered as a subdomain in a slope with multiple layers. Thereafter, a typical realization of the standard Gaussian random field underlying the soil properties in the k^{th} layer is then derived as

$$\boldsymbol{X}^{k,G}(x,y)=\boldsymbol{L}_1^k\boldsymbol{\xi}^k(\boldsymbol{L}_2^k)^T,\ (k=1,2,\cdots N) \tag{5.2}$$

where the superscript G means the standard Gaussian random field; $\boldsymbol{\xi}^k$ is an $n_e^k \times m^k$ sample matrix, which is obtained in the following way: (1) obtain a vector ξ with n independent standard normal samples, in which $n=\sum_{k=1}^{N} n_e^k m^k$; (2) partition the vector ξ into N sub-vectors; and (3) re-arrange each sub-vector as m^k vectors with a dimension of n_e^k, where m^k is the number of simulated random fields associated with soil parameters in the k^{th} layer. $\boldsymbol{L}_1^k$ and $\boldsymbol{L}_2^k$ are lower triangular matrices decomposed from the autocorrelation matrix $\boldsymbol{C}^k$ and the cross-correlated matrix $\boldsymbol{R}^k$, respectively, using the CDT, and they are defined as

$$\boldsymbol{L}_1^k(\boldsymbol{L}_1^k)^T=\boldsymbol{C}^k \tag{5.3}$$

$$\boldsymbol{L}_2^k(\boldsymbol{L}_2^k)^T=\boldsymbol{R}^k \tag{5.4}$$

Thereafter, one realization of the non-Gaussian random field can be achieved by the isoprobabilistic transformation as

$$\boldsymbol{X}_i^{k,NG}(x,y)=F_i^{-1}\left\{\Phi\left[\boldsymbol{X}_i^{k,G}(x,y)\right]\right\},\ (k=1,2,\cdots,N;\ i=1,2,\cdots,m^k) \tag{5.5}$$

where the superscript NG means the non-Gaussian random field; $F_i^{-1}(\bullet)$ is the inverse function of the marginal cumulative distribution of the i^{th} random field in the k^{th} layer; $\Phi(\bullet)$ is the standard Gaussian cumulative distribution function. Repeating the above procedure N_{sim} times will give N_{sim} simulations of the non-stationary random field, based on which the probabilistic slope stability analysis can be performed.

5.2.2 Simulation of stratigraphic boundary uncertainty

In general, the soil profile can be identified based on spot field investigation. However, the volume of the investigation data is commonly not big, which gives rise to a mass of uncertainties. The geological property at an underdetermined location is either interpolated with several available data obtained from the adjacent area of this unknown location (e.g., **Li et al. 2016e; Liu et al. 2017d**) or is estimated based on the posterior probability distribution of the soil (e.g., **Wang et al. 2013**, **2014; Li et al. 2015d**). Therefore, the accuracy or the confidence level of the site investigation data is very critical to the reduction of the uncertainties associated with the aforementioned methods. Meanwhile, the classical method to identify the soil profile in a slope is to simplify it as a single line or panel based upon some borehole data, which is the so-called deterministic stratigraphic boundary (DSB) herein. Therefore, it can be concluded that previous studies have an implicit assumption that the measured data are deterministic and accurate without error or the measurement uncertainty is neglected. However, in geotechnical engineering practice, the measurement uncertainty unavoidably exists due to the judgment and operation errors of practicing engineers. Generally, these errors should be limited to a certain degree. For example, according to the Chinese geotechnical site investigation code, the maximum error of a soil stratum should be within 5 cm (e.g., **PRC and AQSIQ 2009**). Hence, it is more reasonably acceptable to employ a stochastic stratigraphic boundary (SSB) than a DSB to consider the inherent error of the site investigation data. Probabilistic methods provide a good tool to characterize such a stochastic property. Inspired by **Li et al. (2015a)**, the stochastic nature of the stratigraphic boundary is simulated by a discrete random variable model herein, as will be illustrated later. It should be noted that the SBU here merely denotes the inherent error of site investigation data (i.e., the system SBU) and excludes the inherent variation of the soil stratum.

5.3 MCS for slope system reliability analysis and risk assessment

As described in Section 5.1, a slope constituted by multiple soil layers usually presents profound system effects on its stability assessment. To investigate such system effects on the slope stability, MCS is suggested here. In the following, a layered slope with n potential slip surfaces is taken as an example to illuminate the principles of the MCS for system reliability analysis and risk assessment of the slope stability (e.g., **Liu and Cheng 2016; Zhang and Huang 2016**).

5.3.1 MCS for slope reliability analysis

Unlike the conventional deterministic slope stability analysis that considers the soil shear strength parameters as constants, probabilistic slope stability analysis takes the random nature of these parameters into consideration. Suppose the shear strength parameters constitute a vector of random variables $\boldsymbol{X}=(x_1,x_2,\cdots,x_p)$, which are described some specific distributions (e.g., lognormal distributions). Therefore, it is more reasonable to use P_f to consider the effects of the uncertainties associated with those random variables, which is generally defined as

$$P_f = P(g(\boldsymbol{X})\le 0) = \int\cdots\int\int_{g(\boldsymbol{X})\le 0} f_{\boldsymbol{X}}(\boldsymbol{X})\mathrm{d}\boldsymbol{X} \tag{5.6}$$

where $f_{\boldsymbol{X}}(\boldsymbol{X})$ is the joint probability density function (PDF) of $\boldsymbol{X}$; $g(\boldsymbol{X})$ is the performance function of the slope considered, which is formulated so that the slope is unstable if $g(\boldsymbol{X})\le 0$ and stable otherwise, as defined below

$$g(\boldsymbol{X}) = \min_{i=1,2,\cdots,n} FS_i(\boldsymbol{X}) - 1 \tag{5.7}$$

where $FS_i(\boldsymbol{X})$ is the FS of the i^{th} potential slip surface obtained by a deterministic slope stability analysis method (e.g., the limit equilibrium method). Direct integration of the p-fold integral in Eq. (5.7) is not a trivial matter. However, MCS provides an unbiased estimation of P_f in a systematic way, so it is adopted in this study and is described as follows

$$P_f \approx \frac{1}{N_{sim}} \sum_{i=1}^{N_{sim}} I[\min_{i=1,2,\cdots,n} FS_i(\boldsymbol{X}) \le 1] \tag{5.8}$$

where $I[\cdot]$ is an indicator function, which is equal to unity when $\min_{i=1,2,\cdots,n} FS_i(\boldsymbol{X}) \le 1$ and zero otherwise, and N_{sim} is the number of MCS samples. The estimation accuracy of P_f depends highly on the number of samples and is assessed by the coefficient of variation of P_f as per

$$COV_{P_f} = \sqrt{\frac{1-P_f}{N_{sim}P_f}} \tag{5.9}$$

5.3.2 MCS for risk assessment

Traditionally, the risk of a slope failure is calculated as the product of the failure consequence and the failure probability based on the CSS (e.g., **Ang and Tang 1984**). However, there would be a great many multiple potential slip surfaces if the aforementioned uncertainties associated with the soil properties and the stratigraphic boundary are considered, and it is likely that the slope can slide along any single one of these slip surfaces. Hence, the failure consequence is no longer a deterministic value but a variable, since different slip surfaces may have different values of the volume of sliding mass and thus lead to significantly different consequences. This indicates that the traditional approach is no more applicable. Nevertheless, it is relatively easy to account for this uncertainty in the risk assessment by using MCS.

Suppose the failure consequence of sliding along the i^{th} potential slip surface is denoted as C_i. For a given $\boldsymbol{X}$, the slope failure consequence is then identified as $C_m(\boldsymbol{X})$, where m is the index of the slip surface with the minimum FS among all potential slip surfaces, i.e., $m = \arg\min_{i=1,2,\cdots,n} FS_i(\boldsymbol{X})$ (n is the number of potential slip surfaces). In general, the slope failure consequence is highly dependent on the volume or mass of the sliding mass. Therefore, in the literature (e.g., **Huang et al. 2013; Li and Chu**

2016; Zhang and Huang 2016), the volume or area of the sliding mass is widely used to measure the slope failure consequence. Next, a 2-D slope with multiple potential slip surfaces is taken as an example to illustrate the evaluation of the slope failure consequence based on the area of the sliding mass. Suppose A_i denotes the cross-sectional area of the sliding mass associated with the i^{th} slip surface. That is, A_i is equal to the area of the soil mass over the i^{th} slip surface, which can be easily obtained with the help of the LEM. Then, for the entire slope system under a given $\boldsymbol{X}$, if the minimum FS is larger than unity, the slope will be stable, and the failure consequence is equal to zero, i.e., $C_m(\boldsymbol{X})=0$. Otherwise it is unstable, and the failure consequence is equal to the sliding mass that corresponds to the slip surface with the minimum FS, denoted as A_m. The measurement of $C_m(\boldsymbol{X})$ can also be written as

$$C_m(\boldsymbol{X}) = \begin{cases} A_m & \mathrm{g}(\boldsymbol{X}) \le 0 \\ 0 & \mathrm{g}(\boldsymbol{X}) > 0 \end{cases}, \text{ where } m = \underset{i=1,2,\cdots,n}{\arg\min} FS_i(\boldsymbol{X}) \tag{5.10}$$

However, it might be argued that it is of more practical significance to use more complete and realistic indices such as life losses, economic losses and environmental impacts to assess the slope failure consequence (e.g., **Dai et al. 2002; Vega and Hidalgo 2016; Liu et al. 2017c**). To this end, the index of economic losses is adopted in this study, while for simplicity other indices like life losses and environmental impacts are not considered herein because it is generally difficult to quantify the values of these indices (e.g., **Liu et al. 2017c**). According to the author's practical engineering experience in HK and other countries, the consequence of a slope failure is generally proportional to the volume of the sliding mass. For soil slopes without reinforcements such as soil nails, the unit price u_p of the economic losses resulted by the slope failure is estimated as about 100 HK dollars per cubic meter. Thus, the $C_m(\boldsymbol{X})$ in Eq. (5.10) can further be modified in terms of economic losses as

$$C_m(\boldsymbol{X}) = \begin{cases} u_p A_m & \mathrm{g}(\boldsymbol{X}) \le 0 \\ 0 & \mathrm{g}(\boldsymbol{X}) > 0 \end{cases}, \text{ where } m = \underset{i=1,2,\cdots,n}{\arg\min} FS_i(\boldsymbol{X}) \tag{5.11}$$

According to the distribution of $\boldsymbol{X}$ and the definition of risk, the risk of the slope failure considering multiple slip surfaces can be written as

$$R = \int \cdots \int \int C_m(\boldsymbol{X}) f_X(\boldsymbol{X}) \mathrm{d}\boldsymbol{X} \tag{5.12}$$

Similar to the solution to Eq. (5.6), according to MCS, the risk is estimated as the average value of $C_m(\boldsymbol{X})$ with the consideration of uncertainty in $\boldsymbol{X}$. If N_{sim} samples are adopted in an MCS, there will be N_{sim} samples of $C_m(\boldsymbol{X})$, which is denoted as $C_m(\boldsymbol{X}^i)$ $(i = 1, 2, \cdots, N_{sim})$. The estimation of risk is calculated as

$$\hat{R} \approx \frac{1}{N_{sim}} \sum_{i=1}^{N_{sim}} C_m(\boldsymbol{X}^i) \tag{5.13}$$

The estimation of risk $\hat{R}$ could change with the simulated set of samples due to the random nature of $\boldsymbol{X}$. Using the methods for estimating the error of the mean (e.g., **Ang and Tang 1984; Zhang and Huang 2016**), the standard deviation associated with $\hat{R}$ is

$$Std(\hat{R}) \approx \sqrt{\frac{\sum_{i=1}^{N_{sim}} [C_m(\boldsymbol{X}^i) - \hat{R}]^2}{N_{sim}(N_{sim} - 1)}} \tag{5.14}$$

Based on Eqs. (5.13) and (5.14), one can easily obtain the COV of the statistical error of $\hat{R}$ by dividing the $Std(\hat{R})$ by $\hat{R}$. Decision makers can thus judge if the $\hat{R}$ reaches the desirable accuracy based on the value of COV. If not, more MCS samples are required to reduce the variation.

5.4 Implementation tools and procedure

The proposed approaches are accomplished based on an MATLAB toolbox that was developed by the author and has been successfully applied to several previous investigations (e.g., **Liu and Cheng 2016; Liu et al. 2017a; Liu et al. 2017d**). The implementation procedure is schematically shown in Figure 5.1 and is summarized as follows:

1. Collect input data for both deterministic and probabilistic slope stability analyses, which includes but not limited to the slope geometry parameters, the number of the potential slip surfaces n, statistics (e.g., means, COVs, SOFs and PDFs) of the soil property parameters and the probability mass function (PMF) of the stratigraphic boundary.

2. Discretize the study domain into finite elements and extract the centroid coordinates of each element, based on which one can calculate the autocorrelation matrix $\boldsymbol{C}^k$ for each soil layer using Eq. (5.1).

3. Perform MCS and start from i=1

    (a) Draw a vector of independent standard normal random samples, which is then partitioned into N (i.e., the number of soil layers) sub-vectors. Next, re-arrange each subvector as a sample matrix $\boldsymbol{\xi}^k$ with a dimension of $n_e^k \times m^k$.

    (b) Obtain the desirable random fields $\boldsymbol{X}_i^{k,NG}$ using Eqs. (5.2-5.5).

    (c) Evaluate the FS value for each potential slip surface using $\boldsymbol{X}_i^{k,NG}$ as the input and obtain n FS values. Based on these FS values, single out the critical slip surface (or the m^{th} slip surface) corresponding to the minimum FS based on the n FS values obtained in the last step. Meanwhile, save the minimum FS as an output of the i^{th} sample, i.e., $\min_{i=1,2,\cdots,n} FS_i(\boldsymbol{X}^i)$.

    (d) Obtain the failure consequence of the i^{th} sample $C_m(\boldsymbol{X}^i)$ associated with the m^{th} slip surface using Eq. (5.11).

(e) Increase i by one and go back to step 3(a) until i is equal to N_{sim}.

4. Based on the N_{sim} set of outputs from step 3, estimate the slope failure probability P_f and failure risk $\hat{R}$ using Eqs. (5.8) and (5.13), respectively.

5. Calculate the statistical errors associated with P_f and $\hat{R}$. If the COVs of these are too large to be acceptable, then increase the value of N_{sim} and repeat the steps 3 to 5; otherwise, stop the program.

5.5 Illustrative example

In this part, a hypothetical layered slope adapted from **Li et al. (2015a)**, which is characterized by the system SBU and the inherent spatial soil variability, is studied to elaborate the influence of the SSB on the slope reliability and failure risk. As shown in Figure 5.2, the slope is comprised of two soil layers, and has a slope height of 10 m and a slope angle of 45°. The buried depth of the stratigraphic boundary between the two soil layers is 10 m. In general, this boundary is ubiquitously recognized as the real boundary between the two layers. Hence, it is diffusely used as a DSB in the conventional slope stability analysis. However, in engineering practice, this boundary might not be the real one because of the little experience in site investigation as well as of the inadequate supervision of workmanship, which induces uncertainty in the real boundary location. Likewise, the boundary location identified from site investigation is generally uncertain, and is much more reasonably to be considered as an SSB. To describe the variation of the location of the SSB here, a discrete random variable model is assumed, which is written as

$$p(y) = \begin{cases} 0.3, & y=0.5(\text{m}) \\ 0.4, & y=0.0(\text{m}) \\ 0.3, & y=-0.5(\text{m}) \end{cases} \tag{5.16}$$

where $p(y)$ is the PMF of the SSB; y=0.0 indicates the x-coordinate axis is superposed on the DSB; y=0.5 and y=−0.5 denote the possible upper and lower stratigraphic boundary (PUSB and PLSB) limits, respectively, as shown in Figure 5.2. This assumption is reasonably acceptable because the measurement error in practice would not be too large. In addition, Table 5.1 tabulates the soil properties for each soil layer. These parameters are considered the reference case for this study. Specifically, the unit weights of both layers are assumed to be the same constant of 20 kN/m^3, while the cohesion c and friction angle φ in each layer are simulated as cross-correlated lognormal random fields. Statistics for the cohesion and the friction angle are also displayed in the table. For simplicity, SOFs and cross-correlation coefficients in the two layers are assumed to be the same.

5.5.1 Reliability analysis and risk assessment results of the baseline case

This part evaluates the stability of the slope for the reference case as shown in Table 5.1. As can be expected from the above analysis, the location of the stratigraphic boundary would influence the characterization of the soil spatial variation, i.e., the simulation results of the random fields, which can subsequently influence the slope stability results. To this end, Figure 5.3 compares the slope stability results (i.e., FS and sliding mass A) obtained from three different boundary conditions (i.e., DSB, PUSB and PLSB) based on a typical realization of random fields underlying the cohesion and the friction angle for the reference case. In general, under all the three conditions, the figure shows that the cohesion and friction angle fluctuate more heavily in the vertical direction than in the horizontal direction, since the vertical SOF is much smaller than the horizontal SOF (4 m vs. 40 m). In addition, the FS and the corresponding CSS are also shown in the figure. Although the FSs obtained from DSB, PUSB and PLSB conditions are very close (1.094, 1.046 and 1.065, respectively), the locations of the critical slip surfaces present relatively large differences, indicating that slopes with a nominally similar FS might result in quite different consequences. For example, when the traditional DSB is adopted, the slope might slide through the lower layer, which leads to a relatively large consequence. However, the slope fails with the critical slip surface passing through the slope toe when the PLSB is involved, which gives rise to a smaller consequence. Overall, we can conclude that the SBU would affect the system P_f and R results.

Probabilistic stability analysis of this slope is then performed using MCS. The sample size of MCS (i.e., N_{sim}) is very critical to the accuracy of the estimations of P_f and R, which herein is determined by a sensitivity study with N_{sim} varying from 100 to 10,000, as shown in Figure 5.4. It is observed from the figure that the mean value of FS, P_f and R keep nearly invariant as well as their errors when N_{sim} is greater than about 5,000. In particular, both the COVs of P_f and R are below 2.5% when N_{sim} is larger than 5,000, suggesting that a satisfactory accuracy has been obtained. Thus, based on the trade-off between the computational efficiency and accuracy, N_{sim}=5,000 is adopted in this study. Figure 5.5 shows the distributions of the sliding mass under DSB, PUSB and PLSB conditions based on the 5,000 MCS samples. As can be expected from Figure 5.3, the distributions of the sliding mass based on the three boundary conditions are quite different from each other. For instance, the sliding mass obtained from DSB tends to be normally distributed, whereas the result from PUSB is more like a lognormal distribution.

To gain more insights into the influence of the boundary condition on the sliding mass, Figure 5.6 further compares the average sliding mass obtained from different boundary conditions for various FS values. In general, the results increase very slightly with the increase of FS, except for the results from PLSB which are more sensitive to FS. The maximum and minimum results at various safety levels are obtained when using DSB and PUSB, respectively. The only exception is at the FS equal to unity, where the result from PLSB is minimum but very close to the result from PUSB. Nevertheless, all these indicate that the slope will have different failure mechanisms when different boundary conditions are involved. Additionally, the results from SSB, which take the stratigraphic uncertainty into account, are also shown in the figure for an intentional comparison with those obtained from DSB. Similarly, the results from SSB also show little variation with respect to the change of FS and are smaller than those obtained from DSB, suggesting that the traditional deterministic boundary analysis might overestimate the slope failure consequences, thus affecting the decision makers to propose economical prevention measures in engineering practice.

Figure 5.7(a) compares the cumulative distribution functions (CDFs) of FS obtained from DSB and SSB conditions. As shown in the figure, if FS is greater than approximately one, the P_f obtained from DSB may be overestimated, otherwise it can be underestimated, compared with the results obtained from SSB. However, the difference in P_f between SSB and DSB is minimal, as can be expected from Figure 5.3. Figure 5.7(b) shows the variations of the risks obtained based on DSB and SSB conditions with respect to various FSs, i.e., cumulative risk functions (CRFs). Similar to Figure 5.7(a), there is also a critical point (at approximately FS=0.95) where the risks obtained from SSB and DSB are nearly the same. However, what is different from the results in Figure 5.7(a) is that the risk difference between SSB and DSB is relatively larger than the difference of P_f shown in Figure 5.7(a). Again, this can be expected from the above analysis. Finally, it is interesting to find that the shape of CRF is very similar to the shape of CDF under both DSB and SSB because the average slope failure consequence is insensitive to FS (see Figure 5.6), and the risk R is estimated as the expected value of the product of P_f and C_m. This finding is also consistent with those in the literature such as **Xiao et al. (2016)** and **Li et al. (2016c)**.

5.5.2 Influence of $\rho_{c,\varphi}$ on slope failure results

From this subsection, various parametric studies will be performed to investigate the influence of statistics of soil properties on the slope failure probability P_f and risk R. The effect of the $\rho_{c,\varphi}$ is first investigated here. The value of $\rho_{c,\varphi}$ ranges from −0.7 to 0.5, which is suitable for many soil types based on the data reported by **Cho (2010)** and **Li et al. (2015a)** and is thus used in this study. Figure 5.8(a) compares the results of P_f for various values of $\rho_{c,\varphi}$ obtained from DSB and SSB conditions. Generally, the results from both conditions increase with the increase of $\rho_{c,\varphi}$. Meanwhile, when $\rho_{c,\varphi}$ is greater than approximately −0.35, the traditional probabilistic analysis that neglects the stratigraphic uncertainty may overestimate the P_f, whereas it is underestimated when $\rho_{c,\varphi}$ is less than approximately −0.35. Nevertheless, the difference in P_f between DSB and SSB is not large. Figure 5.8(b) shows the variations of risk assessment results obtained from DSB and SSB with respect to $\rho_{c,\varphi}$. Similar to Figure 5.8(a), both results from the two conditions present an increasing trend with respect to $\rho_{c,\varphi}$. However, there is no critical point, and the results by DSB tend to be overestimated for all values of $\rho_{c,\varphi}$. In addition, different from the results in Figure 5.8(a), the difference between DSB and SSB in risk is relatively larger than the difference in P_f, especially for highly positively correlated soils, indicating that decision makers should pay more attention to the consequences of conservative estimations from a traditional probabilistic analysis that neglects the stratigraphic uncertainty.

5.5.3 Influence of COVs on slope failure results

As recognized by many previous studies, statistical errors of soil properties may have significant influence on the slope reliability results (e.g., **Li et al. 2015a; Liu et al. 2017d**). Hence, Figure 5.9 shows probabilities and risks of slope failure for various COVs of cohesion and friction angle (i.e., COV_c and COV_φ). In the figure, COV_c and COV_φ vary from 0.1 to 0.7 and 0.05 to 0.2, respectively. These ranges were selected following **Li et al. (2015a)** and **Cho (2010)**.

Figure 5.9(a) shows the variations of failure probabilities associated with DSB and SSB with respect to COV_c. The results associated with DSB and SSB are in the same variation trends—both of them decrease slightly to a minimum and then increase sharply with the COV_c. The results from DSB begin to be larger than those by SSB when COV_c is greater than approximately 0.3, whereas they are very close to the results of SSB when COV_c is relatively small. Additionally, the difference between SSB and DSB increases with COV_c, but it is generally minimal in the considered range of COV_c. Figure 5.9(b) shows the risks associated with DSB and SSB for various values of COV_c. Obviously, the results estimated from DSB are overestimated for all values of COV_c considered herein. Similar to Figure 5.9(a), there is also a minimum at COV_c=0.3 for both DSB and SSB because the failure probability identified in Figure 5.9(a) reaches the minimum, while the estimated consequence is insensitive to COV_c. Overall, the influence of the stratigraphic boundary uncertainty on R is larger than the influence of the stratigraphic boundary uncertainty on P_f.

Figures 5.9(c) and (d) show the variations of failure probabilities and risks associated with DSB and SSB, respectively, with respect to COV_φ. Different from the effects of COV_c, the failure probabilities obtained from DSB and SSB increase with the increase of COV_φ, and the results with DSB are smaller than those with SSB in the considered range. The results with DSB would be larger than the results with SSB when COV_φ becomes larger than the upper limit (i.e., 0.2) considered herein. In addition, from Figure 5.9(d), there is a critical point (at about COV_φ=0.13), from which the size relationship between risks obtained from DSB and SSB is turned over, although both of the results increase with COV_φ, indicating that the results of DSB are more sensitive to COV_φ than the results of SSB. To conclude, comparing influences of COV_c and those of COV_φ, the slope failure probability and risk are more sensitive to COV_φ than to COV_c.

5.5.4 Influence of SOFs on slope failure results

To investigate the effects of spatial variabilities of soil properties on slope stability, Figure 5.10 shows the slope failure probabilities and risks associated with DSB and SSB for various SOFs. Following **Li et al. (2015a)**, the considered variation ranges of horizontal and vertical SOFs (i.e., δ_h and δ_v) are [10 m, 60 m] and [1 m, 6 m], respectively.

Figures 5.10(a) and (b) compare the slope failure probabilities and risks associated with DSB and SSB for various horizontal SOFs, respectively. According to

Figure 5.10(a), the failure probabilities obtained from both DSB and SSB decrease with the increase of δ_h , and the results associated with DSB are underestimated and overestimated when δ_h is greater than and less than 20 m, respectively. However, regarding the risks shown in Figure 5.10(b), both results are expected to present variation trends similar to those in Figure 5.10(a). What is different from Figure 5.10(a) is that the risks estimated based on DSB are much smaller than the risks based on SSB for all considered values of δ_h , and they can be underestimated by approximately 7%.

Figures 5.10(c) and (d) compare the slope failure probabilities and risks associated with DSB and SSB, respectively, for various vertical SOFs. Different from the effects of δ_h shown in Figure 5.10(a), the failure probabilities obtained from both DSB and SSB increase with the increase of δ_v, and the results associated with DSB are underestimated for all considered values of δ_v. In addition, the difference in P_f between DSB and SSB tends to be enlarged when δ_v is larger than 4 m. On the contrary, according to Figure 5.10(d), the risks estimated based on DSB are underestimated within the investigated range of δ_v. Totally, we can conclude that neglecting the stratigraphic boundary uncertainty would lead to conservative estimates of risk in spatially variable soils.

5.6 Discussions

The above results might be affected by the determination of the discrete random variable y underlying the stratigraphic boundary location. For example, both the number of values and the range of variation of the discrete random variable y would give rise to quite different probabilistic analysis results. Hence, this section further discusses the effects that the number of values and the variation range of the stochastic stratigraphic boundary have on the system failure probability and risk. For this purpose, another two models are considered here. In the first model, compared with the original one shown in Eq. (5.17), the variation range of the location of the stratigraphic boundary increases to [-1 m, 1 m], whereas the number of values for the random variable y here remains invariant, as well as the probability at each value. This model can be written as

$$p(y) = \begin{cases} 0.3, & y=1.0(\mathrm{m}) \\ 0.4, & y=0.0(\mathrm{m}) \\ 0.3, & y=-1.0(\mathrm{m}) \end{cases} \tag{5.17}$$

For the second one, the variation range of the location of the stratigraphic boundary is the same as the first one, but more possible numbers of values are utilized in this model (e.g., **Li et al. 2015a**). Similarly, the second model can also be written in the formula form as

$$p(y) = \begin{cases} 0.061, & y=1.0(\mathrm{m}) \\ 0.245, & y=0.5(\mathrm{m}) \\ 0.388, & y=0.0(\mathrm{m}) \\ 0.245, & y=-0.5(\mathrm{m}) \\ 0.061, & y=-1.0(\mathrm{m}) \end{cases} \tag{5.18}$$

Based on the above two models, a series of reliability and risk analyses were performed, for which the corresponding results are then compared with each other and with those obtained based on the model shown in Eq. (5.17). For a clear presentation of the study, analyses based on the first and second models here are numbered as Case-2 and Case-3, respectively, whereas the analysis based on the aforementioned model in Eq. (5.17) is numbered as Case-1.

Figure 5.11(a) compares the P_f values associated with the three cases for different values of δ_v. The slope reliability results based on the DSB condition are also shown in the figure for reference. The figure shows that the failure probabilities obtained based on all situations increase significantly with the increase in δ_v. The results associated with DSB are smaller than the results associated with SSB conditions (i.e., Case-1, Case-2 and Case-3), indicating the failure probabilities estimated based on DSB might be underestimated. In addition, compared with the results associated with Case-1, the failure probabilities associated with Case-2 are much larger, mainly for the following two reasons: (1) The variation range of the location of the stratigraphic boundary in Case-2 is two times the range in Case-1, which consequently increases the uncertainties. (2) The mean FS is more likely to decrease when the location of the stratigraphic boundary moves up and down, as Figure 5.12 shows. Moreover, curves associated with Case-2 and Case-3 indicate that the failure probabilities will decrease when a greater number of values are assigned to the discrete random variable y, i.e., in Case-3. This can be expected from Eqs. (5.17) and (5.18), where the stratigraphic boundary in Case-3 has more chance than the stratigraphic boundary in Case-2 to be located near the DSB, which subsequently increases the occurrence of larger FS values in Case-3, thereby decreasing the failure probabilities. In fact, the model in Eq. (5.18) is more reasonable and consistent with practice than the model in Eq. (5.17) since it is usually quite difficult for an experienced engineer to locate the stratigraphic boundary with an error so large as ±1 m.

Figure 5.11(b) compares the slope failure risks associated with the four cases for various vertical SOFs. Generally, the figure shows that the risks associated with all cases increase slightly as δ_v increases. However, different from the results in Figure 5.11(a), the risks associated with DSB are larger than the risks obtained based on the other cases, suggesting that the risks estimated based on DSB are overestimated. In addition, compared with Case-1, Case-2 may induce much smaller risks because the slope is prone to slide along a shallow slip surface when the location of the stratigraphic boundary moves up and down, although the FS values are smaller in this case. However, the slope is more likely to have a deep failure mechanism when the location of the stratigraphic boundary has more chance to be located near the DSB in Case-3, thereby inducing larger failure risks than Case-2.

Overall, different failure probabilities and risks can be obtained based on different stochastic models. Nevertheless, we can conclude that the failure probabilities and risks estimated based on DSB are underestimated and overestimated, respectively, thereby highlighting the necessity to incorporate the stratigraphic uncertainty into the probabilistic analysis of slope stability. Finally, the difference in the results in Case-1 and Case-3 is very small, which further validates the reasonability of the assumed model in Eq. (5.15).

5.7 Summary and conclusions

This chapter has explored the influence of the system SBU on the system failure probability and risk of a layered slope with spatially variable soil properties. Various comparisons between probabilistic analysis results (e.g., slope failure probability and risk) obtained from considering and neglecting the stratigraphic boundary uncertainty have been made for different cross-correlation coefficients, COVs and SOFs. Moreover, the influence of the discrete random variable model underlying the stratigraphic boundary location has been discussed. Several conclusions can be drawn from this study and are summarized as follows:

1. The location of the stratigraphic boundary has a significant influence on the slope failure mechanism. Although it may not influence the FS value of the slope too much, different stratigraphic boundary locations would give rise to significantly different failure modes or consequences and thus affect risk assessment.

2. For different safety levels, the average sliding mass estimated based on traditional DSB analysis is much larger than the average sliding mass estimated by SSB analysis, suggesting that the traditional DSB analysis might overestimate slope failure consequences, thereby affecting the decision makers to propose reasonable and economical prevention measures in engineering practice.

3. A difference generally exists between slope failure probabilities obtained

from DSB and SSB. The failure probabilities are not always underestimated or overestimated for different cross-correlation coefficients, COVs and SOFs, except for the considered range of the vertical SOFs, where the results estimated based on DSB are always underestimated. However, the difference between slope failure probabilities obtained from DSB and SSB conditions are generally small for different statistics, except at small values of COV_{φ}.

4. The stratigraphic boundary uncertainty significantly influences the risk assessment. Generally, the difference in slope failure risks estimated based on DSB and SSB is relatively larger than the difference in slope failure probabilities. In addition, the risks estimated based on DSB are overestimated for different statistics, except at small values of COV_{φ}, where the results are underestimated.

5. Although the adopted discrete random variable model can effectively characterize the uncertainty in the stratigraphic boundary, this model neglects the inherent geological uncertainty in soil strata. Hence, future studies should be directed to accounting for the inherent geological uncertainty.

Table 5.1 Statistics of soil properties for the baseline case

Soil properties	Mean	COV	Distribution	SOFs	Cross-correlation coefficient $\rho_{c\varphi}$
c_1 (kPa)	12	0.3	Lognormal	δ_h=40 m, δ_v =4 m	$\rho_{1,c\varphi}$=−0.5
φ_1 (°)	24	0.2	Lognormal	δ_h=40 m, δ_v =4 m	
γ_1 (kN/m³)	20	−	−	−	−
c_2 (kPa)	8	0.3	Lognormal	δ_h=40 m, δ_v =4 m	$\rho_{2,c\varphi}$=−0.5
φ_2 (°)	14	0.2	Lognormal	δ_h=40 m, δ_v =4 m	
γ_2 (kN/m³)	20	−	−	−	−

Note: The symbol "−" means not applicable.

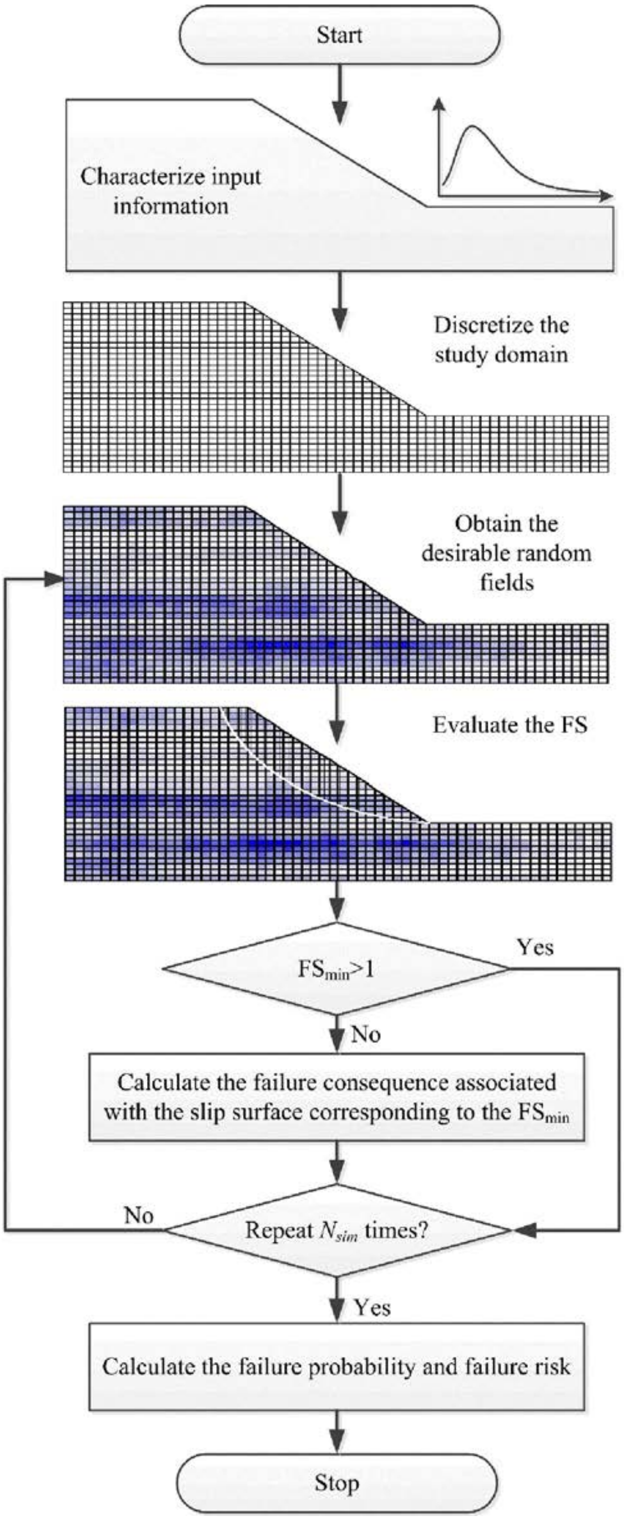

Figure 5.1 Flowchart for addressing the effect of the system SBU on P_f and R

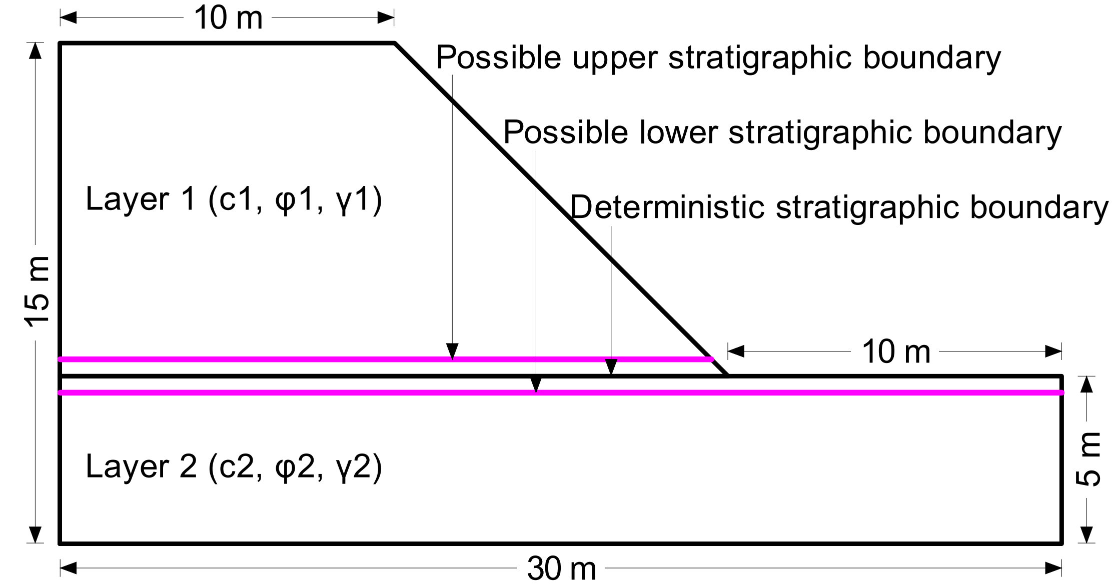

Figure 5.2 Geometry of the analyzed slope

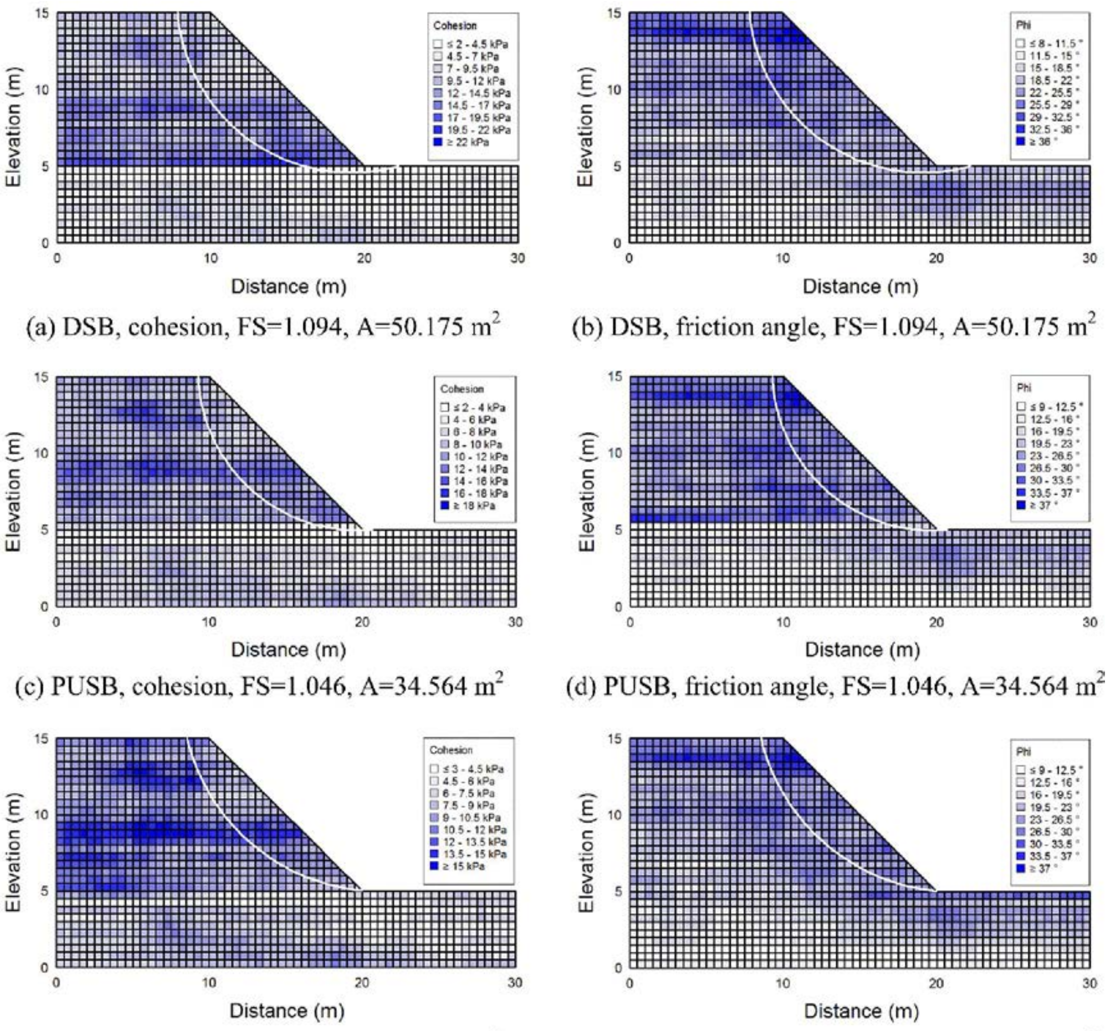

(a) DSB, cohesion, FS=1.094, A=50.175 m^2

(b) DSB, friction angle, FS=1.094, A=50.175 m^2

(c) PUSB, cohesion, FS=1.046, A=34.564 m^2

(d) PUSB, friction angle, FS=1.046, A=34.564 m^2

(e) PLSB, cohesion, FS=1.065, A=32.245 m^2

(f) PLSB, friction angle, FS=1.065, A=32.245 m^2

Figure 5.3 Typical realizations of random fields of cohesion and friction angle and the corresponding slope stability results for the baseline case

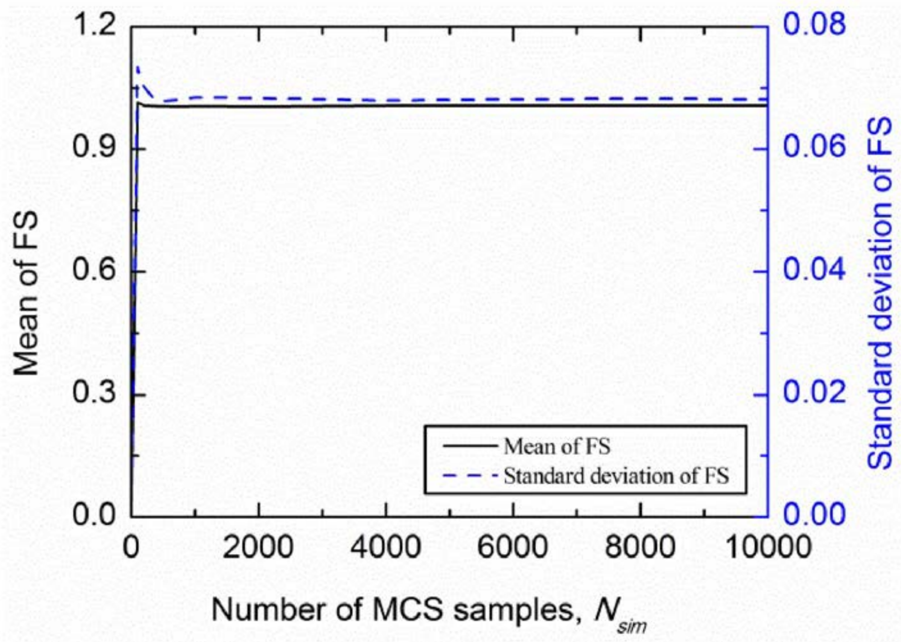

(a) Effect on FS

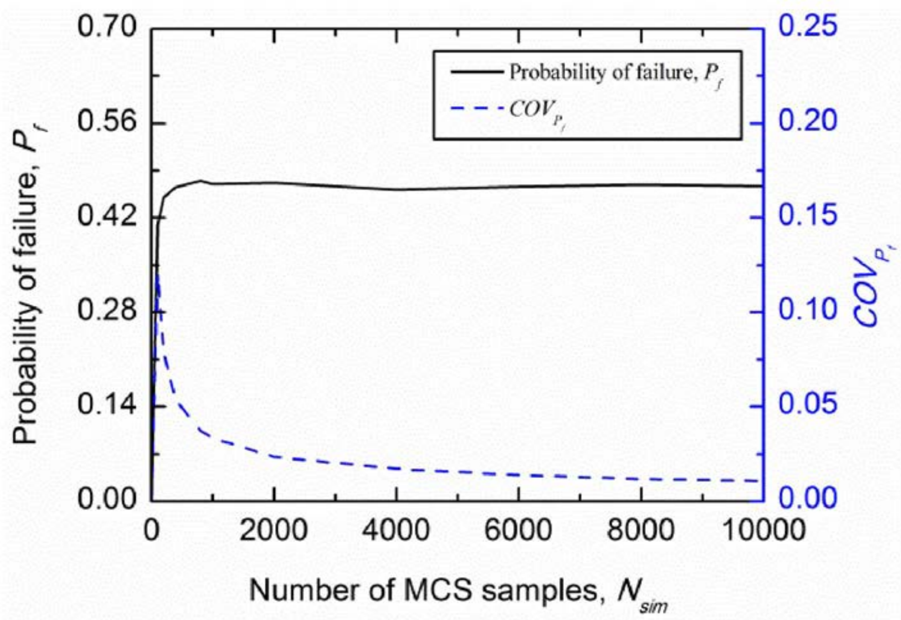

(b) Effect on P_f

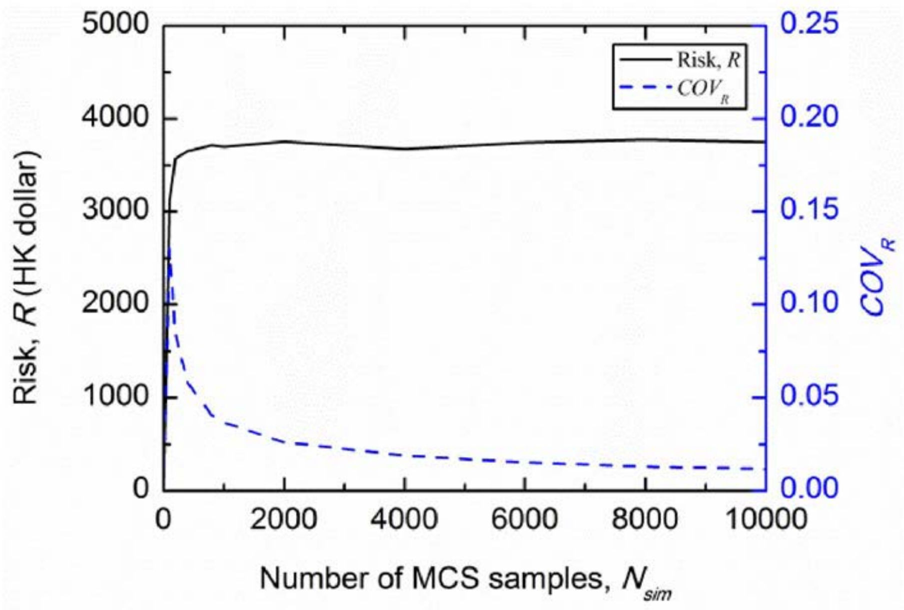

(c) Effect on R

Figure 5.4 Effect of the N_{sim} on FS, P_f and R for the baseline case

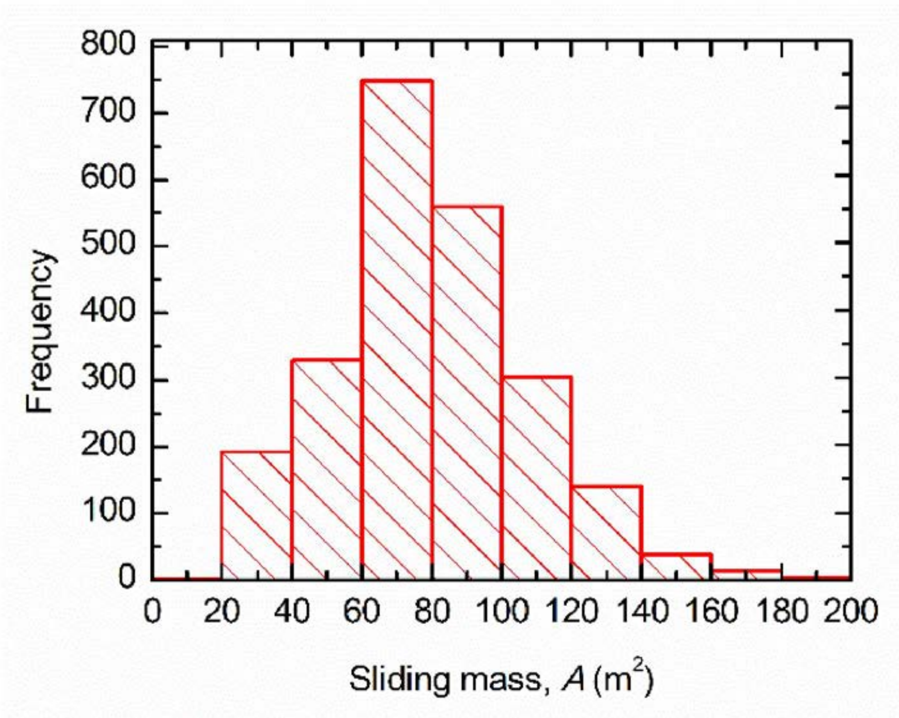

800
700
600
500
400
300
200
100
0
Frequency
0 20 40 60 80 100 120 140 160 180 200
Sliding mass, A (m2)

(a) DSB

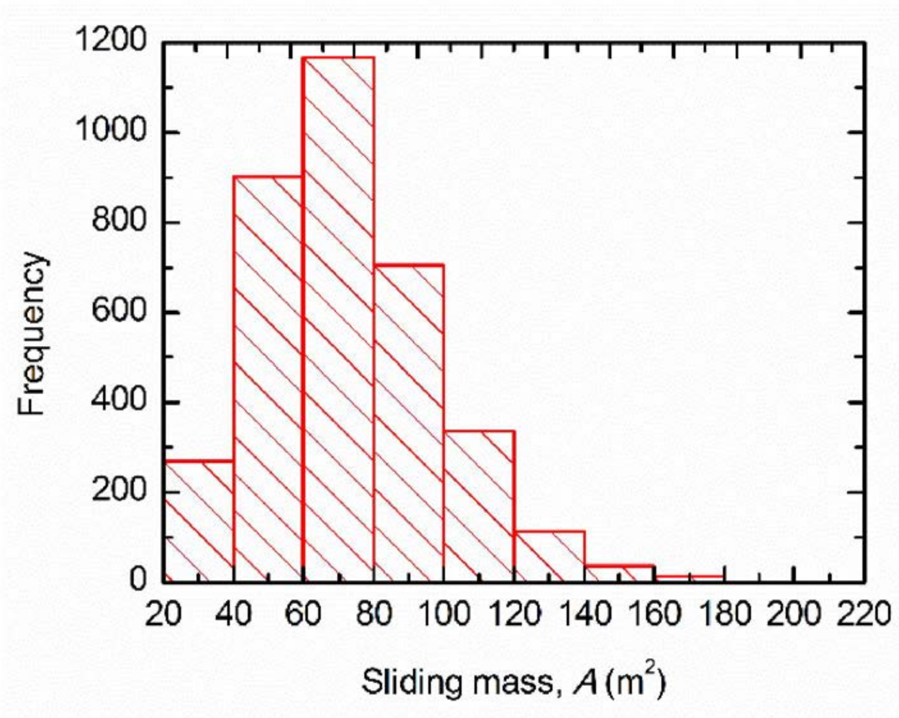

1200
1000
800
600
400
200
0
Frequency
20 40 60 80 100 120 140 160 180 200 220
Sliding mass, A (m2)

(b) PUSB

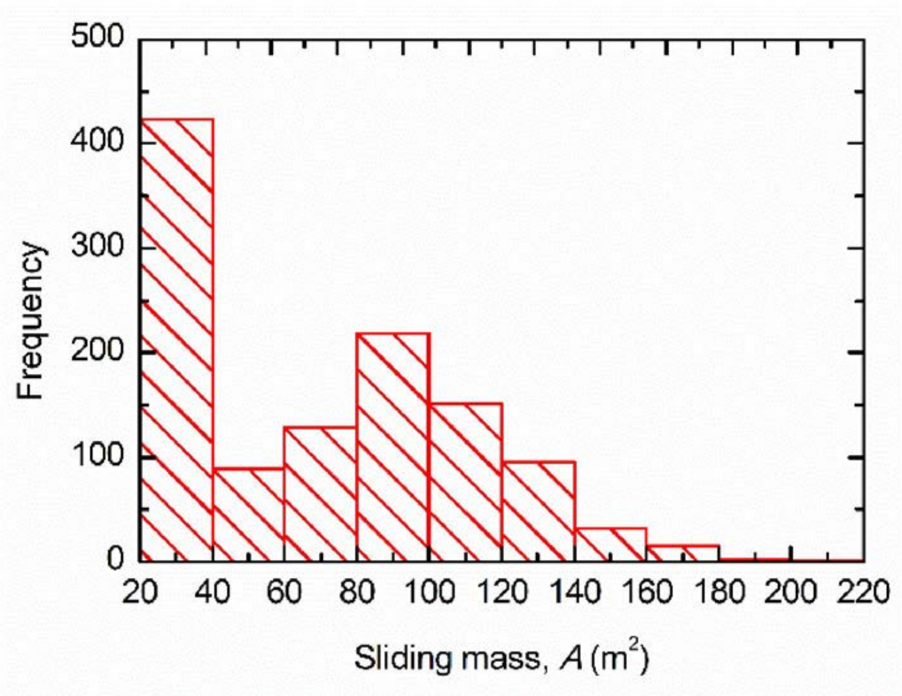

(c) PLSB

Figure 5.5 Histograms of sliding mass for the baseline case

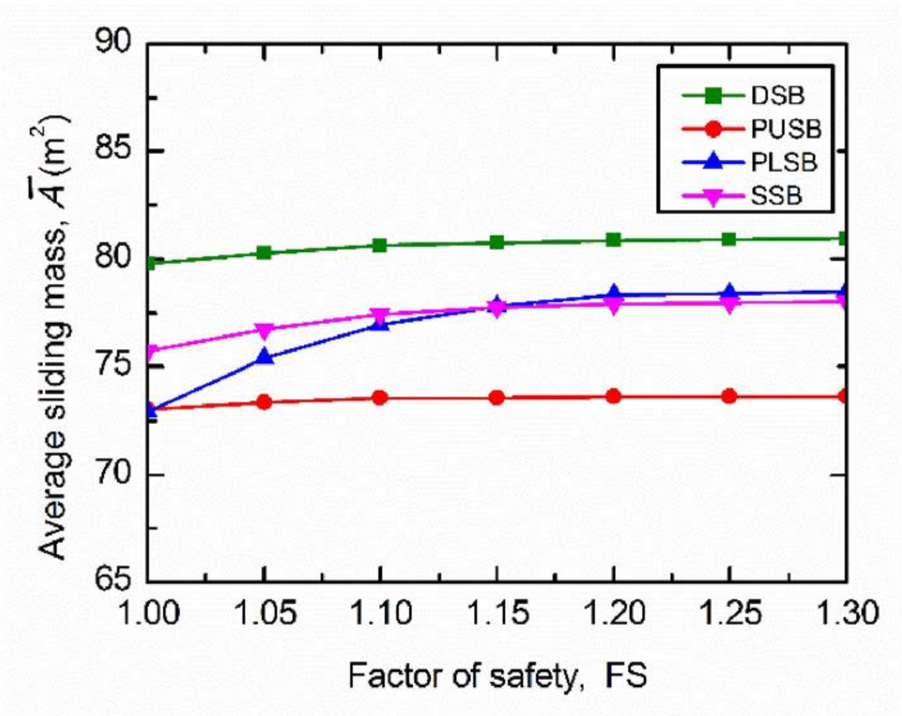

Figure 5.6 Average sliding mass at different safety levels

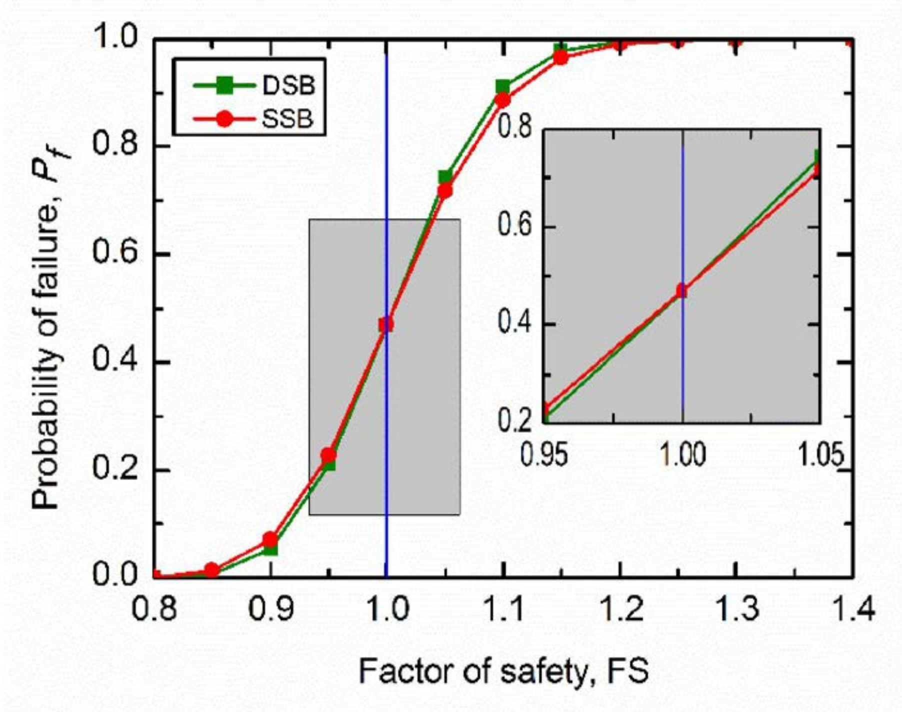

(a) CDF

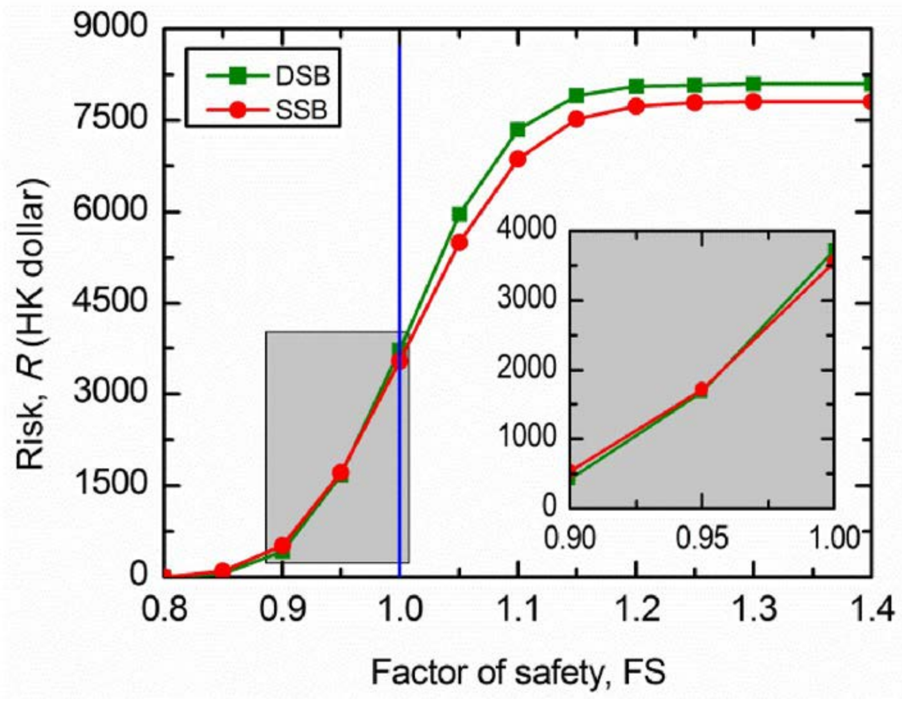

(b) CRF

Figure 5.7 CDFs and CRFs obtained from deterministic and stochastic stratigraphic boundary conditions

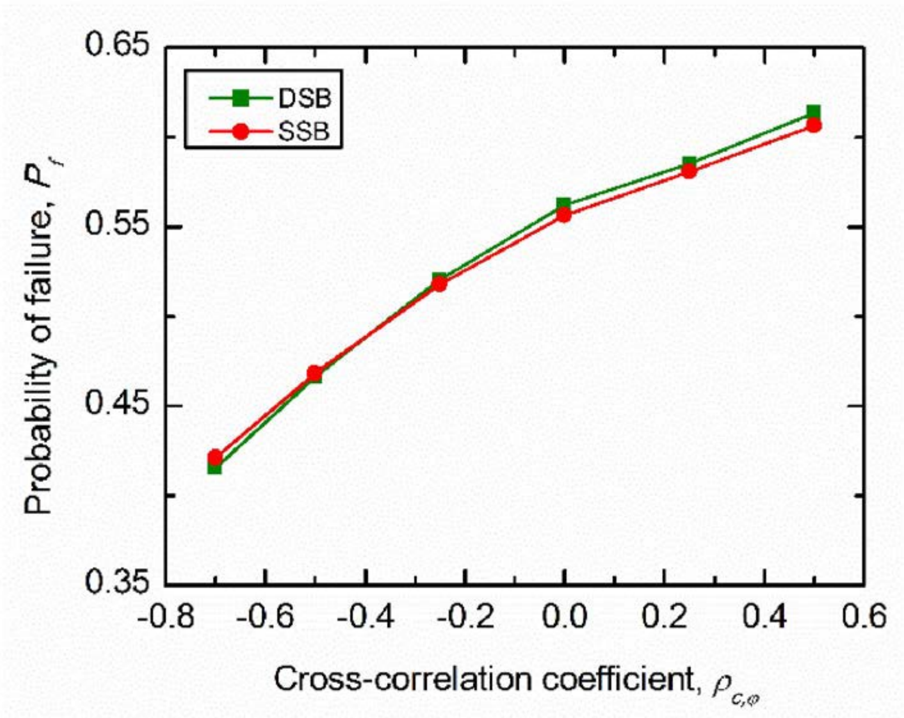

(a) Slope failure probability

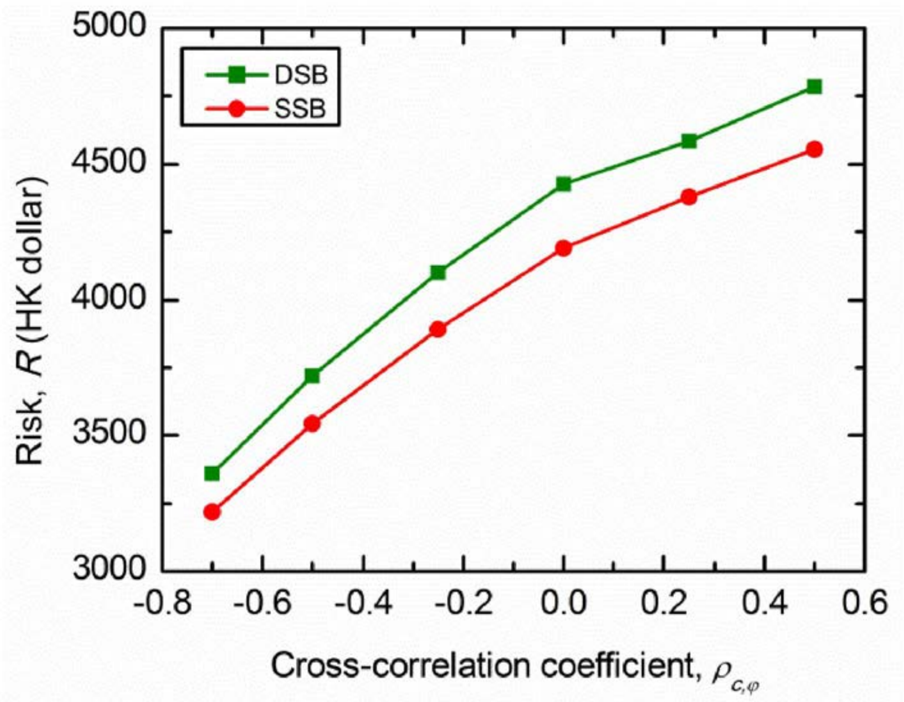

(b) Slope failure risk

Figure 5.8 Variations of P_f and R with $\rho_{c,\varphi}$

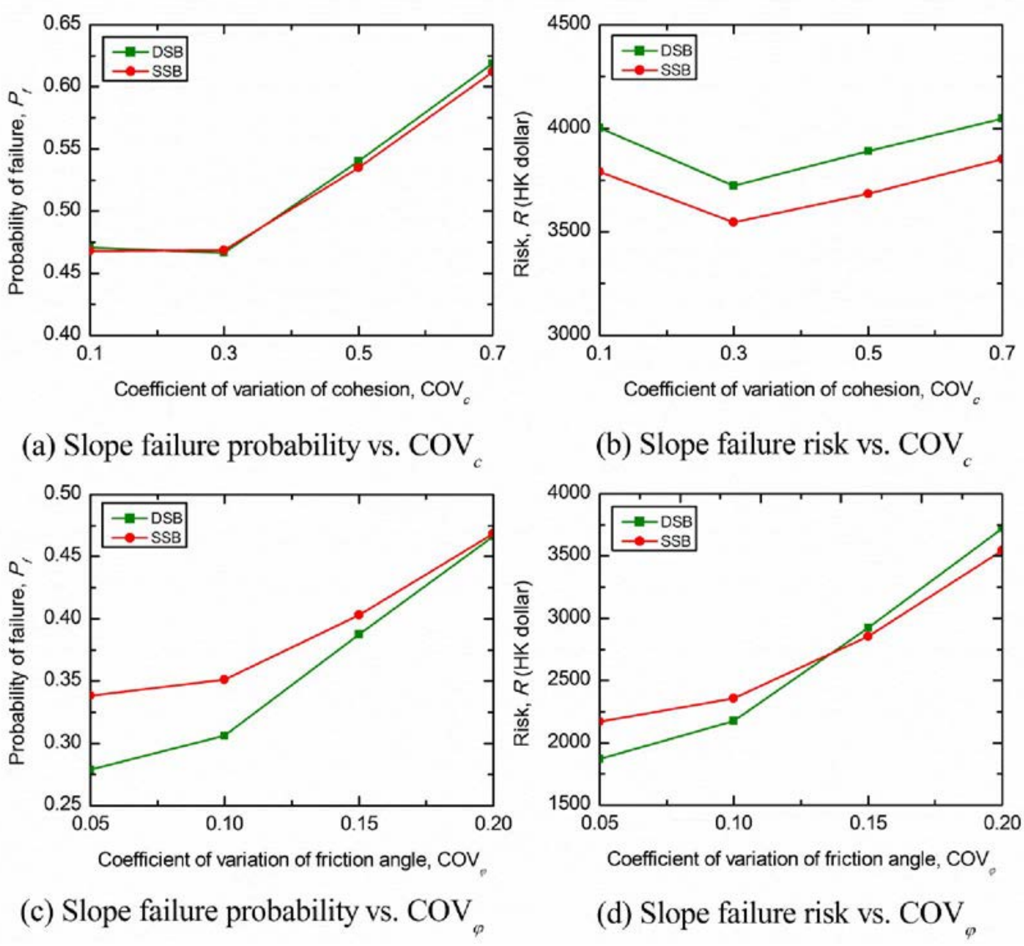

Figure 5.9 Variations of P_f and R with COVs

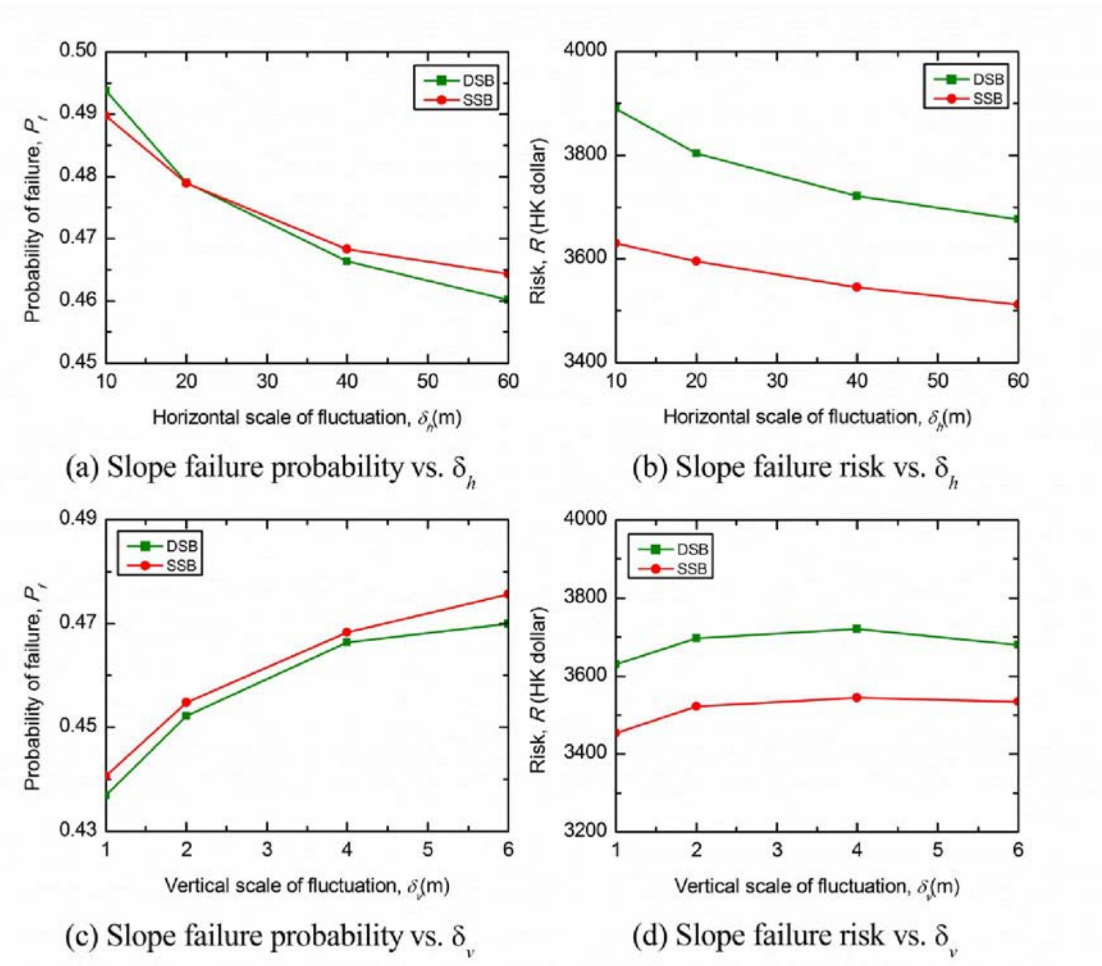

Figure 5.10 Variations of P_f and R with SOFs

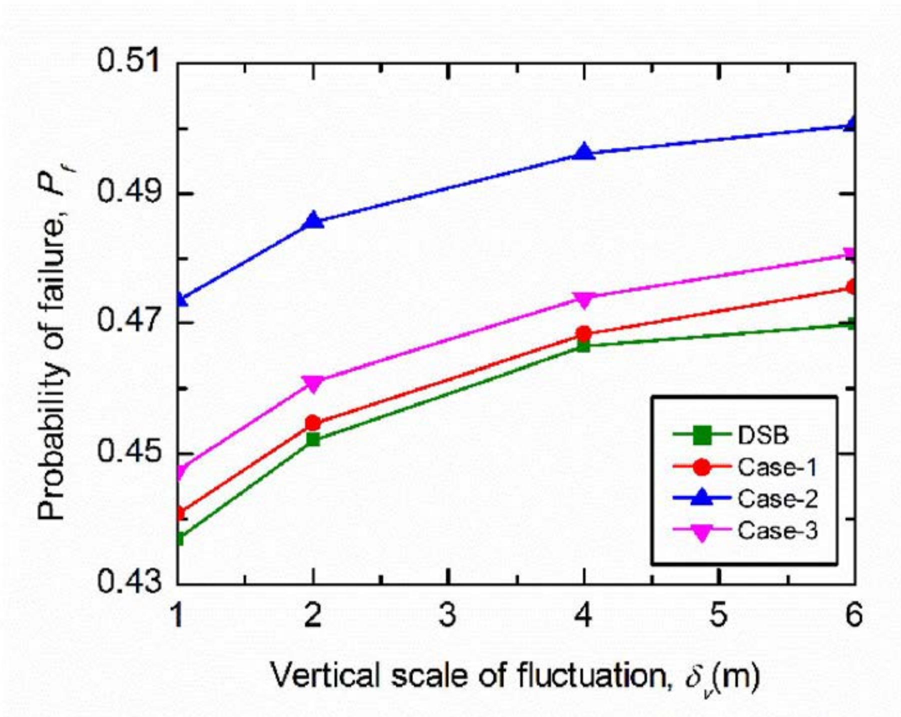

(a) Slope failure probability

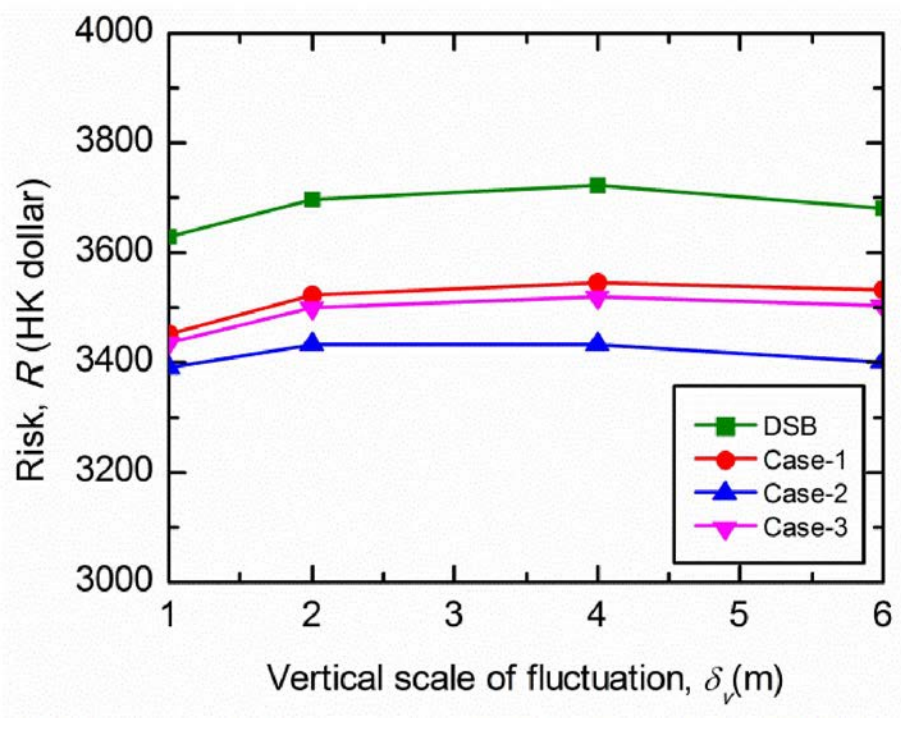

(b) Slope failure risk

Figure 5.11 Results of P_f and R for various situations

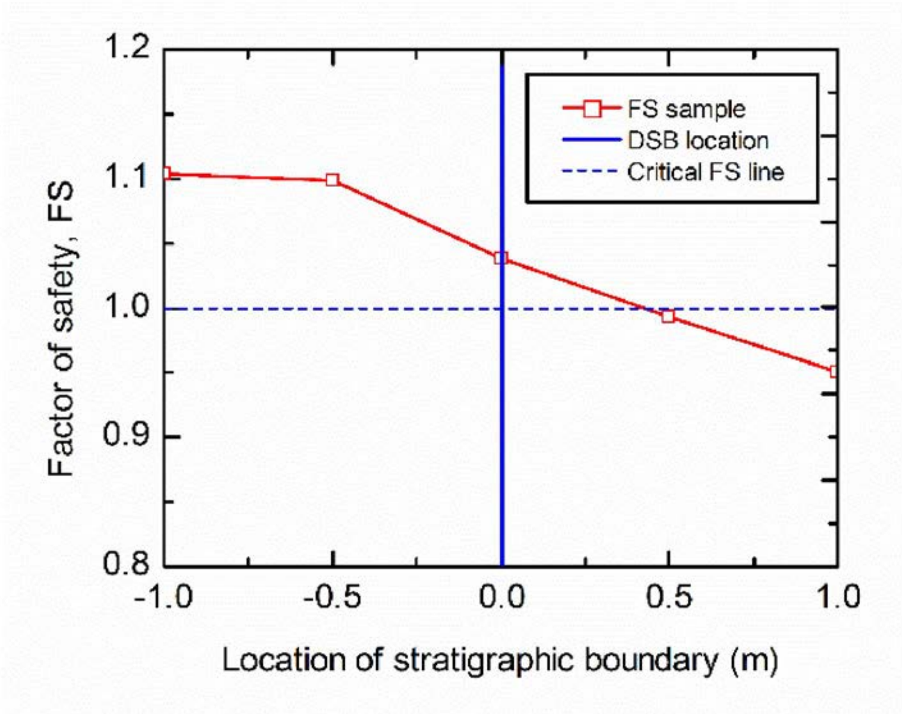

Figure 5.12 Variation of FS with location of the stratigraphic boundary using mean values

CHAPTER 6 EFFECT OF INHERENT STRATIGRAPHIC BOUNDARY UNCERTAINTY ON RELIABILITY ANALYSIS OF SLOPES IN SPATIALLY VARIABLE SOILS

6.1 Introduction

As mentioned in Chapter 1, there are mainly four types of uncertainties in geotechnical engineering practice: inherent physical uncertainty, system uncertainty, epistemic uncertainty and model uncertainty. However, in the literature, only the epistemic uncertainty and inherent spatial variability are frequently investigated, either simultaneously or individually (e.g., **El-Ramly et al. 2002; Griffiths and Fenton 2004; Sivakumar Bubu and Mukesh 2004; Cho 2007; Dasaka and Zhang 2012; Li et al. 2016a; Deng et al. 2017**). The reasons are mainly due to the facts that techniques to incorporate simultaneously all those uncertainties are usually complex and demanding and the influence of the epistemic uncertainty and inherent spatial variability is usually the most dominant compared with the others. Hence, without loss of generality and for convenience purpose, this study mainly aims at investigating the influence that both the epistemic uncertainty and the soil spatial variability have on slope stability analysis, with a particular emphasis on the effect of the stratigraphic boundary uncertainty (SBU) arising from limited site investigation data on the stability of a layered slope.

The motivation of this study is mainly two-fold and described as follows. First, to date, although considerable efforts (e.g., **Griffiths and Fenton 2004; Cho 2010; Suchomel and Mašín 2010; Wang et al. 2011; Jha and Ching 2013; Kim and Sitar 2013; Jiang et al. 2014a; Low 2014; Jiang et al. 2015; Li et al. 2015a; Li and Chu 2015; Pantelidis et al. 2015; Huang et al. 2017; Ji et al. 2017**) have been made by geotechnical reliability community to study the influence of soil spatial variability on slope reliability analysis, few of them have involved the treatment of non-stationary properties underlying the soil parameters because only nominally homogeneous slopes are studied as illustrative examples (e.g., **Griffiths et al. 2009; Wang et al. 2011; Jiang et al. 2015**). Instead, what they mainly want to emphasize is either exploring how soil spatial variability influences the slope stability or developing efficient algorithms to enhance the computation efficiency. For example, **Griffiths and Fenton (2004)** proposed a pioneering probabilistic analysis method for reliability analysis of slopes in spatially variable soils, namely RFEM (Random Finite Element Method), but only a cohesive slope example was studied because the author mainly wants to check the influence of soil spatial variability and local averaging on slope stability using RFEM. In addition, there are also many other researchers (e.g., **Cho 2010; Wang et al. 2011; Jiang et al. 2014a; Jiang et al. 2015; Huang et al. 2017**) devoting themselves to developing new or improving available efficient probabilistic analysis methods, but similarly, only simple slopes are investigated. However, in geotechnical engineering practice, there are always situations where natural or manmade slopes are composed of layered soils, of which the soil properties should be amenable to non-stationary random field treatment. Hence, probabilistic analysis of layered slopes in spatially variable soils has not been fully investigated. Herein, it should be noted that the author is not criticizing the limits of the aforementioned works for dealing with layered slopes, but appealing to our peers to pay more attention to these cases as they are much closer to real situations. Indeed, careful readers might also find that there are tracked recorders that the aforementioned works are applicable to far more complicated cases (e.g., **Li et al. 2015a; Li and Chu 2015; Jiang and Huang 2016; Deng et al. 2017**).

On the other hand, as mentioned above, some attention has been paid to the reliability analysis of layered slopes, but almost without exception, they all implicitly assume that the stratigraphic boundary between arbitrary two soil layers is a deterministic line or surface (e.g., **Li et al. 2015a; Li and Chu 2015**). This may be contradictory to real situations where the stratigraphic boundary is often characterized by a certain fluctuations. Likewise, the deterministic line or surface assumption would definitely underestimate the SBU, which will subsequently affect the slope stability concerned. The only exception might be the very recent work by **Liu et al. (2017c)**, where the influence of SBU on probability of failure (P_f) and risk assessment is investigated. However, the stratigraphic boundary in the work by **Liu et al. (2017c)** is still assumed to be a line, and the uncertainty associated with the stratigraphic boundary is simply considered by allowing the boundary to fluctuate in a limited range. This type of uncertainty actually belongs to the system uncertainty that is led by observers' errors. In other words, such uncertainty can be readily reduced by experienced geotechnical engineers. Additionally, as mentioned before and reported by **Liu et al. (2017c)**, the system uncertainty underlying the stratigraphic boundary has minimal effect on slope failure probability. Hence, if experienced geotechnical engineers can be involved in the initial period of site investigation, such system uncertainty along with the stratigraphic boundary can be easily reduced to an acceptable level. Nevertheless, despite the insignificance of the system uncertainty, the inherent fluctuating uncertainty or epistemic uncertainty of the stratigraphic boundary arising from limited site investigation data may significantly affect the slope stability, which however, remains an outstanding problem.

To address those two limitations in the literature and achieve the aim mentioned above, the key points are to appropriately simulate the aforementioned two types of uncertainties—inherent spatial variability of soil properties and inherent spatial fluctuations of the stratigraphic boundary. In terms of the soil spatial variability, it is relatively easy as many effective techniques available in the literature can be employed, such as the Cholesky decomposition method (e.g., **Li et al. 2015a**). However, as for the simulation of inherent spatial fluctuations of the stratigraphic boundary, a modified one-dimensional conditional Markov chain model (e.g., **Elfeki and Dekking 2001; Elfeki and Dekking 2005; Qi et al. 2016**) is used because it is conceptually simple, geologically interpretable and computationally efficient, although some geostatistical methods (e.g., **Deutsch and Journel 1992**) can also work for this purpose. With these purposes in mind, the remainder of this chapter is outlined as follows. Sections 6.2 and 6.3 introduce respectively the simulation methodologies for characterizing the SBU and inherent spatial variability of soil properties, followed by the numerical implementation procedure of the proposed method in Section 6.4. Thereafter, in Section 6.5, a two-layered soil slope is taken as an illustrative example to investigate the influence of the two types of uncertainties on slope stability using the suggested method. Finally, Sections 6.6 and 6.7 present some discussions and conclusions from this study, respectively.

6.2 One-dimensional conditional Markov chain model for characterizing SBU

Conditional Markov chain model is a random process formed by conditioning the ordinary Markov chain model on some future states such that on the chain the next state depends not only on the present state but also on the future states (e.g., **Elfeki and Dekking 2001)**. Because it allows the consideration of future states, this model can be easily used in combination with borehole data to reduce modelling uncertainty. Additionally, the model has at least the following three advantages: (1) It reserves general properties of ordinary Markov chain model that is conceptually simple and easily implemented; (2) It can be explicitly expressed, which makes it computationally efficient; (3) It can deal with any number of states, and is specially suitable for simulation of geological formations (e.g., **Elfeki and Dekking 2005; Qi et al. 2016**). As such, the model is used in this study to simulate the SBU based on limited borehole data, and it is briefly introduced as follows.

6.2.1 One-dimensional Markov chain theory

A Markov chain is a random process satisfying the following requirement: the next state on the process depends only on the current state and is independent of those states in the past (First-order Markov property is implicitly considered here). Hence, suppose a Markov process consists of *n* random variables $\{Z_1, Z_2, \cdots, Z_n\}$ taking state values from the set $\{S_1, S_2, \cdots, S_m\}$ (*m* is the number of states), there will be

$$P(Z_i = S_k | Z_{i-1} = S_l, Z_{i-2} = S_p, \cdots, Z_1 = S_q) = P(Z_i = S_k | Z_{i-1} = S_l) = p_{lk} \quad (6.1)$$

where $P(Z_i = S_k | Z_{i-1} = S_l, Z_{i-2} = S_p, \cdots, Z_1 = S_q)$ is the probability that $Z_i = S_k$ when $Z_{i-1} = S_l, Z_{i-2} = S_p, \cdots, Z_1 = S_q$; $P(Z_i = S_k | Z_{i-1} = S_l)$ is the probability that $Z_i = S_k$ when $Z_{i-1} = S_l$; p_{lk} is the one-step probability of transition from state S_l to S_k, which is taken from the one-step transition probability matrix (TPM) $\boldsymbol{p} = (p_{lk})_{m \times m}$ that saves the one-step probability of transition between any two states. It should be noted that here we implicitly assume that the Markov chain is homogeneous, which indicates the one-step transition probability is independent of the step, i.e., $P(Z_i = S_k | Z_{i-1} = S_l) = P(Z_{i+1} = S_k | Z_i = S_l)$. This assumption has been widely used in the literature (e.g., **Elfeki and Dekking 2001; Elfeki and Dekking 2005; Qi et al. 2016**).

To facilitate better understanding of the application of the Markov chain model for SBU modelling in this study, it is worthwhile to point out that the state values are characterized by vertical locations and the steps are denoted by a sequence of horizontal distances. For example, Z_1=the vertical location of stratigraphic boundary between 0 m and 0.5 m, Z_2=the vertical location of stratigraphic boundary between 0.5 m and 1.0 m. Note that, for convenience purpose, the stratigraphic boundary in each step is assumed to be a horizontal line. This is reasonable because generally the fluctuation of the stratigraphic boundary will not be significant within a short distance (e.g., in the scale of decimeter).

6.2.2 Conditioning one-dimensional Markov chain on future states

To effectively incorporate borehole data into Markov chain model, **Elfeki and Dekking (2001)** proposed to conditioning the Markov chain on future states (i.e., borehole data) such that on the chain the next state depends not only on the present state but also on the future states. As an illustration, Figure 6.1 schematically show the conditional simulation process, where each cell represents a Markov step, cells on the two extreme ends filled with blue indicate steps with known states obtained from borehole data, and cells in between are steps whose states are to be simulated. If a forward Markov process is adopted, the state of the left cell is considered as initial state, while the state of the right cell is taken as the future state. Conditional Markov process can thus be simulated based on these states. Suppose cells filled with yellow have been simulated and the i^{th} cell is going to be simulated, so given the states of the $(i\text{-}1)^{\text{th}}$ and the last step, we can know the probability that the i^{th} step takes the state of S_k (e.g., **Elfeki and Dekking 2001**) as

$$P\left(Z_i = S_k \middle| Z_{i-1} = S_l, Z_n = S_p\right) = \frac{p_{lk} p_{kp}^{(n-i)}}{p_{lp}^{(n-i+1)}} \tag{6.2}$$

where $p_{kp}^{(n-i)}$ is the $(n\text{-}i)^{\text{th}}$-step probability of transition from state S_k to S_p; $p_{lp}^{(n-i+1)}$ is the $(n\text{-}i\text{+}1)^{\text{th}}$-step probability of transition from state S_l to S_p. Both $p_{kp}^{(n-i)}$ and $p_{lp}^{(n-i+1)}$ can be easily calculated from the one-step TPM $\boldsymbol{p}$, and the reader is referred to **Elfeki and Dekking (2001)** and **Qi et al. (2016)** for details. It should be noted that Eq. (6.2) only conditions on two boreholes, while there would be more than two boreholes in real situations. For this problem, this study simulates the stratigraphic boundary segment by segment until all boreholes are used. Herein, the segment indicates the horizontal interval constituted by two adjacent boreholes.

6.2.3 Estimation of transition probability matrix

It is known from above that estimation of the one-step TPM $\boldsymbol{p}$ is a prerequisite for using the conditional Markov chain model. Theoretically, the TPM can be estimated directly from borehole data, such as the tally matrix used by **Elfeki and Dekking (2001)**. However, for the simulation problem herein, it is rather difficult to count the number of transitions between different states because the stratigraphic boundary data obtained from all boreholes is rather discrete. To this problem, a practical method adapted from **Elfeki and Dekking (2001)** and **Qi et al. (2016)** is suggested in this section and is described as follows.

First, the basic idea that the TPM is assumed to be diagonally dominant with identical off-diagonal elements is accepted from **Elfeki and Dekking (2005)**. This suggests that a state transiting to itself is dominant, which is consistent with general rules of formation of sequence stratigraphy. In addition, the identical off-diagonal elements right reflect that there is no sufficient information to support the transition from one state to another. Within this assumption, the off-diagonal elements are calculated as $p_{ij} = (1 - p_{ii})/(m - 1)$ $(i \neq j)$, where p_{ii} is determined from some candidate probability values that are relatively large, such as $\{0.60, 0.62, \cdots, 0.98\}$ used in the following analysis.

Borehole data is then used to identify the optimal value of p_{ii} from the candidate values. According to **Qi et al. (2016)**, the optimal value is the one that maximizes the occurrence of the observed scenario given the conditional information. This means, for the example shown in Figure 6.2, the optimal p_{ii} should ensure that the likelihood of the i^{th}, j^{th} and k^{th} cells simultaneously and respectively taking the states S_l, S_k and S_p is the largest given the 1st and n^{th} states. However, they did not consider the dependence between states at different cells, i.e., they evaluate the probability that each cell takes a corresponding state independently. Seriously, if a state at one cell (or borehole) is known, it should also be considered as conditional information for estimating the state at another cell. Hence, the likelihood of the occurrence P_l of the observed scenario given the conditional information in Figure 6.2 should be expressed as

$$P_l = \mathrm{P}\left(Z_i = \mathrm{S}_l, Z_j = \mathrm{S}_k, Z_k = \mathrm{S}_m \middle| Z_1 = \mathrm{S}_q, Z_n = \mathrm{S}_p\right)$$

$$= \mathrm{P}\left(Z_i = \mathrm{S}_l \middle| Z_1 = \mathrm{S}_q, Z_n = \mathrm{S}_p\right) * \mathrm{P}\left(Z_j = \mathrm{S}_k \middle| Z_i = \mathrm{S}_l, Z_n = \mathrm{S}_p\right)$$

$$* \mathrm{P}\left(Z_k = \mathrm{S}_m \middle| Z_j = \mathrm{S}_k, Z_n = \mathrm{S}_p\right)$$

$$= \frac{p_{lp}^{(n-i)} \cdot p_{ql}^{(i-1)}}{p_{qp}^{(n-1)}} * \frac{p_{kp}^{(n-j)} \cdot p_{lk}^{(j-i)}}{p_{lp}^{(n-i)}} * \frac{p_{mp}^{(n-k)} \cdot p_{km}^{(k-j)}}{p_{kp}^{(n-j)}} \quad (6.3)$$

For each candidate value of p_{ii}, a value of P_l will be calculated based on Eq. (6.3), and the candidate corresponds to the maximum P_l will be used to consitute the final TPM for the given borehole layout. The effectiveness of the estimated TPM can be checked by the "Engineering approach" suggested by **Elfeki and Dekking (2005)**, which will be illustrated in the example section later. Additionally, it should be noted that for a given borehole layout, all the boreholes are used to estimate the TPM, while the simulation of the conditional Markov chain is following the process described in Section 6.2.2.

6.3 Random field modeling of spatially variable soil properties

The method (procedure) suggested in Section 5.2.1 is used. Repeating this procedure N_{sim} times will give N_{sim} simulations of the non-stationary random field, based on which slope reliability analysis using Monte Carlo simulation (MCS) can be performed.

6.4 Numerical implementation

To facilitate the understanding of the proposed approach and its applications in geotechnical engineering practice, this section introduces in detail the implementation tools and procedure of the approach.

6.4.1 Implementation tools and strategies

The basic tools used in this study are MATLAB and ABAQUS. MATLAB software is used to control the whole probability analysis using an in-house code, while ABAQUS is mainly employed for evaluating the slope stability, i.e., obtaining the factor of safety (FS). In addition, MATLAB is also used to equip ABAQUS with the ability to consider the soil spatial variability in slope stability analysis. This can be achieved by directly revising the ABAQUS input file suffixed by ".inp" based on the random fields underlying the soil properties using a programming language such as MATLAB. The reason is because by using ABAQUS, the FS is deduced from the ABAQUS results file suffixed by ".odb" that can be obtained through the evaluation of the ".inp" file by the ABAQUS/Standard. For illustration purpose, Figure 6.3 schematically shows the strategies employed in this study for enabling the ABAQUS to consider the spatial variability of soil properties. In general, three steps are involved and are detailed as follows:

1. *Preparation*. In this step, one needs to prepare a data file consisting of a set of random fields data that can be generated by any kind of code, such as the MATLAB code by the author. Meanwhile, an ABAQUS input file (e.g., the "Slope.inp" file here) including information of slope geometry and FEM mesh should also be prepared, which can be obtained by directly coding in a Python editor or through the ABAQUS/CAE model, whichever is more convenient for yourself.

2. *Analysis*. This is the major step that consists of incorporating the random fields data into the "Old" "Slope.inp" file to obtain the "New" "Slope.inp" file and invoking the ABAQUS solver to evaluate the "New" "Slope.inp" file to finish the slope stability analysis. Because the built-in language in ABAQUS is Python, so an MATLAB-Python interface function is preferably used by the author to realize the former purpose. As for the latter one, an MATLAB-ABAQUS interface function is coded to submit the "New" "Slope.inp" file to the ABAQUS solver for evaluating the slope stability.

3. *Results*. After finishing step (2), an ABAQUS result file "Slope.odb" will be automatically generated. This file saves all information of FEM calculation results such as stress and displacement at each node, which however, should be read by ABAQUS Python script because of the built-in characteristic of the data structure in the file. Hence, another MATLAB-Python interface function is required.

With the above strategies in mind, a full MCS can be easily performed to evaluate the P_f while considering both the inherent strategraphic boundary uncertainty and spatial soil variability. It should be noted that since the strategraphic boundary uncertainty only affects the distributions of different soil types, the major input of the whole analysis is still the random fields data for each MCS realization, and thus how to incorporate this type of uncertainty into ABAQUS is unnecessary. Detailed procedure for a full MCS will be introduced in the following section.

6.4.2 Implementation procedure

As mentioned above, this section introduces the detailed implementation procedure of the proposed method step by step. In general, the whole procedure mainly consists of 9 steps, which can be quickly learned from Figure 6.4. By referring to this figure, each step is detailed as follows:

1. Collect data that is necessary for slope stability modelling, including but not limited to slope geometrical parameters (e.g., slope height and slope angle), stratigraphic boundary information and soil physical-mechanical parameters (e.g., cohesion c and friction angle φ). In addition, determine the corresponding statistics such as means, coefficients of variation (COVs), distributions, SOFs and ACFs for those spatially varied soil parameters that are amenable to random field treatment.

2. Build an initial FEM model using the available slope geometrical parameters and the mean values of the spatially varied soil parameters with the help of ABQUS/CAE. Likewise, the basic model information, which includes but is not limited to slope geometry, FEM mesh and constitutive relation of soil, is saved in an ABAQUS input file suffixed by ".inp", e.g., "Slope.inp" herein. It should be noted that in this file, the soil parameters are constant over the slope domain and the SBU has not yet been considered. Hence, to differentiate this file with the ".inp" file that considers both the SBU and inherent spatial variability of soil properties, the "Slope.inp" herein is marked by "Old" in case of confusing.

3. Interpret the stratigraphic boundary information obtained from some specific boreholes into Markov states. Then, use the method suggested in Section 6.2.3 to estimate the Markov chain TPM. The Markov states at unknown locations finally can be simulated based on the known states and the TPM using the method suggested in Section 6.2.2. All Markov states, including the known ones and those simulated ones, contribute together to form the stratigraphic boundary. Herein, it is worthwhile to point out that, for the purpose of convenience, the Markov step used in this study is kept consistent with the size of the finite element in FEM model.

4. Incorporate the simulated stratigraphic boundary (also known as Markov chain) into the slope stability model such that the entire slope domain is divided into several non-overlapped subdomains to differentiate different soil layers.

5. Discretize each subdomain into some finite random field elements and simulate the spatial variability of soil properties in each domain using the CDT introduced in Section 6.3. Likewise, a typical realization of random fields of soil properties while considering the SBU is obtained. Note that the random field element size is the same as that of finite element, which is again for the convenient purpose.

6. Incorporate the random field data obtained above into the initial FEM model to form a new model that is capable of considering both the SBU and inherent spatial variability of soil properties. This can be achieved by directly replacing the mean soil properties in the ABAQUS input file (i.e., the "Old" "Slope.inp") with the corresponding random field values through calling the aforementioned MATLAB-Python interface function. To differentiate the new model with the original one, the new model is saved as "Slope.inp" but marked by the tag "New" (see Figure 6.3).

7. Submit the "New" "Slope.inp" file to the ABAQUS solver for the evaluation of slope stability with the help of an inhouse MATLAB code—MATLAB-ABAQUS interface function, which finally results in an ABAQUS results file, named "Slope.odb"

for example.

8. Extract the FS value from the "Slope.odb" file using another MATLAB-Python interface function.

9. Perform MCS simulation. Repeat steps (3)-(8) for N_{sim} times will generate N_{sim} FS values, based on which statistical analysis of FS can be performed and the P_f of slope stability considering both SBU and inherent spatial variability of soil properties can also be calculated by dividing the number (e.g., N_f) of FS values less than 1 by N_{sim}, i.e., $P_f = N_f / N_{sim}$.

6.5 Illustrative example

In this section, the proposed approach is applied to analyze the stability of a layered soil slope, based on which the effectiveness of the approach is verified and the influence of the inherent SBU on slope stability is investigated. In particular, various borehole layout schemes are designed to explore the influence of the number and locations of the boreholes on slope stability. Details are described as follows.

6.5.1 Example description and deterministic slope stability analysis

The slope to be investigated is adapted from the work by **Liu et al. (2017c)**, and its geometry is schematically shown in Figure 6.5. As can be seen from the figure, the slope has a height of 10 m and an angle of 45° and the soil mass of the slope extends to 15 m below the slope top. In addition, the slope is composed by two types of soils—clay and sand, and the sand layer is laid beneath the clay layer. The stratigraphic boundary between the two soil layers is generally unknown without enough site investigation data. Hence, if only few data is available in hand, for example three boreholes (numbered as ZK1 to ZK3) as shown in Figure 6.5, the boundary is very likely to be considered as a horizontal line or a deterministic line (e.g., the blue dash line in Figure 6.5) located 10 m below the slope top by engineers, which is the common practice in slope design. However, the real situation could be that the boundary is a curved line (e.g., the red solid line in Figure 6.5) with a certain degree of fluctuations due to complex geological and environmental process of deposition. Likewise, the deterministic line assumption has no doubt underestimated the uncertainty associated with the stratigraphic boundary, thus affecting the stability assessment of the slope.

Figure 6.6 shows slope stability results under the two boundary conditions based on the mean values of soil parameters in Table 6.1 where cohesion c and frictional angle φ are considered spatially variable with a zero cross-correlation coefficient $\rho_{c\varphi}$ and unit weight γ, elastic modulus E and Poisson's ratio υ are assumed to be constants. Obviously, the slope stability results are quite different in terms of both FS values and critical slip surfaces when different stratigraphic boundary conditions are used. Firstly, the slope will be considered less stable if the boundary is assumed to be a line compared with the real situation (i.e., 1.163 vs. 1.248), which would finally lead to a conservative design in geotechnical engineering practice. Secondly, the slope failure consequence would be underestimated when the boundary is simplified as a line, because under this assumption the slope tends to slide along a shallow surface, while the slope is more likely to have a deep failure mode. As such, it is of great practical significance to consider the SBU in stability analysis of this kind of slope.

6.5.2 Borehole data

To model the SBU, a certain amount of borehole data is a prerequisite. Therefore, nine boreholes are designed in this section, and the layout of the boreholes is schematically shown in Figure 6.7. In general, it can be seen from the figure that the boreholes are marked by three different colors. This is mainly to reflect the real geotechnical site investigation process that usually starts with a preliminary exploration, then a detailed exploration followed by an added exploration. With this idea in mind, the boreholes here are designed in the following three phases. In Phase I, three boreholes (i.e., boreholes numbered as ZK1-3 and marked by blue) are preliminarily drilled at the slope left boundary, slope crest and slope toe, respectively, which is often the case when no sufficient prior information is available. One can see that the horizontal interval between two adjacent boreholes in this phase is relatively large, because we want to cover all potential influence areas as much as possible. Then, in Phase II, another two boreholes, numbered as ZK4 and ZK5 and marked by yellow, are placed in the intervals among the three boreholes in Phase I. The purpose is to explore more details about the stratigraphic information in the investigation area, because the borehole interval in Phase I is generally large, which may miss some important changes in stratigraphic boundary. For example, the three boreholes in Phase I reveal almost the same stratigraphic information, which, obviously, does not catch the variation trend of the real boundary and would be misleading. Finally, in Phase III, to gain more insights into the fluctuation of the real stratigraphic boundary (RSB), four more boreholes marked by green (i.e., ZK6-9) are located at the intervals that are formed by the boreholes drilled in Phase I and II.

All boreholes from the three phases constitute the available data for SBU modelling herein. The revealed stratigraphic information from all boreholes can also be noticed from Figure 6.7 by referring to the simplified stratigraphic boundary (i.e., the red broken line) that is simplified from the real boundary in Figure 6.5. In addition, it should be noted that in practical engineering there might not be so many boreholes with such a high density, hence such design of boreholes herein is mainly for research purpose, which is expected to work out a useful guidance for an effective borehole design. To this end, several borehole layout schemes are further designed based on the nine boreholes to investigate the influence of borehole location and borehole number on SBU modelling and thus on the slope stability. The schemes are summarized in Table 6.2, where the countermark indicates the corresponding borehole is included in a scheme. In other words, each scheme is actually a combination of several boreholes in Figure 6.7. However, it is noted that the boreholes ZK1 and ZK3 are included in all schemes. This is because of the prerequisite for using the conditional Markov chain analysis, as described in Section 6.2. For each layout scheme, the SBU can be simulated using the suggested method in Section 6.2.2, as will be introduced in the following.

6.5.3 One-dimensional Markov chain conditioned on borehole data for SBU modelling

6.5.3.1 Estimation of TPM

To simulate the SBU based on the abovementioned borehole data, the one-step TPM should be firstly estimated following the suggested method in Section 6.2.3. Note that the Markov step length herein is set as 0.5 m, which is consistent with the random field element size as well as the finite element size, as shown in Figure 6.7. The reason for choosing this value is mainly two-fold: (1) The soil strata will generally not show very significant variations within a very short distance; (2) Although the step length has a significant effect on the estimation of the TPM, the simulated Markov chain (or stratigraphic boundary) will not change too much with the step length, because the effects of the TPM and the step length on the simulated Markov chain could be balanced out (e.g., **Qi et al. 2016**).

Figure 6.8 shows the variations of the likelihood of occurrence of the observed information P_l with respect to various candidate values of p_{ii} for the seven borehole layout schemes. According to the analysis in Section 6.2.3, the TPM for each layout scheme can be determined by locating the p_{ii} value that maximizes the P_l in the figure. Likewise, it can be seen that different schemes have different TPMs. This can be expected from the borehole positions and quantity in each scheme. For example, three boreholes are used in Scheme 1 and all of them indicate the stratigraphic boundary is located 10 m below the slope top, suggesting that the stratigraphic boundary state has a very high probability to transit to itself. Hence, the p_{ii} is determined as 0.98 for Scheme 1. On the contrary, there are more transitions from a state to another different state in Schemes 2-4, so the p_{ii} value for these cases tends to be smaller. Furthermore, for Schemes 5-7, the P_l increases first with the p_{ii} to a peak and then decreases. This phenomenon is expected because in these schemes a stratigraphic boundary state can transit not only to itself but also to other states. Under this circumstance, larger p_{ii} values will lead to a longer extension of the state as the self-transition probability of the state is large, while the smaller p_{ii} values will give rise to frequent transitions between different states. Hence, the optimal p_{ii} is finally located in between the minimal and maximal candidate values. In the following part, the effectiveness of the proposed method for estimating the TPM is validated.

6.5.3.2 Verification of the proposed method for TPM estimation

This section verifies the effectiveness of the proposed method for TPM estimation, which is achieved by comparing the estimated TPM with the real TPM. Since there is no available data to know the real TPM for the studied case in Figure 6.7, four TPMs, with the diagonal elements (i.e., p_{ii}) equalling to 0.6, 0.8, 0.9 and 0.98, respectively, are predefined as replacements of four kinds of real situations. As such, the TPMs estimated in Figure 6.8 for the seven borehole layout schemes might be changed because the real states at all boreholes could be different from the original ones in Figure 6.7, and thus cannot be used directly to compare with the predefined TPMs. Hence, different "real boundaries" for the four situations should be obtained first. In this study, the real boundary for each situation is determined as an arbitrary realization of the one-dimensional conditional Markov chain model that is performed based on the corresponding predefined TPM and the utmost two boreholes (i.e., ZK1 and ZK3) in Figure 6.7. Then, the states at the intermediate boreholes are updated by extracting the states from the real boundary at the same locations, based on which new TPMs can be estimated using the proposed method in Section 6.2.3. Finally, the effectiveness of the proposed method can be judged by comparing the estimated TPM and the predefined TPM, and the estimated TPM is considered effective if it is similar to the real one (e.g., **Qi et al. 2016**).

Figure 6.9 schematically compares the predefined and estimated p_{ii} values for various schemes when real situations are considered. Generally, the accuracy of the suggested approach herein increases with the increase of the p_{ii}. In other words, the estimated TPM can be very close with the real TPM when the real TPM is strongly diagonally dominant (e.g., $p_{ii} > 0.8$), which also matches well with the observation by **Qi et al. (2016)**. For example, the estimated p_{ii} values for all schemes are equal to the predefined one when p_{ii} is 0.98. This is because the potential stratigraphic boundary is more likely to be a line when p_{ii} is 0.98, which results in the same known states at all boreholes, thus further leading to the same TPM for all schemes. However, it might be argued that the method is also accurate enough when p_{ii} is weakly diagonally dominant (e.g., $p_{ii} = 0.6$). The reason might be the fact that the optimal p_{ii} can be the minimal candidate value (e.g., 0.6 herein) when the predefined p_{ii} is very small because there are more state transitions between different states, according to the analysis in Section 6.2.3. Therefore, the estimated p_{ii} could indeed be much lower than 0.6, thus showing large difference between the estimated and predefined TPM. Furthermore, it is also noticed that the proposed method is still less accurate when $p_{ii} > 0.8$ for some schemes, Scheme 1 at $p_{ii} = 0.9$ for example. This is mainly because the number of boreholes used is too less to characterize the stratigraphic state transitions. In other words, this kind of error is mainly attributed by lack of site investigation data. Overall, the proposed method can be effectively used herein because the TPM of soil transitions in reality is often strongly diagonally dominant (e.g., **Qi et al. 2016**).

6.5.3.3 Influence of borehole layout scheme on realization of stratigraphic boundary

Having demonstrated the effectiveness of the estimated TPMs for the aforementioned borehole layout schemes, the stratigraphic boundary in the above slope example can subsequently be simulated. Since different layout schemes might provide different simulation results, it is necessary here to investigate the influence of different borehole layout schemes on the stratigraphic boundary modelling before investigating their influence on the slope stability. Therefore, a total of 50,000 simulations of the 1-D conditional Markov chain model are conducted for each scheme. The purpose is to obtain the most probable stratigraphic boundary that can be simulated by the proposed method for each scheme. It should be noted that here we are not focusing on an arbitrary realization of the stratigraphic boundary that many previous studies (e.g., **Li et al. 2016a; Liu et al. 2017c**) focused on. This is because the real boundary can be a typical realization of the stratigraphic boundary modelling, which makes it much more convenient to compare the real boundary with the most probable one. It is also worthwhile to point out that the number of 50,000 is more than enough to obtain a convergent result for each scheme through lots of internal studies. In fact, a very small number is also sufficient for convergence for some cases, as pointed out in the literature (e.g., **Elfeki and Dekking 2005; Li et al. 2016a**). However, the number of 50,000 is still employed here because it does not influence the computation efficiency very much.

Figure 6.10 shows the simulated most probable stratigraphic boundaries based on different borehole layout schemes, and for a convenient comparison the real boundary is also plotted in the figure. In general, due to the fact that the number and locations of boreholes used in each scheme is different, the difference between different layout schemes is significant. For example, comparing Figures 6.10(a), (d), and (g), where 3, 5 and 9 evenly distributed boreholes are used, respectively, it is found that the most probable stratigraphic boundary simulated in Figure 6.10(a) is far less accurate, which, however, becomes more consistent with the real boundary when the number of boreholes is increased to 9 in Figure 6.10(g). This is because in Figure 6.10(a) the three boreholes reveal the same boundary state and provide no information about the fluctuation of the real boundary. Thus, the simulated boundary is a horizontal line, substantially underestimating the boundary uncertainty. By contrast, since more boreholes are added in Figures 6.10(d) and (g) to provide more information on the lower and upper bounds of the real boundary, the simulation results are more and more sound. On the other hand, comparing Figures 6.10(b) and (c), where the same number (i.e., 4) of boreholes are used, it is also noticed that the simulated results are quite different. This can be forecasted from Figure 6.7 and Table 6.2, where only one borehole location is different in Schemes 2 and 3 and the difference is exactly consistent with that appeared in Figures 6.10(b) and (c). Furthermore, similar results can be found between Figures 6.10(e) and (f), and similar reasons can be attributed to. Hence, both the location and number of boreholes have significant influence on the stratigraphic boundary simulation, and thus on the slope stability, as will be investigated later.

6.5.4 Influence of SBU on slope stability without considering soil spatial variability

As showed above, different borehole layout schemes will result in different degrees of SBU, which may propagate to the slope stability analysis. In view of this, a series of FEM analyses of slope stability are conducted in this section within the framework of MCS for various borehole layout schemes so as to check the influence of SBU on slope stability. Since the sample size of MCS influences not only the accuracy of the estimations of the FS statistics but also the computational efficiency, it should be carefully determined on the basis of the compromise between the computational efficiency and accuracy. In this study, this is achieved by a parameter study of the FS statistics for Scheme 2 with the number of MCS samples, and the results are shown in Figure 6.11. It is observed from the figure that both the mean and standard deviation of FS (i.e., μ_{FS} and σ_{FS}, respectively) start converging to a reasonably stable level when the number of MCS samples reaches about 4,000. This indicates that the size of 4,000 MCS samples is sufficient to obtain reasonably stable estimations of the FS statistics, and hence it is used to estimate the μ_{FS} and σ_{FS} in the following analysis.

Figure 6.12(a) shows the values of μ_{FS} for various borehole layout schemes. As references, the FS values calculated for DSB and RSB are also plotted in this figure. In general, with the increase of the borehole number, the μ_{FS} does not present a monotonic variation. For example, the μ_{FS} estimated for Scheme 2 with four boreholes (ZK1-4) is lower than that for Scheme 1 with three boreholes (ZK1-3) and those for the other schemes with more than four boreholes [e.g., Scheme 4 with five boreholes (ZK1-5) and Scheme 7 with nine boreholes (ZK1-9)]. This mainly arises from the different distributions of soil types caused by different stratigraphic boundary simulations associated with different schemes, which can be seen from Figure 6.10. According to Figure 6.10, the stratigraphic boundary simulated based on Scheme 2 generally results in the largest ratio of sand volume to clay volume in the whole slope body compared with the other schemes. As such, the μ_{FS} estimated for Scheme 2 would be the smallest because the shear strength of sand is much lower than that of clay, as can be judged from Table 6.1. However, except for Scheme 2, the estimated μ_{FS} increases gradually as increasing the number of boreholes. For example, the μ_{FS} obtained by using three boreholes (i.e., Scheme 1) is nearly the same with that for the DSB case, both are about 1.163. This is not surprising and is expected as the three boreholes (ZK1-3) used in Scheme 1 reveal the same boundary information (see Figure 6.7), which results in nearly the same boundary simulation with the deterministic one that we often assumed. By contrast, when the number of boreholes is increased to nine (Scheme 7), the μ_{FS} (i.e., 1.212) is much closer to the real FS value (i.e., 1.248) for the RSB case. This is not only because the number is relatively large but also due to the fact that all the nine boreholes have successfully identified the key variation trends of the RSB. Therefore, if more boreholes (i.e., larger than nine) are drilled, the estimated μ_{FS} will converge to the "correct" result.

It is also observed from Figure 6.12(a) that the location of the boreholes has a significant influence on the slope stability results. This can be seen from the schemes that use the same amount but different distributions of the boreholes—Schemes 2 and 3 with four boreholes and Schemes 5 and 6 with seven boreholes. For example, the μ_{FS} estimated for Scheme 2 (ZK1-4) is the lowest (i.e., 1.138), while the μ_{FS} for Scheme 3 (ZK1-3 and ZK5) is 1.190. Obviously, the value of 1.190 is much closer to the correct FS for the RSB case, while the value of 1.138 could even be more conservative than that (i.e., 1.163) for the DSB case. Such a significant difference is no doubt induced by the different locations of boreholes ZK4 and 5 as the other three boreholes in Schemes 2 and 3 are the same. This indicates that the location of ZK5 is more important than that of ZK4 for evaluating the slope stability. In fact, this can be understood from Figure 6.6, where the critical slip surface is going deeper and deeper when the stratigraphic boundary evolves from the DSB case to the RSB case, suggesting that the valley or its around location of the RSB plays a more important role in the stability of the slope. Since the borehole ZK5 reveals exactly the potential location of the valley of the RSB but ZK4 cannot, the uncertainty existed in this area is reduced by Scheme 3 and the clay volume for Scheme 3 is much larger than that for Scheme 2. Likewise, the μ_{FS} for Scheme 3 is increased and is more accurate than that for Scheme 2 because the clay has higher shear strengths than the sand has. In the literature (e.g., **Sivakumar Babu et al. 2006; Li et al. 2016a; Deng et al. 2017**), the area that influences the slope stability, like the valley of the RSB here, is referred to as the influence zone. To be consistent with the previous works, this term is also used in the following study. Similarly, compared with Schemes 5, the μ_{FS} for Scheme 6 is much closer to the correct FS because the extra two boreholes (ZK8-9) in addition to those (ZK1-5) also used by Scheme 5 are all located in the influence zone, while the extra two boreholes in Scheme 5 are not and only one (i.e., ZK7) is located in the influence zone, as will be illustrated later. Hence, it is suggested here to design more boreholes in the influence zone in priority so as to effectively reduce the SBU and then to accurately evaluate the FS of slope stability.

To gain more insights into the effective design of boreholes in geotechnical engineering practice, it is necessary here to find out where the influence zone is exactly located. For this purpose, some further analyses based on Figure 6.12(a) are conducted. Firstly, the schemes in Table 6.2 are compared with each other, and in particular the following groups are considered: (Scheme 1, Scheme 2), (Scheme 3, Scheme 4), (Scheme 5, Scheme 7) and (Scheme 6, Scheme 7). Note that in each group the latter scheme has one or two more boreholes than the former one. The redundant boreholes in the latter schemes are expected to be located either in or outside of the influence zone such that this zone can be effectively found out. From the comparison of (Scheme 1, Scheme 2) and that of (Scheme 3, Scheme 4), it is roughly found that ZK4 is outside the influence zone while ZK5 is inside the zone, because ZK5 has a larger influence on the slope stability while ZK4 does not, as mentioned above. Due to limited space, the reason is not repeated here. Therefore, the preliminary left boundary of the influence zone can be marked by the location of ZK4, while the right boundary is expected to be on the right of ZK5. Then, compared with Scheme 5 and Scheme 7, the μ_{FS} for Scheme 7 is closer to the correct result because, in addition to those boreholes used in Scheme 5, two more boreholes (ZK8-9) are used in Scheme 7 and they are probably located in the influence zone. This shows that the influence zone can probably extends to the location of ZK9, as there is at least no significant evidence to exclude the influence of ZK9. Finally, compared with Scheme 6, Scheme 7 has a higher result of FS due to ZK6 and ZK7 joined in Scheme 7. Assuming that the influence zone is continuous and considering that ZK6 is on the left of ZK4 that has been demonstrated to have little influence on the slope stability, it can be concluded that ZK7 is still located in the influence zone. This suggests that the possible left boundary of the influence zone could be further updated to be located in between ZK4 and ZK7. Overall, from the above analyses, the influence zone in this study is identified as [6 m, 17 m]. It is worthwhile to point out that this interval is generally consistent with the major deformation area of the slope, as can be seen from Figure 6.6. Therefore, it is suggested herein that the influence zone can be roughly estimated as the area with relatively large strain based on conventional slope stability analysis, if there are no sufficient boreholes in hand. In addition, the emphasize is that it has better to judge in advance the location of the influence zone by using methods such as the suggested one before drilling boreholes so as to save project cost as much as possible.

Figure 6.12(b) shows the values of σ_{FS} for various borehole layout schemes. Similar to Figure 6.12(a), the σ_{FS} is not monotonically influenced by the number of boreholes. This is mainly attributed to the following two reasons: (1) The locations of the added boreholes are outside the influence zone; (2) The added boreholes provide new stratigraphic boundary information, which introduces extra uncertainty to the Markov chain simulation. For example, compared with Scheme 1 with only three boreholes, the σ_{FS} for Scheme 2 with four boreholes is much larger, because there is no extra information on the influence zone while the added borehole ZK4 provides a significantly different boundary state with the other three boreholes. However, the σ_{FS} is seen to decrease with the increasement of the boreholes. This is expected as from Scheme 2 to Scheme 7 the number of boreholes in the influence zone increases. Note that the lowest result for Scheme 1 does not mean this Scheme provides the closest stratigraphic boundary simulation to the real one, but simply because the three boreholes used in this scheme reveals the same borehole information, thus reducing the uncertainty of the Markov chain analysis. Therefore, this further highlights the importance of the effective design of boreholes based on the influence zone, as mentioned above.

Figure 6.12(c) plots the CDFs for various borehole layout schemes. Note that the CDF for each scheme in this figure is estimated based on more MCS samples (i.e., 10,000) than the μ_{FS} and σ_{FS} so as to obtain a more accurate and smooth curve. As can be seen from the figure, the borehole layout scheme has a significant influence on the CDF of FS. The P_f of the slope stability presents a similar variation trend with respect to the increase of the number of boreholes. For example, the P_f for Scheme 2 is the largest, as can be expected from Figures 6.12(a) and (b). Meanwhile, with the uncertainty in the influence zone being decreased by more boreholes, the P_f for Scheme 2 to 7 decreases accordingly. To sum up, the commonly assumption on DSB would overestimate the P_f of the slope stability herein when the soil spatial variability is ignored.

6.5.5 Influence of SBU on slope stability with considering soil spatial variability

Since soil spatial variability is widely recognized in geotechnical engineering practice, this part further investigates how the slope stability changes with different borehole layout schemes when the soil spatial variability is considered. Similar to Section 6.5.4, MCS is adopted to estimate the FS statistics and P_f of the slope for various borehole layout schemes. In particular, the FS statistics are estimated based on 4,000 MCS samples, which is deemed appropriate from a similar parameter study to Figure 6.11; whereas the P_f is evaluated based on more samples (i.e., 5000), which is also reasonably acceptable for the problem herein. The results are plotted in Figure 6.13. Note that, as a reference, the corresponding results for DSB and RSB conditions are also provided in the figure. In addition, except the seven borehole layout schemes in Table 6.2, one more scheme consisting of 17 boreholes (i.e., ZK1-17) is considered here in order to capture the convergence rate of the results as increasing the number of boreholes, because more uncertainties are involved when spatial soil variability is considered. Here, it is worthwhile to point out that the boreholes ZK10-17 are successively located in the middle of the eight borehole intervals formed in Scheme 7, for example ZK10 is located in the middle of ZK1 and ZK6. In the following, for convenience purpose, the added scheme is numbered as Scheme 8.

Figure 6.13(a) shows the values of μ_{FS} for various borehole layout schemes when the soil spatial variability is considered. In general, the variation trend of μ_{FS} with respect to the number of boreholes is very similar to that in Figure 6.12(a) where the soil spatial variability is ignored, i.e., μ_{FS} does not monotonically change with the number of boreholes. Again, the reason mainly lies in the fact that different schemes provide different borehole information, which may lead to significantly different boundary simulation results. In addition, similar to Figure 6.12(a) and as expected, the μ_{FS} for Scheme 1 matches very well with that obtained based on the DSB condition. The reason is similar to that for Figure 6.12(a) and thus not repeated here. It is also observed that the μ_{FS} will converge gradually to the correct answer obtained based on the RSB case when the number of boreholes increases. For example, the relative error of the estimated result decreases from 4.74% to 0.77% when the number of boreholes increases from 3 to 17. This can be expected, as more boreholes being used in the conditional Markov chain analysis will finally lead to more similar boundary simulations to the RSB. However, unlike Figure 6.12(a), more boreholes in the influence zone would not always increase the accuracy of the estimation of μ_{FS}, although the convergence trend of μ_{FS} to the correct answer can be captured with increasing the borehole numbers. For example, the μ_{FS} decreases from 1.164 to 1.157 when the scheme is transferred from Scheme 6 to Scheme 7. The possible reasons may be two-fold: (1) The soil spatial variability can increase the negative effect of boreholes outside the influence zone on the FS here; (2) The negative effect brought by the boreholes outside the influence zone cannot be balanced out by the positive effect by the boreholes added in the influence zone, when the ratio of the number of boreholes added in the influence zone to that of the original boreholes in the influence zone is relatively small. Actually, similar observations can also be tracked in the work reported by **Deng et al. (2017)**. Furthermore, for schemes with the same number of boreholes but different borehole distributions (e.g., Scheme 2 and Scheme 3, Scheme 5 and Scheme 6), the results are significantly different because the borehole location also plays an important influence on the slope stability results.

Figures 6.13(b) and (c) show the σ_{FS} and P_f for various borehole layout schemes when the soil spatial variability is considered. As seen from the figures, similar findings to μ_{FS} are observed, that is the increasement in borehole number dose not ensure a monotonically decrease of σ_{FS} and P_f. Possible reason may be that the added boreholes introduce new boundary states, suggesting an increasement in the SBU. This can be readily understood from Table 6.2 and Figure 6.7. However, it can be observed and expected that the σ_{FS} and P_f can generally converge to the correct answers as increasing the number of boreholes. This is because more boreholes being used in the conditional Markov chain analysis will finally lead to more similar boundary simulations to the RSB. In addition, when all the conditional boreholes provide the same information (i.e., Scheme 1), the corresponding results are nearly the same with those provided based on DSB. Again, this is expected, as the simulated boundary will be very similar with the DSB, as shown in Figure 6.10(a). To conclude, both the borehole number and location influence the stability of the slope, and particularly the boreholes in the influence zone are very important for accurately assessing the stability of the slope. Meanwhile, the common assumption on DSB would overestimate the P_f of the slope stability herein when the soil spatial variability is considered. However, the spatial variation of soil properties is considered with a fixed degree of uncertainty (i.e., the SOFs are predefined), so it is natural to question how the relative error of the P_f estimated based on DSB compared with the P_f obtained based on RSB changes with different degrees of soil spatial variability, as will be studied later.

6.5.6 Influence of soil spatial variability on the assessment of $\mathbf{P_f}$ estimated based on DSB

Figure 6.14 compares the results of the P_f estimated based on DSB and RSB as increasing the vertical SOF δ_v. The comparative results represented by relative error are also plotted in the figure. Note that only the influence of the vertical SOF is considered here because previous studies have shown that the horizontal SOF has little influence on the slope reliability results (e.g, **Li et al. 2015a**). As seen from the figure, the results estimated for both the two conditions increase with the increase of δ_v. This is expected and is similar to those reported in the literature (e.g., **Li et al. 2015a**). In addition, it is observed that the P_f estimated based on DSB is significantly overestimated, because the underlying SBU is underestimated. However, such difference shows a decreasing trend with the δ_v. For example, the difference decreases from approximately 90% to about 46% when δ_v increases from 1 m to 6 m. The reason is that the soil spatial variability is substantially reduced when δ_v increases from 1 m to 6 m. Nevertheless, the difference is unacceptably large, which may result in significantly different design outputs in engineering practice. Furthermore, compared with the effect of the system SBU in Chapter 5, the inherent SBU is far more important to be considered in slope reliability analysis.

6.6 Conclusions

This chapter investigates the influence of the inherent SBU on slope reliability analysis using the one-dimensional conditional Markov chain model and MCS. A modified TPM estimation method is proposed. Detailed procedure for implementing the proposed approach on commonly used commercial software (e.g., ABAQUS and MATLAB) is described. Finally, the approach is illustrated and validated by a hypothetical slope example characterized by different degrees of SBU and soil spatial variability. The following conclusions can be made from this chapter as:

1. Slope stability evaluated based on different stratigraphic boundary conditions can be significantly different in terms of the FS value and location of the critical slip surface.

2. Different borehole layout schemes may provide significantly different stratigraphic boundary states information, thus bringing different degrees of uncertainty. The one-dimensional conditional Markov chain model can well simulate the stratigraphic boundary based on some given boreholes. The modified TPM estimation method is demonstrated to be effective when the TPM of soil transitions in reality is strongly diagonally dominant.

3. Both the location and number of boreholes have significant influence on the stratigraphic boundary simulation. Whether the soil spatial variability is neglected or not, the FS statistics and P_f do not increase or decrease with the borehole number, because there is an influence zone in the slope body and the boreholes located in this zone play a dominant role in the stability of the slope. However, the FS statistics and P_f can converge to the correct results if more and more boreholes are drilled.

4. When the soil spatial variability is neglected, it seems that the FS statistics and P_f can be more and more accurate as increasing the number of boreholes in the influence zone. In contrast, the increase of the number of boreholes in the influence zone may not ensure a more accurate result when the soil spatial variability is considered.

5. Conventional reliability analysis with an implicit assumption of DSB

condition may overestimate the slope reliability. The difference between the DSB and RSB decreases with the increase of the vertical scale of fluctuation.

6. Compared with the effect of the system SBU in Chapter 5, the inherent SBU is far more important to be considered in slope reliability analysis.

Table 6.1 Statistics of soil parameters

Soil layer	Statistics	c (kPa)	φ (°)	γ (kN/m^3)	E (Mpa)	υ
Clay	Mean	18	30	20	30	0.3
	COV	0.3	0.2	–	–	–
	$\rho_{c\varphi}$	0		–	–	–
	SOF	$\delta_h = 40$ m, $\delta_v = 4$ m		–	–	–
Sand	Mean	2	20	20	50	0.3
	COV	0.3	0.2	–	–	–
	$\rho_{c\varphi}$	0		–	–	–
	SOF	$\delta_h = 40$ m, $\delta_v = 4$ m		–	–	–

Table 6.2 Borehole layout schemes

Scheme No.	Borehole number	ZK1	ZK6	ZK4	ZK7	ZK2	ZK8	ZK5	ZK9	ZK3
1	3	√				√				√
2	4	√		√		√				√
3	4	√				√		√		√
4	5	√		√		√		√		√
5	7	√	√	√	√	√		√		√
6	7	√		√		√	√	√	√	√
7	9	√	√	√	√	√	√	√	√	√

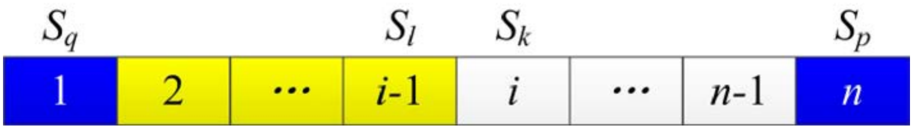

Figure 6.1 Schematic illustration of one-dimensional conditional Markov chain. (For interpretation of color description in this figure, please refer to the web version of this thesis.)

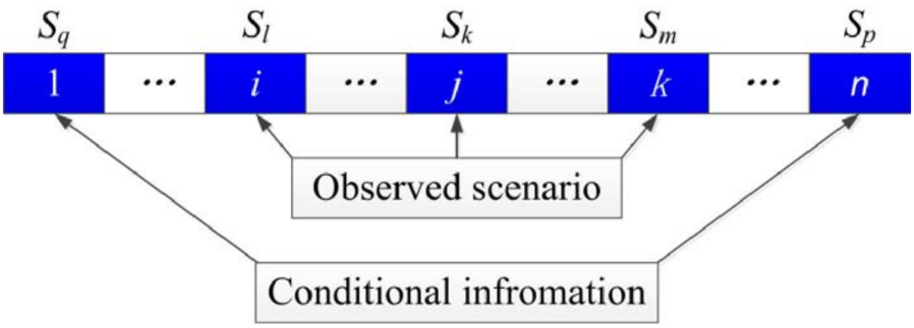

Figure 6.2 Borehole information used for TPM estimation

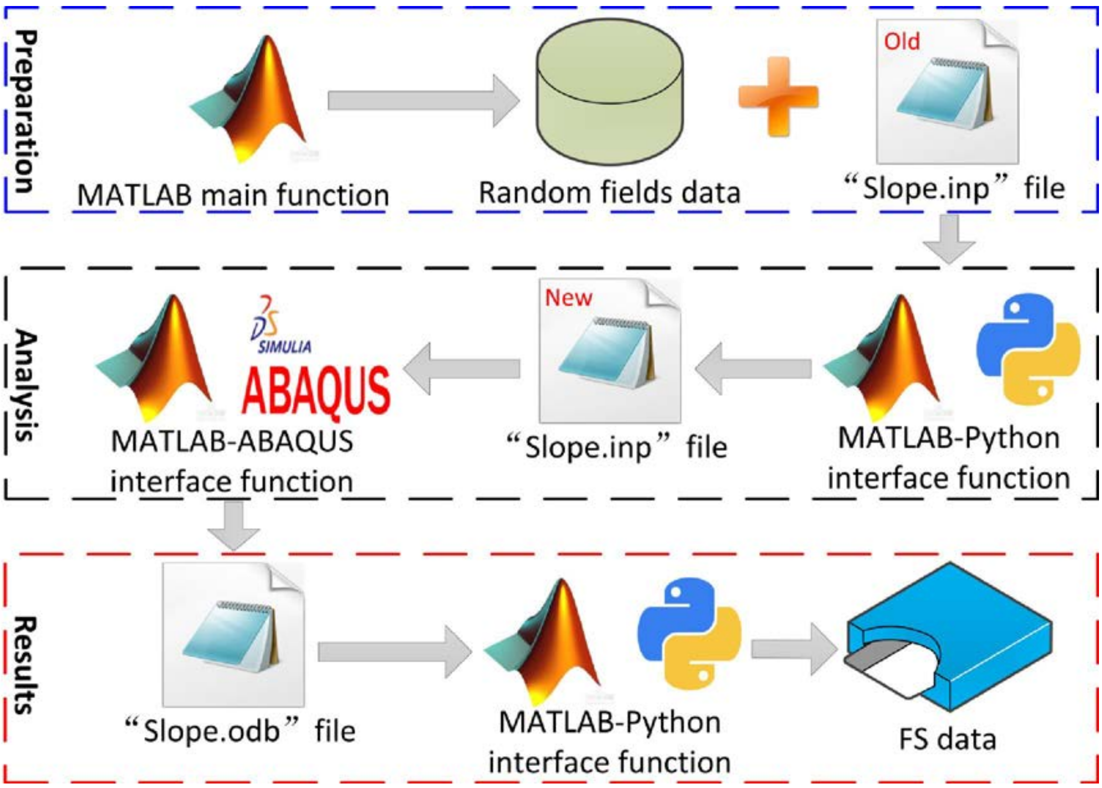

Figure 6.3 Strategies for incorporating spatial soil variability into ABAQUS

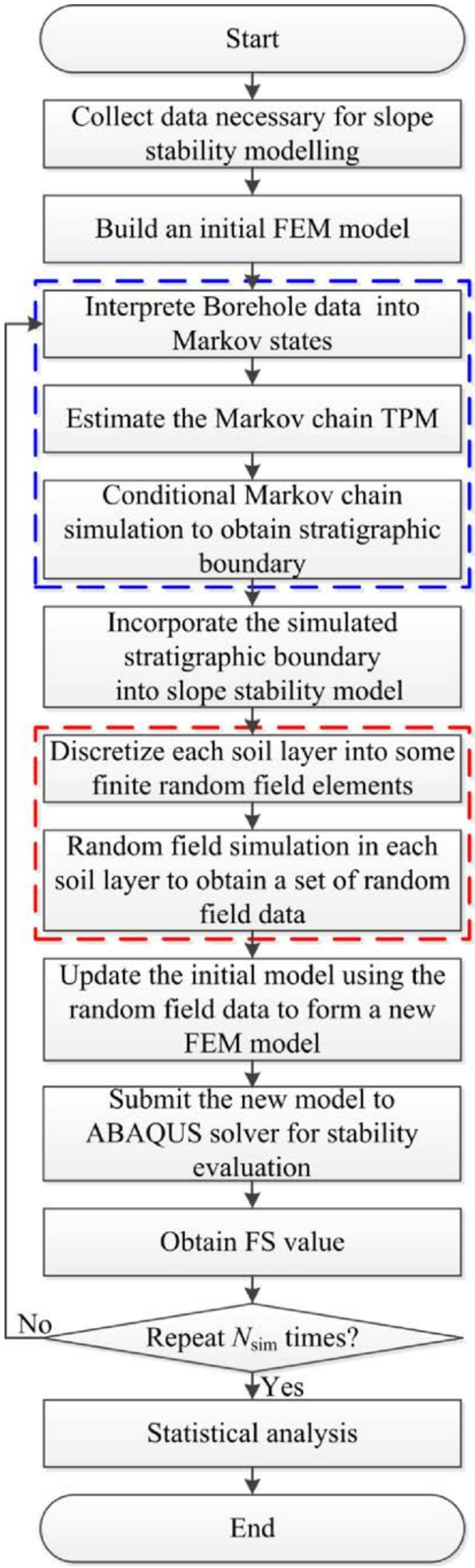

Figure 6.4 Flow chart of the proposed approach

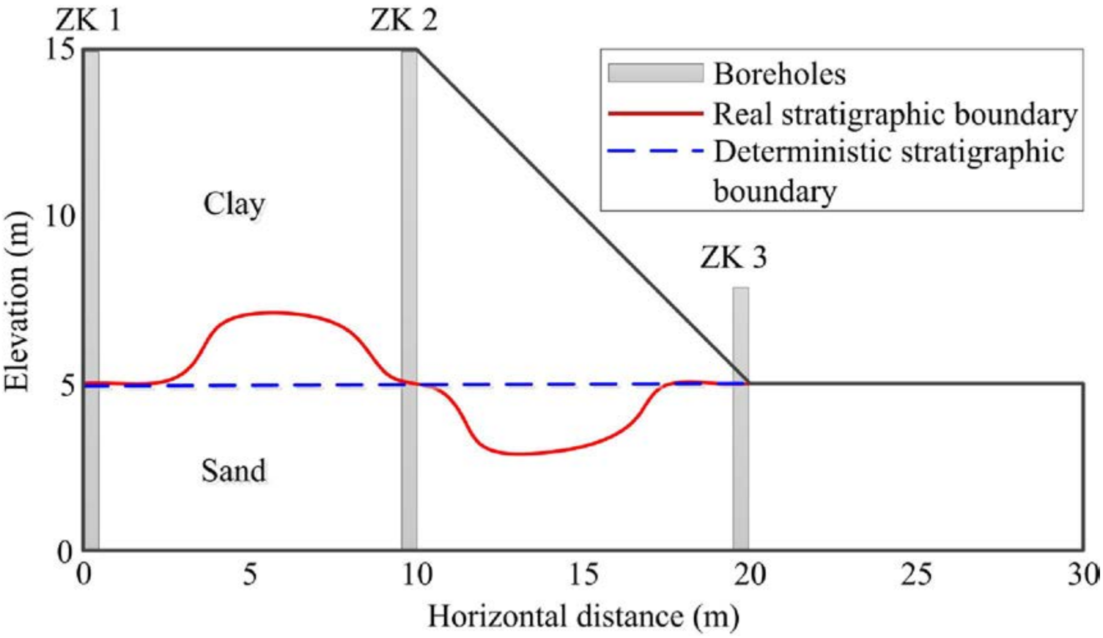

Figure 6.5 Geometry of the studied slope

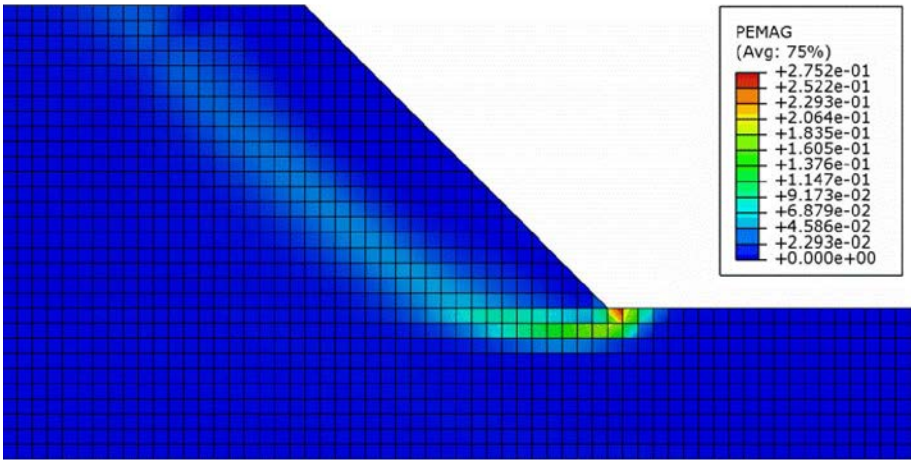

(a) Deterministic stratigraphic boundary (DSB), FS=1.163

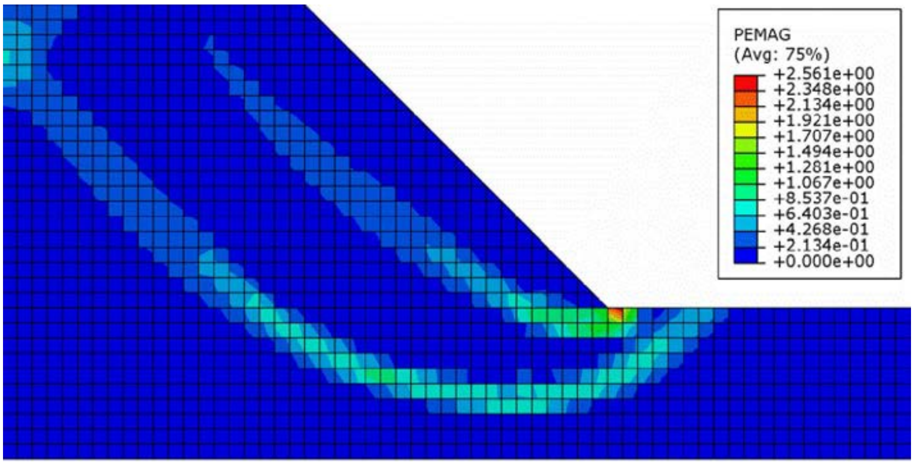

(b) RSB, FS=1.248

Figure 6.6 Slope stability results based on FEM

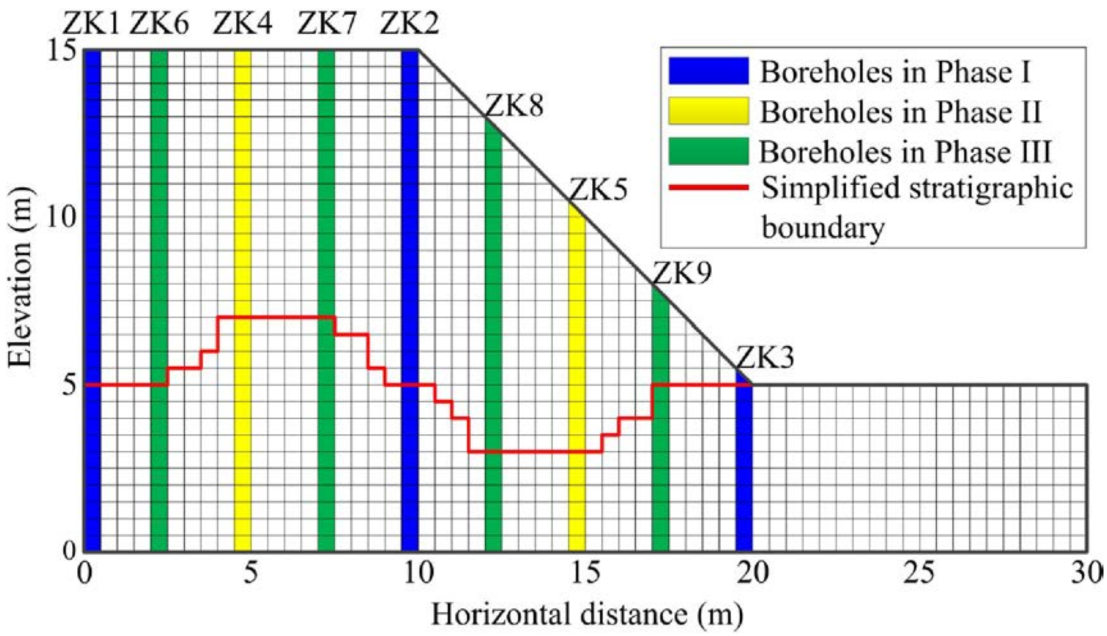

Figure 6.7 Borehole locations and random field element size

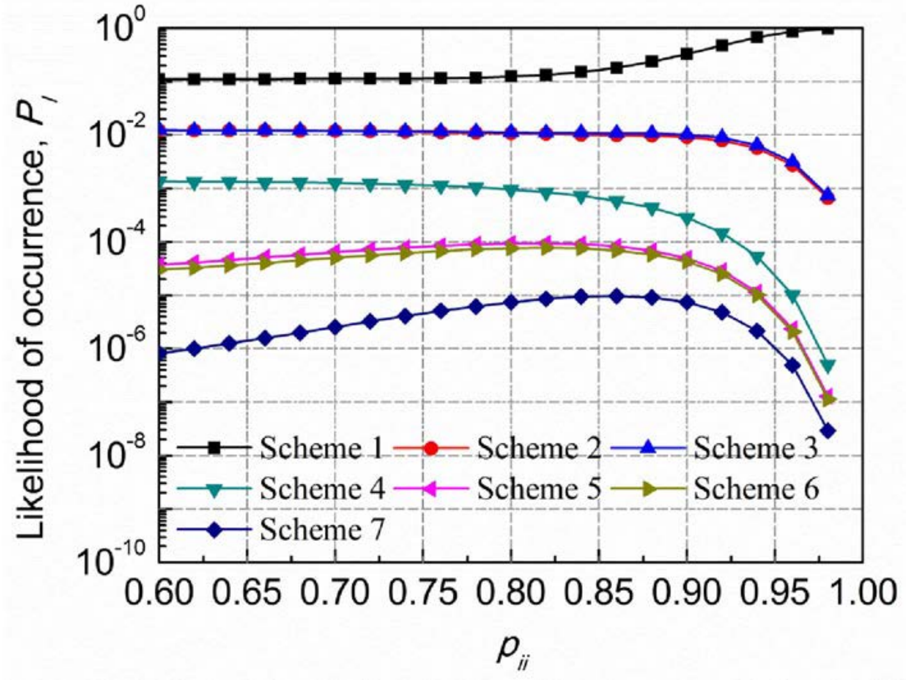

Figure 6.8 Variation of P_l with respect to different p_{ii} values

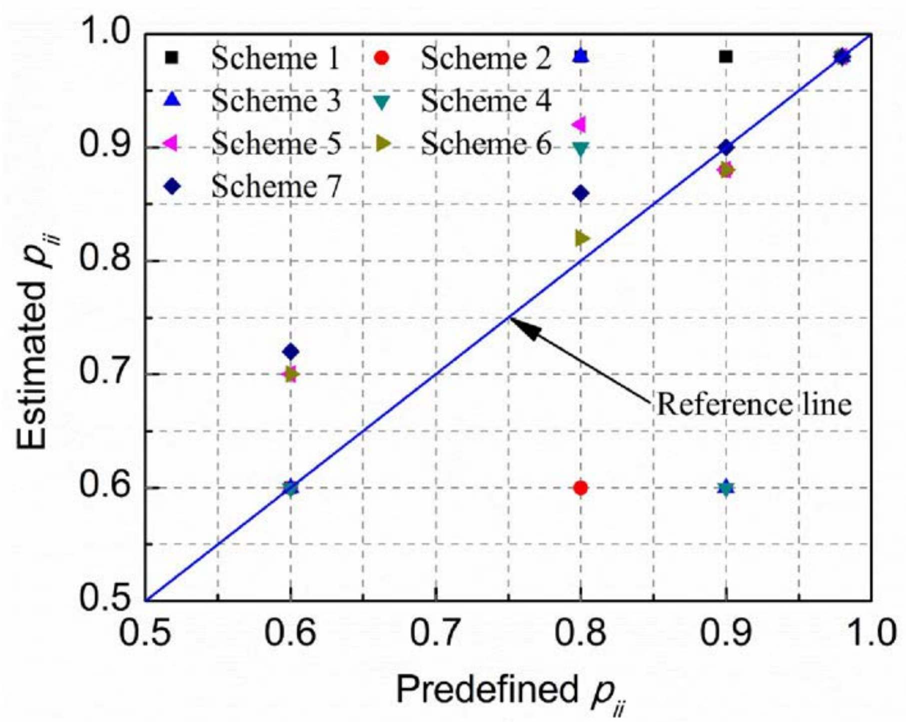

Figure 6.9 Comparison of the predefined and estimated p_{ii} values for various schemes

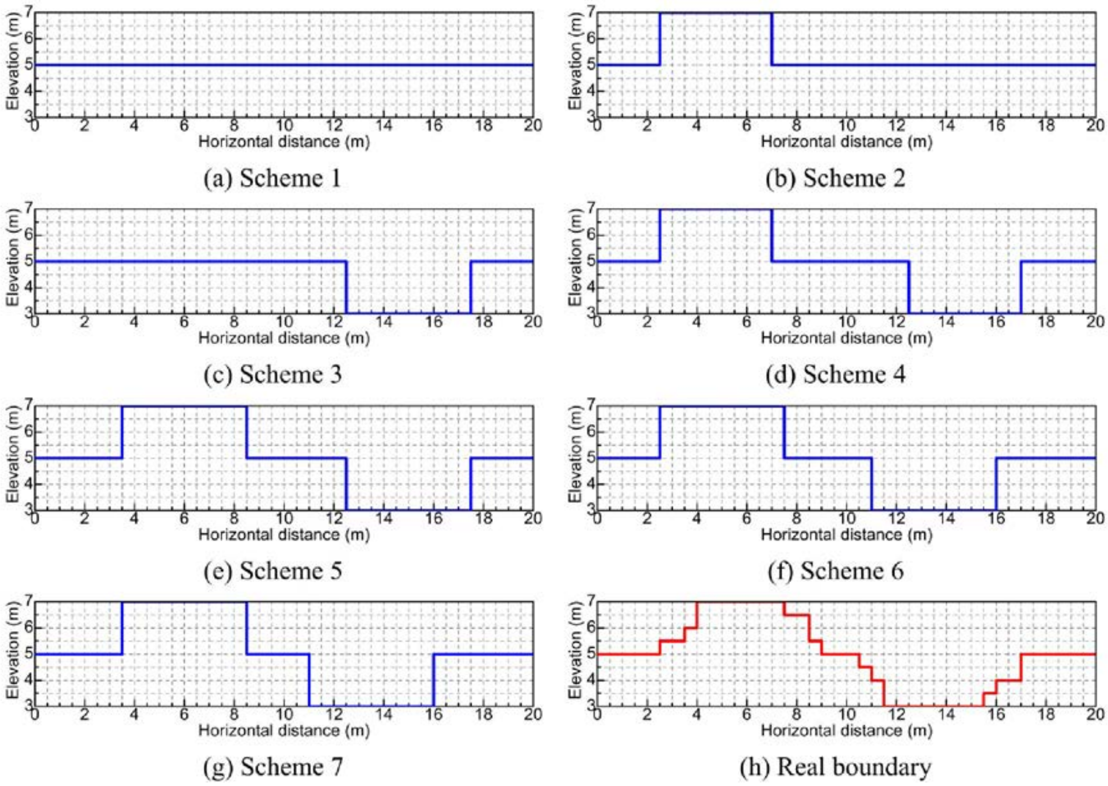

Figure 6.10 Simulated most probable stratigraphic boundaries based on different borehole layout schemes

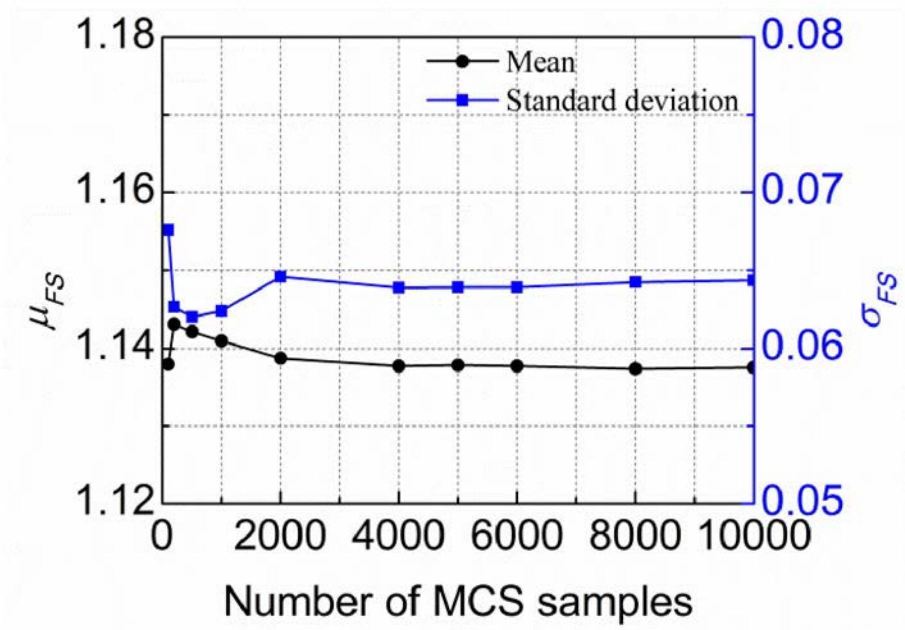

Figure 6.11 Convergence of FS statistics for Scheme 2 with the number of MCS samples

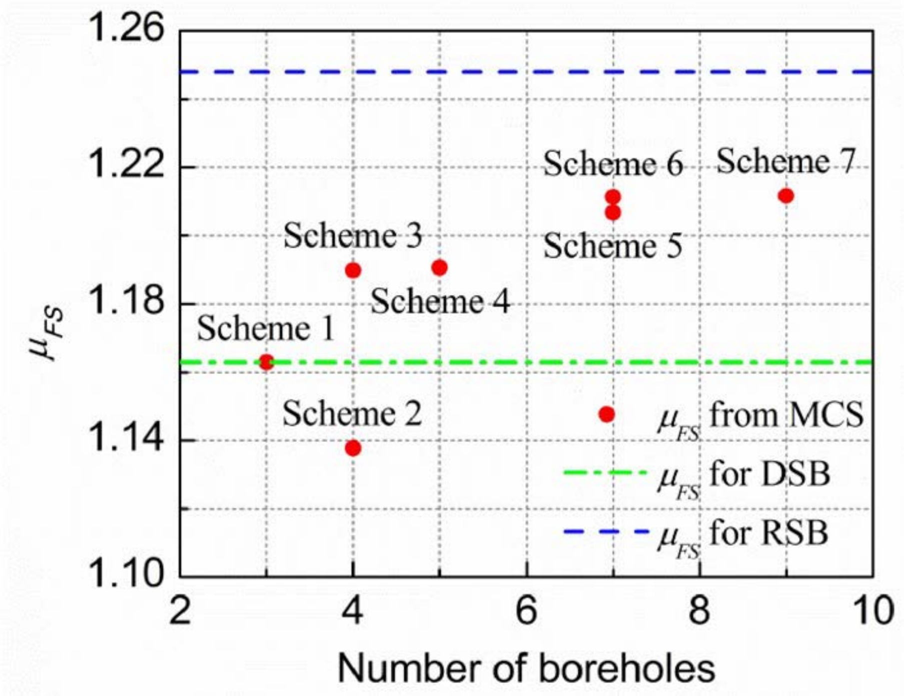

(a) μ_{FS}

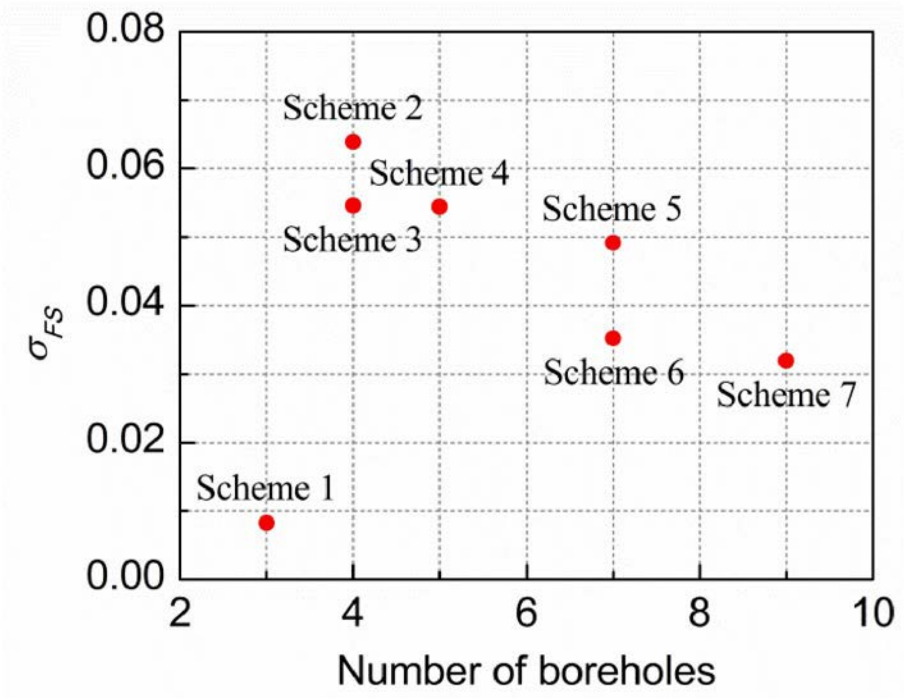

(b) σ_{FS}

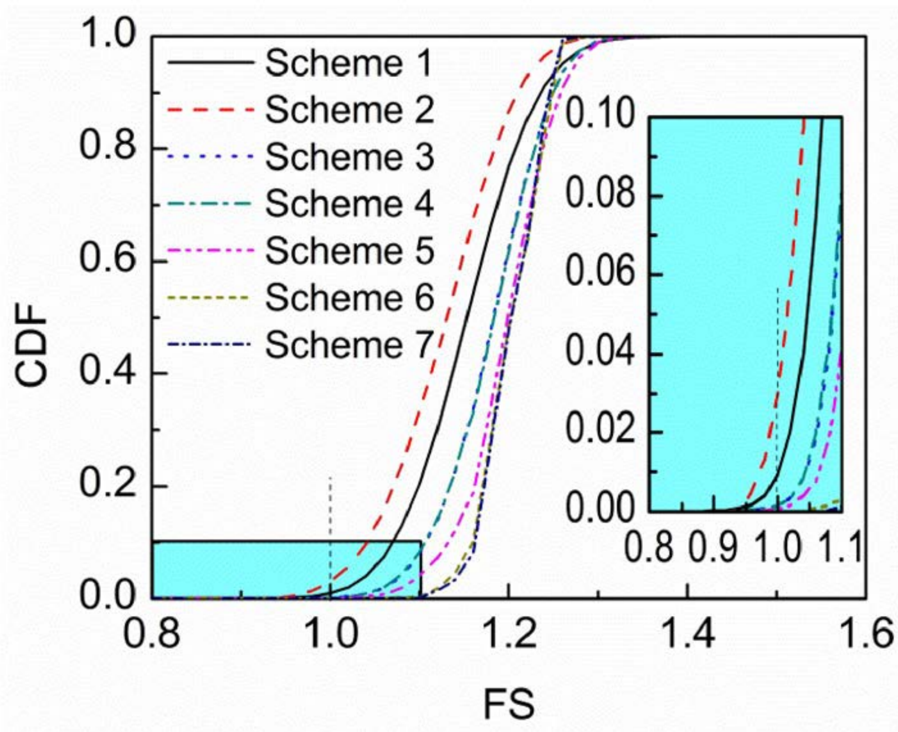

(c) CDF

Figure 6.12 FS statistics for various borehole layout schemes without considering soil spatial variability

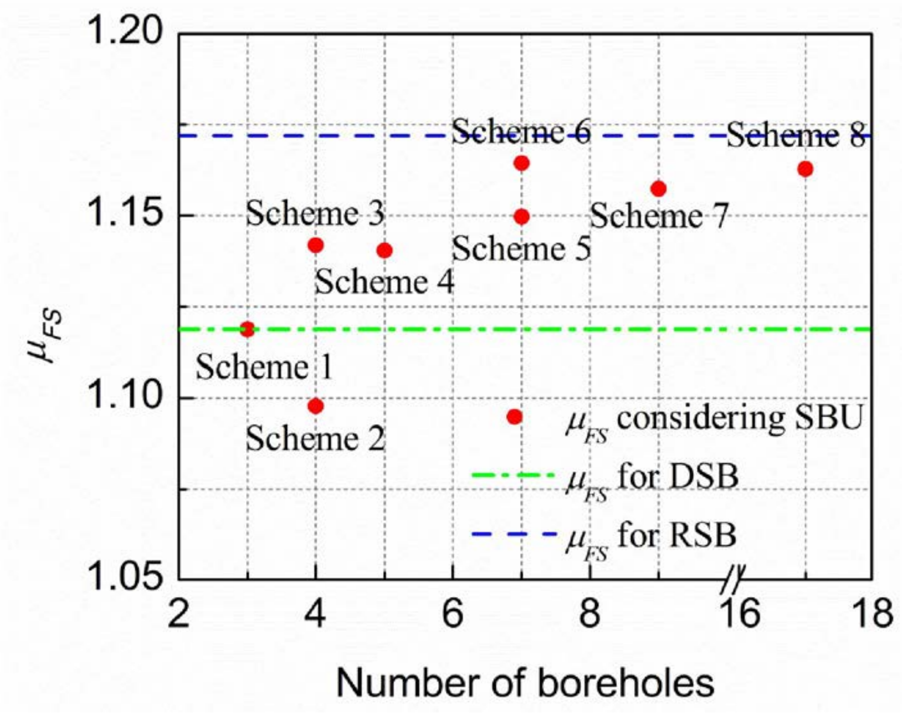

(a) μ_{FS}

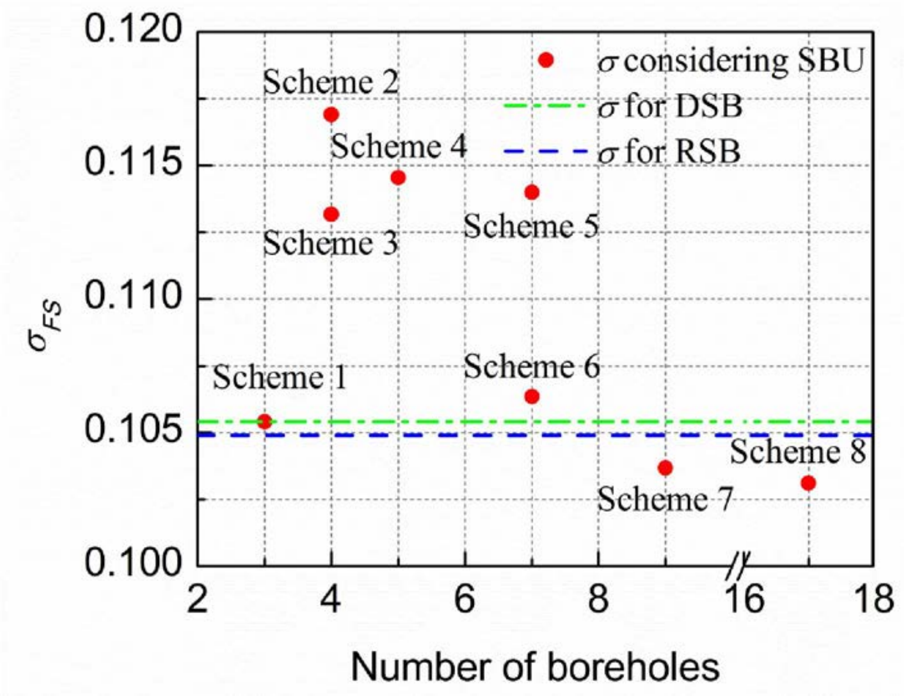

(b) σ_{FS}

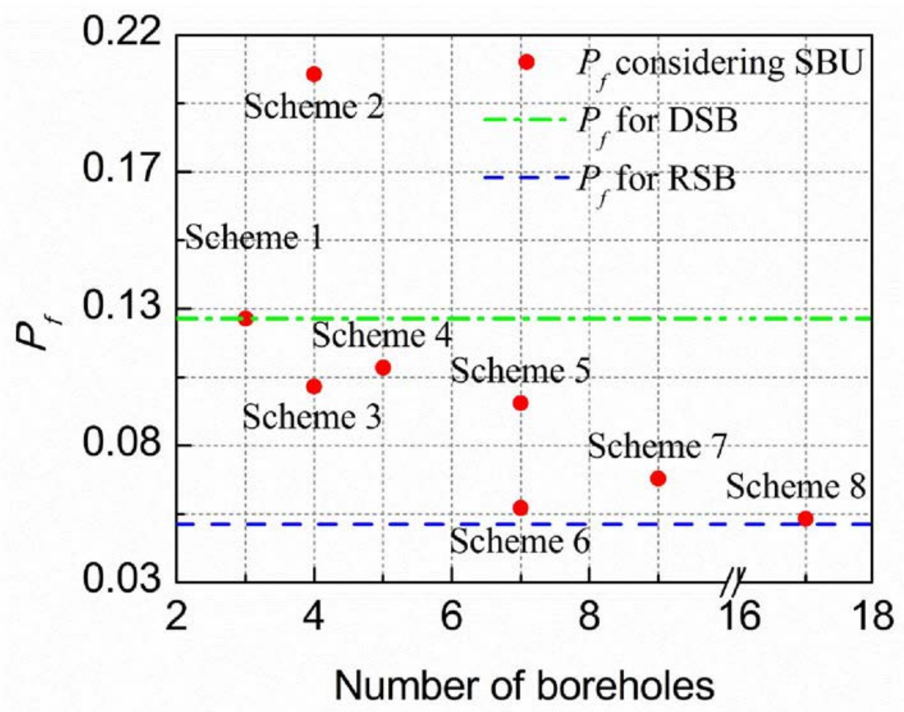

(c) P_f

Figure 6.13 FS statistics and P_f for various borehole layout schemes with considering soil spatial variability

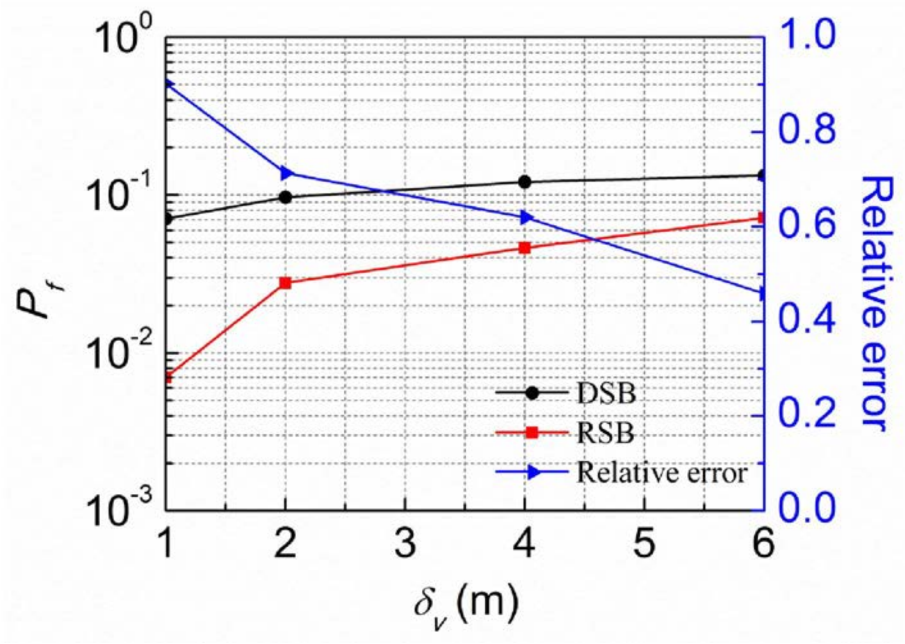

Figure 6.14 Variation of P_f with respect to the soil spatial variability

CHAPTER 7 CONCLUSIONS AND RECOMMENDATIONS FOR FUTURE WORKS

7.1 Conclusions

This thesis aims at proposing an efficient approach for slope reliability analysis by considering the soil spatial variability and incorporating borehole/measurement data (i.e., conditional information) into slope reliability analysis. In particular, this work has mainly contributed to: (1) proposing an efficient approach for system reliability analysis of slopes in spatially variable soils; (2) performing conditional random field reliability analysis to investigate the effect of borehole data from site investigation and the effect of different layouts of cored samples on slope reliability; (3) investigating the effects of the system SBU on the system reliability and risk of a layered slope in spatially variable soils; (4) incorporating the inherent SBU into the reliability analysis of slopes in spatially variable soils using one-dimensional conditional Markov chain model, so as to investigate the influence of different borehole layout schemes on slope reliability analysis with and without considering the spatial soil variability. Based upon these studies, the major contributions and conclusions of this thesis are summarized as follows:

1. A simplified framework based on multiple response surface method (MRSM) and Monte Carlo simulation (MCS) for efficient system reliability analysis of slopes in spatially variable soils is proposed. The proposed simplified framework can well deal with slope reliability analysis in spatially variable soils, providing sound results that are comparable with those by MCS and reported in the literature. It is robust against changes of various cross-correlations, COVs and ACDs. Meanwhile, the proposed framework is much more efficient than direct MCS, especially for reliability problems with low probability levels (e.g., $P_f \leq 10^{-3}$). However, compared with MRSM, its relative efficiency is case dependent. For the slope where the number of

random field elements is relatively large and more than one type of shear strength is dealt with, the proposed framework is much more efficient; otherwise, it is less efficient. Nevertheless, the proposed framework offers a useful strategy for performing system reliability analysis of slopes where the spatially varied soil properties are considered.

2. The conditional random field can effectively reduce the simulation variance of the underlying random fields if the Kriging method can accurately reflect the spatial variation of the soil properties based on a specific amount of known data; otherwise, the established conditional random fields are of no practical significance. The realization of a CRF is heavily relied on the ratio of the sample distance to the ACD. It is found in this study that the random fields can be accurately simulated when the ratios in the horizontal and vertical direction are less than or equal to 1 and 3, respectively. A smaller ratio of the sample distance to the ACD would provide a better simulation result.

3. The variation of the FS obtained by the conditional random field simulation increase with the cross-correlation coefficients, the COVs of the soil properties, and decrease with the ACDs. Of great importance is the fact that the variation of the FS obtained by the conditional random field simulation is smaller than that obtained by the unconditional random field simulation. Furthermore, the spatial variation of the critical slip surface is also narrower when conditional random fields are considered.

4. The failure probabilities can be reduced significantly by the CRF simulation. In general, the probabilities of failure follow similar trends as the results obtained by the unconditional random field simulation with respect to the cross-correlation coefficients and the COVs of the soil properties. However, the probabilities of failure present inverse trends with respect to the ACDs, suggesting that the conditional random field simulation is of significant benefit at relatively large ACDs.

5. The location of the stratigraphic boundary plays an important role in

identifying the slope failure mechanism. Although it may not influence the FS value of the slope too much, different stratigraphic boundary locations would give rise to significantly different failure modes or consequences and thus affect risk assessment. For different safety levels, the average sliding mass estimated based on traditional DSB analysis is much larger than the average sliding mass estimated by SSB analysis, suggesting that the traditional DSB analysis might overestimate slope failure consequences, thereby affecting the decision makers to propose reasonable and economical prevention measures in engineering practice.

6. A difference generally exists between slope failure probabilities obtained from the DSB and SSB. The failure probabilities are not always underestimated or overestimated for different cross-correlation coefficients, COVs and SOFs, except for the considered range of the vertical SOFs, where the results estimated based on DSB are always underestimated. However, the difference between slope failure probabilities obtained from DSB and SSB conditions are generally small for different statistics, except at small values of COV_{φ}. In contrast, the difference in slope failure risks estimated based on DSB and SSB is relatively larger than the difference in slope failure probabilities. The risks estimated based on DSB are overestimated for different statistics, except at small values of COV_{φ}, where the results are underestimated.

7. Both the location and number of boreholes have significant influence on the stratigraphic boundary simulation. Whether the soil spatial variability is neglected or not, the FS statistics and P_f do not increase or decrease with the borehole number, because there is an influence zone in the slope body and the boreholes located in this zone play a dominant role in the stability of the slope. However, the FS statistics and P_f can converge to the correct results if more and more boreholes are drilled. When the soil spatial variability is neglected, it seems that the FS statistics and P_f can be more and more accurate as increasing the number of boreholes in the influence zone. In contrast, the increase of the number of boreholes in the influence zone may not ensure a more accurate result when the soil spatial variability is considered.

Conventional reliability analysis with an implicit assumption of DSB condition may overestimate the slope reliability. The difference between the DSB and RSB decreases with the increase of the vertical SOF.

8. Compared with the effect of the system SBU, the inherent SBU is far more important to be considered in slope reliability analysis.

7.2 Recommendations for future works

Although some progress has been made in developing efficient reliability analysis approaches for slope stability analysis in spatially variable soils and studying the effect of borehole/measurement data on slope reliability in the present work, there are still some limitations and rooms for further improvement. They are listed as follows:

1. Although the proposed simplified approach in Chapter 1 can deal with more than one type of shear strength parameter and has been demonstrated effective and efficient, it is only suitable for simple slopes, for example the nominally homogeneous slopes. In addition, the influence of variance reduction factor has not been investigated. Thereafter, future work should be directed to efficient reliability analysis of complicated slopes with more soil layers and more types of strengths, and to study the influence of the variance reduction factor.

2. The effect of conditional random fields is investigated only for a hypothetical homogeneous cohesion-frictional slope in Chapter 2 because the computational demand increases sharply when heterogeneous slopes are considered. Although SS can enhance the simulation efficiency to some extent, it still requires several thousands of evaluations of the deterministic stability model. In addition, the current conditional information focuses only on a specific number of samples and does not consider practical borehole layouts. Hence, further research is required to study the influence of borehole locations on the practical slope reliability, therein employing more advanced probabilistic approaches.

3. The system SBU is modeled by a discrete random variable model, which is relatively simple. In addition, for simplicity and convenience purposes, the admissible error of the stratigraphic boundary location is slightly large, which may not be the case in real engineering projects. Hence, the effect of different models on the simulation of the system SBU should be considered in the future study while keeping the error of the stratigraphic boundary location to a reasonably acceptable range. This underlines the need for much finer discretization of the random field elements and more efficient reliability analysis approach to be adopted.

4. Although the effect of the system SBU on slope reliability has been successfully investigated in Chapter 6, the slope example used to illustrate the effect of the system SBU on slope reliability is hypothetical and the slope size is relatively small. In engineering practice, the borehole density would not be as dense as used herein. Collecting real borehole data for real slopes in geotechnical practice to identify characterize the system SBU is reserved for further study. In addition, the question of which kind of uncertainty is more important remains to be answered.

5. The reliability analysis conditioned on some known soil properties and that conditioned on real stratigraphic boundary from site investigation data are separately considered in this study, which is a kind of simplification. In reality, the soil properties and the stratigraphic information can be obtained simultaneously from site investigation. Therefore, it is suggested that future study consider different kinds of conditional information simultaneously so as to reflect the reality as closely as possible.

6. In the present study, only two-dimensional slope stability problems have been studied, whereas the influence of three-dimensional soil spatial variability on the slope reliability and slope failure mechanism has been neglected. In fact, due to the assumption of the plain strain on two-dimensional slope stability model, the failure probability estimated at this situation would be underestimated, which would finally lead to conservative assessment of the real performance of the slope. Hence, it is of

more practical significance to explore the influence of three-dimensional soil spatial variability on the slope stability.

7. The slopes studied herein are simple, thus the proposed approaches cannot be directly applied to the slopes reinforced with soil nails or piles. However, it is more important to employ reliability-based approaches to evaluate the performance of those reinforced slopes. Hence, study on reliability analysis of reinforced slopes while considering conditional measurement data is also a meaningful research topic.

REFERENCES

Al-Bittar T, Soubra AH (2013) Bearing capacity of strip footings on spatially random soils using sparse polynomial chaos expansion. Int J Numer Anal Meth Geomech 37: 2039-2060

Ang AH-S, Tang WH (2007) Probability concepts in engineering: emphasis on applications to civil and environmental. Wiley, New York

Ang AHS, Tang WH (1984) Probability concepts in engineering planning and design: design, risk and reliability, vol. 2. Wiley, New York

Angelikopoulos P, Papadimitriou C, Koumoutsakos P (2015) X-TMCMC: Adaptive kriging for Bayesian inverse modeling. Comput Method Appl M 289: 409-428

Au SK, Beck JL (2001) Estimation of small failure probabilities in high dimensions by subset simulation. Probabilistic Eng Mech 16(4): 263-277

Au SK, Beck JL (2003) Subset Simulation and its Application to Seismic Risk Based on Dynamic Analysis. J Eng Mech 129(8): 901-917

Au SK, Cao ZJ, Wang Y (2010) Implementing advanced Monte Carlo simulation under spreadsheet environment. Struct Saf 32(5): 281-292

Au SK, Ching J, Beck JL (2007) Application of subset simulation methods to reliability benchmark problems. Struct Saf 29(3): 183-193

Au SK, Wang Y (2014) Engineering risk assessment with subset simulation John Wiley & Sons, Singapore

Bucher CG, Bourgund U (1990) A fast and efficient response surface approach for structral reliability problems. Struct Saf 7(1): 57-66

Cadini F, Santos F, Zio E (2014) An improved adaptive kriging-based importance technique for sampling multiple failure regions of low probability. Reliab Eng Syst Saf 131: 109-117

Cafaro F, Cherubini C (2002) Large sample spacing in evaluation of vertical strength variability of clayey soil. J Geotech Geoenviron Eng 128(7): 558-568

Cai JS, Yan EC, Yeh TCJ, Zha YY, Liang Y, Huang SY, Wang WK, Wen JC (2017) Effect of spatial variability of shear strength on reliability of infinite slopes using analytical approach. Comput Geotech 81: 77-86

Cheng Q, Luo SX, Gao XQ (2000) Analysis and discuss of calculation of scale of fluctuation using correlation function method. Chin J Rock Soil Mech 21(3): 281-283

Cheng YM, Lansivaara T, Wei WB (2007) Two-dimensional slope stability analysis by limit equilibrium and strength reduction methods. Comput Geotech 34(3): 137-150

Ching J, Phoon KK (2013) Effect of element sizes in random field finite element simulations of soil shear strength. Comput Struct 126: 120-134

Ching JY, Phoon KK, Hu YG (2009) Efficient evaluation of reliability for slopes with circular slip surfaces using importances sampling. J Geotech Geoenviron Eng 135(6): 758-777

Cho SE (2007) Effects of spatial variability of soil properties on slope stability. Eng Geol 92(3-4): 97-109

Cho SE (2009) Probabilistic stability analyses of slopes using the ANN-based response surface. Comput Geotech 36(5): 787-797

Cho SE (2010) Probabilistic assessment of slope stability that considers the spatial variability of soil properties. J Geotech Geoenviron Eng 136(7): 975-984

Cho SE (2012) Probabilistic analysis of seepage that considers the spatial variability of permeability for an embankment on soil foundation. Eng Geol 133-134: 30-39

Cho SE (2013) First-order reliability analysis of slope considering multiple failure modes. Eng Geol 154: 98-105

Cho SE (2014) Probabilistic stability analysis of rainfall-induced landslides considering spatial variability of permeability. Eng Geol 171: 11-20

Cho SE, Park HC (2010) Effect of spatial variability of cross-correlated soil properties on bearing capacity of strip footing. Int J Numer Anal Meth Geomech 34: 1-26

Chowdhury RN, Xu DW (1994) Slope system reliability with general slip surfaces. Soils Found 34(3): 99-105

Chowdhury RN, Xu DW (1995) Geotechnical system reliability of slopes. Reliab Eng Syst Saf 47(3): 141-151

Christian JT, Ladd CC, Baecher GB (1994) Reliability applied to slope stability analysis. J Geotech Eng 120(12): 2180-2207

Dai FC, Lee CF, Ngai YY (2002) Landslide risk assessment and management: an overview. Eng Geol 64: 65-87

Dasaka SM, Zhang LM (2012) Spatial variability of in situ weathered soil. Géotechnique 62(5): 375-384

Deng ZP, Li DQ, Qi XH, Cao ZJ, Phoon KK (2017) Reliability evaluation of slope considering geological uncertainty and inherent variability of soil parameters. Comput Geotech 92: 121-131

Deutsch CV, Journel AG (1992) GSLIB: Geostatistics Software Library and user's guide. Oxford Univ., New York

Dithinde M, Phoon K-K, Ching J, Zhang L, Retief JV (2016a) Chapter 5 Statistical characterization of model uncertainty. Reliability of Geotechnical Structures in ISO2394, CRC Press/Balkema, pp 127-158

Dithinde M, Phoon KK, Ching J, Zhang LM, Retief JV (2016b) Reliability of Geotechnical Structures in ISO2394. In: Phoon KK and Retief JV (eds) Reliability of Geotechnical Structures in ISO2394, CRC Press, Balkema,

Ditlevsen O (1979) Narrow reliability bounds for structural systems. Mech Based Des Struc 7(4): 453-472

Echard B, Gayton N, Lemaire M, Relun N (2013) A combined Importance Sampling and Kriging reliability method for small failure probabilities with time-demanding numerical models. Reliab Eng Syst Saf 111: 232-240

El-Ramly H, Morgenstern NR, Cruden DM (2002) Probabilistic slope stability analysis for practice. Can Geotech J 39(3): 665-683

Elfeki A, Dekking M (2001) A Markov Chain Model for Subsurface Characterization: Theory and Applications. Math Geol 33(5): 569-589

Elfeki AMM, Dekking FM (2005) Modelling Subsurface Heterogeneity by Coupled Markov Chains: Directional Dependency, Walther's Law and Entropy. Geotech Geol Eng 23(6): 721-756

Fenton GA (2007) Probabilistic Methods in Geotechnical Engineering. In: Griffiths DV and Fenton GA (eds) Data analysis/geostatistics, Springer, New York, pp 51-73

Fenton GA, Griffiths DV (2003) Bearing-capacity prediction of spatially random c-φ soils. Can Geotech J 40(1): 54-65

Fenton GA, Griffiths DV (2005) A slope stability reliability model. Ontario, London,

Fenton GA, Griffiths DV (2008) Risk assessment in geotechnical engineering. Wiley, New York

Fenton GA, Vanmarcke EH (1990) Simulation of random fields via local average subdivision. J Eng Mech 116(8): 1733-1749

Fuglstad GA, Simpson D, Lindgren F, Rue H (2014) Does non-stationary spatial data always require non-stationary random fields? Spat Stat 14: 505-531

Gong WP, Juang CH, Martin JR, Ching JY (2015) New Sampling Method and Procedures for Estimating Failure Probability. J Eng Mech, 10.1061/:

Griffiths DV, Fenton GA (1993) Seepage beneath water retaining structures founded on spatially random soil. Géotechnique 43(4): 577-587

Griffiths DV, Fenton GA (2001) Bearing capacity of spatially random soil-the undrained clay Prandtl problem revisited. Géotechnique 51(4): 351-359

Griffiths DV, Fenton GA (2004) Probabilistic slope stability analysis by finite elements. J Geotech Geoenviron Eng 130(5): 507-518

Griffiths DV, Huang J, Fenton GA (2009) Influence of spatial variability on slope reliability using 2-D random fields. J Geotech Geoenviron Eng 135(10): 1367-1378

Griffiths DV, Huang J, Fenton GA (2011) Probabilistic infinite slope analysis. Comput Geotech 38(4): 577-584

Griffiths DV, Lane PA (1999) Slope stability analysis by finite elements.

Géotechnique 49(3): 387-403

Griffiths DV, Yu X (2015) Another look at the stability of slopes with linearly increasing undrained strength. Géotechnique 65(10): 824-830

Hasofer A, Lind N (1974) Exact and invariant second moment code format. J Eng Mech 100: 194-208

Henderson CR (1975) Best linear unbiased estimation and prediction under a selection model. Biometrics 31(2): 423-447

Hicks MA, Chen J, Spencer WA (2008) Influence of spatial variability on 3D slope failures. In Sixth International Conference on Computer Simulation Risk Analysis and Hazard Mitigation,

Hicks MA, Nuttall JD, Chen J (2014) Influence of heterogeneity on 3D slope reliability and failure consequence. Comput Geotech 61: 198-208

Hicks MA, Spencer WA (2010) Influence of heterogeneity on the reliability and failure of a long 3D slope. Comput Geotech 37(7-8): 948-955

Hsu SC, Nelson PP (2006) Material spatial variability and slope stability for weak rock masses. Journal of Geotechnical and Geoenvironmental Engineering 132(2): 183-193

Huang J, Fenton G, Griffiths DV, Li D, Zhou C (2016) On the efficient estimation of small failure probability in slopes. Landslides 14(2): 491-498

Huang J, Fenton G, Griffiths DV, Li D, Zhou C (2017) On the efficient estimation of small failure probability in slopes. Landslides 14(2): 491-498

Huang J, Griffiths DV (2015) Determining an appropriate finite element size for modelling the strength of undrained random soils. Comput Geotech 69: 506-513

Huang J, Griffiths DV, Fenton GA (2010) System reliability of slopes by RFEM. Soils Found 50(3): 343-353

Huang J, Lyamin AV, Griffiths DV, Krabbenhoft K, Sloan SW (2013) Quantitative risk assessment of landslide by limit analysis and random fields. Comput Geotech 53: 60-67

Huang SP, Quek ST, Phoon KK (2001) Convergence study of the truncated Karhunen–Loeve expansion for simulation of stochastic processes. Int J Numer Meth Eng 52(9): 1029-1043

Isukapalli SS, Roy A, Georgopoulos PG (1998) Stochastic response surface methods for uncertainty propagation: application to environmental and biological systems. Risk Anal 18(3): 351-363

Javankhoshdel S, Bathurst RJ (2014) Simplified probabilistic slope stability design charts for cohesive and cohesive-frictional (c-ϕ) soils. Can Geotech J 51(9): 1033-1045

Jha SK, Ching JY (2013) Simplified reliability method for spatially variable undrained engineered slopes. Soils Found 53(5): 708-719

Ji J (2013) Reliability analysis of earth slopes accounting for spatial variation. PhD Thesis, Nanyang Technological University

Ji J, Liao HJ, Low BK (2012) Modeling 2-D spatial variation in slope reliability analysis using interpolated autocorrelations. Comput Geotech 40: 135-146

Ji J, Low BK (2012) Stratified response surfaces for system probabilistic evaluation of slopes. J Geotech Geoenviron Eng 138(11): 1398-1406

Ji J, Zhang C, Gao Y, Kodikara J (2017) Effect of 2D spatial variability on slope reliability: a simplified FORM analysis. Geosci Front, 10.1016/j.gsf.2017.08.004:

Jiang SH, Huang J, Yao C, Yang J (2017) Quantitative risk assessment of slope failure in 2-D spatially variable soils by limit equilibrium method. Appl Math Model 47: 710-725

Jiang SH, Huang JS (2016) Efficient slope reliability analysis at low-probability levels in spatially variable soils. Comput Geotech 75: 18-27

Jiang SH, Li DQ, Cao ZJ, Zhou CB, Phoon KK (2015) Efficient system reliability analysis of slope stability in spatially variable soils using Monte Carlo simulation. J Geotech Geoenviron Eng 141(2): 04014096

Jiang SH, Li DQ, Zhang LM, Zhou CB (2014a) Slope reliability analysis considering spatially variable shear strength parameters using a non-intrusive stochastic finite element method. Eng Geol 168: 120-128

Jiang SH, Li DQ, Zhou CB, Phoon KK (2014b) Slope reliability analysis considering effect of autocorrelation functions Chin J Geotech Eng 36(3): 508-518

Jimenez-Rodriguez R, Sitar N, Chacón J (2006) System reliability approach to rock slope stability. Int J Rock Mech Min Sci 43(6): 847-859

Johari A, Khodaparast AR (2015) Analytical stochastic analysis of seismic stability of infinite slope. Soil Dyn Earthquake Eng 79: 17-21

Johari A, Lari AM (2016) System reliability analysis of rock wedge stability considering correlated failure modes using sequential compounding method. Int J Rock Mech Min Sci 82: 61-70

Kang F, Han S, Salgado R, Li J (2015) System probabilistic stability analysis of soil slopes using Gaussian process regression with Latin hypercube sampling. Comput Geotech 63: 13-25

Kang F, Li J (2016) Artificial Bee Colony Algorithm Optimized Support Vector Regression for System Reliability Analysis of Slopes. J Comput Civ Eng 30(3): 04015040

Kang F, Xu Q, Li J (2016) Slope reliability analysis using surrogate models via new support vector machines with swarm intelligence. Appl Math Model 40(11-12): 6105-6120

Kim JM, Sitar N (2013) Reliability approach to slope stability analysis with spatially correlated soil properties. Soils Found 53(1): 1-10

Krahn J (2006) The limitations of the strength reduction approach. GEO-SLOPE | Direct Contact, GEO-SLOPE International Ltd., Calgary, Alberta, Canada

Laloy E, Rogiers B, Vrugt JA, Mallants D, Jacques D (2013) Efficient posterior exploration of a high-dimensional groundwater model from two-stage Markov chain Monte Carlo simulation and polynomial chaos expansion. Water Resour Res 49(5): 2664-2682

Li D, Chen Y, Lu W, Zhou C (2011a) Stochastic response surface method for reliability analysis of rock slopes involving correlated non-normal variables. Comput Geotech 38(1): 58-68

Li DQ, Jiang SH, Cao ZJ, Zhou W, Zhou CB, Zhang LM (2015a) A multiple response-surface method for slope reliability analysis considering spatial variability of soil properties. Eng Geol 187: 60-72

Li DQ, Jiang SH, Chen YF, Zhou CB (2011b) System reliability analysis of rock slope stability involving correlated failure modes. KSCE J Civ Eng 15(8): 1349-1359

Li DQ, Qi XH, Cao ZJ, Tang XS, Phoon KK, Zhou CB (2016a) Evaluating slope stability uncertainty using coupled Markov chain. Comput Geotech 73: 72-82

Li DQ, Qi XH, Phoon KK, Zhang LM, Zhou CB (2014) Effect of spatially variable shear strength parameters with linearly increasing mean trend on reliability of infinite slopes. Struct Saf 49: 45-55

Li DQ, Shao KB, Cao ZJ, Tang XS, Phoon KK (2016b) A generalized surrogate response aided-subset simulation approach for efficient geotechnical reliability-based design. Comput Geotech 74: 88-101

Li DQ, Tang XS, Phoon KK (2015b) Bootstrap method for characterizing the effect of uncertainty in shear strength parameters on slope reliability. Reliab Eng Syst Saf 140: 99-106

Li DQ, Xiao T, Cao ZJ, Zhou CB, Zhang LM (2016c) Enhancement of random finite element method in reliability analysis and risk assessment of soil slopes using Subset Simulation. Landslides 13: 293-303

Li DQ, Zheng D, Cao ZJ, Tang XS, Phoon KK (2016d) Response surface methods for slope reliability analysis: Review and comparison. Eng Geol 203: 3-14

Li HS, Ma YZ, Cao ZJ (2015c) A generalized Subset Simulation approach for estimating small failure probabilities of multiple stochastic responses. Comput Struct 153: 239-251

Li J, Cassidy MJ, Huang J, Zhang L, Kelly R (2016e) Probabilistic identification of soil stratification. Géotechnique 66(1): 16-26

Li KS, Lumb P (1987) Probabilistic design of slopes. Can Geotech J 24(4): 520-535

Li L, Chu X (2016) Risk assessment of slope failure by representative slip surfaces and response surface function. KSCE J Civ Eng 20(5): 1783-1792

Li L, Chu XS (2015) Multiple response surfaces for slope reliability analysis. Int J Numer Anal Meth Geomech 39(2): 175-192

Li XY, Zhang LM, Gao L, Zhu H (2017) Simplified slope reliability analysis considering spatial soil variability. Eng Geol 216: 90-97

Li XY, Zhang LM, Li JH (2015d) Using conditioned random field to characterize the variability of geologic profiles. J Geotech Geoenviron Eng, 10.1061/(asce)gt.1943-5606.0001428: 04015096

Liu L, Cheng Y, Wang X (2017a) Genetic algorithm optimized Taylor Kriging surrogate model for system reliability analysis of soil slopes. Landslides 14: 535-546

Liu LL, Cheng YM (2016) Efficient system reliability analysis of soil slopes using multivariate adaptive regression splines-based Monte Carlo simulation. Comput Geotech 79: 41-54

Liu LL, Cheng YM, Jiang SH, Zhang SH, Wang XM, Wu ZH (2017b) Effects of spatial autocorrelation structure of permeability on seepage through an embankment on a soil foundation. Comput Geotech 87: 62-75

Liu LL, Cheng YM, Wang XM, Zhang SH, Wu ZH (2017c) System reliability analysis and risk assessment of a layered slope in spatially variable soils considering stratigraphic boundary uncertainty. Comput Geotech 89: 213-225

Liu LL, Cheng YM, Zhang SH (2017d) Conditional random field reliability analysis of a cohesion-frictional slope. Comput Geotech 82: 173-186

Lloret-Cabot M, Fenton GA, Hicks MA (2014) On the estimation of scale of fluctuation in geostatistics. Georisk 8(2): 129-140

Lloret-Cabot M, Hicks MA, van den Eijnden AP (2012) Investigation of the reduction in uncertainty due to soil variability when conditioning a random field using Kriging. Geotech Lett 2(3): 123-127

Low BK (2003) Practical probabilistic slope stability analysis. 12th Panamerican conference on soil mechanics and geotechnical engineering and 39th US rock mechanics symposium, MIT, Cambridge, Massachusetts,

Low BK (2007) Reliability analysis of rock slopes involving correlated nonnormals. Int J Rock Mech Min Sci 44(6): 922-935

Low BK (2014) FORM, SORM, and spatial modeling in geotechnical engineering. Struct Saf 49: 56-64

Low BK, Gilbert RB, Wright SG (1998) Slope reliability analysis using generalized method of slices. J Geotech Geoenviron Eng 124(4): 350-362

Low BK, Lacasse S, Nadim F (2015) Slope reliability analysis accounting for spatial variation. Georisk 1(4): 177-189

Low BK, Tang WH (2007) Efficient spreadsheet algorithm for first-order reliability method. J Eng Mech 133(12): 1378-1387

Lu ZM, Zhang DX (2007) Stochastic simulations for flow in nonstationary randomly heterogeneous porous media using a KL-based moment-equation approach. Multiscale Model Sim 6(1): 228-245

Luo XF, Cheng T, Li X, Zhou J (2012a) Slope safety factor search strategy for multiple sample points for reliability analysis. Eng Geol 129-130: 27-37

Luo XF, Li X, Zhou J, Cheng T (2012b) A Kriging-based hybrid optimization algorithm for slope reliability analysis. Struct Saf 34(1): 401-406

Luo Z, Atamturktur S, Cai Y, Juang CH (2012c) Simplified Approach for Reliability-Based Design against Basal-Heave Failure in Braced Excavations Considering Spatial Effect. J Geotech Geoenviron Eng 138(4): 441-450

Luo Z, Atamturktur S, Juang CH, Huang HW, Lin PS (2011) Probability of serviceability failure in a braced excavation in a spatially random field: Fuzzy finite element approach. Comput Geotech 38: 1031–1040

Mari DD, Kozt S (2001) Correlation and dependence. Imperial College Press, UK

Mašín D (2015) The influence of experimental and sampling uncertainties on the probability of unsatisfactory performance in geotechnical applications. Géotechnique 65(11): 897-910

Metya S, Bhattacharya G (2015) Reliability Analysis of Earth Slopes Considering Spatial Variability. Geotechnical and Geological Engineering 34(1): 103-123

Namikawa T (2016) Conditional Probabilistic Analysis of Cement-Treated Soil Column Strength. Int J Geomech 16(1): 04015021

Nataf A (1962) Détermination des distributions de probabilités dont les marges sont données. Comptes Rendus de l' Académie des Sciences 225: 42-43

Oka Y, Wu TH (1990) System reliability of slope stability. Journal of Getechnical Engineering 116(8): 1185-1189

Pan Q, Dias D (2017) Probabilistic evaluation of tunnel face stability in spatially random soils using sparse polynomial chaos expansion with global sensitivity analysis. Acta Geotechnica 12(6): 1415-1429

Pan Q, Jiang Y-J, Dias D (2017) Probabilistic stability analysis of a three-dimensional rock slope characterized by the Hoek-Brown failure Criterion. J Comput Civ Eng 31(5): 04017046

Pantelidis L, Gravanis E, Griffiths DV (2015) Influence of spatial variability on rock slope reliability using 1-D random fields. 10.1007/978-3-319-09057-3_216: 1235-1238

Peng M, Li XY, Li DQ, Jiang SH, Zhang LM (2014) Slope safety evaluation by integrating multi-source monitoring information. Struct Saf 49: 65-74

Phoon KK, Ching J (2014) Risk and reliability in geotechnical engineering. CRC Press, Boca Raton

Phoon KK, Huang SP, Quek ST (2002) Implementation of Karhunen–Loeve expansion for simulation using a wavelet-Galerkin scheme. Probabilistic Eng Mech 17(3): 293-303

Phoon KK, Kulhawy FH (1999a) Characterization of geotechnical variability. Can Geotech J 36(4): 612-624

Phoon KK, Kulhawy FH (1999b) Characterization of geotechnical variability. Can Geotech J 36: 612-624

Phoon KK, Kulhawy FH (1999c) Evaluation of geotechnical property variability. Can Geotech J 36: 625-639

PRC MC, AQSIQ (2009) State Standard of the People's Republic of China. Code for investigation of geotechnical engineering (GB50021-2001), China Architecture & Building Press, Beijing

Qi XH, Li DQ, Phoon KK, Cao ZJ, Tang XS (2016) Simulation of geologic uncertainty using coupled Markov chain. Eng Geol 207: 129-140

Rennen G (2008) Subset selection from large datasets for Kriging modeling. Struct Multidisc Optim 38(6): 545-569

Rosenblueth E (1975) Point estimates for probability moments. National Academy of Science:

Sivakumar Babu GL, Srivastava A, Murthy DS (2006) Reliability analysis of the bearing capacity of a shallow foundation resting on cohesive soil. Can Geotech J 43(2): 217-223

Sivakumar Bubu GL, Mukesh MD (2004) Effect of soil variability on reliability of soil slopes. Géotechnique 54(5): 335-337

Suchomel R, Mašín D (2010) Comparison of different probabilistic methods for predicting stability of a slope in spatially variable c–φ soil. Comput Geotech 37(1-2): 132-140

Sundar V (2015) A short report on MATLAB implementation of subset simulation. 10.13140/RG.2.1.3041.7444:

Tang XS, Li DQ, Chen YF, Zhou CB, Zhang LM (2012) Improved knowledge-based clustered partitioning approach and its application to slope reliability analysis. Comput Geotech 45: 34-43

Vanmarcke E (1977a) Reliability of earth slopes. J Geotech Eng Div 103(11): 1247-1265

Vanmarcke EH (1977b) Probabilistic Modeling of Soil Profiles. J Geotech Eng Div 103(11): 1227-1246

Vanmarcke EH (2010) Random Fields: Analysis and Synthesis (revised and expanded). World Scientific Publishing Co. Pte. Ltd., Singapore

Vega JA, Hidalgo CA (2016) Quantitative risk assessment of landslides triggered by earthquakes and rainfall based on direct costs of urban buildings. Geomorphology 273: 217-235

Vořechovský M (2008) Simulation of simply cross correlated random fields by series expansion methods. Struct Saf 30(4): 337-363

Wang X, Li Z, Wang H, Rong Q, Liang RY (2016) Probabilistic analysis of shield-driven tunnel in multiple strata considering stratigraphic uncertainty. Struct Saf 62: 88-100

Wang Y, Cao ZJ, Au SK (2010) Efficient Monte Carlo Simulation of parameter sensitivity in probabilistic slope stability analysis. Comput Geotech 37(7-8): 1015-1022

Wang Y, Cao ZJ, Au SK (2011) Practical reliability analysis of slope stability by advanced Monte Carlo simulations in a spreadsheet. Can Geotech J 48: 162-172

Wang Y, Huang K, Cao Z (2013) Probabilistic identification of underground soil stratification using cone penetration tests. Can Geotech J 50(7): 766-776

Wang Y, Huang K, Cao Z (2014) Bayesian identification of soil strata in london clay. Géotechnique 64(3): 239-246

Wong FS (1985) Slope reliability and response surface method. J Geotech Eng 111(1): 32-53

Wu ZJ, Wang SL, Ge XR (2009) Slope reliability analysis by random FEM under constraint random field. Chinese J Rock Soil Mech 30(10): 3086-3092

Xiao T, Li DQ, Cao ZJ, Au SK, Phoon KK (2016) Three-dimensional slope reliability and risk assessment using auxiliary random finite element method. Comput Geotech 79: 146-158

Yi P, Wei K, Kong X, Zhu Z (2015) Cumulative PSO-Kriging model for slope reliability analysis. Probabilistic Eng Mech 39: 39-45

Ying L (2012) Application of Stochastic Response Surface Method in the Structural Reliability. Procedia Eng 28: 661-664

Zhang J, Huang HW (2016) Risk assessment of slope failure considering multiple slip surfaces. Comput Geotech 74: 188-195

Zhang J, Huang HW, Phoon KK (2013) Application of the Kriging-based response surface method to the system reliability of soil slopes. J Geotech Geoenviron Eng 139(4): 651-655

Zhang J, Zhang LM, Tang WH (2011a) Kriging numerical models for geotechnical reliability analysis. Soils Found 51(6): 1169-1177

Zhang J, Zhang LM, Tang WH (2011b) New methods for system reliability analysis of soil slopes. Can Geotech J 48(7): 1138-1148

Zhao HB (2008) Slope reliability analysis using a support vector machine. Comput Geotech 35(3): 459-467

Zhao HL, Yue ZF, Liu YS, Gao ZZ, Zhang YS (2015) An efficient reliability method combining adaptive importance sampling and Kriging metamodel. Appl Math Model 39(7): 1853-1866

Zhu H, Griffiths DV, Fenton GA, Zhang LM (2015) Undrained failure mechanisms of slopes in random soil. Eng Geol 191: 31-35